Development of responsive polymers for drug delivery applications

Benzeval, Ian

Award date:
2009

Awarding institution:
University of Bath

Development of Responsive Polymers for Drug Delivery Applications

submitted by Ian David Benzeval

A thesis submitted for the degree of Doctor of Philosophy

University of Bath
Department of Chemical Engineering

January 2009

COPYRIGHT

Ian David Benzeval

Abstract

In this thesis, glucose responsive hydrogels based on cross-linked dextran molecules were studied to determine the diffusion rate of an insulin analogue. Investigations of the interaction between concanavalin A and dextran, both in free solution and in the form of glucose responsive hydrogels were conducted.

The free solution results have shown that there is an increase of association constant between concanavalin A and dextran when the molecular mass of the dextran is increased. Free solution viscometric tests have shown that increasing the molecular mass or the concentration of the dextran increases the viscosity.

The hydrogels have been shown to form for dextrans of molecular mass 43kD or greater. Smaller molecular mass dextrans were found to coalesce into small beads which appeared to prevent hydrogel formation with these materials.

Experiments conducted with hydrogel membranes in a diffusion cell have shown that the batch to batch reproducibility of hydrogel transport properties is low. This is partly due to the weak mechanical nature of the hydrogel and partly due to the heterogeneous nature of the precursor dextrans. However, clear evidence of glucose enhanced transport was obtained and these results were compared with predictions obtained from a theoretical model of gel permeability that accounts for competitive displacement of affinity cross links. Oscillatory rheological tests of gelation mixtures which showed an increase in complex viscosity at the gel point with increasing molecular mass of dextran were in agreement with empirical observations that gels formed from the highest molecular mass dextrans were more physically robust and easier to handle.

Swelling rate experiments have shown that the rate of hydration of a hydrogel in the presence of glucose is decreased due to the osmotic pressure of the glucose.

This work has shown that the multivalent nature of concanavalin A may not be a necessary pre-requisite for this type of hydrogel due to spatial constraints decreasing the number of potential affinity bonds per tetramer. In-house production of more tightly defined dextrans (molecular mass and branching ratio) might be expected to reduce heterogeneity and improve the reproducibility of this type of hydrogel membrane.

Acknowledgments

I would like to thank Dr. John Hubble for always being available to give invaluable advice throughout this work.

Thanks are also due to Dr. Adrian Bowyer for his knowledge of Mechanical Engineering, which provided interesting alternative viewpoints. Mrs. Suzanne Barkley and Mr. Richard Bull should be thanked for the essential technical support they provided and I would also like to thank the late Professor Robert Eisenthal for the help he provided.

Finally I would like to thank the EPSRC for their financial support of my work.

Contents

Section 1. Literature Review 1

Section 1.1. Diabetes Mellitus and the Role of Insulin 1

Section 1.1.1. Diabetes Mellitus 1

Section 1.1.2. Insulin 2

Section 1.1.3. Treatment 3

Section 1.2. Responsive Polymers - Hydrogels 6

Section 1.2.1. Temperature Sensitive Hydrogels 7

Section 1.2.2. pH Sensitive Hydrogels 7

Section 1.2.3. Antigen – Antibody 8

Section 1.2.4. Glucose Sensitive Hydrogels – Phenylboronic Acid 8

Section 1.2.5. Glucose Sensitive Hydrogels – Concanavalin A 9

Section 1.2.6. Other Responsive Polymers and their Stimuli 10

Section 1.2.7. Mannose Binding Lectin (MBL) 11

Section 1.2.8. Summary of Current Thinking on Hydrogels 12

Section 1.3. Lectins 13

Section 1.4. Mono- and Polysaccharides 14

Section 1.5. ConA / Dextran Interaction Characterisation 15

Section 1.5.1. Isothermal Titration Calorimetry (ITC) 16

Section 1.5.2. Surface Plasmon Resonance (SPR) 18

Section 1.6. Hydrogel Production Methods 18

Section 1.6.1. Production 18

Section 2. Materials and Methods 20

Section 2.1. Materials 20

Section 2.2. Buffer Solution 20

Section 2.3. Carboxymethyl Dextran 21

Section 2.4. Dextran Branching - NMR 22

Section 2.5. Dextran Summary 26

Section 2.6. Hydrogel Production and Casting 27

Part 1 – Investigation of Concanavalin A / Dextran Interaction 28

Section 3. Isothermal Titration Calorimetry 29

Section 3.1. Theory 29

Section 3.1.1. Isothermal Titration Calorimetry 29
Section 3.1.2. Thermodynamics of the System 31
Section 3.1.3. Lectin / Saccharide Binding 32
Section 3.1.4. Sequential Sites Mathematical Model 34
Section 3.1.5. Parameter 'c' 35
Section 3.2. Experimental Conditions and Data Analysis 35
Section 3.2.1. Experimental Conditions 35
Section 3.2.2. Model Accuracy and Error Calculation 36
Section 3.2.3. Model Selection 37
Section 3.2.4. Model Instability 38
Section 3.3. Results and Discussion 40
Section 3.4. Conclusion 45
Section 3.5. Nomenclature 46
Section 4. Surface Plasmon Resonance 47
Section 4.1. Theory 47
Section 4.1.1. Surface Plasmon Resonance 47
Section 4.1.2. Kinetic Experiments 49
Section 4.1.3. Analysis 50
Section 4.2. Experimental Conditions 51
Section 4.2.1. Experimental Conditions 51
Section 4.2.2. Binding ConA or Dextran to the Sensor Chip Surface 51
Section 4.3. Data Analysis and Results 52
Section 4.3.1. Binding Type Analysis 53
Section 4.3.2. Binding Type Summary and Discussion 58
Section 4.3.3. Results 60
Section 4.4. Conclusions 62
Section 4.5. Nomenclature 62
Part 1 - Conclusions 63
Part 2 - Production and Evaluation of Dextran / Concanavalin A Hydrogels 64
Section 5. Rheology 65
Section 5.1. Theory 65
Section 5.1.1. Cone and Plate Measuring System 65
Section 5.1.2. Rheological Solutions 66

Section 5.2. Viscosity of Pure Dextran 66
Section 5.2.1. Experimental Procedure 66
Section 5.2.2. Results and Discussion 67
Section 5.2.3. Conclusions 69
Section 5.3. Rheology of Gelation mixture 70
Section 5.3.1. Viscoelastic Materials 70
Section 5.3.2. Oscillatory Tests 71
Section 5.3.3. Experimental Procedure 73
Section 5.3.4. Results and Discussion 74
Section 5.3.5. Conclusions 78
Section 5.4. Nomenclature 79
Section 6. Diffusion Rate Experiments 80
Section 6.1. Hydrogel Theory 80
Section 6.2. Hydrogel Production 80
Section 6.3. Experimental Conditions and Data Analysis 82
Section 6.3.1. In-House Diffusion Chamber 82
Section 6.3.2. Experimental Conditions 83
Section 6.3.3. Data Analysis 87
Section 6.3.4. Swelling Model 88
Section 6.4. Results and Discussion 92
Section 6.4.1. Experimental Data 92
Section 6.4.2. Swelling Model 95
Section 6.5. Conclusions 104
Section 6.6. Nomenclature 106
Section 7. Swelling Rate of Hydrogels 107
Section 7.1. Swelling Rate Theory 107
Section 7.1.1. Calculations 107
Section 7.2. Experimental Conditions 108
Section 7.3. Results and Discussion 109
Section 7.4. Conclusions 110
Section 7.5. Nomenclature 111
Part 2 - Conclusions 112
Part 3 – Overall Conclusions and Future Work 113

Section 8. Overall Conclusions 113
Section 9. Future Work Plans 116
Section 10. References 118
Appendix 1. NMR Traces 126
Appendix 2. Isothermal Titration Calorimetry Binding Theory 131
Appendix 2.1. One Site Model 131
Appendix 2.2. Two Site Model 133
Appendix 3. Isothermal Titration Calorimetry Models 135
Appendix 3.1. One Site Model 135
Appendix 3.2. Two Site Model with Constant K and ΔH values 136
Appendix 3.3. Two Site Model with Variable K and ΔH Values 137
Appendix 3.4. Three Site Model with Constant K and ΔH Values 139
Appendix 3.5. Three Site Model with Variable K and ΔH Values 140
Appendix 3.6. Four Site Model with Constant K and ΔH Values 141
Appendix 3.7. Four Site Model with Variable K and ΔH Values 143
Appendix 3.8. One Site Model with Two Populations of Dextran 144
Appendix 4. Isothermal Titration Calorimetry Raw Data 146
Appendix 5. Surface Plasmon Resonance Binding Theory 151
Appendix 5.1. Langmuir Model 151
Appendix 5.2. Bivalent Model 152
Appendix 5.3. Heterogeneous Ligand Population Model 152
Appendix 5.4. Additional Effects 153
Appendix 6. Surface Plasmon Resonance Models 155
Appendix 6.1. Langmuir Model 155
Appendix 6.2. Langmuir Model with Mass Transfer 156
Appendix 6.3. Bivalent Model 156
Appendix 6.4. Heterogeneous Model 157
Appendix 6.5. Heterogeneous Bivalent Model 158
Appendix 7. Surface Plasmon Resonance Data 160
Appendix 7.1. Deconvoluted SPR data 160
Appendix 7.2. SPR Raw Data 162
Appendix 8. Rheology - Maxwell Model for Viscoelasticity 166

Appendix 9. Mathematics of an Oscillator 169
Appendix 10. Oscillatory Rheology 171
Appendix 11. Complex Number Theory 175
Appendix 12. Swelling Model for a Hydrogel..... 177
Appendix 13. Power Basic Model of Hydrogel Swelling..... 180

List of Figures

Figure 1-1 Diagram of proinsulin molecule. 3
Figure 1-2 Depiction of the binding of insulin to a charged Boronic acid group and its disruption by free glucose (Taken from [33]). 9
Figure 1-3 Structure of a dextran molecule with an α(1-3)- branch. 14
Figure 1-4 The energy release profile of 0.1mM conA when titrated with 24.77mM 2000kD dextran 17
Figure 2-1 Structure of α-D-glucose molecule. 23
Figure 2-2 ^{1}H spectra for 17kD Dalton dextran. 24
Figure 2-3 ^{1}H spectra for 17kD Dalton dextran (Blue) and maltotriose (green) taken at 55^{o}C in a 400MHz Bruker NMR Spectrometer. 25
Figure 3-1 Raw Data of titration of D-glucose into conA. 30
Figure 3-2 Plots A and B both represent 31 5µl injections of 11kD dextran into 0.1mM conA. ……...33
Figure 3-3 Moles of primary and secondary complex formed by 30 injections of 0.15mM 500kD dextran with 0.1M conA. 39
Figure 3-4 Energy release of primary and secondary complex formation by 30 injections of 0.15mM 500kD dextran into 0.1M conA. 39
Figure 3-5 Intrinsic association constant of primary binding of glucose, maltose (a glucose dimer), maltotriose (a glucose trimer) and various dextrans with conA..... 42
Figure 3-6 Enthalpy change of primary binding of glucose, maltose (a glucose dimer), maltotriose (a glucose trimer) and various dextrans with conA. 43
Figure 3-7 Structure of a conA tetramer, consisting of two pairs of dimers on top of each other. 44
Figure 4-1 Depiction of the standard amine binding process 47

Figure 4-2 Schematic of SPR technology: L: light source, D: photodiode array, P: prism, S: sensor surface, F: flow cell. 48
Figure 4-3 Injections of ConA over 2000kD Dextran. Concentration of conA (1.1μM, 2.5μM, 4.3μM, 6.8μM and 10.2μM) increasing in direction of arrow. 49
Figure 4-4 Graph showing the first 2000 seconds of the data using the 2000kD dextran activated surface. 53
Figure 4-5 Graph representing data analysis of an injection of 10.2μM conA (monomer concentration) over a 2000kD dextran activated surface. 54
Figure 4-6 Graph representing data analysis of an injection of 10.2nM conA (monomer concentration) over a 2000kD dextran activated surface. 55
Figure 4-7 Graph representing a heterogeneous model, with refractive index, for all the concentrations of conA. 56
Figure 4-8 Graph representing a bivalent heterogeneous model, with refractive index, for all the concentrations of conA. 57
Figure 4-9 Graph of response components that comprise the total seen response of an injection of 10.2μM conA over 2000kD dextran. 59
Figure 4-10 Graph showing normalised injection data for the blank sensor surface and that activated by 43, 500 and 2000kD dextran 61
Figure 5-1 Cone and plate measuring system, of radius, *r*, and angle, α. 65
Figure 5-2 Viscosity test of 20wt% 43kD dextran 67
Figure 5-3 Viscosity of dextran solutions, shear rate increasing 68
Figure 5-4 Viscosity of dextran solutions, shear rate decreasing 68
Figure 5-5 Depiction of a Maxwell model, incorporating a Hookean spring and a Newtonian dashpot in series 71
Figure 5-6 Application of an oscillating shear strain and the resulting shear stress (from [112]) 72
Figure 5-7 Oscillation at 1Hz and 0.5% of a 500kD dextran based gelation 73
Figure 5-8 Time for gel point to be reached for hydrogel mixtures (43, 64, 500 and 2000kD – average of three replicates, error bars show +/- 1 standard deviation) 75
Figure 5-9 Complex and elastic modulus value at gel point (43, 64, 500 and 2000kD – average of three replicates, error bars show +/- 1 standard deviation) 75

Figure 5-10 Rate of change of phase angle at gel point (43, 64, 500 and 2000kD – average of three replicates, error bars show +/- 1 standard deviation) 76
Figure 5-11 Final phase angle of hydrogel (43, 64, 500 and 2000kD – average of three replicates, error bars show +/- 1 standard deviation) 77
Figure 5-12 Final complex modulus of hydrogel (43, 64, 500 and 2000kD – average of three replicates, error bars show +/- 1 standard deviation) 78
Figure 6-1 Schematic of diffusion cell..... 82
Figure 6-2 Photograph of diffusion cell..... 83
Figure 6-3 Schematic of flow cell set-up..... 84
Figure 6-4 Absorption spectrum of cytochrome C showing the strong absorbance at 410nm. ……85
Figure 6-5 Calibration graph of various concentrations of cytochrome C, enabling conversion of spectrometric data from absorbance units to concentration units. 86
Figure 6-6 Time course of cytC passage through a 500kD dextran hydrogel. 87
Figure 6-7 Diffusion ratio with respect to glucose concentration for 17-500kD hydrogels……93
Figure 6-8 Diffusion ratio with respect to glucose concentration for 43-500kD hydrogels……93
Figure 6-9 Diffusion ratio with respect to glucose concentration for 500kD hydrogels ……94
Figure 6-10 Diffusion ratio with respect to glucose concentration for 500-2000kD hydrogels……94
Figure 6-11 Concentration flux variation with glucose for 500kD hydrogel – Base model using data from Table 6-1 and Table 6-2. (Inset displays trend for all glucose concentrations) 95
Figure 6-12 Concentration flux variation with glucose for 500kD hydrogel – Terminal glucose group variation 97
Figure 6-13 Concentration flux variation with glucose for 500kD hydrogel – ConA concentration variation..... 98
Figure 6-14 Concentration flux variation with glucose for 500kD hydrogel – Number average molecular mass between covalent cross-links variation..... 99
Figure 6-15 Concentration flux variation with glucose for 500kD hydrogel – ConA/dextran association constant variation..... 100

Figure 6-16 Concentration flux variation with glucose for 500kD hydrogel – ConA/glucose association constant variation 100
Figure 6-17 Concentration flux variation with glucose for 500kD hydrogel – Flory characteristic ratio variation 101
Figure 6-18 Concentration flux variation with glucose for 500kD hydrogel – Unit length of backbone variation 102
Figure 6-19 Concentration flux variation with glucose for 500kD hydrogel – Membrane thickness variation 103
Figure 6-20 SEM image of conA/dextran hydrogel.Taken from [1]. 105
Figure 7-1 Swelling rate with respect to dextran molecular mass. 109

List of Tables

Table 1-1 Summary of advantages and disadvantages of the methods being investigated for treatment of type I diabetes. 12
Table 2-1 Degree of carboxymethylation by dextran molecular mass 22
Table 2-2 Branching ratio by dextran molecular mass 26
Table 3-1 Comparison of data analysis models based on size of error 37
Table 3-2 Variability of binding parameters depending upon initial estimates 38
Table 3-3 Branching Concentrations from ITC experiments 40
Table 3-4 Binding Parameters from ITC experiments 41
Table 4-1 Number of parameters in the various models used for data analysis 57
Table 4-2 Table of parameters fitted to experimental data using Scientist® 60
Table 4-3 Calculated values of association constants from the experimental data 60
Table 5-1 Rheological Properties of Gelation 74
Table 6-1 Swelling model parameters for 500kD hydrogel 91
Table 6-2 Mesh size, diffusivity and flux calculation parameters for 500kD hydrogel ... 92
Table 7-1 Osmotic Pressures of cuvette swelling experiments, 500kD hydrogel 110

List of Equations

Equation 1-1 8
Equation 1-2 16
Equation 1-3 16
Equation 3-1 31

Equation 3-2 31
Equation 3-3 32
Equation 3-4 34
Equation 3-5 35
Equation 3-6 36
Equation 5-1 65
Equation 5-2 65
Equation 5-3 65
Equation 5-4 70
Equation 5-5 70
Equation 5-6 71
Equation 6-1 89
Equation 6-2 89
Equation 6-3 90
Equation 6-4 90
Equation 6-5 90
Equation 6-6 90
Equation 6-7 91
Equation 7-1 107
Equation 7-2 108
Equation 7-3 109
Equation A2-1 131
Equation A2-2 131
Equation A2-3 131
Equation A2-4 131
Equation A2-5 131
Equation A2-6 132
Equation A2-7 132
Equation A2-8 132
Equation A2-9 132
Equation A2-10 132
Equation A2-11 132
Equation A2-12 132

Equation A2-13 132
Equation A2-14 132
Equation A2-15 133
Equation A2-16 133
Equation A2-17 133
Equation A2-18 133
Equation A5-19 151
Equation A5-20 151
Equation A5-21 151
Equation A5-22 151
Equation A5-23 151
Equation A5-24 152
Equation A5-25 152
Equation A5-26 152
Equation A5-27 152
Equation A5-28 152
Equation A5-29 152
Equation A5-30 153
Equation A5-31 153
Equation A5-32 153
Equation A5-33 153
Equation A5-34 153
Equation A5-35 153
Equation A8-36 166
Equation A8-37 166
Equation A8-38 166
Equation A8-39 167
Equation A8-40 167
Equation A8-41 167
Equation A8-42 167
Equation A8-43 167
Equation A9-44 169
Equation A9-45 170

Equation A10-46 171
Equation A10-47 171
Equation A10-48 171
Equation A10-49 171
Equation A10-50 172
Equation A10-51 172
Equation A10-52 172
Equation A10-53 172
Equation A10-54 172
Equation A10-55 172
Equation A10-56 173
Equation A10-57 173
Equation A10-58 173
Equation A10-59 173
Equation A10-60 173
Equation A10-61 174
Equation A10-62 174
Equation A10-63 174
Equation A10-64 174
Equation A10-65 174
Equation A12-66 177
Equation A12-67 177
Equation A12-68 177
Equation A12-69 177
Equation A12-70 178
Equation A12-71 178
Equation A12-72 178
Equation A12-73 178
Equation A12-74 179

Abbreviations

CM-dextran	Carboxymethyl-dextran
ConA	Concanavalin A
CytC	Cytochrome C
EDC	1-Ethyl-(3-3-dimethylaminopropyl) carbodiimide hydrochloride
FAD	Flavin adenine dinucleotide
G-Ins	Glycosylated insulin
GDH	Glucose dehydrogenase
GOD	Glucose oxidase
ITC	Isothermal titration calorimetry
MBL	Mannose binding lectin
NAD	Nicotinamide adenine dinucleotide
NHS	*N*-hydroxysuccinimide
PAA	poly(Acrylic acid)
PBA	Phenylboronic acid
SPR	Surface plasmon resonance

Nomenclature

a	Amplitude of the wave (m)
A	Surface area of hydrogel (m^2)
c	Wiseman feasibility parameter
C	Concentration of free lectin (M) – equivalent to *[M]* (Section 4)
C	Concentration of solute (gm^{-3}) (Section 7)
C_d	Concentration of cytC, donor side (mgL^{-1})
C_n	Flory characteristic ratio
C_r	Concentration of cytC, receiving side (mgL^{-1})
D	Concentration of dye (gml^{-1})
D_{gel}	Gel phase diffusivity (m^2s^{-1})
D_l	Liquid phase diffusivity of the solute (m^2s^{-1})
F	Force (N)
g	Gravitational constant = $9.81ms^{-2}$
ΔG	Gibbs free energy change ($calmol^{-1}$ or $Jmol^{-1}$)

G	Spring modulus (Pa)
G^*	Complex modulus (Pa)
G'	Storage modulus (Pa)
G''	Loss modulus (Pa)
ΔH	Enthalpic change ($calmol^{-1}$ or $Jmol^{-1}$)
i	Imaginary number = $-1^{0.5}$
J	Flux ($mgm^{-2}min^{-1}$)
J_C	Concentration flux ($mgL^{-1}min^{-1}$)
K	Association constant (M^{-1})
KI	Intrinsic association constant (M^{-1})
k	Spring constant of the spring (Nm^{-1})
k_a	Association rate ($M^{-1}s^{-1}$)
k_d	Dissociation rate (s^{-1})
l	Length of unstretched spring (m)
l	Unit length along the polymer backbone (m)
M	Molecular mass of solute ($gmol^{-1}$)
M_D	Mass of dye (g)
m	Mass (kg)
$\overline{M_c}$	Number average molecular mass of the polymer chain between cross-links ($gmol^{-1}$)
$\overline{M_n}$	Number average molecular mass of the polymer chain ($gmol^{-1}$)
M_r	Molecular mass of repeat unit ($gmol^{-1}$)
$[M]_i$	Concentration of free lectin (conA) (M)
$[MX]_i$	Concentration of conA/dextran complex (M)
$[MXX]_I$	Concentration of conA/dextran/dextran complex (M)
$[M_{TOT}]$	Total conA sites, bound and unbound (M)
n_s	Stoichiometric coefficient
n	Number of data points
n_p	Number of parameters
Q	Swelling ratio
Q_i	Total energy released (cal or J)
dQ_i	Energy change over one injection (cal or J)
r	Modulus of complex number

r	Hydrodynamic radius of the solute (m)
R	Universal gas constant = 1.986 $calmol^{-1}K^{-1}$ / 8.314 $JK^{-1}mol^{-1}$
R	SPR signal at time t (RU) – equivalent to $[MX]$
R_i	Refractive index effect due to conA in solution (RU M^{-1})
R_{max}	Maximum dextran binding capacity (RU) – equivalent to $[X_{TOT}]$
ΔS	Entropic change ($calmol^{-1}K^{-1}$ or $Jmol^{-1}K^{-1}$)
SR	Swelling Ratio
t	Time (s)
T	Temperature (K)
V_C	Volume of sample cell (L)
V_{inj}	Volume of injection i (L)
$\bar{v}$	Partial specific volume of the polymer
V_g	Volume of gel (ml)
V_l	Volume of liquid (ml)
V_{tot}	Total volume (ml)
V	Volume of receiving side (m^3)
V_1	Molar volume of water (m^3g^{-1})
$v_{2,r}$	Polymer fraction of the gel after gel formation (gg^{-1})
$v_{2,s}$	Polymer fraction of the gel at equilibrium swelling (gg^{-1})
$x(t)$	Displacement from equilibrium position (m)
$[X]_i$	Free dextran binding ligands at injection, i (M)
$[X_{TOT}]$	Total dextran ligands, bound and unbound (M)
Y	Ratio of the two binding populations, $[X_1]$ and $[X_2]$
$y(t)$	Displacement from baseline (m)
z	Complex number
γ^*	Complex shear strain
γ_0	Peak shear strain
$\dot{\gamma}$	Shear strain rate (s^{-1})
δ	Phase Angle (^{o})
δ_G	Thickness of hydrogel (m)
η	Viscosity (Pas)
θ	Argument of complex number

λ	LDE factor (s^{-1})
ξ	Mesh size (m)
Π	Osmotic pressure (Pa)
σ^*	Complex shear stress (Pa)
σ_0	Peak shear stress (Pa)
$\dot{\sigma}$	Shear stress rate (Pas^{-1})
τ_m	Time constant = η/G (s)
χ^2	Size of error (chi^2)
χ_1	Flory polymer-solvent interaction parameter
ω	Frequency of oscillation (Hz)
ω_n	Natural frequency (s^{-1})

Introduction

Drug delivery is traditionally performed as single point introductions of the desired compound, be this through injection or ingestion. Many of these drugs are now being formulated so that they are released slowly into the body over a period of time, rather than the sudden increase followed by a long tail-off period associated with single point introductions. The concept of responsive polymers and hydrogels is that they can actually respond in real time to the needs of the patient without any user or doctor input required, much in the same way as the human body does naturally.

The main focus of this work is to investigate hydrogels incorporating concanavalin A and dextran which potentially could be used to supply insulin to a patient with Type I Diabetes Mellitus. The rate of supply of insulin is greatly dependent upon the patient's situation; exercise undertaken, food eaten and sleep patterns are all influential, hence a need to move away from single point introductions which cannot mimic the natural response of the pancreas.

Current approaches to insulin delivery all depend upon monitoring of glucose levels by the patient, or estimating the glucose levels based on the behaviour of the patient in order to supply the correct dose. This is far from ideal.

Section One of this report contains a literature review, in which the disease Diabetes Mellitus is studied and the possible treatment types investigated. The materials used in the experimental work are then assessed for their viability and finally the approach to producing and analysing hydrogels is considered. Section Two details the materials and methods used to create the hydrogels.

The main thesis is split into two parts. Firstly, sections Three and Four detail the investigation of the dextran / concanavalin A interaction in a free situation. Secondly, sections Five, Six and Seven detail the investigation of the hydrogels.

Sections Eight and Nine evaluate the results obtained and detail possible future work.

Aims and Objectives

The aim of this work was to investigate the use of hydrogels for responsive drug delivery, with the primary consideration being for the delivery of insulin to patients with type I diabetes. Hydrogels have been produced by Zhang *et al.* from dextran and concanavalin A to respond to the presence of glucose in solution [1]. The first phase of the work in this thesis was to investigate how the molecular mass of the dextran molecule used in the hydrogel affected the interaction with concanavalin A. This was done using two specialised techniques. Firstly, isothermal titration calorimetry was used to investigate the thermodynamics of the interaction. Secondly, surface plasmon resonance was used to investigate the kinetics of the interaction.

The second phase of this work involved investigating the behaviour of the hydrogels themselves. This was done using oscillatory rheology to study the strength of the hydrogels; diffusion cell experiments were performed to investigate the rate of diffusion of protein through a hydrogel and finally the hydrogel mixture was allowed to set within UV-spectrophotometer cuvettes and the rate of swelling of the hydrogels tested.

During the course of all work, where possible experiments were conducted at physiological conditions to ensure the relevance of the data obtained to those expected from a patient.

Section 1. Literature Review

This work's primary focus is to investigate responsive hydrogels aimed at providing insulin release systems for sufferers of type I diabetes. A basic understanding of the disease is required, though the effects of insulin on the body are too numerous to be thoroughly studied here. Once the relevant aspects of the illness have been considered current treatments will be reviewed. Approaches to design and production of responsive hydrogels will be the last aspect reviewed.

Section 1.1. Diabetes Mellitus and the Role of Insulin

Section 1.1.1. Diabetes Mellitus

Diabetes (full name diabetes mellitus) is the third leading cause of death in the United States (only cancer and heart disease cause more)[2] and is estimated to affect 200 million people worldwide [3]. Diabetes is concerned with the body's ability to produce and / or use insulin and comes in two forms. Type I diabetes, or juvenile onset diabetes, is caused by the pancreas (β cells) ceasing to produce insulin. The destruction of the β cells within the pancreas is thought to be an autoimmune response, but the reasons behind it are not fully understood. Statistical evidence has been found to suggest that environmental factors have an effect, though more evidence is required [4]. Type II diabetes, or maturity onset diabetes, is believed to be caused by a problem with the insulin receptors on cells as tests have shown that the level of insulin in the body is not low [2, 3, 5, 6]. The work undertaken here is to investigate responsive polymers for treatment of type I diabetes and type II will not be considered further.

In a healthy human body, glucose levels are held at a concentration of 3.5-5.5mM with increases due to digestion being rapidly controlled. In diabetic patients, the aim is to maintain the level at 4-8mM [5, 7]. Concentrations outside of this range for a long period can be harmful, particularly in the brain for which glucose is the primary fuel. When the level of glucose in the blood gets too low (hypoglycaemia) the brain will become starved of glucose and the patient can become comatose. In the long term, hypoglycaemia and hyperglycaemia (levels of glucose too high) can cause a range of problems. The symptoms are mainly caused by the effect of the fluctuating glucose level on the blood vessels.

Damage to the retina (retinopathy – developed by 30% of patients [3]), to the glomerulus in the kidneys (nephropathy – 20-30% incidence for type I sufferers [3]) and damage to the nerves in the extremities (peripheral neuropathy - incidence widely affected by period of time with the disease and ability to manage glycaemic levels) and the circulatory system nerves (autonomic neuropathy) are all caused by damage to the microvascular blood vessels. Damage to the macrovascular blood vessels can lead to coronary heart disease and atherosclerosis (heart disease being the most common cause of death in type II sufferers and is also prevalent in type I sufferers [3]) [2, 3, 5, 6, 8].

Section 1.1.2. Insulin

Under normal physiological conditions there are several hormones which regulate glucose homeostasis. Insulin, produced in the β islets of the pancreas, is a polypeptide hormone of approximately 5800 Daltons. It facilitates the reduction in blood-glucose levels by activating the production of glycogen, though it also stimulates, amongst other functions, lipid and protein synthesis. Increasing the level of glucose in the body is facilitated by several hormones; glucagon, adrenaline, cortisol and growth hormone. [3]

Glucose not used directly by the body for metabolic purposes is stored as glycogen, primarily in the skeletal muscle and the liver. It consists of long chains of α(1-4) linked glucose molecules with α(1-6) branches every 8 to 12 glucose residues (see Section 1.4 for details) [9].

Insulin does not directly interact with glucose; it binds to surface receptors and stimulates glucose transport, glycogen synthesis, lipid synthesis, protein synthesis, potassium ion entry to cells and sodium ion retention in renal tubes. It also inhibits gluconeogenesis (glucose production from C_3 non-hexose precursors), glycogenolysis (the breakdown of glycogen), lipolysis and proteolysis (the breakdown of fats and proteins respectively). [3] Ultimately, insulin is the only known control mechanism used by the body to reduce glucose concentration.

When there is an excess of glucose in the body, the production of proinsulin is triggered. This is a protein consisting of a chain of amino acids that can be considered as three

sections, A, B and C (see Figure 1-1 below). Proinsulin forms a structure in which sections A and B can bind together via two disulphide links. The C chain is then proteolytically excised from A and B, which remain bound together as the functional version of insulin [2].

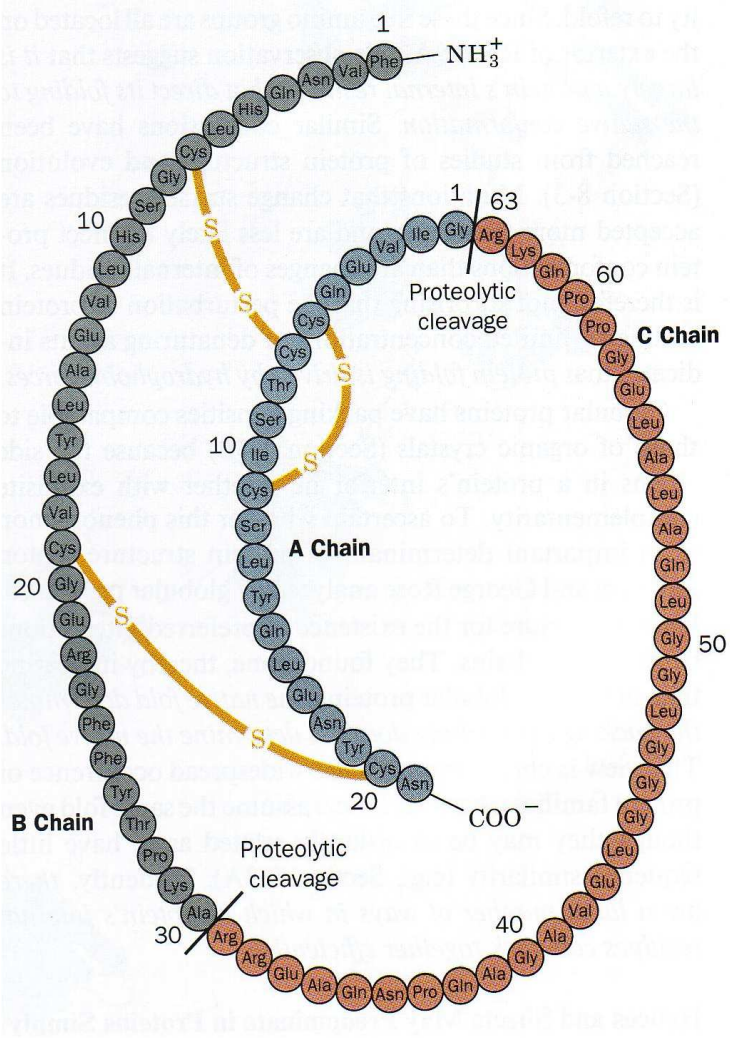

Figure 1-1 Diagram of proinsulin molecule.

Once the disulphide bridges are formed, the C chain (in brown) is proteolytically cleaved from the A and B chains (in blue) to leave the functional insulin molecule (Taken from [2], p.193).

Section 1.1.3. Treatment

For people with type 1 diabetes the approach to regulate glucose levels that most patients currently use is regular injection of insulin, though there are other options under investigation. In order for any treatment to work there must be either measurement or

estimation of the glucose concentration in the body so that the correct dose can be administered. They must also overcome the problem of insulin having a short biological half-life: only 3-4 minutes in the circulatory system [10].

Section 1.1.3.1. Methods for Treating Diabetes

There are many ways of treating diabetes, with individual patients having to find what is best suited to their condition and their desired lifestyle. As the disease progresses it is often necessary to alter the treatment to reflect changes in the condition.

The best way to avoid complications arising from diabetes is to maintain the correct level of glucose in the blood and brain. Keeping a regular and sensible diet is a major step, particularly the reduction of simple sugars (sugar in tea etc) which are very rapidly absorbed and thus can cause sudden changes in the blood-glucose levels. Exercise is another way of helping control the blood-glucose levels by metabolising the glucose for energy. Hypoglycaemia may be a problem though and the first few days of each exercise should be monitored to see how the individual patient responds. [3, 5, 8]

For the majority of type I sufferers, dietary control is not enough to completely control glycaemic levels. There is therefore a need to control the blood-glucose levels, primarily through the injection of insulin. There are several analogues of insulin available for injection, based on whether it is desired to be fast or slow acting in the body. The rate of absorption of the injected material is also affected by other factors. It is known that injections into the abdomen are absorbed faster than those into the arm, which are in turn more rapid than those into the thigh, though each of these is also dependant upon any exercise undertaken as heat generated in a moving limb can alter the absorbance rates [3, 5, 8].

As well as subcutaneous injections, peritoneal, intranasal, gastrointestinal and pulmonary routes have been investigated for the administration of insulin. The peritoneal route (the peritoneum is the sack which contains the abdominal internal organs) is a similar method to peritoneal dialysis. The peritoneum can be filled with an insulin solution, its large surface area enables uptake to the circulatory system. Tests have shown that this approach can help reduce severe hypoglycaemic episodes, but delivery time is much greater than for

subcutaneous injections [11]. The intranasal route is an idea based on the large surface area available in the nose and the fact that no needles are required, unlike the subcutaneous or peritoneal routes [12]. The primary obstacle to overcome in the preparation of an intranasal delivery system is the nose's ability to recognise and expel foreign matter. The insulin must be able to be absorbed rapidly enough to overcome this, whilst not providing too great a peak in concentrations of insulin in the blood. The gastrointestinal approach to insulin delivery is not easy. Insulin is broken down in the gut and so must be transported past the stomach before release. This can be done with pH sensitive gels (Section 1.2.2), but initial studies have not been successful. Inhalation studies using preprandial human insulin inhalation powder (HIIP), have produced results which suggest it can be as effective as subcutaneously injected insulin [13, 14].

Section 1.1.3.2. Methods for 'Curing' Diabetes

Effective treatment of diabetes, though desirable, is not the whole story. Ideally it should be possible to remove the necessity of external insulin administration altogether. This can be done on a limited basis by pancreas transplantation from organ donors, but this has all the usual complications of rejection associated with organ transplants and there can be additional complications with the kidneys [3]. A number of institutions have tried transplants of just the β islets from various sources, but these have had limited success – the longest recorded duration of a patient not requiring insulin treatment was less than six years [3]. One of the major problems with β islet transplantation is that they make up ≤ 2% of the cells within the donor pancreas [15]. Work is being performed to try and improve this, but is still not clinically viable [15]. Gene therapy is also being investigated, primarily by altering hepatocytes from the patient themselves to produce and secrete insulin [3].

In between approaches to treatments for diabetes and 'cures' for diabetes there is the artificial pancreas approach. This is where a device is produced which behaves in the same way as the β islets, recognising the presence of glucose and proportionally releasing insulin, but without the risk of rejection and other complications that arise through transplantation of actual pancreas or β islet tissue. The primary focus of the work performed thus far, and the main focus of this thesis, is hydrogels. These are polymeric membranes which are capable of swelling, and therefore increasing porosity, when in the presence of a variety of stimuli [16]. This is discussed further in Section 1.2.

Section 1.1.3.3. Methods for Blood-Glucose Concentration Measurement or Estimation

Insulin treatment must be administered carefully as under- or overdose can lead to hyper-or hypoglycaemia respectively, both of which have health complications (as discussed in Section 1.1.1). The obvious course of action is to measure the blood-glucose level so that the amount of insulin required can be calculated. This can, however, be inconvenient and can also be unpleasant for the patient as the most common approach involves a pinprick to a finger [8]. There is also a need to keep a detailed record and to fully understand how and how fast the insulin will affect the blood-glucose level, else there will be very little control and the long-term complications will still arise.

Blood-glucose monitoring is also possible by monitoring the amount of glucose or ketones in the patient's urine. There is a threshold glucose level, over which damage to the kidneys occurs. There is evidence that some drugs including aspirin, paracetamol, iodine and dopamine can cause false readings in the tests performed on the patient's urine, so care must be taken [8].

Non-invasive techniques are being investigated to remove the need for a blood sample. Infra-red spectroscopy through the skin has been investigated, but so far the signal to noise ratio through the skin is too great [11]. Reverse iontophoresis has also been investigated, the concept being that the electrical current applied to the skin draws through salts, which in turn draw through water which contains glucose [11]. Accurate calibration is essential for this process and levels of perspiration and thickness of skin can have very noticeable effects on the results.

Due to the inconvenient nature of testing, and the fact that a dozen tests per day is still not frequent enough due to the fluctuations that can occur in the body, responsive hydrogels that continuously deliver insulin based on glucose levels in the patient are highly attractive.

Section 1.2. Responsive Polymers - Hydrogels

There are many stimuli with which responsive polymers can be made to react, with each having specific advantages and disadvantages. The polymers that are used tend to be classified as hydrogels [16-20]. At a conference for hydrogel research in the 1970s, B.D.

Ratner suggested, "A hydrogel can be defined as a polymeric material which exhibits the ability to swell in water and retain a significant fraction (e.g. >20%) of water within its structure, but which will not dissolve in water." [21]

The swelling associated with a hydrogel is normally designed such that the 'pores' between the polymer strands increase in size, thus allowing diffusion of an entrapped molecule. In the case of the responsive hydrogels that are reviewed here, the general concept is that when the relevant stimulus is present, the gel is allowed to swell, thus releasing the drug to be delivered. Ideally, these gels will react to release insulin, either by directly removing bonds holding the insulin to the hydrogel, or by increasing the permeability of insulin through the hydrogel.

Section 1.2.1. Temperature Sensitive Hydrogels

Temperature based changes in the swelling of a polymer are reasonably simple to achieve. However, hydrogels designed for insulin release must operate within the human body, with a base temperature of 37^{o}C and with only very small changes acceptable. The majority of hydrogels that have been developed to react to temperature changes require large (~10^{o}C) changes for any significant changes in swelling to occur, though some have been made to work over a temperature change of only 2^{o}C [22-24].

Section 1.2.2. pH Sensitive Hydrogels

Hydrogels which are responsive to pH are also relatively simple to achieve, Akala *et al.* [25] have developed pH sensitive hydrogels aimed at being stable in the acidic conditions of the stomach, and which then start to release the drug in the more pH neutral conditions of the colon. However, as with the temperature sensitive gels, the pH changes within the human body (outside of the gastro-intestinal tract) are tiny, based around a core value of pH 7.4 [7].

There is the possibility of using a secondary compound to produce a localised pH change which would allow the required change within the hydrogel. Several different approaches have been attempted using glucose oxidase (GOD) within the hydrogel and glucose as the trigger. The overall concept is that in the presence of glucose, the glucose oxidase catalyses the production of gluconic acid, thus lowering the pH of the surrounding environment. It

has been demonstrated that GOD can be used to both increase and decrease the swelling of hydrogels, depending upon the backbone utilised [26-30]. In the case of an increase in swelling in the presence of glucose, the associated increase in porosity allows insulin to permeate through; where shrinkage occurs the insulin is squeezed out within the fluid expelled by the contracting hydrogel.

$$glucose + O_2 + H_2O \xrightarrow{GOD} gluconic\ acid + H_2O_2 \qquad \textbf{Equation 1-1}$$

Kim *et al.* have also demonstrated that liposomes infused with GOD can respond to differing glucose concentrations, the pH change causing destabilisation of the outer membrane [10].

The primary problem with using GOD is that the by-product of the conversion of glucose to gluconic acid is hydrogen peroxide. The bacterium that produces GOD, *Aspergillus niger*, also produces a peroxidase to remove the hydrogen peroxide. This would need to be included in any implant as hydrogen peroxide is very harmful inside the human body and also leads to rapid inactivation of the GOD which produces it. Oxygen is also a limiting factor of this reaction making it possible for the presence of glucose to not be enough to trigger the response.

Section 1.2.3. Antigen – Antibody

Miyata *et al.* [31, 32] have proposed hydrogels which contain antibodies and immobilised antigens. The concept is that in the presence of free antigen, *i.e.* when the patient is ill, the antibody-antigen binding within the gel is displaced allowing the natural swelling effect to take place, releasing the relevant molecule. There are however no known antigen-antibody reactions relevant to type I diabetes. Similar approaches do exist for insulin, though, and are further examined in Section 1.2.4 to Section 1.2.6.

Section 1.2.4. Glucose Sensitive Hydrogels – Phenylboronic Acid

Phenylboronic acid (PBA) has been used to produce two types of hydrogel. Shiino *et al.* have produced a hydrogel in which the PBA binds to gluconated insulin (G-ins) [33, 34]. When glucose is then introduced it displaces the binding between the PBA and the glucose

moiety of the G-ins, thus releasing the G-ins (Figure 1-2). However this only occurs satisfactorily at pH 8.4, and is thus not suitable for direct inclusion in the body (human physiological pH = 7.4 [7]).

PBA hydrogels have also been developed such that the PBA binding is to a backbone within the hydrogel structure and the insulin is free within the hydrogel. When glucose is present it disrupts the binding between the PBA and the backbone, increasing the porosity of the hydrogel thus allowing the release of the insulin [35-37]. Both of these systems work most effectively at pH values above that desired by human physiology, though it is possible to reduce this by altering the amine groups present.

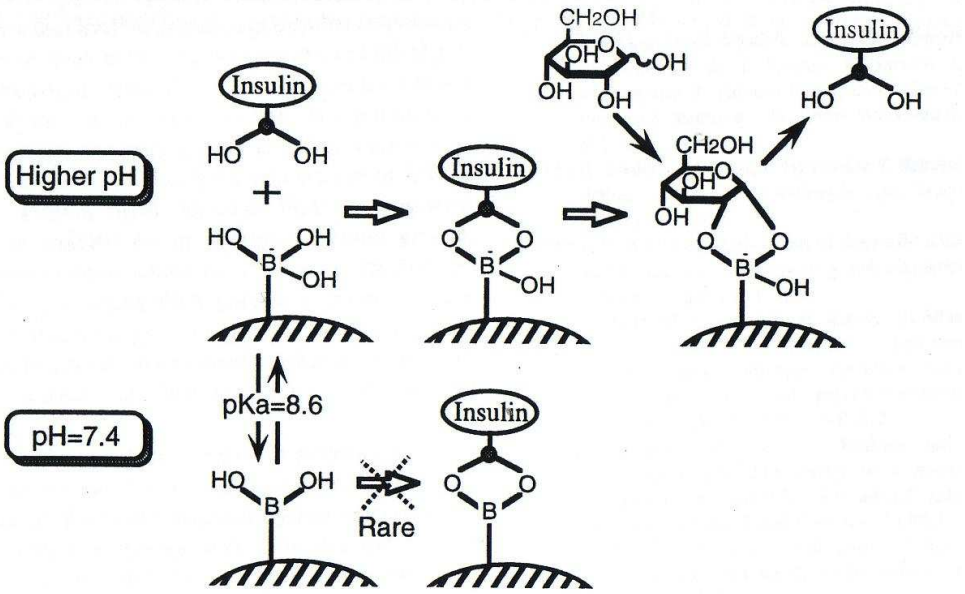

Figure 1-2 Depiction of the binding of insulin to a charged Boronic acid group and its disruption by free glucose (Taken from [33]).

Section 1.2.5. Glucose Sensitive Hydrogels – Concanavalin A

Concanavalin A (conA) is a lectin produced by jack beans. It is known to bind some mono- and polysaccharides including glucose and dextran [38] (see Section 1.3 for details). Several groups have performed work using conA, either creating hydrogels with dextran or directly binding modified insulin to the lectin.

Two groups, led by Obaidat [39, 40] and by Taylor and Tanna [41-45], have produced hydrogels using Acrylamide-allyl glucose copolymer (Obaidat) and glycogen / carbopols /

dextran (Taylor) to supply the binding backbone for the conA. In all cases, the binding between the glucose moiety and the conA is the only structure present. When glucose is introduced into the gel the entire structure collapses (assuming sufficient glucose). This sol-gel response allows proteins, such as insulin, to permeate through. Both systems have been shown to be reversible, which is essential for diabetes patients. However, both will require a secondary membrane which will allow the insulin through into the body, but prevent conA from being released as it is required to reform the gel and because it is mitogenic (see Section 1.3 for details).

A more direct approach was taken by Brownlee *et al.* [46], Makino *et al.* [47] and Kim *et al.* [48-51], whereby the insulin was glycosylated (G-ins) and bound directly to the conA. The presence of glucose therefore directly unbound the insulin which was then capable of permeating through the microporous capsule in which the conA mixture was held.

Tang and Zhang *et al.* [1, 52] have developed a conA-dextran system in which the conA is covalently bonded to a cross-linked dextran backbone. This results in the gel not being reduced to a solution in the presence of glucose, but which allows swelling and therefore an increase in porosity. These gels have been shown to be reversible and to give varying levels of permeability depending upon the concentration of the glucose.

Ballerstadt *et al.* [53] have also used conA with dextran to try to devise a glucose sensor based on the large viscosity differences between conA-dextran and conA-dextran-glucose solutions.

Section 1.2.6. Other Responsive Polymers and their Stimuli

Section 1.2.6.1. Glucose Oxidase

Ito *et al.* have used glucose oxidase, in a similar manner to Section 1.2.2, to control the release of insulin [54, 55]. In their approach, the glucose oxidase (GOD) is bound to the surface of a membrane so that it is near the pores through the membrane. The pores themselves are filled with poly(acrylic acid) such that the pore is blocked by reduced carboxylic acid groups, all of which repel each other. When glucose is present, it is oxidised by the GOD, producing gluconic acid, which in turn protonates the poly(acrylic

acid) (see Equation 1-1). When protonated, the repulsion forces within the poly(acrylic acid) are no longer present, resulting in their collapse and the unblocking of the pores. It is suggested that this system responds more rapidly than hydrogels that use GOD, but there is no information as to how long the poly(acrylic acid) would survive being protonated and then deprotonated, as would happen continuously in a patient. There is also an issue with the GOD reaction with glucose as hydrogen peroxide is one of the by-products. Ito *et al.* have also used GOD bound directly to insulin via a disulphide bridge, the bridge is then severed when glucose is catalysed to gluconic acid by GOD [56].

Cartier *et al.* have also produced membranes with carboxylic acid groups acting as the barrier. They found that the basal transport rate was too high and no follow-up work has been published [57].

Section 1.2.6.2. Glucose Dehydrogenase

Glucose dehydrogenase (GDH) has been used to facilitate the cleavage of covalently bound insulin from a backbone by supplying an electron [58]. GDH, NAD (Nicotinamide adenine dinucleotide), FAD (Flavin adenine dinucleotide) and insulin are all covalently bound to a backbone. The GDH reacts with glucose to form gluconolactone. The electron taken by the GDH is passed to NAD, on to FAD and on to the disulphide bridge holding the insulin to the backbone. The disulphide bridge breaks when the electron reaches it, releasing the insulin. Once the electron has been passed on the GDH, NAD and FAD are all ready to perform the action again. It is also possible to perform this with the GDH in solution, rather than bound to the backbone, but this would then result in a need to prevent its release into the body.

Section 1.2.7. Mannose Binding Lectin (MBL)

Human mannose binding lectin is a potential replacement for conA in hydrogel systems. It is known to bind to glucose as well as mannose and will not have the toxic problems of conA because it is from a human source [59-61]. MBL is also being investigated for other therapeutic applications which would aid its approval for *in vivo* use.

Section 1.2.8. Summary of Current Thinking on Hydrogels

Section 1.2.1 to Section 1.2.7 shows that there have been many attempts to find hydrogels that can be used in the treatment of type 1 diabetes. All have specific advantages and disadvantages associated with them. These are summarised in Table 1-1.

Table 1-1 Summary of advantages and disadvantages of the methods being investigated for treatment of type I diabetes.

Process	Advantages	Disadvantages	Ref.
pH sensitive, GOD	Correct pH range can be targeted	H_2O_2 is a by-product, requires oxygen	[26-30]
PBA	Useable with normal or glycosylated insulin, reversible	Only active at pH >8.4	[33-37]
ConA, Sol-Gel	Reversible, glucose is not rendered useless in reaction	Secondary membranes required to prevent leakage, conA is mitogenic	[39-45]
ConA, G-Ins	Direct release, swelling ratio not important	Secondary membranes required to prevent leakage, conA is mitogenic	[46-51]
ConA, cross-linked	No membrane required, reversible, glucose is not rendered useless in reaction	ConA is mitogenic	[52]
GOD, PAA	Diffusion rate controlled by membrane	No reversibility data, requires oxygen, H_2O_2 is a by-product	[54, 55]
GDH, NAD/FAD	Direct release, swelling ratio not important	Requires three components to work	[58]
MBL	From human source, is not mitogenic	No work yet performed	[59-61]

Section 1.3. Lectins

The hydrogels that are to be developed in this work are to be based around a lectin (concanavalin A (conA)) – dextran system. The reasons for using dextran are discussed in Section 1.4.

Lectins are proteins produced by a range of organisms to bind specifically to one or more types of carbohydrate. They were first found in 1888 owing to their ability to agglutinate erythrocytes, and it was not until many years later that it was discovered that the binding was taking place with saccharide moieties on the surface of the erythrocytes [62-64]. ConA is a lectin produced by the Jack Bean (*Canavalia ensiformis*) and is probably the most investigated lectin in science [38, 65-71]. When used in a hydrogel, conA is capable of reversibly binding to any glucose or mannose moiety present without chemically altering itself or the compound to which it is bound.

Under physiological conditions (pH7.4 [7]) conA exists as a tetramer, each monomer being a 25500 Dalton, 237 amino acid residue molecule. At lower pH it exists as a dimer and at a pH less than 4 it exists as a monomer [72]. The advantage of the tetrameric form is that it will generate a more highly cross-linked hydrogel when in the presence of dextran. The dextrans used have the ability to bind the terminus of every chain (non-anomeric end plus branches) to each monomer unit. The active form of a conA monomer contains three binding sites, two for metal ions, Mn^{2+} and Ca^{2+}, as well as a third for the saccharide. The manganese ion can be replaced by other transition metal ions, but one plus the calcium ion are needed before the saccharide binding can occur [62, 66].

The primary problem with conA is that it is mitogenic and capable of agglutinating erythrocytes [62]. Given these problems, it is not feasible to implant conA directly into the patient. Ballerstadt *et al.* have shown that the amount of conA used for a sensor would not be hazardous, but the mass of conA in a hydrogel would be greater than that of a sensor [73]. Even with cross-linking to lock the conA into a gel or membranes to block its release, it is an unsuitable choice. The solution to this is to use a protein from a human source which should have no toxic effects when implanted into a patient. Human Mannose Binding Lectin (MBL) would make a suitable candidate though currently it is not

commercially available, it must be purified from serum [74]. Therefore, this work will be based on developing the concept of the hydrogel using conA such that future work on MBL will have a base on which to build [60].

Section 1.4. Mono- and Polysaccharides

In the work for this thesis it has been decided to use dextran as the backbone to the hydrogel. Dextran is a primarily α(1-6) glucose polymer with α(1-3) and occasional α(1-4) branches also present depending on the bacteria used for production [9]. Clinically, it is produced primarily by *Leuconostoc mesenteroides*, though there are other sources. In theory, most glucose polymers would provide the necessary binding sites (chemical conformation allowing), but dextran has been deemed to offer the most suitable option for the reasons discussed below.

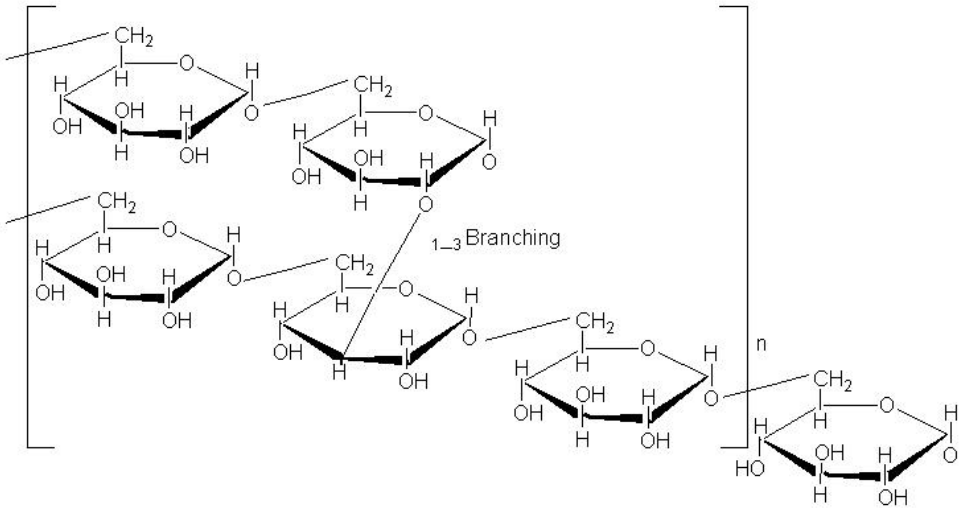

Figure 1-3 Structure of a dextran molecule with an α(1-3)- branch.

It is also possible for dextran to have α(1-4)- branches.

There are several other possible polymers: amylose (solely α(1-4)), amylopectin (α(1-4) with α(1-6) branches ~every 24-30 residues), cellulose (β(1-4)), glycogen (α(1-4) with α(1-6) every 8-12 residues), maltose (dimer of glucose) and maltotriose (a trimer of glucose) [9]. Amylose and amylopectin are collectively known as starch (a storage molecule for glucose within plants) and cellulose is the structural material in plants. None of these is particularly soluble in water, particularly at low (physiological) temperatures,

making them impractical for this application. Glycogen, the animal equivalent of starch, has been used to make hydrogels with conA [41], but is not as soluble as dextran. Maltose and maltotriose would be too short to provide good cross-linking between conA molecules.

Therefore dextran was the polymer of choice because it is very soluble in water at physiological temperatures, can be cheaply obtained at a variety of molecular masses and has been approved for use *in vivo*. Dextran can be obtained in varying molecular masses, from 6000 to 2,000,000 Daltons. Much work has been done to try and identify the branching ratio of these products based on the bacterial strain used to grow the dextran [75-81] and the operating conditions of the fermentation reactor [82]. Though the majority of the work, performed in the 1950s and 1960s, suggests that the majority of bacteria (and in particular the strain used to produce the dextran as used here, supplied by Sigma Aldrich) produce branching ratios of 5% (1 branch per 20 glucose residues) there is a suggestion in Kim's work [82] that this is by no means guaranteed.

Without knowing the branching ratio of the dextrans, the effective ligand density is unknown and so it will not be possible to accurately obtain the binding kinetics and equilibrium constants for the system. Therefore part of the study reported here concerns the determination of branching ratios for the dextran preparations used.

Much work has been performed by Dam *et al.* [68, 83-85] which shows that, as the number of mannotriose moieties on a dendrimer increase, the association constant of binding to conA also increases. It will therefore be interesting to investigate the affect of varying molecular mass of the dextran to see if a similar pattern exists.

Section 1.5. ConA / Dextran Interaction Characterisation

The preceding sections of this literature review have suggested that the most attractive materials to make glucose-responsive hydrogels are dextran and conA. The conA used will only have concentration as a variable (i.e. site density). The dextran, however, can be obtained with varying molecular masses and branching densities allowing gel density and ligand concentration to be varied independently within the gels.

In order for the gel to work correctly in a human, the gel must respond at physiological blood-glucose levels and must swell to release the necessary amount of insulin for the level of glucose [3, 5, 7, 8]. Therefore it is necessary to characterise how the size of the dextran molecule affects the binding with the conA.

The reversible binding of a molecule to a lectin is characterised primarily by the association constant (K_a) and the enthalpic change (ΔH) of the reaction. Linked with these, there is also the entropic change of reaction (ΔS) and the rates of association and dissociation (k_a and k_d respectively). Each of these parameters are linked, based on the thermodynamics of the reaction:

$$K_a = \frac{k_a}{k_d} \qquad \textbf{Equation 1-2}$$

$$\Delta G = -RT \ln K_a = \Delta H - T\Delta S \qquad \textbf{Equation 1-3}$$

Where R is the universal gas constant (8.314 $Jmol^{-1}K^{-1}$) and T is the temperature of the reaction (K).

For a reaction to proceed spontaneously, the Gibbs free energy change (ΔG) must be negative, thus implying that the association rate must be greater than the dissociation rate.

There are several commercially available instruments which can be used to follow these binding interactions. Two which will be used here are the MicroCal™ isothermal titration calorimeter (ITC) and the Biacore® X which utilises surface plasmon resonance (SPR) to quantify binding where one component is immobilised to a sensor chip.

Section 1.5.1. Isothermal Titration Calorimetry (ITC)

The MicroCal™ ITC is capable of providing the data needed to evaluate Equation 1-3. The machine consists of an active cell and a reference cell. One of the two components of the reaction, typically the protein, is placed in the active cell at the desired concentration. Over a given time period the second component is injected into the cell and the reaction proceeds. The cell itself is held within a Peltier element which is capable of adding or removing known amounts of energy depending upon the endo- or exothermic nature of the

reaction respectively to maintain the cell at a constant temperature (hence isothermal). Once the series of injections is complete, a profile of the energy released for each given amount of injectant is produced:

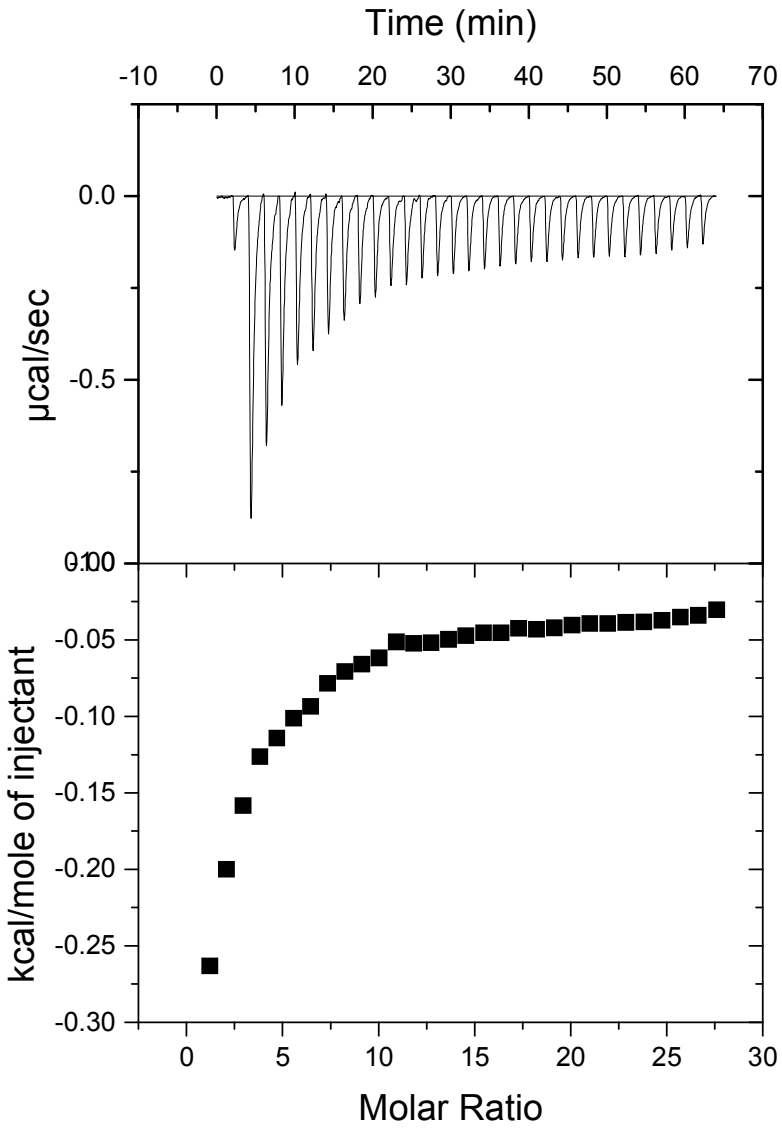

Figure 1-4 The energy release profile of 0.1mM conA when titrated with 24.77mM 2000kD dextran

(Concentration is of branch ends assuming 1 branch per 20 glucose residues)

The software supplied with the machine is capable of matching a curve to the data based on a stipulated number of binding sites and the relevant concentrations. This matched curve

provides values for the association constant (K_a) and the enthalpic change (ΔH). From these two parameters the entropic change (ΔS) can be inferred.

Section 1.5.2. Surface Plasmon Resonance (SPR)

The Biacore® X utilises surface plasmon resonance (SPR) to obtain information about the binding kinetics of a system. Within the machine a chip with a gold surface can be mounted which has dextran bound to one face (other types of chip are available). It is recommended that the protein, in this case conA, is covalently bound to the dextran using appropriate chemistry and any remaining dextran chains deactivated. The ligand is then passed over the surface, allowing association to take place. After an allocated time the liquid passing over the cell is changed from buffer with ligand to just buffer, enabling the dissociation to be monitored in a similar manner to the association. The resulting mass of material affects the surface of the gold producing the plasmons from a beam of light incident upon the opposite surface (see Section 4.1.1), it is then possible for the supplied software to produce values for the association and dissociation rates of the reaction. These should then coincide, using Equation 1-2, with the measured values from the ITC.

Section 1.6. Hydrogel Production Methods

Section 1.6.1. Production

There are two published approaches to forming hydrogels which use lectins as one of the binding groups. Taylor and Tanna [41-44] take the sol/gel approach of mixing the lectin with the secondary material (dextran, glycogen etc.) and allowing the structure to completely disintegrate when the competing ligand (glucose) is present. However this results in the need for membranes to prevent leakage of the materials into the body of the patient. The second approach, which will be the one used in this work, is to covalently cross-link the two components together such that the competing ligand disruption only leads to an increase in swelling, rather than complete dissolution. Currently under investigation at the University of Bath is a third option whereby it has been demonstrated that low molecular mass dextran, when in solution, will irreversibly aggregate [86]. Therefore there is a possibility of entrapping lectins within these structures, thereby removing the need for chemical cross-linking and additional membranes.

Covalent cross-linking of the hydrogels has been demonstrated using two approaches. The first utilises divinyl sulphone, ethylene diamine, cyanuric chloride and triazine to create covalent bonds between dextran and conA and has been demonstrated by Tang *et al.* [52]. The second approach, used by Zhang [87], involves carboxymethylation of the dextran chains with sodium chloroacetate, the cross-linking is then achieved using 1-ethyl-(3-3-dimethylaminopropyl) carbodiimide hydrochloride (EDC) and *N*-hydroxysuccinimide (NHS). This gives a 'zero-length' bond and introduces no toxic components which makes it the preferred approach. Both of these methods create a binding site on the dextran for an amine group. It is likely that some of the reversible binding sites on the conA molecules are disrupted by the cross-linking positions. However, careful control of the degree of cross-linking should enable fine-tuning of the hydrogel so that it still works correctly.

Section 2. Materials and Methods

This section contains details of the generic materials used throughout this project. More specific information for ITC, SPR and gel synthesis can be found in the relevant sections.

Section 2.1. Materials

The dextrans used in this work were all purchased from Sigma-Aldrich (11, 17, 43, 64, 500 and 2000kD) with the exception of the 6kD dextran which was purchased from Fluka Biochemika. The D-glucose, L-glucose, maltose, concanavalin A (conA), cytochrome C (cytC), adenosine and insulin were all purchased from Sigma-Aldrich.

The following standard reagents were purchased from Sigma-Aldrich: TRIZMA base, NaN_3, $MnCl_2.4H_2O$, Na_2HPO_4, sodium chloroacetate, ethanolamine and ethylenediamine. $MgCl_2.6H_2O$, $CaCl_2.2H_2O$, NaCl, NaOH and HCl were purchased from Fisher Scientific. EDC was purchased from Alfa Aesar and NHS from Lancaster Synthesis.

Section 2.2. Buffer Solution

This work is based around using concanavalin A (conA) to bind to glucose moieties on dextran molecules. It is known that a conA monomer contains one calcium and one manganese ion and that these are needed to ensure the correct conformation of the saccharide binding site [66]. To prevent leakage from the protein these ions were included in the buffer solution that was used through the majority of this work. The complete buffer solution comprised: 20mM TRIS (TRIZMA base), 150mM sodium chloride and 0.5mM calcium chloride, magnesium chloride and manganese chloride, corrected to pH7.4. For those solutions not being frozen once prepared, 0.02wt% sodium azide was added to prevent microbial growth. The pH correction was performed using hydrochloric acid or sodium hydroxide, additional sodium and chlorine ions from the pH correction being negligible compared to the overall concentration of sodium chloride.

Section 2.3. Carboxymethyl Dextran

Carboxymethyl dextran (CM-dextran) was produced for use in the surface plasmon resonance (SPR) work and for use in the hydrogels.

The carboxymethylation process involves the addition of sodium chloroacetate to a dextran solution. The reaction is initiated by raising the pH using sodium hydroxide and by heating the solution to 60^{o}C. The length of time the reaction is allowed to proceed controls the degree of reaction. The reaction is stopped by returning the mixture to pH 7 using hydrochloric acid.

Typically: 5g of dextran, dissolved in 75ml of distilled water
5g of sodium chloroacetate is added
Reaction initiated by 25ml of 8M NaOH
Reaction allowed to proceed for 15 minutes at 60^{o}C
6M HCl added until pH 7
Solution added to 300ml absolute ethanol, resulting in precipitation, left to stand overnight
Precipitate redissolved in distilled water and exhaustively dialysed against distilled water
Dialysed solution freeze-dried for storage

Owing to the rejection characteristics of the dialysis tubing it was decided not to dialyse CM-dextran produced from the 6, 11 or 17kD dextrans. Instead the CM-dextran, once redissolved after the ethanol precipitation step, was precipitated again with a similar quantity of ethanol. This was repeated twice (for a total of three precipitations for each sample preparation) and produced a freeze-dryable solution of purity similar to the dialysed solutions.

The degree of carboxymethylation was determined by UV spectroscopy. Adenosine, a nucleoside with one amine group and no carboxylic acid groups, was bound to the CM-dextran using EDC and NHS (for chemistry see Section 4.1.1). The adenosine-CM-Dextran (ACM-dextran) was dialyzed for one day, with the water being replaced twice, and then

lyophilised. The ACM-dextran will have an absorption peak at 260nM corresponding to the heterocyclic aromatic ring structure within adenosine. Use of the Beer-Lambert law to calibrate the absorption values allowed for quantification of the adenosine and thus of the carboxylic acid groups.

Table 2-1 Degree of carboxymethylation by dextran molecular mass

RMM of Dextran	Number of glucose residues per -COOH	Number of COOH per molecule
6000	818	<0.1
11000	433	0.2
17000	64	1.1
43000	90	2.9
64000	695	0.6
500000	25	121.3
2000000	57	217.0

Section 2.4. Dextran Branching - NMR

Dextran molecules are produced as exopolysaccharides by various strains of bacteria. These have been shown to have variable rates of branching, depending upon the conditions in which the bacteria are grown [2-4]. The calculation of the branching rate was performed using ^{1}H nuclear magnetic resonance (NMR) spectroscopy. (The raw data traces can be found in Appendix 1).

Some atomic nuclei, in the right conditions, can behave like bar magnets. Under an applied magnetic field these nuclei can be aligned and excited with a radio wave. Those frequencies absorbed by the nuclei are dependent upon the surrounding molecular conditions and the energy the nucleus contains. The frequencies absorbed from the radio wave are naturally emitted by the nuclei as they 'spin down' from the higher state of excitation. These emitted radio waves are detected and can be converted into a spectrum specific to the molecule being investigated. The frequency of each nucleus is calculated in terms of an internal standard (in this case residual HOD arising from incomplete deuteration of the D_2O

solvent) and the operating frequency of the machine. This gives values in parts per million (ppm) of the applied field [88].

At room temperature, C_1 hydrogen absorption was found to partially overlap with the HOD peak. The spectra were therefore taken at an elevated temperature as this causes a shift in the spectra due to the additional energy of the nuclei. In this case this resulted in the C_1 hydrogen absorption being shifted downfield (to a greater ppm) of the HOD peak - facilitating analysis.

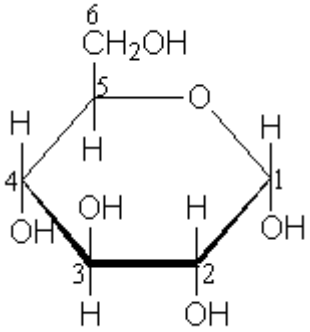

Figure 2-1 Structure of α-D-glucose molecule.

It is possible to have α(1-6) bonds (resulting in the loss of the C_1 hydroxyl and the H of the C_6 hydroxyl) of the main chain or α(1-3) bonds (resulting in the loss of the C_1 hydroxyl and the H of the C_3 hydroxyl) of the branches.

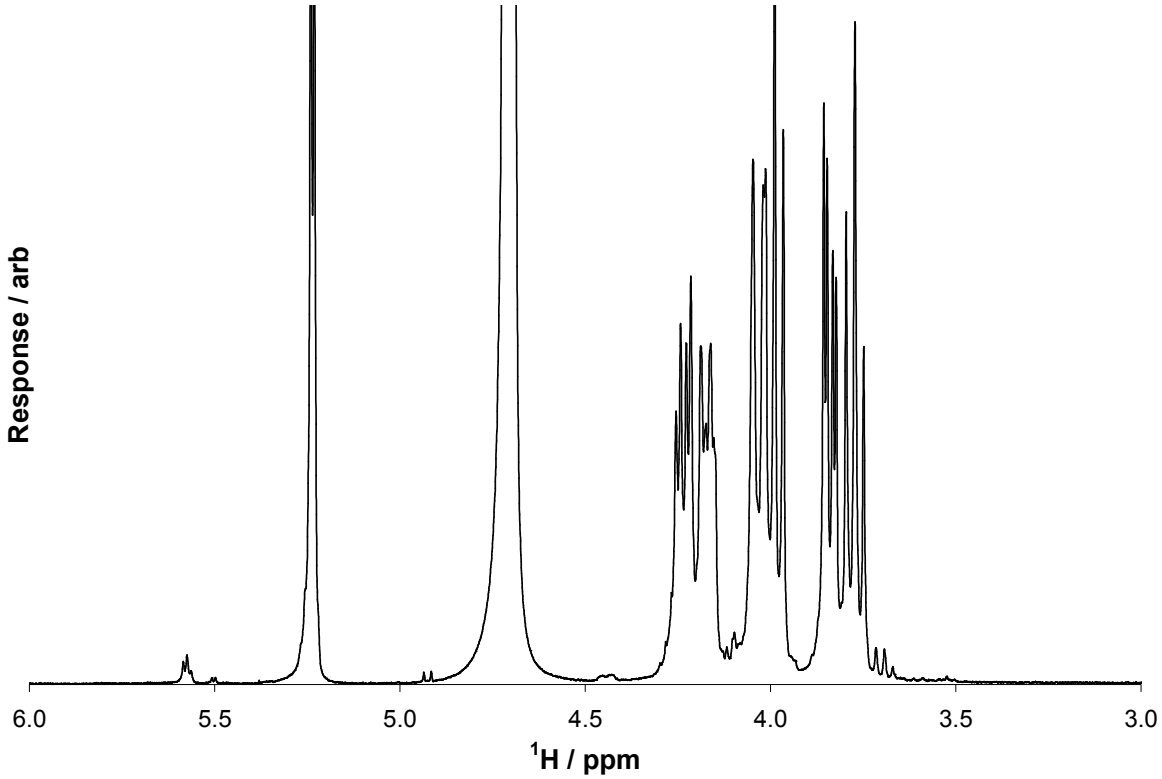

Figure 2-2 ^{1}H spectra for 17kD Dalton dextran.

Taken at 55^{o}C in a 400MHz Bruker NMR Spectrometer. The peaks between 3.5 and 4.5ppm correspond to the C_2 to C_6 hydrogen atoms. The peak at 4.75ppm is the HOD (solvent impurity) peak. Peaks from 4.8 to 5.8ppm correspond to the C_1 hydrogen atoms and these are enlarged in Figure 2-3 for clarity. [89-93]

The spectra shown in Figure 2-2 and Figure 2-3 do not show the hydrogen of the hydroxyl groups. This peak is not visible beneath the HOD solvent. The ratio of the magnitudes of the remaining peaks can be used to calculate the branching ratio. The total area of the C_2 to C_6 hydrogen peaks compared to the C_1 peaks should be 6:1. The ratio of the main chain α(1-6) groups to the branch α(1-3) will equal the branching ratio.

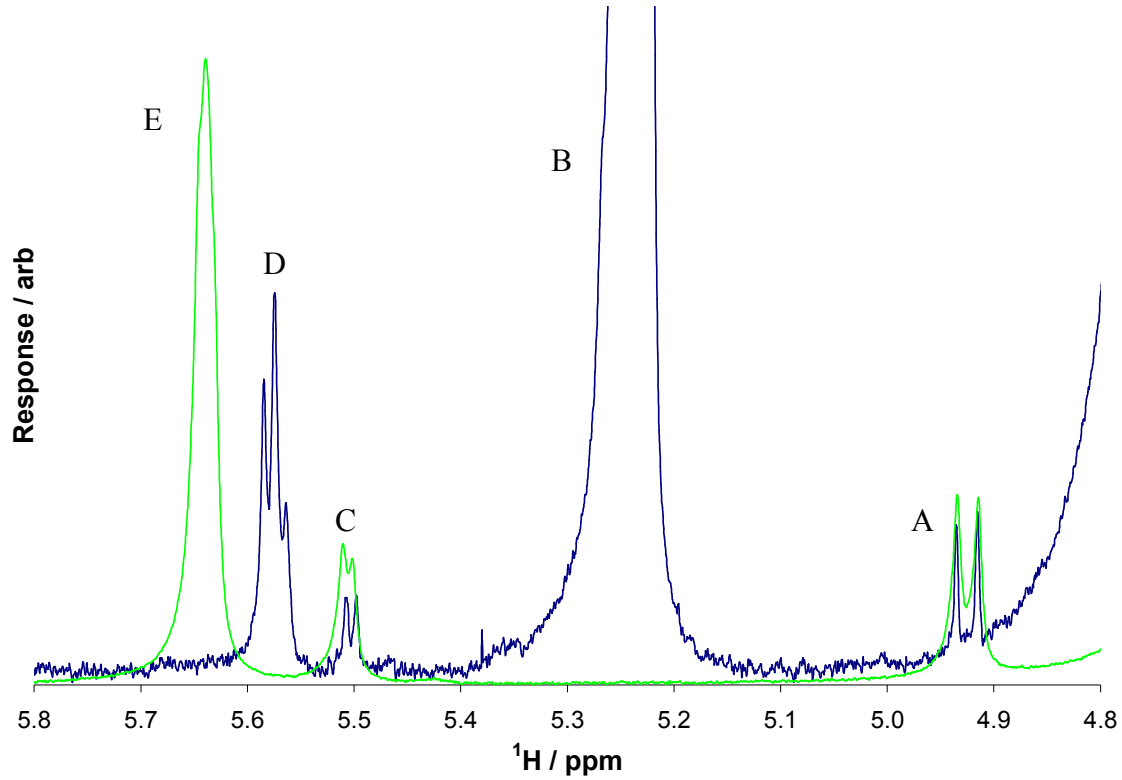

Figure 2-3 ^{1}H spectra for 17kD Dalton dextran (Blue) and maltotriose (green) taken at 55^{o}C in a 400MHz Bruker NMR Spectrometer.

Comparison of the dextran spectrum to maltotriose in Figure 2-3 enables identification of the type of branches in the dextran. The maltotriose spectrum, in green, has three peaks in the C_1 region. The doublets A and C (4.9 and 5.5ppm respectively) correspond to the β and α configurations of the reducing end C_1 [92]. The third peak, E (between 5.6 and 5.7ppm) must therefore be due to the two α(1-4) linkages in maltotriose. This is confirmed by the ratio of areas of peaks E : A+C being 2:1. For the dextran spectrum, peaks A and C are the same as those of maltotriose. Peaks B and D must therefore correspond to the linkages of the main chain and of the branches, respectively. The main chain linkages are known to be α(1-6) in dextran whilst the branches can either be α(1-3) or α(1-4), depending on the species used for production [9, 92]. The triplet, D, does not appear at the same signal as the maltotriose peak, E. Therefore, given that the maltotriose peak is known to be α(1-4), the dextran branches from this species must be α(1-3). The ratio of peak D to peak B will give the branching ratio of the dextran.

Table 2-2 Branching ratio by dextran molecular mass

RMM of Dextran	Branching ratio / %
6000	5.5
11000	3.0
17000	3.9
43000	3.9
64000	4.8
500000	4.6
2000000	4.1

Section 2.5. Dextran Summary

The branching ratio of the different dextran sizes available fluctuates around the literature value of 5%, with no noticeable trend between them. The degree of carboxymethylation showed a noticeable difference between the molecular masses. The lower mass dextrans have very few groups attached. This may be due to the smaller dextrans naturally forming insoluble beads in solution [86, 94]. The beads reduce the amount of dextran available for modification from a given dissolved mass.

Section 2.6. Hydrogel Production and Casting

All of the hydrogels were produced using the following recipe:

1g of dextran, dissolved in 4.2ml of distilled water
210mg of EDC and 30mg of NHS, dissolved in 1.5ml of distilled water
The two solutions are combined and stirred gently for 10 minutes
130mg of conA, dissolved in 3ml of buffer added to solution
Mixture poured into mould and placed in fridge to set overnight.

The dextran used was the carboxymethylated version so as to allow covalent cross-linking within the gel. The mass of the dextran was always 50% 500kD with the other 50% being one of the seven molecular masses available (6, 11, 17, 43, 64, 500 and 2000kD). This is to ensure a reasonable level of structure within the hydrogels. The moulds were made from acetate sheet. The top and bottom glass plates were covered in Parafilm to prevent adhesion to the glass. Ethanol was pipetted between the gel and Parafilm (by peeling back a corner) to separate them once the gel had set and was ready for use.

Part 1 – Investigation of Concanavalin A / Dextran Interaction

The interaction of unmodified dextran with conA was studied using two techniques: isothermal titration calorimetry (ITC) and surface plasmon resonance (SPR). This work was carried out in order to investigate the differences, if any, between the various available dextran sizes and their interaction with conA.

The ITC experiments were performed in order to identify the type of binding that occurs between the polysaccharide and the lectin and to identify any trends between the molecular mass of the dextran and the binding equilibria. This was achieved by use of an isothermal titration calorimeter.

SPR experiments were performed to investigate the kinetics of the binding between the various dextran sizes and conA molecules. This is achieved by use of an SPR machine produced by BIAcore®.

These two techniques complemented each other. The ITC work provided data on the strength of the binding and the energy released during this process. The SPR results allow quantification of the interaction kinetics.

Section 3. Isothermal Titration Calorimetry

ITC (Isothermal Titration Calorimeter) experiments were performed in a MicroCal™ VP-ITC MicroCalorimeter (MicroCal, LLC. Northampton, MA, 01060-2327, USA) which is used to evaluate the association binding constant (K), enthalpic change (ΔH) and entropic change (ΔS) of a reaction or binding interaction (see Section 1.5.1).

Section 3.1. Theory

Section 3.1.1. Isothermal Titration Calorimetry

The MicroCal™ ITC comprises two cells, one for the sample and one as a reference. These are held within a heated shield which is set to the temperature required by the user. A constant reference power is fed to the reference cell, the magnitude of which is dependent upon the amount of heat expected to be released by the interaction under investigation (in this description, it will always be assumed that the interaction in question is exothermic). The temperatures of the two cells are monitored and the difference between the two calculated. If the sample cell is of a different temperature to the reference cell, a Peltier element supplies or removes energy to equalise the temperature of the two cells.

The titrations are added to the sample cell at a set rate and volume (typically 5µl every 2 minutes). The energy evolved from the interaction results in the sample cell requiring less energy from the Peltier element to achieve the same temperature as the reference cell. Hence a trace of the energy input to the cell is produced over time with troughs corresponding to the amount of energy produced by the interaction (see Figure 3-1).

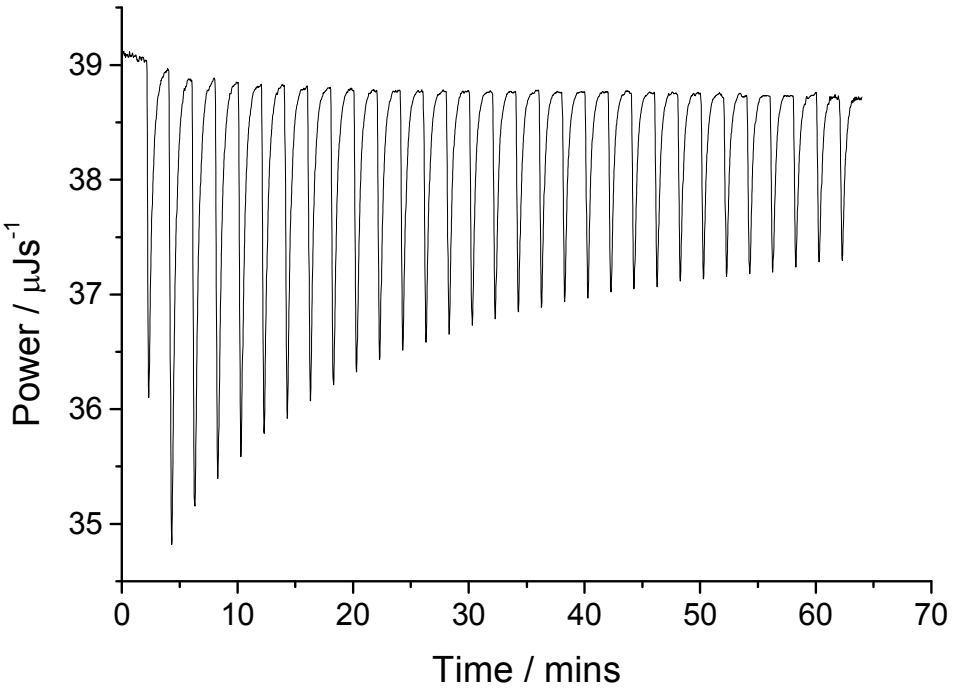

Figure 3-1 Raw Data of titration of D-glucose into conA.

Reference power set to 42μJs^{-1}. Thirty one 5μl injections, one injection every 2 minutes.

Figure 3-1 shows a series of 31 injections of D-glucose into conA. The system, once all the solutions are in place, takes approximately 20 minutes to equilibrate at the required temperature before the first injection can occur. Due to diffusion caused by the rotating syringe (ca. 400rpm) during the equilibration period the first injection is always slightly erroneous and MicroCal™ recommend removing it from subsequent analysis [95].

The baseline of the injections (at approximately 39μJ/s in this case) corresponds to the amount of energy supplied to the sample cell when there are no injections and is equivalent to the reference power supplied to the reference cell (There is a small difference due to energy from the stirrer). The injections then show the reduction in energy input due to the energy released from the molecular interactions. With each subsequent injection, fewer new interactions are formed and so less energy is released and the size of the troughs from the reference baseline decrease. The energy released per injection is calculated by integrating

the area between the curve and the reference line. The total concentration of dextran and conA (bound and unbound) can be calculated from a mass balance over the cell. It should be noted that, in order to keep the size of the sample cell constant, each injection pushes the equivalent volume of liquid out of the sample cell, resulting in a small reduction in conA concentration and a loss of energy due to the interacting species within this volume.

The quantity of conA / dextran complexes were calculated using the derivation detailed in Appendix 2. In summary, mass balances were taken across the sample cell for each component. These were then related to the experimental data using the enthalpic energy change. The binding association constant, K, and the enthalpy change, ΔH, were estimated and mathematical models (see Section 3.2.3) used iteratively to find a 'best fit', in this case a minimised chi squared value, for the data.

Section 3.1.2. Thermodynamics of the System

The enthalpic and entropic changes of the reaction are an indication of the reaction's "likelihood of occurring". The enthalpic change, ΔH, and the association constant, K, are obtained from the solving of the equations detailed in Appendix 2. They were used to determine the Gibbs free energy, ΔG, from Equation 3-1, and in turn Equation 3-2 was used to determine, ΔS:

$$\Delta G = -RT \ln K \qquad \textbf{Equation 3-1}$$

$$\Delta S = \frac{\Delta H - \Delta G}{T} \qquad \textbf{Equation 3-2}$$

The Gibbs free energy is a measure of the overall energy change of a reaction. If it has a negative value, the reaction can happen spontaneously, though there may be activation energies which need to be supplied. If the value is positive the reaction will not proceed without external energy input.

Section 3.1.3. Lectin / Saccharide Binding

In order to analyse the experimental data, the type of binding had to be considered. The ITC control package incorporates Origin™, a graphics and data analysis package, to provide a non-linear least squares fit to the appropriate binding isotherm equation. The two main options are single site and sequential site models. The single site model is based on the concept that each ligand and each binding site have the same chance of combining, irrespective of the amount of binding that has already occurred. This is the model described in detail in Appendix 2.1.

The sequential binding model is based on the concept that once one ligand has bound, a second binding to the same conA molecule is either made easier or harder (positive and negative cooperativity respectively) [96].

$$[M]_i + [X]_i \underset{k_{d1}}{\overset{k_{a1}}{\Leftrightarrow}} [MX]_i$$
$$[MX]_i + [X]_i \underset{k_{d2}}{\overset{k_{a2}}{\Leftrightarrow}} [MXX]_i$$

Equation 3-3

Figure 3-2 shows two attempts at modelling a dataset. Image A shows a Langmuir type binding, image B shows a sequential sites model. C and D are residual plots for A and B respectively.

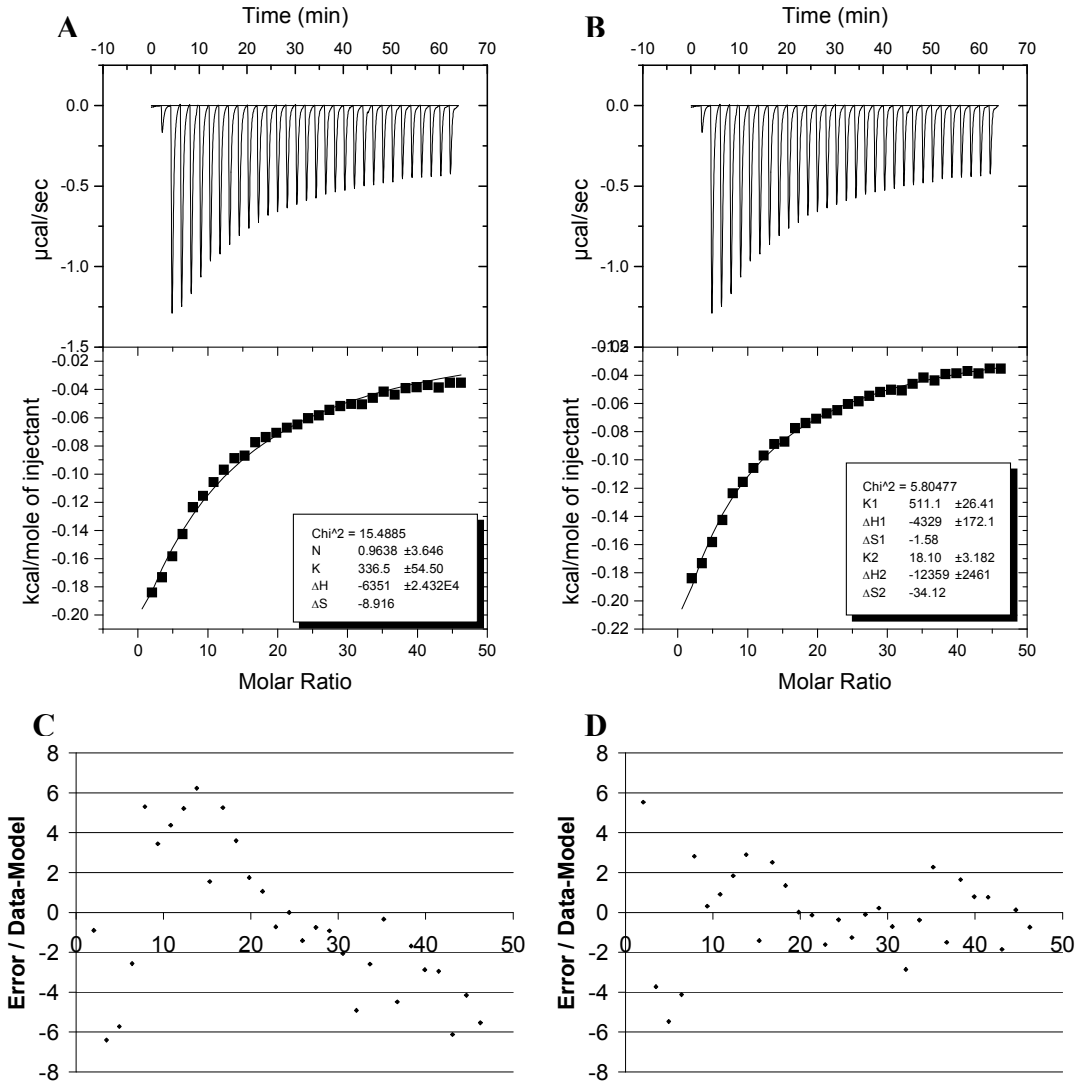

Figure 3-2 Plots A and B both represent 31 5µl injections of 11kD dextran into 0.1mM conA.

The line of best fit in figure A shows a Langmuir type binding, figure B shows a sequential sites model. Plots C and D are the residual errors (C applies to A, D applies to B) (1µCal = 4.184µJ).

It is clear from Figure 3-2 that a single site model is not ideal. The line of best fit in A (Langmuir) shows systematic deviation from the data, as confirmed in the residual plot, C. In B, where a sequential binding model was used, the corresponding residual plot, D, shows a more random residual distribution.

Section 3.1.4. Sequential Sites Mathematical Model

ConA is a tetrameric protein. It is possible, therefore, to have up to four stages of sequential binding, with each subsequent attachment releasing a different quantity of energy and having a different binding strength. It was decided to produce each of the four models, whereby the maximum degree of binding is either [*MX*], [*MXX*], [*MXXX*] or [*MXXXX*].

The modelling of the four sequential site models was done based on the principle that Adair postulated in 1925 [96] when examining Haemoglobin. When the first dextran branch binds to a free conA molecule, statistically there are four possible binding sites, for the second there will only be three available. Similarly, when a conA tetramer is fully bound there are four possible dextran branches to lose and so on. Therefore the equilibrium equations should be written thus:

$$K_1 = \frac{4}{1} KI_1 = \frac{[MX]}{[M][X]}$$
$$K_2 = \frac{3}{2} KI_2 = \frac{[MXX]}{[MX][X]}$$
$$K_3 = \frac{2}{3} KI_3 = \frac{[MXXX]}{[MXX][X]}$$
$$K_4 = \frac{1}{4} KI_4 = \frac{[MXXXX]}{[MXXX][X]}$$

Equation 3-4

The *K* values are the apparent, overall, association constants, the *KI* values are the intrinsic association constants. The numerator and denominator of the *KI* values are the statistical attachment and detachment chances respectively. In order to consider whether or not there is cooperativity, the intrinsic association constants must be considered as they are the fundamental constants.[96-98]

The modelling of the one site model resulted in a quadratic equation which could be simply solved. The sequential site systems, if solved in a similar manner result in cubic, or higher, equations. Though possible to solve analytically, they can be complex and may result in non-real roots. Therefore they were solved numerically (see Appendix 2.2).

Section 3.1.5. Parameter 'c'

Wiseman *et al.* [99], in their initial description of isothermal titration calorimetry defined a parameter, *c*, as a function of the association constant of the reaction and the concentration of the analyte in the sample cell:

$$c = n_s K[M_{TOT}] \qquad \textbf{Equation 3-5}$$

Ideally the *c* value should be between 5 and 100. This will give a sensible energy signature without inducing macromolecular problems.

The stoichiometric coefficient, n_s, is unity when the concentration of conA ($[M_{TOT}]$) is measured in terms of monomer units rather than tetramers. Work by Santori [100] and Zhang [101] has shown *K* for glucose to be of the order $10^2 - 10^3$ M^{-1}. Visual observations of conA solutions showed that a concentration of 0.1mM was the highest feasible given that viscosity effects will begin to affect the 'well-mixed' status of the system. This gives, at most, a *c* value of 0.1, constrained by the weak binding constant and high molecular mass of the dextran.

Section 3.2. Experimental Conditions and Data Analysis

Section 3.2.1. Experimental Conditions

All experiments with the ITC were performed in the buffer detailed in Section 2.2 and at 37^{o}C. This meant the experiments were at physiological temperature and pH. The solutions were found to be more stable, particularly the conA solution, if they were frozen after being made and only thawed prior to use each day. In all experiments 31 injections of 5µl were injected at 2min intervals. The first injection, due to diffusion during the temperature equilibration period prior to the experimental run, is always smaller than expected and is thus removed from the subsequent analysis [95]. The concentration of conA in the cell, as stated in Section 3.1.5, was kept at 0.1mM, this being the highest usable concentration without viscosity effects. The dextrans were used at as high a concentration as possible without making the solution unduly viscous. The dextrans used were of 6, 11, 17, 43, 64, 500 and 2000kD molecular mass.

The dextran solutions used were initially planned to have the same binding concentration irrespective of molecular mass, assuming 5% branching. This was, however, not feasible as the larger mass dextrans produce highly viscous solutions at relatively high concentrations (see Section 5.2 for more detail). Therefore an initial solution was made at the desired concentration and its viscosity visually observed. An estimate was then made as to the reduction in concentration required to produce a freely flowing solution. The final concentrations used are detailed in Table 3-3.

To eliminate thermal changes due to dilution effects, background runs were performed. This involved injecting the same dextran solutions as used in the standard tests into buffer devoid of conA. This shows the energy signature of the dilution effects of the buffer, which can then be subtracted from the standard run to give the energy signature that is solely due to the binding interactions.

Section 3.2.2. Model Accuracy and Error Calculation

The accuracy of a binding model is calculated as a χ^2 value. This is a summation of the square of the error between the model and data, divided by the number of degrees of freedom:

$$\chi^2 = \frac{\sum (Model - data)^2}{(n_p - p)} \qquad \textbf{Equation 3-6}$$

The number of degrees of freedom is found by subtracting the number of parameters, p, from the number of data points, n_p. This is to identify the statistical quality of the model. In pure mathematical terms, if the number of parameters is increased the model will fit the data set more accurately. However, each parameter introduced must be meaningful in terms of the biology of the system. This can be monitored statistically using Equation 3-6. As the number of parameters is increased, the denominator decreases in size. Hence, if the reduction in the error (numerator) due to an additional parameter is not significant it will not offset the reduction in the magnitude of the denominator and χ^2 will not be reduced. This equation will be used to compare the different models as well as to identify the values of the parameters within a given model.

Section 3.2.3. Model Selection

The analysis of the dextrans must be performed using one of the four models detailed in Section 3.1.4. In order to do this, one set of data was selected and analysed using each of the models and their error (χ^2) compared. Each of the models was written in the software package *Scientist*® (Version 2.0), a computer program from MicroMath® for mathematical modelling of non-linear and implicit equations. (see Appendix 3 for coding). The program was split into two halves. The first calculated the various concentrations and the energy release for an injection, *i*, using the equations listed in Section 3.1.4. The second half performed the same calculations, but for the injection *i+1*. The energy values were then calculated. The whole system was performed for each injection systematically and the parameters estimated with each iteration.

Each model was run in two modes. The first allowed each of the intrinsic association constants and enthalpy values to be different for each binding site (cooperativity), the second prevented them from varying relative to each other (no cooperativity). An additional model was also written whereby the conA was viewed as a monomer, but as if there were two populations of dextran, with differing binding strengths. This would show if there was a notable difference between branches of different lengths. Each of these models was run using a data set of 500kD dextran.

Table 3-1 Comparison of data analysis models based on size of error

		KI, ΔH equal			*KI, ΔH* different			2x Dextran
ConA Units	1	2	3	4	2	3	4	
Number of parameters	2	2	2	2	4	6	8	4
χ^2	3.200	3.400	3.619	5.421	0.491	0.609	0.615	3.200

From Table 3-1 it can be seen that the best is the two site model with cooperativity. The models with no cooperativity get progressively worse as the number of conA units considered increases. The model with two sets of dextran branches provides no improvement on the one site model. The two, three and four site cooperative models are significantly better than the non-cooperative models and the two site is the best of these.

Section 3.2.4. Model Instability

The modelling process was found to produce variable results depending upon the initial estimates entered into Scientist®. Table 3-2 below shows three separate pairs of binding constants and enthalpy values for a 500kD dextran data set (the same as used in Section 3.2.3).

Table 3-2 Variability of binding parameters depending upon initial estimates

	1		2		3	
	Estimate	Fit	Estimate	Fit	Estimate	Fit
KI_1 / M^{-1}	1000	8630	1000	2500	10000	2410
ΔH_1 / $kJmol^{-1}$	-10000	-23.2	-10000	-19.8	-10000	-20.3
KI_2 / M^{-1}	10	456	100	132	10	13.1
ΔH_2 / $kJmol^{-1}$	-10000	682	-10000	-93.5	-10000	-837
χ^2	0.516		0.491		0.517	

The primary binding site parameters are of the same order of magnitude for each fitted set. The secondary site parameters vary over orders of magnitude without greatly affecting the error. This weaker dependence on the secondary site is due to the respective energy releases of the two binding sites. Of the total energy produced during this titration 31% was generated by the secondary binding, hence a larger difference in the K and ΔH values does not have as large a bearing on the fitting process.

Figure 3-3 and Figure 3-4 show the number of complexes formed and the respective energy release of injecting 500kD dextran into conA. The number of secondary complexes, [MXX], being formed is significantly less than the primary complex, [MX], but the amount of energy released per mole is greater resulting in the small number of secondary complexes having a significant effect on the binding fit.

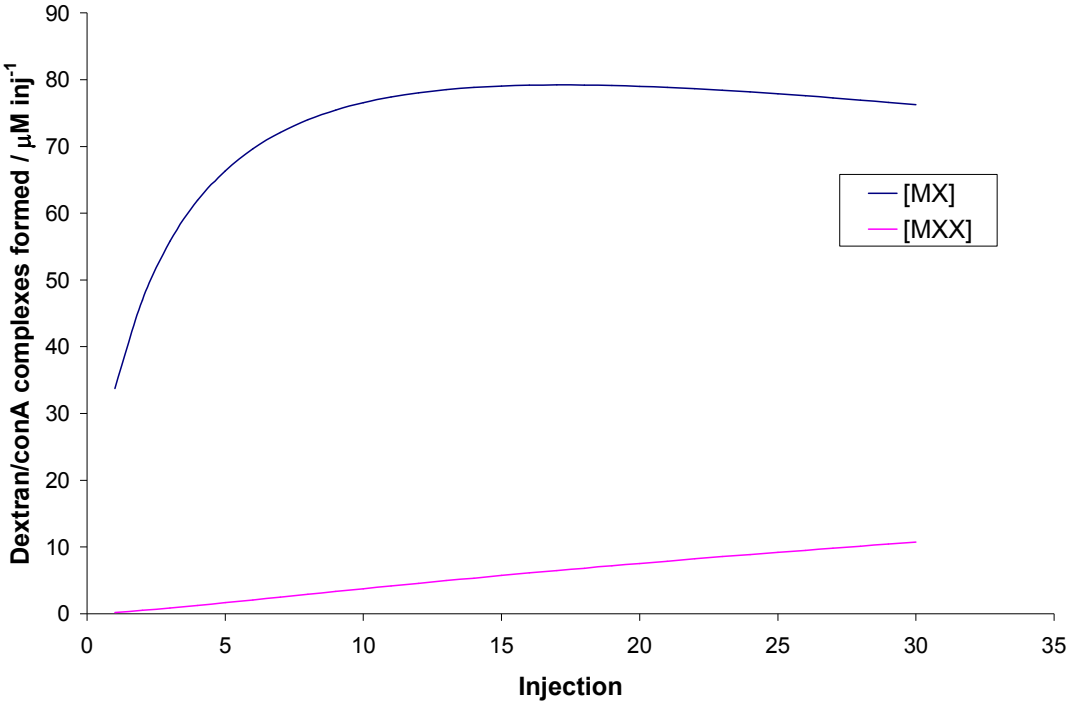

Figure 3-3 Moles of primary and secondary complex formed by 30 injections of 0.15mM 500kD dextran with 0.1M conA.

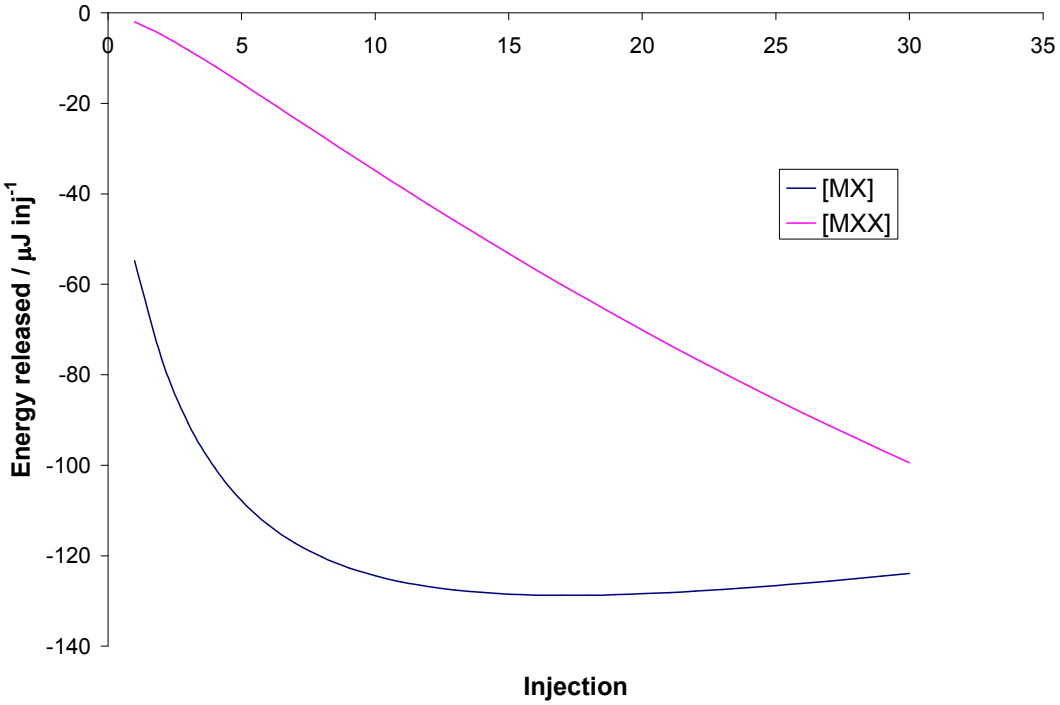

Figure 3-4 Energy release of primary and secondary complex formation by 30 injections of 0.15mM 500kD dextran into 0.1M conA.

Section 3.3. Results and Discussion

Each of the dextran sizes, D-glucose, maltose and maltotriose were run in duplicate and the data modelled in Scientist® using the two site binding model described previously to obtain the binding parameters. The modelling for glucose, maltose and maltotriose was performed using the monomeric concentration of conA as there are no size constraints associated with tese small molecules. Data shown is for the 'best' two experimental runs. Several of the dextrans required five or six repeats to achieve two similar sets of data. This is due to the energy release of this type of interaction being low (see Section 3.1.5). (The raw data graphs can be found in Appendix 4).

Table 3-3 Branching Concentrations from ITC experiments

Dextran MW / kD	Branch Ratio / %	Concentration / mM	Branch ends concentration / mM
Glucose – rep1	-	134.03	-
Glucose – rep2	-	134.03	-
Maltose – rep1	-	68.14	-
Maltose – rep2	-	70.36	-
Maltotriose – rep1	-	68.25	-
Maltotriose – rep2	-	69.16	-
6 – rep1	5.5	11.89	36.1
6 – rep2	5.5	11.89	36.1
11 – rep1	3.0	11.42	34.7
11 – rep2	3.0	11.48	34.9
17 – rep1	3.9	9.18	46.7
17 – rep2	3.9	9.70	49.5
43 – rep1	3.9	3.00	34.1
43 – rep2	3.9	3.00	34.1

Table 3-3 cont.

Dextran MW / kD	Branch Ratio / %	Concentration / mM	Branch ends concentration / mM
64 – rep1	4.8	1.44	28.7
64 – rep2	4.8	1.44	28.7
500 – rep1	4.6	0.15	21.4
500 – rep2	4.6	0.15	21.4
2000 – rep1	4.1	0.04	20.3
2000 – rep2	4.1	0.04	20.3

Table 3-4 Binding Parameters from ITC experiments

Dextran MW / kD	KI_1 / M^{-1}	ΔH_1 / $kJmol^{-1}$	KI_2 / M^{-1}	ΔH_2 / $kJmol^{-1}$	[MXX] energy release / %
Glucose – rep1	159	-10.2	-	-	-
Glucose – rep2	189	-8.31	-	-	-
Maltose – rep1	1380	-8.60	-	-	-
Maltose – rep2	1500	-9.02	-	-	-
Maltotriose – rep1	568	-18.4	-	-	-
Maltotriose – rep2	569	-32.9	-	-	-
6 – rep1	1190	-34.1	109	-155	38.2
6 – rep2	1470	-27.3	225	-73.1	44.8
11 – rep1	683	-82.0	14.5	-1320	9.9
11 – rep2	740	-79.9	35.1	-427	7.7
17 – rep1	376	-128	2.07	-17700	15.1
17 – rep2	307	-218	1.02	-29000	8.2
43 – rep1	714	-27.5	200	-106	49.0
43 – rep2	556	-111	125	-417	31.1

Table 3-4 cont.

Dextran MW / kD	KI_1 / M^{-1}	ΔH_1 / $kJmol^{-1}$	KI_2 / M^{-1}	ΔH_2 / $kJmol^{-1}$	[MXX] energy release / %
64 – rep1	1710	-28.6	676	-53.3	37.3
64 – rep2	1600	-30.2	6.93	-2160	16.0
500 – rep1	2500	-19.8	132	-93.4	30.8
500 – rep2	1940	-17.3	198	-51.1	31.7
2000 – rep1	2700	-25.6	6.15	-333	2.1
2000 – rep2	2910	-34.5	0.35	-54100	12.5

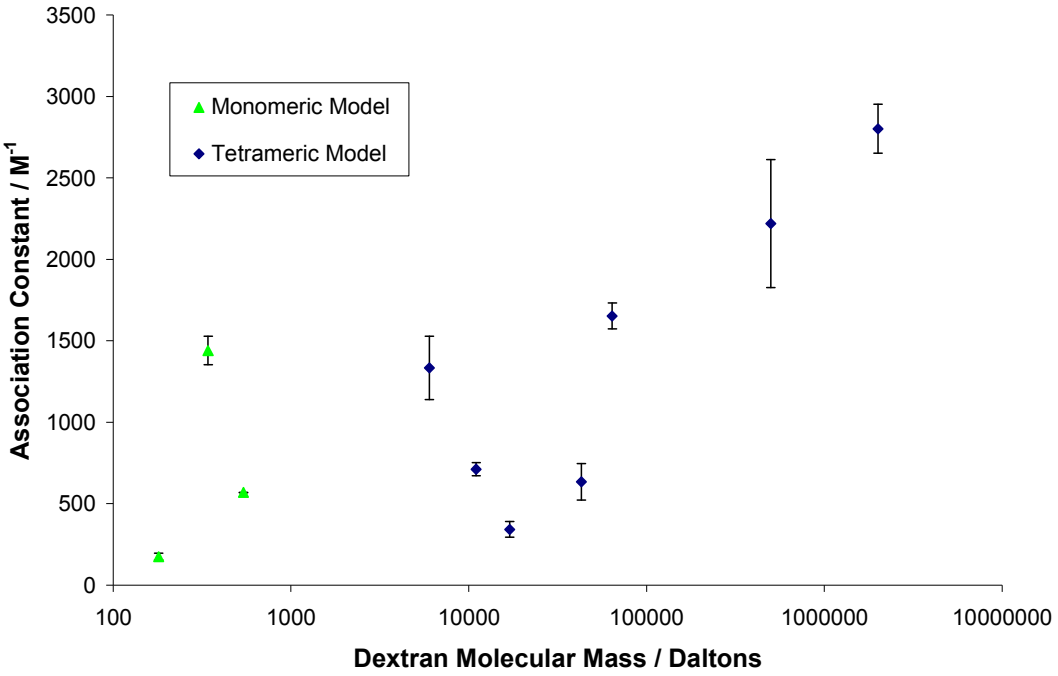

Figure 3-5 Intrinsic association constant of primary binding of glucose, maltose (a glucose dimer), maltotriose (a glucose trimer) and various dextrans with conA.

Data is mean of two replicates, error bars are +/- 1 standard deviation. Dextran data modelled using tetrameric conA concentration. Non dextran data modelled using monomeric concentration of conA.

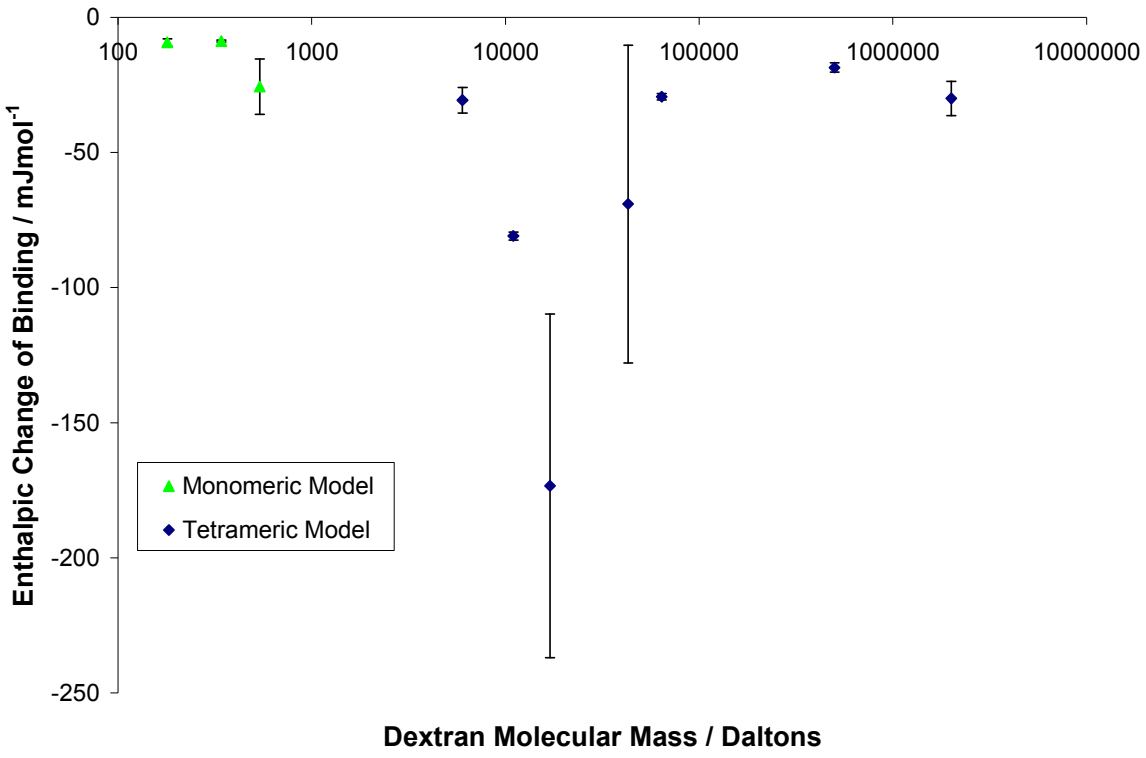

Figure 3-6 Enthalpy change of primary binding of glucose, maltose (a glucose dimer), maltotriose (a glucose trimer) and various dextrans with conA.

Data is mean of two replicates, error bars are +/- 1 standard deviation. Dextran data modelled using tetrameric conA concentration. Non dextran data modelled using monomeric concentration of conA.

The association constant of the primary binding site, Figure 3-5, has a general correlation of increasing binding strength with increasing molecular mass. The amount of energy released by these complexes does not follow a similar correlation, Figure 3-6. The data for the secondary binding site, Table 3-4, is a lot more variable both between replicates and between molecular masses. The energy released by the secondary binding sites ranges from ~10% for 11kD dextran to ~40% for the 6 and 43kD dextrans. The lower this figure, the harder it is for the fitting process to accurately predict the values. The greater strength of association for maltose, compared to glucose, follows the knowledge of how lectins bind to saccharides (see Section 1.3) but this does not follow through for maltotriose.

Mangold *et al.* [102] have performed similar tests on monomeric and dimeric conA using ITC. Titrations of various dendrimers with terminal mannose groups have shown that the association constant of binding increases as the number of terminal groups increases. The modelling performed in their work did not include sequential binding for the dimeric conA. The crystallographic work performed by Reeke *et al.* [67] produced an image of the structure of conA.

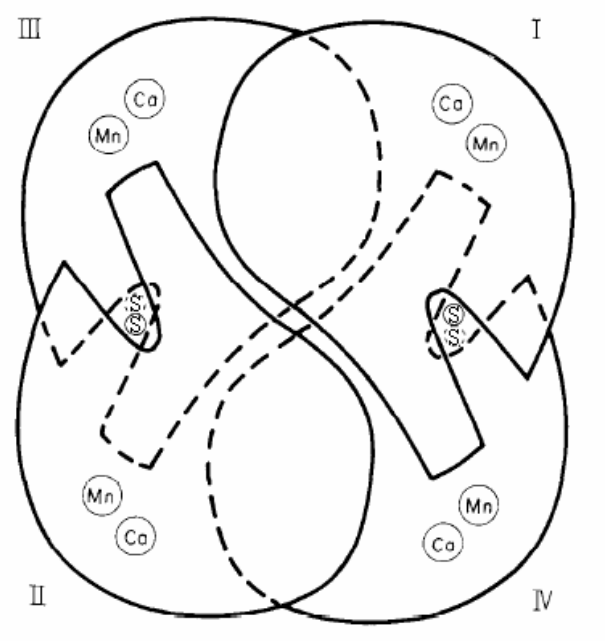

Figure 3-7 Structure of a conA tetramer, consisting of two pairs of dimers on top of each other.

Ca, Mn and S represent the calcium ion, manganese ion and substrate binding sites respectively. Each sub-unit is approximately 4x4x4 nm.

The size of each monomer is approximately 4x4x4 nm. Figure 3-7 shows that a conA tetramer exists as two planes of substrate binding sites. Units I and II have approximately 5nm between their binding sites with III and IV in a similar position on the opposite face of the tetramer. The hydrodynamic radius of dextran has been shown to be between 1.5 and 30nm for dextrans up to 2000kD [103, 104]. It is therefore unlikely that more than two dextran molecules can bind to a conA simultaneously due to the physical constraints. This is supported by the sequential site analysis which showed the three and four site models to be inappropriate and the glucose, maltose and maltotriose data which allowed full tetrameric binding. The weak strength of the secondary bind compared to the primary can also be explained by the size restrictions.

Section 3.4. Conclusion

The interaction between conA and dextran has been thermodynamically investigated. It has been shown that a weak prediction of the primary association constant can be made from the size of the dextran molecule. No prediction of the enthalpic change of binding is possible.

Lectin binding sites are shallow compared to those of enzymes and antibodies [105], with binding being enhanced by secondary effects of the molecule "lying" across the surface of the protein, reflecting the biological role of oligosaccharide recognition. As the length of the dextran chain increases the amount of additional binding should increase, making the binding stronger.

There is a suggestion that the secondary binding is weaker than the primary binding, implying negative cooperativity. This is likely to be due to physical constraints, similar to those that prevent tertiary and quaternary binding, rather than changes in chemical conformation. It is therefore possible to state that, should this work be continued to test non-toxic proteins with dextran, that the number of monomers bound together is not the important factor - the relative position and distance between the saccharide binding sites is the essential characteristic.

Section 3.5. Nomenclature

c	Wiseman feasibility parameter
ΔG	Gibbs free energy change ($Jmol^{-1}$)
ΔH	Enthalpic change ($Jmol^{-1}$)
K	Apparent association constant (M^{-1})
KI	Intrinsic association constant (M^{-1})
k_a	Association rate ($M^{-1}s^{-1}$)
k_d	Dissociation rate (s^{-1})
$[M]$	Concentration of free lectin (conA) (M)
$[MX]$	Concentration of conA/dextran complex (M)
$[MXX]$	Concentration of conA/dextran/dextran complex (M)
$[M_{TOT}]$	Total conA sites, bound and unbound (M)
n_s	Stoichiometric coefficient
n_p	Number of data points
p	Number of parameters
Q_i	Total energy released (J)
dQ_i	Energy change over one injection (J)
R	Universal gas constant = 8.31 $Jmol^{-1}K^{-1}$
ΔS	Entropic change ($Jmol^{-1}K^{-1}$)
t	Time (s)
T	Temperature (K)
V_C	Volume of sample cell (L)
V_{inj}	Volume of injection i (L)
$[X]$	Free dextran binding ligands at injection, i (M)
$[X_{TOT}]$	Total dextran ligands, bound and unbound (M)
χ^2	Size of error

Section 4. Surface Plasmon Resonance

The SPR (Surface Plasmon Resonance) experiments were performed using a BIAcore® X, (BIAcore AB, S-754 50 Uppsala, Sweden), which can be used to evaluate the kinetics (association and dissociation rates of binding) of the dextran / conA binding.

Section 4.1. Theory

Section 4.1.1. Surface Plasmon Resonance

SPR experiments are conducted in a system where the receptor is bound to a surface such that the rate of association and dissociation can be found when the ligand passed through the system in solution is bound. The standard technique, when using CM5 sensor chips, involves covalent binding of ligand via an amine group.

The surface of the chip is coated in dextran with carboxylic acid moieties. These are activated by a set regimen involving ethyl-(3-3-dimethylaminopropyl) carbodiimide hydrochloride (EDC) and *N*-hydroxysuccinimide (NHS). This produces a surface capable of binding amine groups (see Figure 4-1).

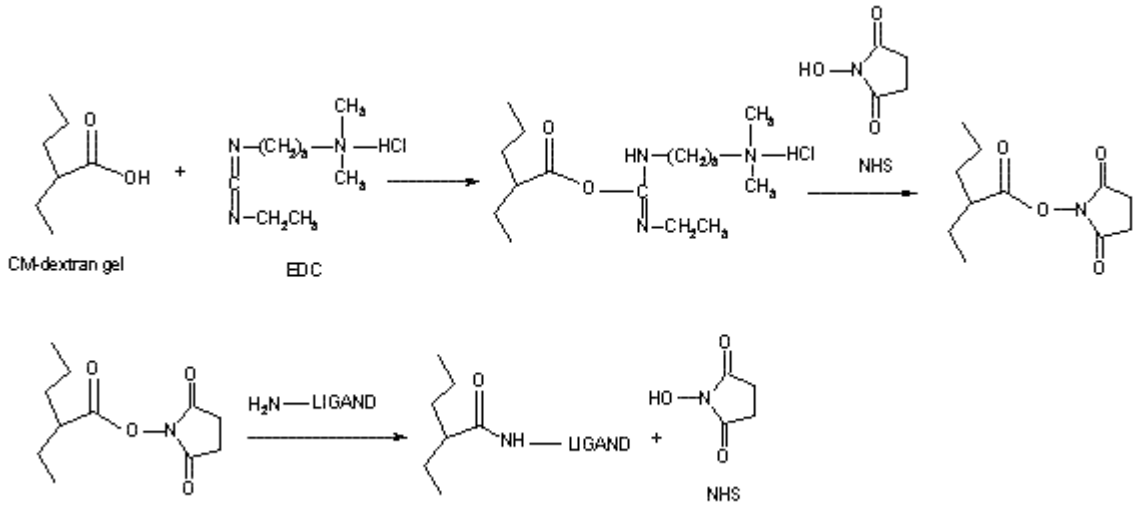

Figure 4-1 Depiction of the standard amine binding process

The material desired to be bound is then passed over the surface (typically for 7 minutes at 5μLmin^{-1}). If more than one amine group is present on the injectant then a heterogeneous

surface will be produced because there is no way of controlling the molecular orientation within the cell. The binding process is concluded by passing ethanolamine through the system. This blocks any remaining active groups from the EDC/NHS phase which haven't bound with amine groups.

SPR works on the principle that some metals, particularly gold and silver, are capable of propagating plasmons along their surface. A plasmon, a quasiparticle, is caused by a photon of light at a specific wavelength striking a free electron on the surface of the metal. At the correct incidence angle the plasmon will propagate along the surface rather than being reflected to the photodiode array. The refractive index of the metal film affects the occurrence of surface plasmons and it is this refractive index which is affected by the presence of material bound to the opposite side of the metal layer (see Figure 4-2).

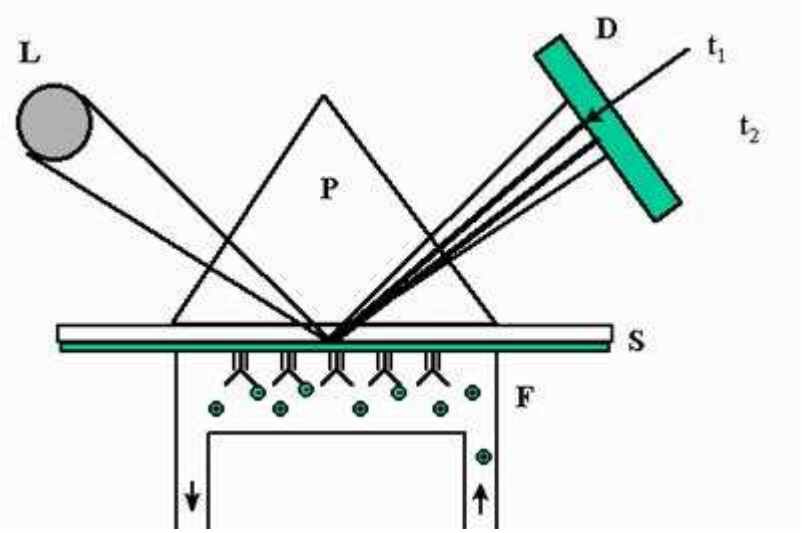

Figure 4-2 Schematic of SPR technology: L: light source, D: photodiode array, P: prism, S: sensor surface, F: flow cell.

The two dark lines in the reflected beam projected on to the detector symbolise the light intensity drop following the resonance phenomenon at time = t1 and t2. The line projected at t1 corresponds to the situation before binding of antigens to the antibodies on the surface and t2 is the position of resonance after binding.

Section 4.1.2.Kinetic Experiments

The kinetic parameters of an interaction, the association and dissociation rates, can be found experimentally using SPR. Kinetic experiments were performed by passing a ligand solution across the activated chip for a given length of time, then followed by buffer without ligand at the same rate. This allows association and then dissociation to occur. The data is recorded and analysed. To obtain kinetic data it is recommended to pass solutions of increasing concentration of ligand through the cell. This will give a set of data as illustrated in Figure 4-3. The use of several concentrations is to ensure that the data analysis is not hindered by localised effects. It is possible for too high concentrations to have mass transfer limitations or bulk refractive index problems and for too low concentrations to produce data at the level of the noise of the detection system; if the kinetic model can produce a good fit for all the concentrations used it is more likely to be accurate.

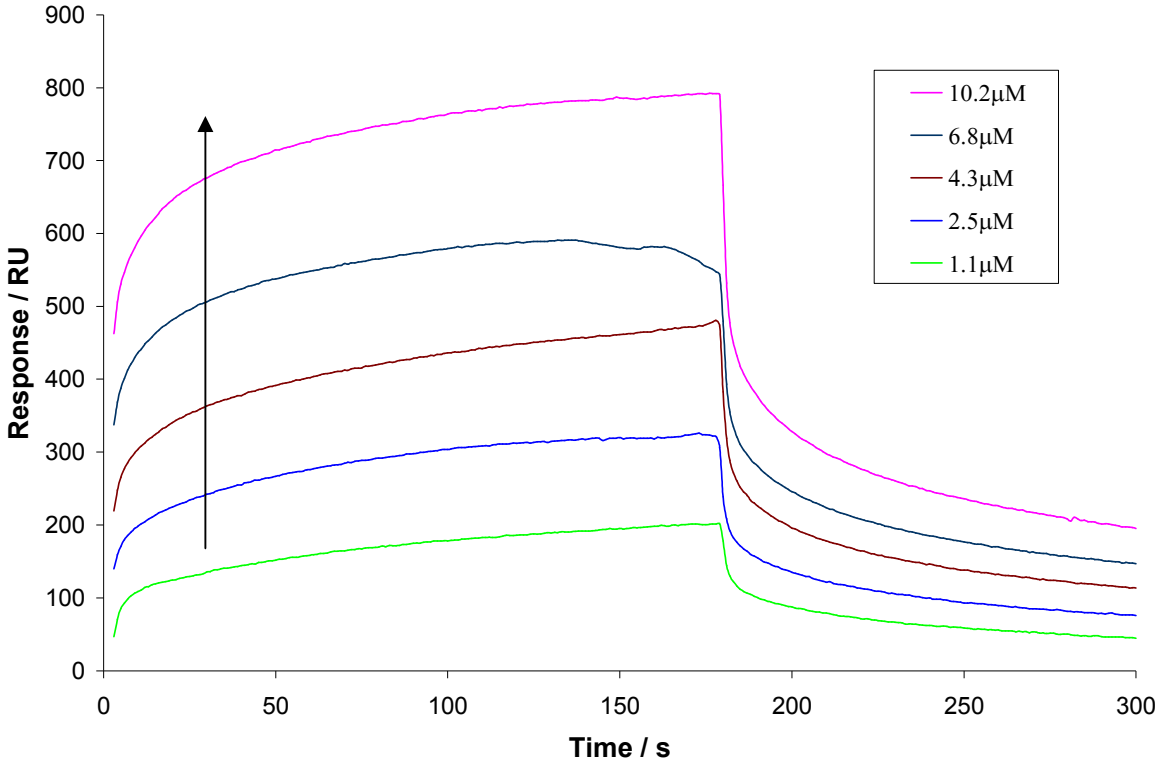

Figure 4-3 Injections of ConA over 2000kD Dextran. Concentration of conA (1.1µM, 2.5µM, 4.3µM, 6.8µM and 10.2µM) increasing in direction of arrow.

At t = 180s flow returned to just buffer with no conA.

The injected sample should be preceded by an air gap (as recommended by BIAcore). This prevents effects similar to that seen in the 6.8μM injection in Figure 4-3. At the end of the association phase the response begins to decrease, rather than continuing towards the equilibrium state. This is because the injected fluid has diffused into the previous samples still present in the sample loop. The air gap provides a physical barrier against diffusion, maintaining the injection concentration throughout the course of the association phase.

Section 4.1.3. Analysis

The analysis of the SPR data is based around the type of interaction it is believed is occurring. There are several binding models built into the BIAcore evaluation software of which the following three are most applicable.

Langmuir type binding assumes a simple 1:1 ratio of binding sites to ligands. The association and dissociation rates are calculated iteratively from an estimation of the total binding sites available on the sensor chip surface and the concentrations known to have been passed through the system. A least squares fit can be performed, similar to Section 3.2.2 (but only incorporating the size of the error, not the number of parameters or data points) to calculate the accuracy of the rates. Details of the equations are in Appendix 5.

At physiological pH conA is a tetramer. Therefore assuming a Langmuir type binding is likely to be an inappropriate model. The next option is a bivalent model which assumes that the binding of a second dextran ligand to a conA tetramer has different association and dissociation rates than the primary bind. The modelling process is similar to that of the Langmuir binding, but with two sets of association and dissociation rates. The difference between the first and second bind to a conA molecule could have a positive or a negative effect. There may be conformational changes caused by the first binding which facilitate the other binding sites, or there could be problems caused by the dextran orientation of the conA when it is bound to the sensor chip surface.

The third type of model assumes a heterogeneous ligand population. This is based on the fact that the dextran is not a homogenous material. It is possible that branches or different lengths will bind to conA with different strengths. Therefore this binding model assumes that there are two populations of dextran which in total account for all of the binding.

Section 4.1.3.1. Additional Effects

There are two additional effects which can alter the response detected by the BIAcoreX. The first is mass transfer, *MT*. It is possible, due to the potentially large and tangled bulk of dextran on the surface of the sensor chip that there is a diffusion limitation on the dextran before all the terminal groups can reach the conA binding sites.

The second potential effect is that of bulk refractive index, R_i. The solution passing over the sensor surface during the association phase contains a significant amount of material, which could potentially enhance the response of the system. This effect can be incorporated as a simple multiple of the injectant concentration.

Section 4.2. Experimental Conditions

Section 4.2.1. Experimental Conditions

Throughout the experiments the buffer detailed in Section 2.2 was used, except during the surface preparation when the standard amine coupling technique was followed. Flowrates were set to 20μlmin^{-1} throughout. The time allowed for association was 180s with a 150s dissociation phase. Rejuvenation of the sensor chip surface (removal of remaining dextran) was performed using a 1M phosphoric acid solution, as recommended by Mann *et al.* [106]. The BIAcore approved technique of adding air gaps to the injectant to isolate from previous solutions was followed at all times.

Section 4.2.2. Binding ConA or Dextran to the Sensor Chip Surface

The technique recommended by BIAcore involves binding at a pH below the pK value of the protein, for conA, this is pH4.5. However this means that the ConA will be binding when in its dimeric form, not the tetrameric form that was used in the ITC or to make the hydrogels. Two other problems were also found with binding the conA to the surface of the SPR chip. The orientation of the binding was not known, and so it is likely that many of the binding sites were inaccessible to the large dextran molecules. The second problem was related to an issue raised by Hubble [107, 108], who suggested that when there is multivalency, the dissociation rate is based on the statistical probability of all bonds dissociating at the same time. Assuming 5% branching, the number of branches varies from

3 on a 6kD molecule to over 600 for the 2000kD dextran. The sensorgrams produced with conA bound to the SPR suggested that this was indeed a problem; the dextran, once bound, was very difficult to remove.

Preparing the surface with conA not being productive, it was decided to bind the dextran to the surface of the SPR chip. This was achieved by using the carboxymethylated dextran that was to be used in the hydrogel production (see Section 2.3). The binding protocol described in Section 4.1.1 was then followed, but with diaminoethane bound to the EDC/NHS prepared surface. Once the ethanolamine had been passed through the system the carboxymethylated dextran (CM-dextran), dissolved in an EDC/NHS solution, was then passed through until sufficient was believed to be bound to the surface. It was not known where the carboxymethyl groups were positioned on the dextran molecule and it was likely that some of them, once bound to the sensor surface, would prevent some branch terminals from binding to conA. However, as the same protocol was used to cross-link the hydrogels, this would provide a more accurate representation of the binding occurring within a hydrogel. Once bound it was possible to pass conA through in solution at pH 7.4 (thus tetrameric) with the maximum bound points of a molecule in solution being 4 rather than the much larger figures possible with the larger dextran molecules.

Section 4.3. Data Analysis and Results

A set of kinetic experiments were performed for the 43, 500 and 2000kD dextrans. Data was also obtained for the 'blank' sensor surface as this was made from CM-dextran and would in theory also be able to bind to conA. (The raw data can be found in Appendix 7.2). The resulting data was then condensed down into a set of five injections of varying concentration. An example section of data from the 2000kD dextran activated surface can be seen in Figure 4-4. The supplied BIAcore software is incapable of fixing the ratio of the species of binding sites for heterogeneous sites; a factor which logic suggests should be constant for a given dextran surface. Therefore this binding would have to be evaluated in Scientist®. For consistency, it was decided that all the data should be evaluated in the same computer package, thus the BIAcore software was not used for data analysis.

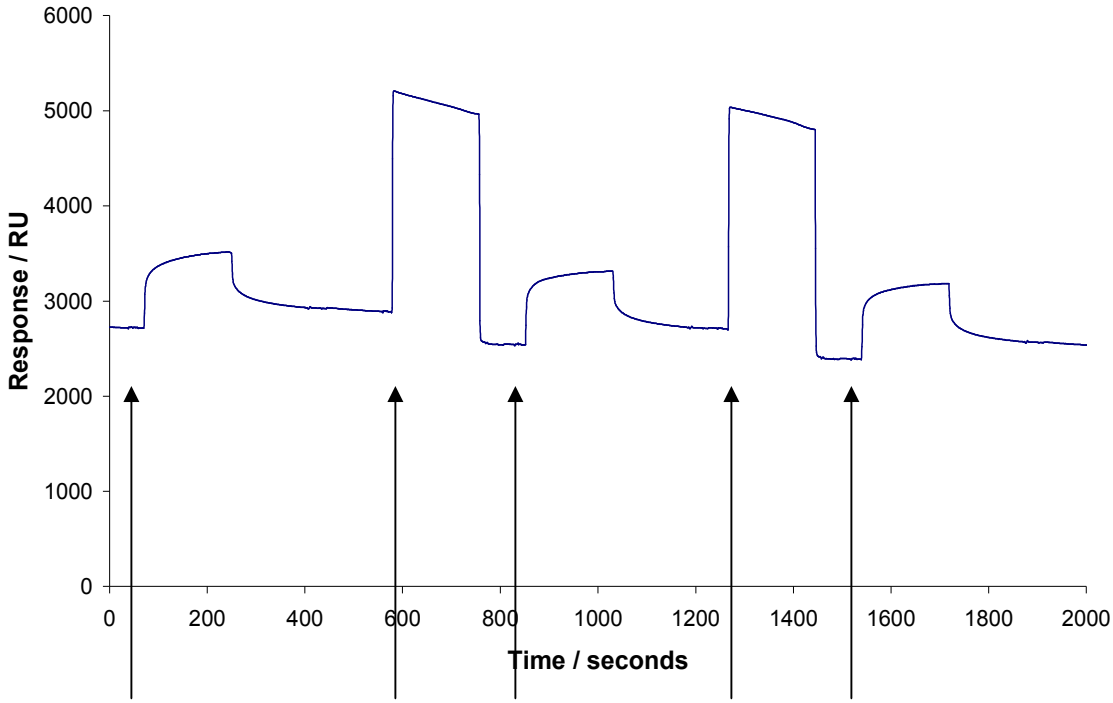

Figure 4-4 Graph showing the first 2000 seconds of the data using the 2000kD dextran activated surface.

This section of data contains five injections, starts of which indicated by the arrows. The first, third and fifth injections are of conA, the second and fourth are cleaning injections of phosphoric acid.

Section 4.3.1. Binding Type Analysis

The binding analysis involved finding the correct model to describe the data. There were two parts to this – the primary half involved finding the appropriate model based on the molecular nature of the materials such as whether the conA was capable of all four of its binding sites being used. The second half incorporated the bulk refractive index and mass transfer terms. The material being injected over the surface of the sensor chip can cause response effects even if there is no binding. This is known as the bulk refractive index term and is represented by a constant value during the association phase, linked to the concentration of the injectant. The mass transfer affect requires the calculation of the concentration on the surface of the chip, rather than in the bulk stream. This is done as a mass transfer coefficient multiplied by the concentration difference.

Figure 4-5 to Figure 4-8, below, show the attempted data analysis of a 10.2μM conA solution over a 2000kD dextran activated sensor surface, the four remaining injections (at 1.1μM, 2.5μM, 4.3μM and 6.8μM) are not shown for clarity, though all were analysed together to ensure that the estimated parameters are applicable for all data. Figure 4-5 shows all the attempts using a Langmuir binding. It is clear that this is not an appropriate model, and it is not enhanced by the addition of mass transfer or bulk refractive index functions, though the equilibrium state at the end of the association phase is more accurate with a refractive index term. In both the case of pure Langmuir and Langmuir with a refractive index term, the mass transfer term produces no discernible benefit.

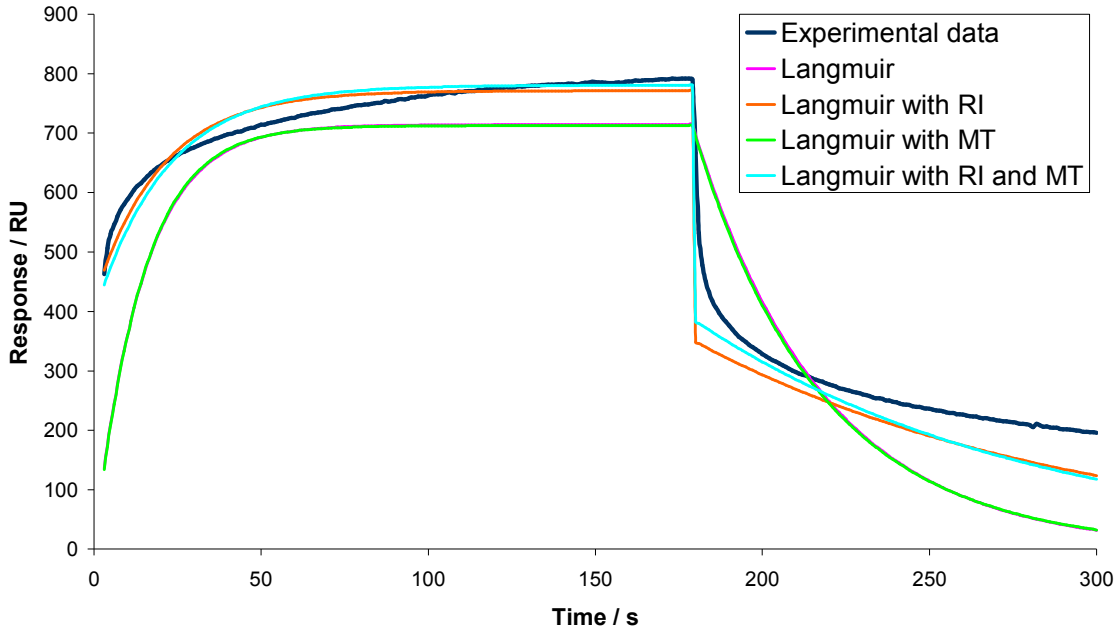

Figure 4-5 Graph representing data analysis of an injection of 10.2μM conA (monomer concentration) over a 2000kD dextran activated surface.

Injection is stopped at 180s to allow dissociation to be recorded. The data recorded is shown as the experimental data line. Type of binding is Langmuir throughout (see Appendix 5.1) with inclusion of a bulk refractive index term (R_i) and / or a mass transfer term (*MT*). (Pink and green lines are superimposed on top of each other due to lack of influence of the *MT* term)

Figure 4-6 shows that a bivalent model for the binding of conA to dextran is not appropriate either, again without any great benefit from either the refractive index or the

mass transfer term. In the case of both the Langmuir and bivalent models the refractive index term aids the model in reaching the equilibrium state at the end of the association phase. However neither model is showing suitably rapid association or dissociation at the beginning of each phase. The fact that very rapid association occurs underlines the reason for the mass transfer term being ineffectual. Mass transfer effects will no longer be considered, whereas refractive index effects will be permanently employed.

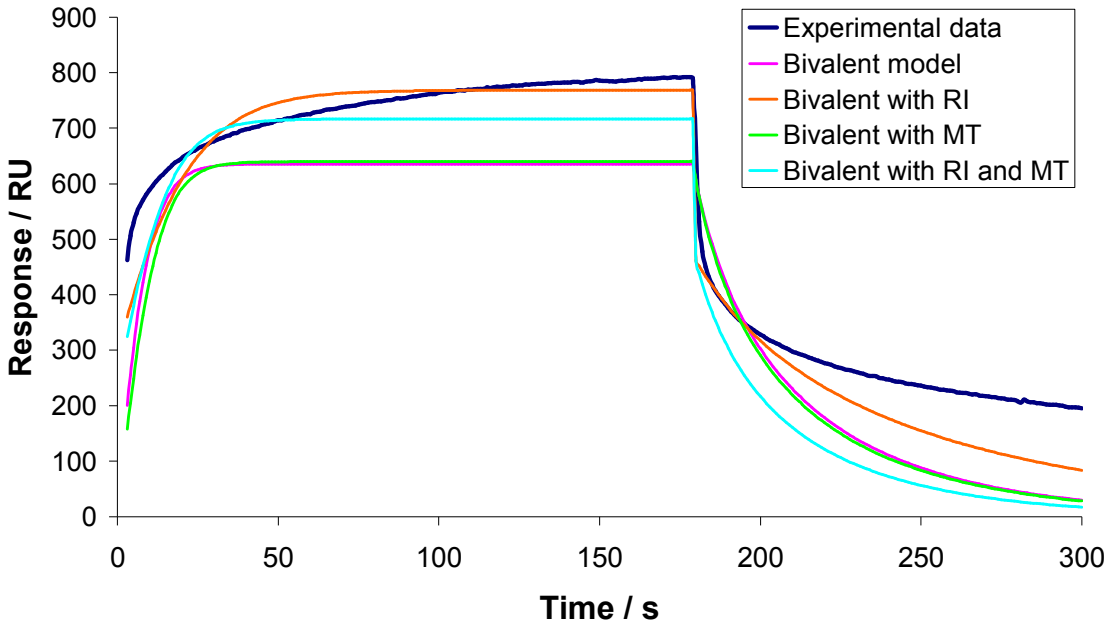

Figure 4-6 Graph representing data analysis of an injection of 10.2nM conA (monomer concentration) over a 2000kD dextran activated surface.

Injection is stopped at 180s to allow dissociation to be recorded. The data recorded is shown as the experimental data line. Type of binding is Bivalent throughout (see Appendix 5.2) with inclusion of a bulk refractive index term (R_i) and / or a mass transfer term (*MT*).

The heterogeneous model, with refractive index, (see Figure 4-7) is far superior to both the Langmuir and bivalent models. This model entails there being more than one population of sites bound to the surface of the sensor chip. In particular the latter half of the association phase and the dissociation phase are not well approximated in the other models. This model is further improved, in Figure 4-8, by applying a bivalent binding to each of the two populations of binding sites, though this additional improvement in the error calculation may be due to the large increase in the number of parameters (see Table 4-1).

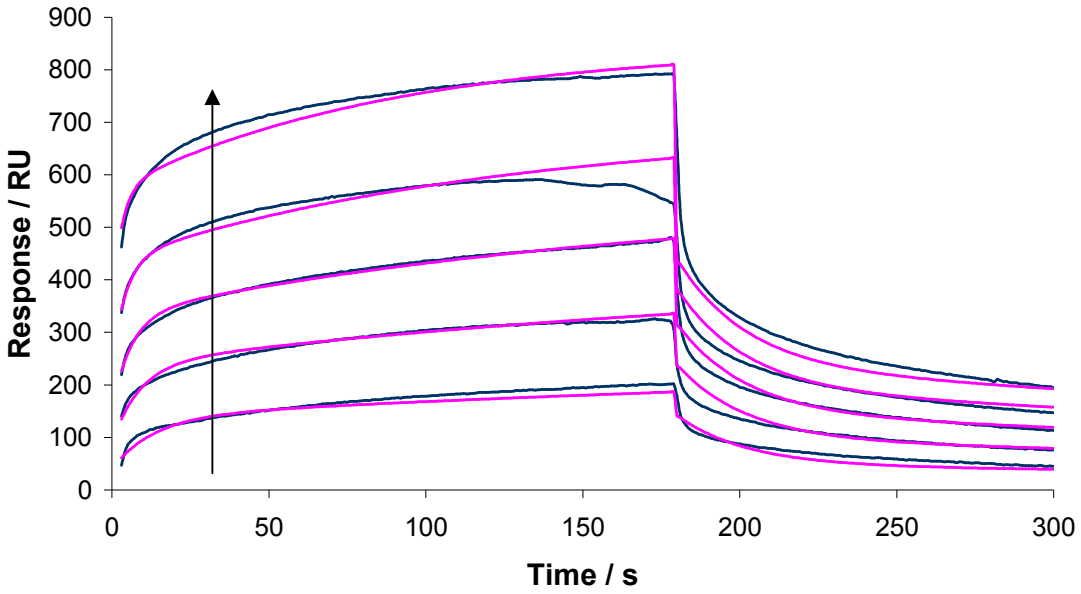

Figure 4-7 Graph representing a heterogeneous model, with refractive index, for all the concentrations of conA.

(1.1μM, 2.5μM, 4.3μM, 6.8μM and 10.2μM – arrow indicates increasing concentration). Blue lines represent the experimental data, pink lines represent the heterogeneous model.

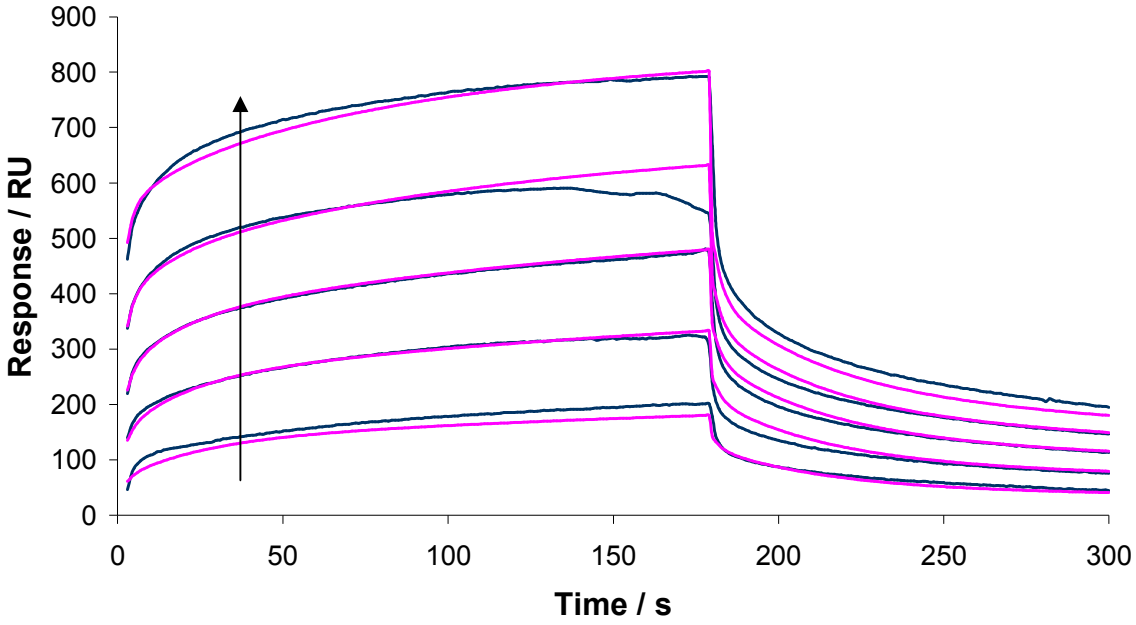

Figure 4-8 Graph representing a bivalent heterogeneous model, with refractive index, for all the concentrations of conA.

(1.1μM, 2.5μM, 4.3μM, 6.8μM and 10.2μM – arrow indicates increasing concentration). Blue lines represent the experimental data, pink lines represent the heterogeneous model.

Table 4-1 Number of parameters in the various models used for data analysis

Model	Number of parameters	with RI factor
Langmuir	3	4
Bivalent	5	6
Heterogeneous	6	7
Heterogeneous / Bivalent	10	11

Section 4.3.2. Binding Type Summary and Discussion

In Section 4.3.1 it was shown that a simple Langmuir or bivalent binding model is not an appropriate approximation of the interaction between conA and bound dextran. Addition of a refractive index term, suggesting that the conA in solution is also affecting the SPR response, showed improvement in the analysis. A mass transfer limited model was ruled out due to the rapid association at the start of the interaction, something which would not occur to this extent if there was a mass transfer limitation.

The heterogeneous sites model, where it is suggested that the bound dextran is not uniform, from the perspective of the conA, is far superior to the simpler models and again is improved with a refractive index term but unchanged by a mass transfer term. This is conceivable as it has been shown by Sidebotham [109] that chain length and dextran molecular size can affect the binding. Such a variable material being bound to a fixed surface would result in some binding sites being more favourable and thus the association and dissociation rates varying. The addition of bivalent binding to the heterogeneous model shows that there may be other factors altering the binding of the conA, particularly as it is a tetramer.

The analysed response for the 10.2μM injection across the 2000kD dextran activated chip has been deconstructed in Figure 4-9 to its five components, that of the primary and secondary bindings for two populations of dextran ligands and the refractive index contribution.

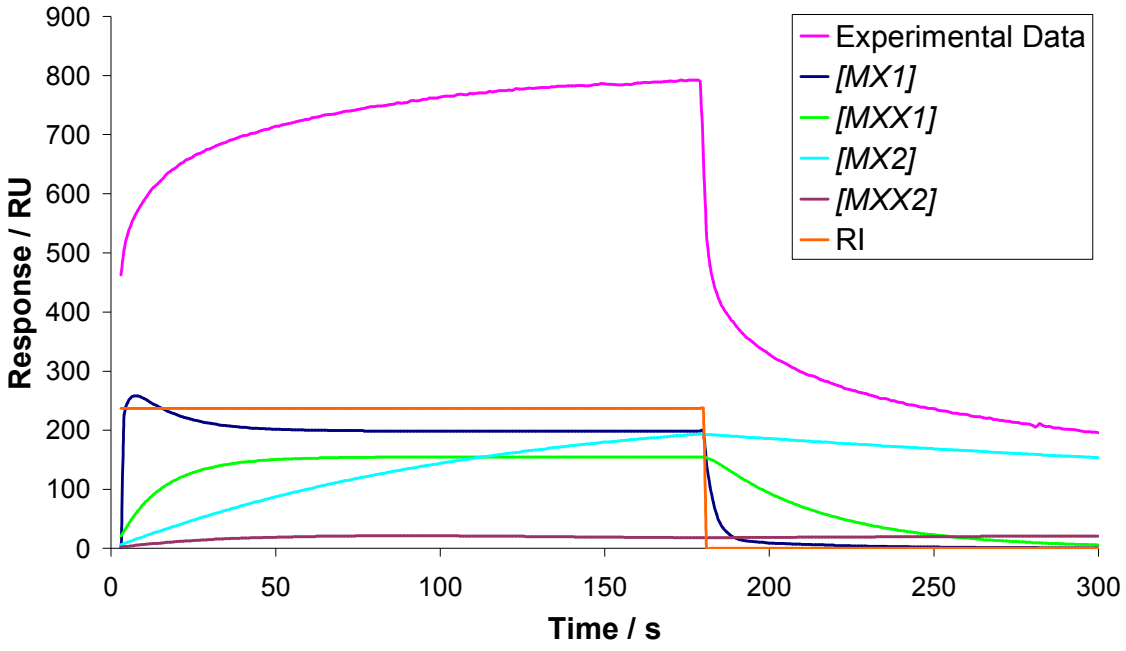

Figure 4-9 Graph of response components that comprise the total seen response of an injection of 10.2μM conA over 2000kD dextran.

Model is Heterogeneous with bivalency and bulk refractive index term.

The deconvoluted data in Figure 4-9 describes how the binding is being modelled. The first population of dextran ligands (creating complex $[MX_1]$ and $[MXX_1]$ - dark blue and green respectively) show that there is a rapid binding up to an equilibrium state after 50s and that this is a dynamic equilibrium. Once the free conA is removed from solution, at 180s, the concentration rapidly decreases. Conversely, the second dextran ligand population (creating complex $[MX_2]$ and $[MXX_2]$ – light blue and purple respectively) takes a long time to build up and does not readily dissociate once the free conA has been removed. The secondary binding to create $[MXX_2]$ virtually doesn't exist. The interactions seen with an active layer of 43kD, 500kD and the blank sensor chip behaved in a similar manner (see Appendix 7.1).

This can be clarified thus; there is a standard interaction between conA and dextran which rapidly reaches equilibrium in the presence of excess conA, and which then rapidly dissociates in the absence of an excess of conA. This interaction may contain negative cooperativity towards a second bond to the same conA molecule. There is a second binding

process, here viewed as a second population of dextran sites, which does not readily dissociate until the phosphoric acid cleaning solution is passed through the system.

Section 4.3.3. Results

The bivalent heterogeneous model has been used to analyse data produced from injecting varying concentrations of conA across a blank sensor surface and across sensor surfaces activated with 43kD, 500kD and 2000kD dextran.

Table 4-2 contains the parameter values from the data analysis and Table 4-3 contains the calculated association constants (Subscripts 1,2,3 and 4 correspond to $[MX_1]$, $[MXX_1]$, $[MX_2]$ and $[MXX_2]$ respectively).

Table 4-2 Table of parameters fitted to experimental data using Scientist®

	Blank	43kD	500kD	2000kD
R_{Max}	2.4×10^{3}	1.4×10^{3}	1.3×10^{3}	1.1×10^{3}
k_{a1} / M^{-1} s^{-1}	6.7×10^{3}	11.4×10^{3}	8.4×10^{3}	9.2×10^{3}
k_{d1} / s^{-1}	3.8×10^{-2}	3.3×10^{-2}	4.5×10^{-2}	32.9×10^{-2}
k_{a2} / M^{-1} s^{-1}	4.1×10^{-4}	16.9×10^{-4}	36.1×10^{-4}	0.7×10^{-4}
k_{d2} / s^{-1}	4.0×10^{-2}	16.4×10^{-2}	40.6×10^{-2}	1.7×10^{-2}
k_{a3} / M^{-1} s^{-1}	3.9×10^{2}	3.5×10^{2}	3.4×10^{2}	4.6×10^{2}
k_{d3} / s^{-1}	2.7×10^{-33}	3.3×10^{-18}	2.7×10^{-33}	1.8×10^{-3}
k_{a4} / M^{-1} s^{-1}	4.0×10^{-47}	2.7×10^{-1}	3.8×10^{-2}	3.4×10^{-2}
k_{d4} / s^{-1}	5.3×10^{-18}	18.4	18.5	14.3
Y	0.79	0.66	0.72	0.73
R_i	3.4×10^{7}	2.4×10^{7}	1.9×10^{7}	2.3×10^{7}

Table 4-3 Calculated values of association constants from the experimental data

	Blank	43kD	500kD	2000kD
K_{a1} / M^{-1}	1.8×10^{5}	3.4×10^{5}	1.9×10^{5}	0.3×10^{5}
K_{a2} / M^{-1}	10.2×10^{-3}	10.3×10^{-3}	8.9×10^{-3}	4.5×10^{-3}
K_{a3} / M^{-1}	1.4×10^{35}	1.1×10^{20}	1.2×10^{35}	2.5×10^{5}
K_{a4} / M^{-1}	7.5E-30	14.7×10^{-3}	2.0×10^{-3}	2.4×10^{-3}

The primary observation concerns the rate of dissociation of the complexes. Figure 4-10 shows the highest concentration injection for each dextran type, normalised so that the

maximum response value is set to 1. The association phase is dependent upon the concentration of the injected conA (not constant across the range of dextrans) and is also dependent upon the amount of material bound during the activation stage, something which is not controllable. The dissociation phase, however, is purely dependent upon the dissociation rates. The shorter dextran molecules have lower dissociation rates, resulting in the conA binding to them more strongly.

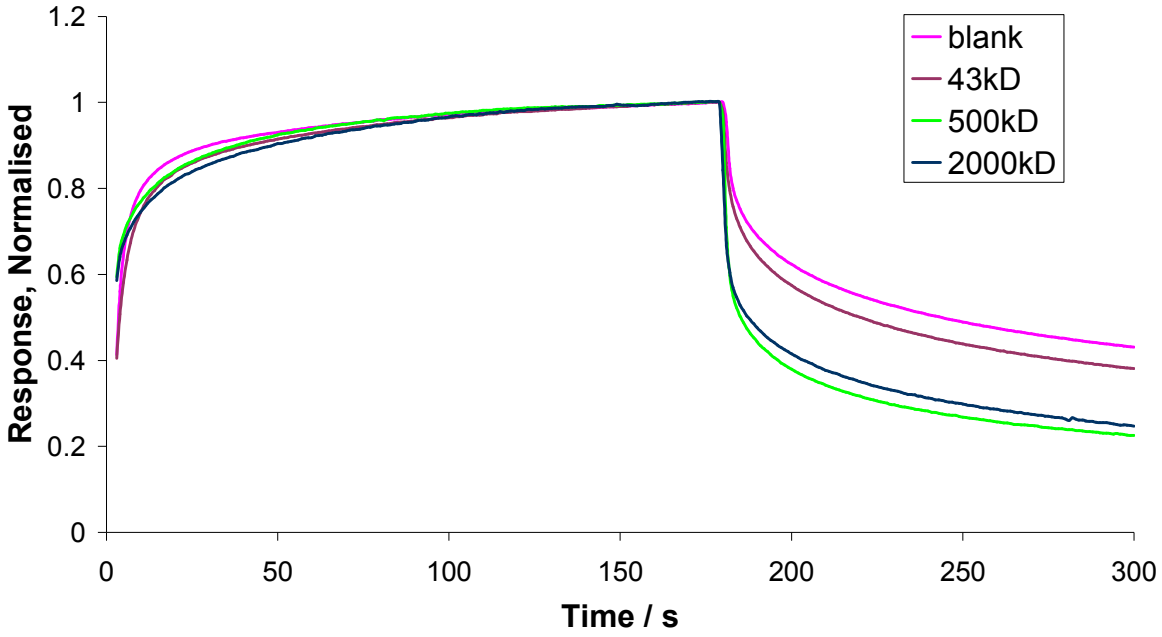

Figure 4-10 Graph showing normalised injection data for the blank sensor surface and that activated by 43, 500 and 2000kD dextran

The maximum response, R_{Max} (see Table 4-2), is greatest for the unmodified surface of the sensor chips. This implies that the CM-dextran applied to the surface is not as accessible to binding.

Section 4.4. Conclusions

This investigation into the rates of association and dissociation of the interaction between conA and dextran has shown some potentially interesting facts. Primarily that, as with the thermodynamic data from Section 3.3, there is a difference in the binding characteristics depending upon the size of the dextran chain. However, the data for the primary binding site shows that the association constant decreases as the molecular mass of dextran increases – this is contrary to the ITC data. This difference could be caused by the dextran being immobile on the sensor chip, resulting in the larger dextran molecules being harder to access than the smaller molecules. There is strong evidence to suggest that some of the interactions are very hard to dislodge without the introduction of phosphoric acid. This could result in hydrogels maintaining structural strength in the presence of glucose, as some bonds will not dislodge, or could result in a maximum swelling ratio.

Further work was not performed due to the expense of the sensor chips when compared with the likelihood of improved data.

Section 4.5. Nomenclature

K_a	Association constant (M^{-1})
k_a	Association rate ($M^{-1}s^{-1}$)
k_d	Dissociation rate (s^{-1})
$[M]_i$	Concentration of free lectin (conA) (M)
$[MX]_i$	Concentration of conA/dextran complex (M)
$[MXX]_i$	Concentration of conA/dextran/dextran complex (M)
R	Response (RU)
R_t	Total response (RU)
R_{max}	Max. dextran binding capacity (RU)
R_i	Refractive index effect (RU M^{-1})
t	Time (s)
$[X]_i$	Free dextran binding ligands at injection, i (M)
$[X]_{TOT}$	Total dextran ligands, bound and unbound (M)
χ^2	Size of error

Part 1 - Conclusions

The results from the ITC work have shown that, though conA exists as a tetramer at physiological pH, it is only possible for two separate dextran molecules to bind. This has been confirmed by a study of the relative sizes of the molecules and the arrangement of the binding sites. It has also shown that there is a general trend of increasing binding strength with increasing molecular mass, though this is not universal.

The ITC and SPR work have not provided comparable data. This was due to the SPR not being effective in measuring the association and dissociation rate of conA / dextran binding. This was due to the multivalent nature of the components.

The combination of these two sections allows the conclusion that the larger dextrans will be more suited to the hydrogels. The increased binding strength, combined with the higher achievable number of carboxylic acid groups result in stronger hydrogels being produced from the larger dextran molecules.

Part 2 - Production and Evaluation of Dextran / Concanavalin A Hydrogels

The second part of this work investigated the characteristics of the hydrogels produced with dextran and conA. Three techniques were used to characterise the gelling process itself and the response of the hydrogels to glucose.

The first section details the rheological work performed on the gelation process. This entailed mixing the hydrogel and allowing it to set between the plates of the rheometer. The change in the viscosity properties were then measured as the hydrogel set.

The second section investigated the diffusional properties of the hydrogels when placed into a flow chamber. Hydrogels were cast in a mould and then placed into a two compartment flow cell. Cytochrome C was then used as a tracer to investigate the diffusion rates possible though the hydrogels.

The third section details the swelling rate of the hydrogels when cast within a cuvette. A large molecular mass dye was used to measure the rate of uptake of water into the hydrogel.

Section 5. Rheology

Rheological experiments were performed in a Bohlin CVOR200 rheometer.

Section 5.1. Theory

The Bohlin CVOR200 rheometer was set up with a cone and plate configuration (see Section 5.1.1). Approximately 1.5ml of solution was poured onto the bottom, flat, plate. The upper plate (4^o cone) was then lowered into position. Any excess solution was removed from the edge of the cone to ensure no interference from solution not in the measuring system. The cone was then rotated in the desired manner and the resulting response was measured by the lower plate.

Section 5.1.1. Cone and Plate Measuring System

The oscillatory tests were performed in a cone and plate measuring system. This configuration has a flat plate as the lower section of the system. The upper section is a cone of a low angle.

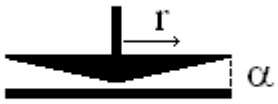

Figure 5-1 Cone and plate measuring system, of radius, *r*, and angle, *α*.

The shear rate on the fluid is found by dividing the velocity, *v*, of the upper plate by the thickness, *z*, of the fluid it is shearing. In this case, assuming that the angle is small (angular velocity = ω):

$$v = \omega r \qquad \textbf{Equation 5-1}$$

$$z = r\tan(\alpha) \approx r\alpha \qquad \textbf{Equation 5-2}$$

$$\dot{\gamma} = \frac{\omega r}{\alpha r} = \frac{\omega}{\alpha} \qquad \textbf{Equation 5-3}$$

Therefore the shear rate across the fluid is independent of the radius, greatly simplifying the conversion of experimental data into viscometric terms.

Section 5.1.2. Rheological Solutions

An ideal Newtonian solution has a constant viscosity when sheared. It is highly unlikely that dextran behaves in this way. Many solutions show either pseudoplastic or thixotropic behaviour, that is the viscosity decreases with increasing shear rate and time respectively. More rare are dilatant and rheopectic solutions whose viscosity increases with shear rate and time respectively. Viscoelastic materials are those that show both viscous and elastic response to stress, resulting in more complex responses to applied stresses [110-113].

Section 5.2. Viscosity of Pure Dextran

Section 5.2.1. Experimental Procedure

The rheometer was set to use a 20mm 4^{o} cone and plate system. The shear rate was ramped from $10s^{-1}$ to $500s^{-1}$ and back over the course of 2000 seconds. The steady state viscosity found in the low shear rate portion was recorded as the viscosity of the solution. Each dextran was tested at 15, 20 and 25wt% in the standard buffer (Section 2.2). The viscosity data was recorded on both the upsweep and downsweep of the experiment.

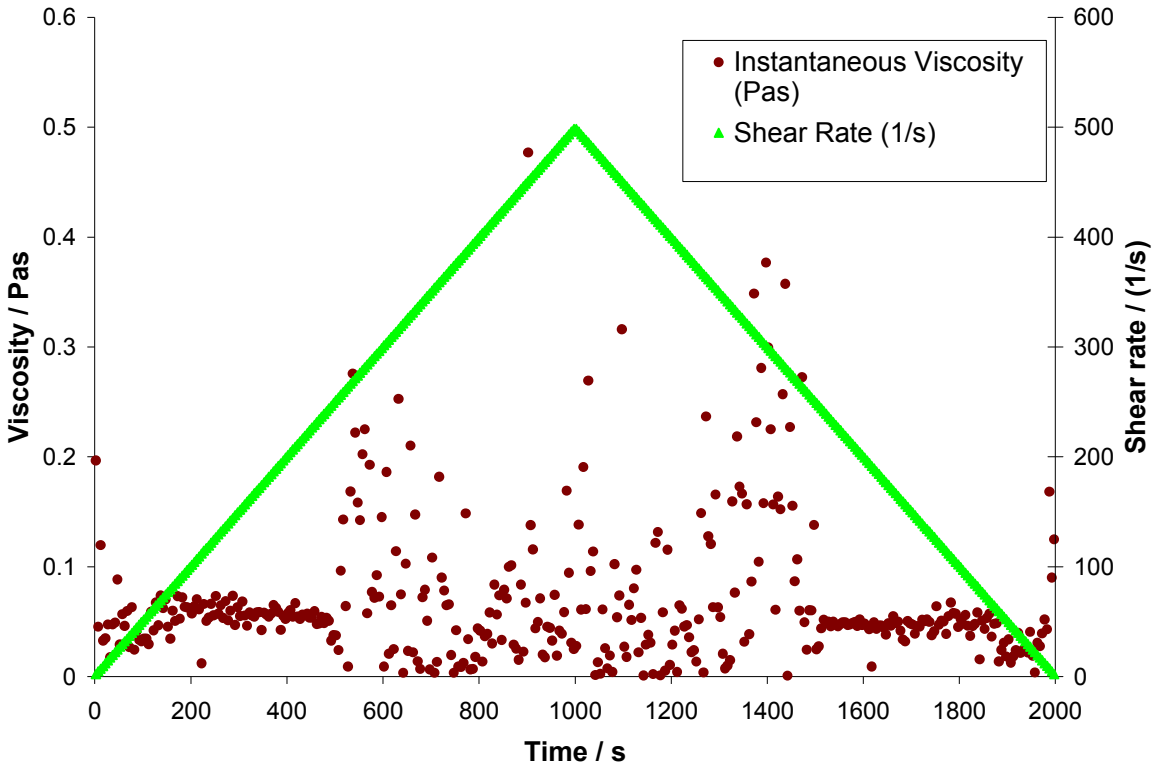

Figure 5-2 Viscosity test of 20wt% 43kD dextran

Shear rate increased linearly from 10 to 500s^{-1} and back over 2000 seconds. Viscosity recorded every 5 seconds

Section 5.2.2. Results and Discussion

The data shown in Figure 5-2 represents a 20wt% solution of 43kD dextran. It can be seen that, after an initial fluctuation, the viscosity is relatively constant prior to a shear rate of approximately 250s^{-1}. The viscosity then fluctuates unpredictably until the shear decreases below the same rate. This was observed for all dextran samples. Further tests performed using other fluids and measuring systems within the same rheometer implied that this was likely a problem with the machine rather than an actual change in the viscosity of the solution. The rheometer is able to directly control either strain rate or stress meaning this problem is unlikely to be due to the control system. However, it could be due to the rate of rotation not changing smoothly, or due to an uneven mass distribution on the rotating head.

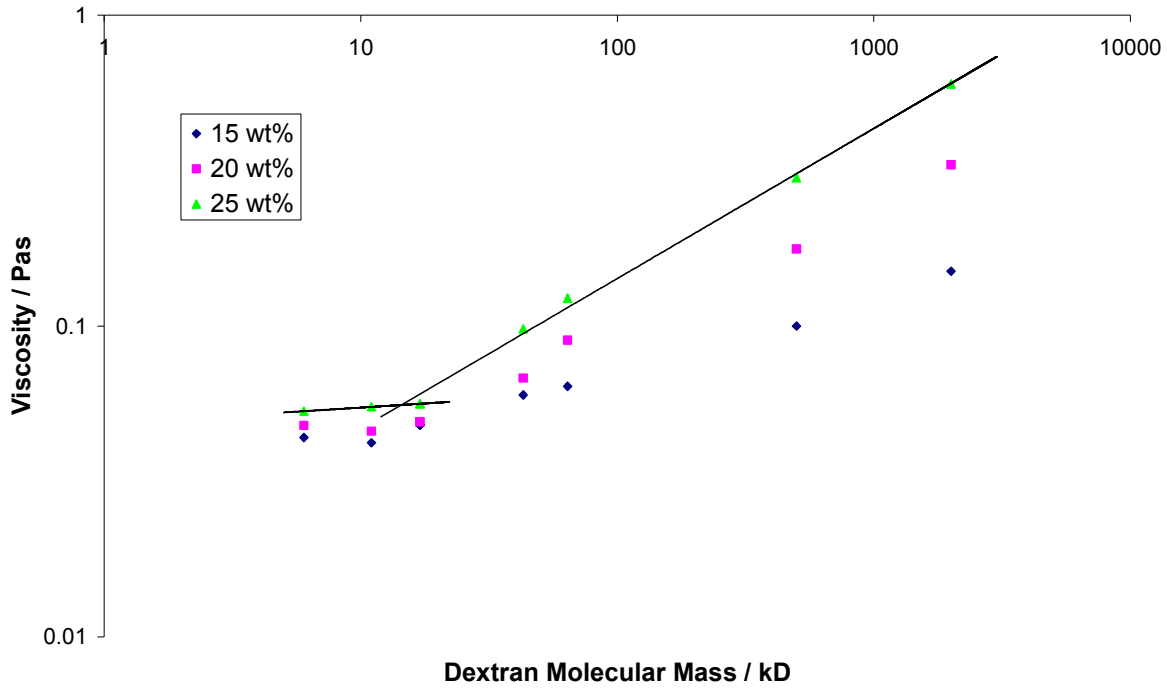

Figure 5-3 Viscosity of dextran solutions, shear rate increasing

Dextran at 15, 20 and 25wt% in standard buffer (Section 2.2)

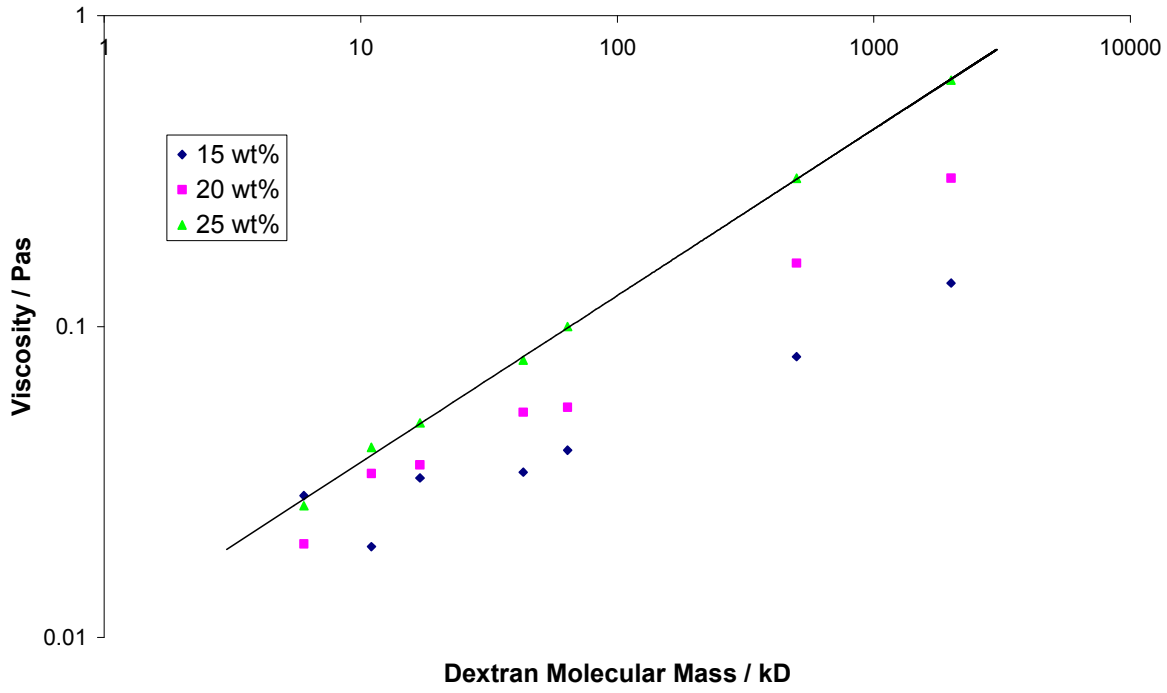

Figure 5-4 Viscosity of dextran solutions, shear rate decreasing

Dextran at 15, 20 and 25wt% in standard buffer (Section 2.2)

The viscosity values show the same overall pattern during both an increasing shear rate sweep and a decreasing shear rate sweep. As the molecular mass and the concentration increase, the viscosity increases.

The values during the decreasing sweep are generally slightly lower than those of the increasing sweep, implying pseudoplastic behaviour, though the effect is only slight. The lower molecular mass dextrans show an additional feature. The viscosity on the increasing sweep is near constant between 6, 11 and 17 kD dextrans, but at a critical dextran size, the viscosity increases much more rapidly. On the decreasing sweep the data fits one trend for all dextran sizes, though the low molecular masses do not perfectly fit this trend at the lower concentrations. It is known that low molecular mass dextran readily forms beads [86, 94] and it is likely that the initial viscosities recorded are for a combination of a dextran solution and a dextran bead suspension. The high shear rate in the middle of the experiment fully dissolves the beads that were present, making the solution more uniform and therefore fit the overall trend seen in the remaining data.

Section 5.2.3. Conclusions

The dextran solutions produced followed the expected trend of increasing viscosity with increasing molecular mass and increasing concentration. Some signs of pseudoplastic behaviour were observed, but this was a small factor. The change in viscosity of the lower molecular mass dextran implies the initial small beads created in dextran solutions are broken apart by the shearing force.

Section 5.3. Rheology of Gelation mixture

Section 5.3.1. Viscoelastic Materials

Dextran solutions do not exhibit pure Newtonian behaviour. Tests in Section 5.2 showed that the viscosity decreased with time during a ramped shear rate experiment. Other tests showed that the viscosity was not very stable at constant shear rates. The dextran solutions are likely to be viscoelastic in nature as the dextrans have been shown to form solid regions, in the form of beads, when in solution [86, 94].

In order to model the behaviour of dextran solutions they must be viewed as having both viscous and elastic properties. These can be defined by the equations for a Newtonian solution and by Hooke's law for a spring:

$$\sigma = \eta\dot{\gamma} \qquad \textbf{Equation 5-4}$$

$$\sigma = G\gamma \qquad \textbf{Equation 5-5}$$

It can be seen from these two equations that the shear stress for a solution is proportional to the rate at which it is being sheared. For a spring the stress is proportional to the magnitude of the strain.

Maxwell [111] developed a model which contained a Hookean spring and a Newtonian dashpot in series.

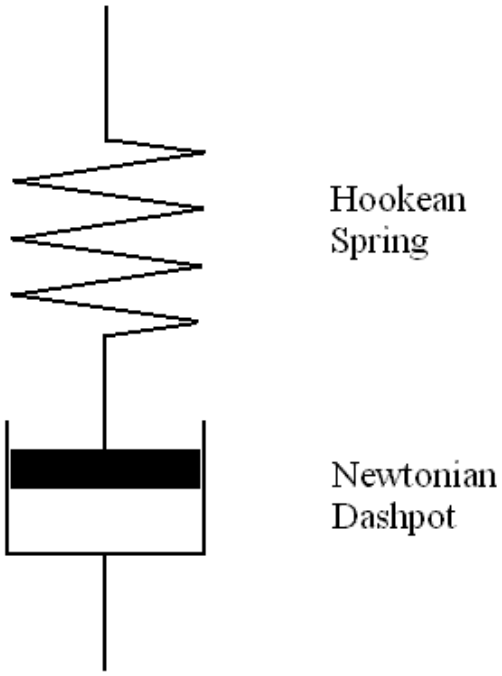

Figure 5-5 Depiction of a Maxwell model, incorporating a Hookean spring and a Newtonian dashpot in series

For a finite shear strain applied constantly over time, the spring will respond, giving a maximum stress. The dashpot will gradually release that stress through movement of the piston in the fluid. Combining Equation 5-4 and Equation 5-5 will enable the description of a viscoelastic fluid from the strain applied to it:

$$\dot{\gamma} = \frac{\dot{\sigma}}{G} + \frac{\sigma}{\eta} \qquad \textbf{Equation 5-6}$$

However it is still difficult to perform viscometric tests to obtain the values for the spring modulus and the viscosity.

Section 5.3.2. Oscillatory Tests

The nature of a viscoelastic material means that it cannot simply be sheared at a known rate such that viscosity can be calculated from the resulting stress. Oscillatory tests, known as dynamic mechanical spectroscopy, have been developed to investigate the combination of

the elastic and viscous properties [112]. Two specific values are obtained from oscillatory tests: that of the complex modulus, $|G^*|$, and the phase difference, δ. The complex modulus is the ratio of the peak shear strain applied to a substance and the resulting peak shear stress. The phase difference is a measure of the contributions of the two properties. A purely viscous solution would have a phase difference of 90^o as the stress would be proportional to the rate of shear strain. A purely elastic solid would have a phase difference of 0^o because the stress is directly proportional to the magnitude of the shear strain.

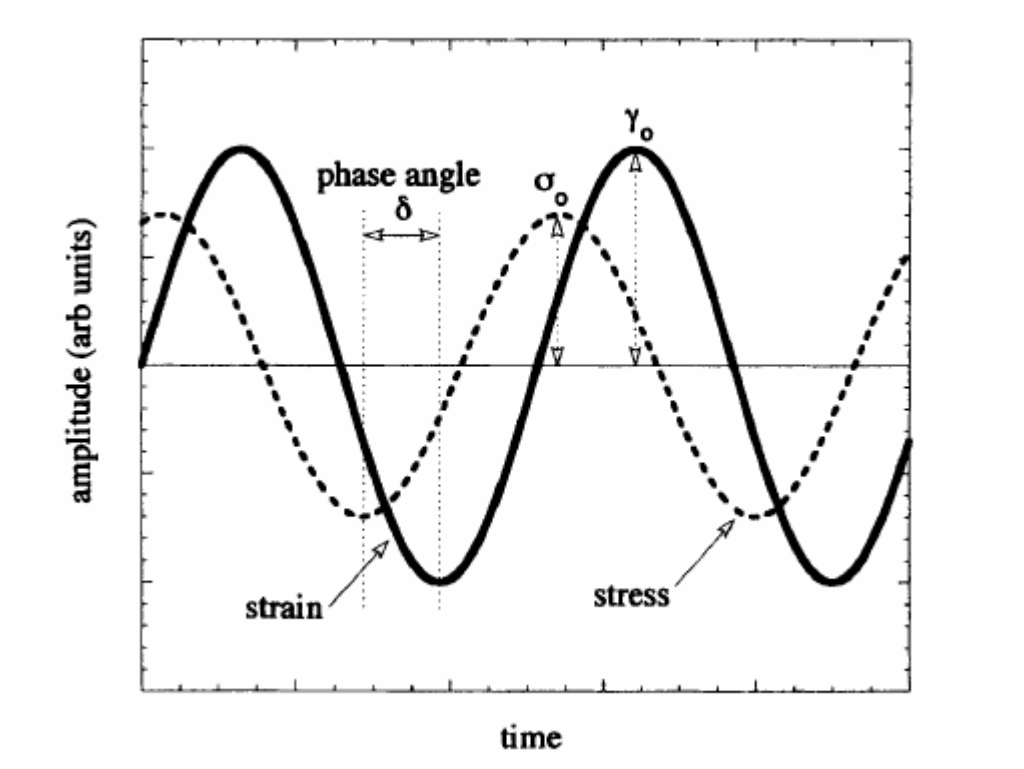

Figure 5-6 Application of an oscillating shear strain and the resulting shear stress (from [112])

Using the Maxwell model as a starting point, it is possible to model oscillatory shear strain and stress to obtain values for the complex modulus and the phase difference. (The derivation can be found in Appendix 8 and Appendix 10.)

Monitoring of the gelation process under an oscillatory strain shows the gel point and fluidity of the final hydrogel.

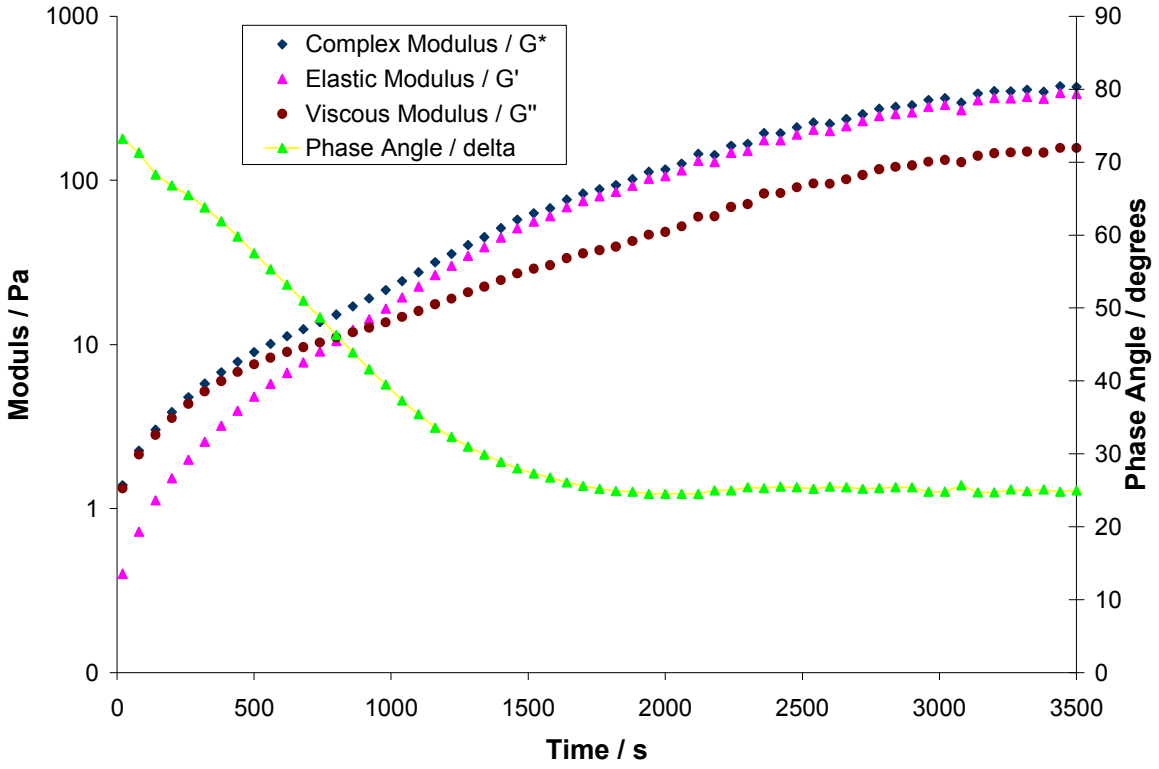

Figure 5-7 Oscillation at 1Hz and 0.5% of a 500kD dextran based gelation

In Figure 5-7 the phase angle describes the nature of the hydrogel mixture. Initially the mixture has a phase angle of over 70°, suggesting that the mixture is predominantly fluid. As time progresses the creation of covalent bonds between the conA and the carboxylic acid groups of the dextran, as well as the reversible interactions with the terminal glucose groups, causes the hydrogel to become more solid. At approximately 800s the phase angle decreases below 45°. It is now more solid than liquid, as confirmed by the elastic modulus now having a greater magnitude than the viscous modulus. This is known as the gel point [114, 115]. As time progresses the gelation process finishes and the phase angle reaches equilibrium. The final value of the phase angle, the time at the gel point and the rate of gelation at the gel point are characteristic of the gelation of a given mixture.

Section 5.3.3. Experimental Procedure

The gelation process was measured within a cone and plate system. The cone was oscillated at a frequency of 1Hz and a strain of 0.5%. The size of the strain was kept small to avoid deformation of the hydrogel as it began to set. The hydrogel mixture was produced as described in Section 2.6. The mixture was then placed onto the lower plate and the cone

lowered into place. Any excess mixture was removed to avoid interference with the measurements. The cone was then set to oscillate and the resulting stress measured.

Section 5.3.4. Results and Discussion

The dextrans of 50% 43, 64, 500 and 2000kD dextran (with the other 50% always being 500kD) were allowed to gel within the cone and plate system. The hydrogels made with 6, 11 and 17kD dextran did not have sufficient initial viscosity for the gelation process to begin, this problem being increased due to the mechanical work performed on the mixture by the oscillating plate. Due to this they did not produce viable results.

Table 5-1 Rheological Properties of Gelation

Dextran / kD	Gel Point Time / s	Gel Point G' and G" / Pa	Gel Point $\Delta\delta \times 10^2$ / ^{o}	Final Phase Angle / ^{o}	Final G* / Pa
43 – rep1	980	1.6	2.9	18.2	670
43 – rep2	620	1.5	4.9	14.2	1410
43 – rep3	2000	1.3	2.4	17.7	690
64 – rep1	440	1.7	4.7	19.8	2000
64 – rep2	300	2.8	8.4	15.9	4150
64 – rep3	280	2.5	7.5	15.1	4030
500 – rep1	840	10.7	3.5	24.8	350
500 – rep2	560	6.9	6.7	17.0	2690
500 – rep3	440	9.0	7.1	21.0	8000
2000 – rep1	560	26.0	7.2	17.9	7000
2000 – rep2	620	37.0	5.5	-*	-*
2000 – rep3	740	21.0	5.9	21.0	2830

*Experiment ended before steady state was reached

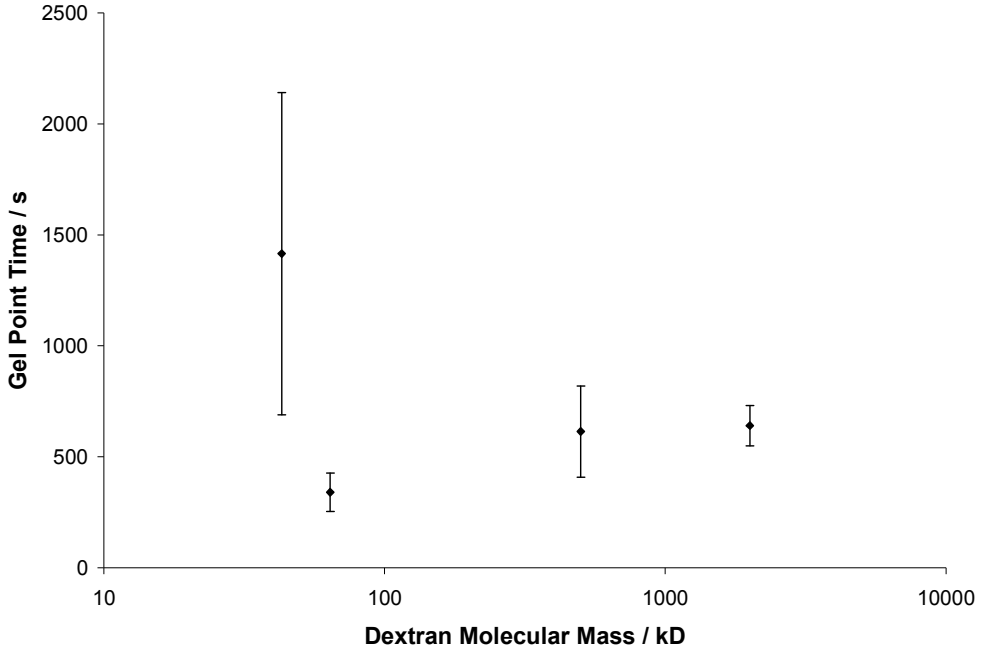

Figure 5-8 Time for gel point to be reached for hydrogel mixtures (43, 64, 500 and 2000kD – average of three replicates, error bars show +/- 1 standard deviation)

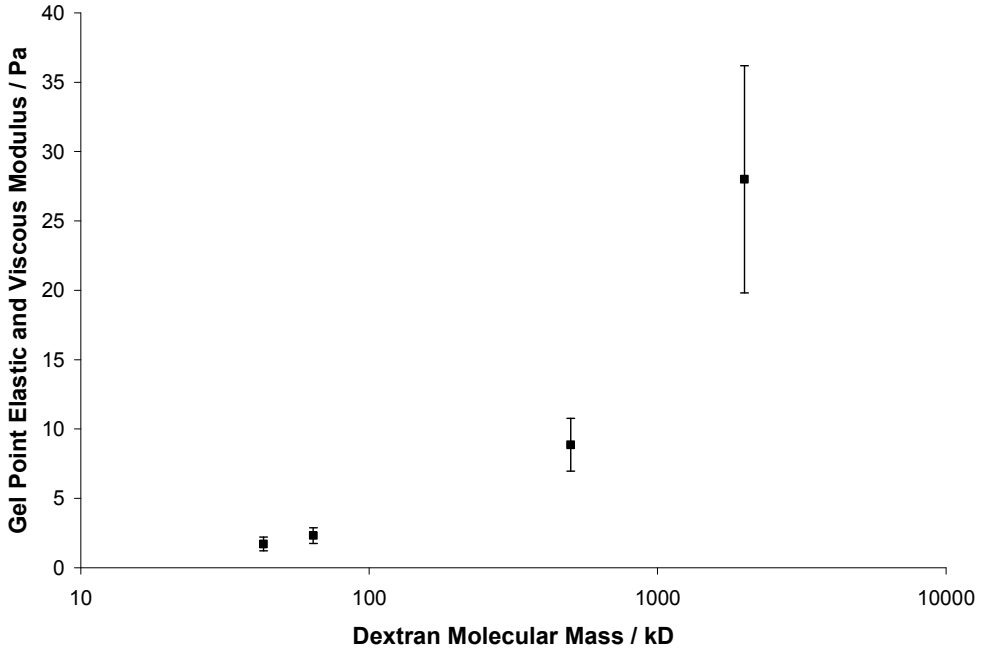

Figure 5-9 Complex and elastic modulus value at gel point (43, 64, 500 and 2000kD – average of three replicates, error bars show +/- 1 standard deviation)

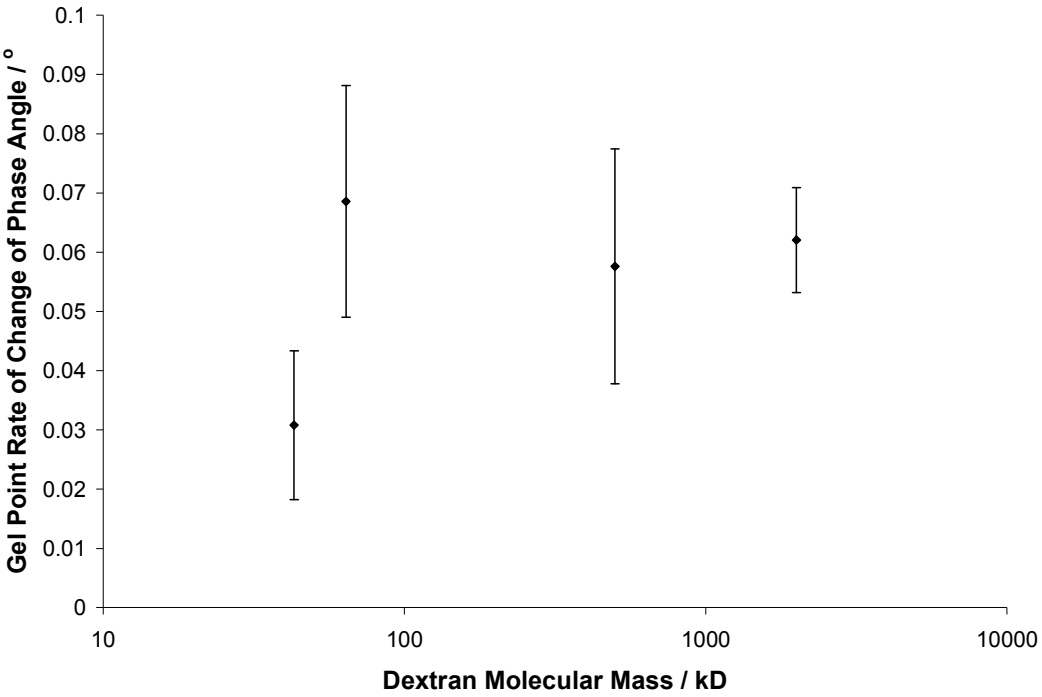

Figure 5-10 Rate of change of phase angle at gel point (43, 64, 500 and 2000kD – average of three replicates, error bars show +/- 1 standard deviation)

The data taken at the gel point is shown in Figure 5-8 - Figure 5-10. The value of the elastic and viscous modulus at the gel point shows a clear trend, similar to that of the viscosity of pure dextran solutions (see Section 5.2). The larger dextran molecules will reduce the amount of flexibility due to the increased number of interactions per molecule. This in turn increases the amount of force required to achieve the same shear, thereby increasing the modulus values.

The time for the gel point to be reached is difficult to quantify as there was a finite time to mix a solution and pour it onto the lower plate of the rheometer. There was also a delay whilst the upper plate is lowered into place and excess material removed. The inherent variability in this process is seen in Figure 5-8. The variability is greater for the weaker gels. This is unsurprising as the weaker gels have fewer affinity interactions and therefore will be more susceptible to the variability of the dextrans. The gel point, from this data, could be viewed as always occurring after the same period of time.

The rate of change of the phase angle at the gel point is also very variable. Once the gel is well mixed and within the rheometer, the conA and dextran will start to interact. The rate of the gelation is dependent upon the kinetics of the carboxylic acid group binding to the protein and the creation of new affinity interactions. The lack of a trend in this data would suggest, again, that the dextrans have an inherent variability in their production.

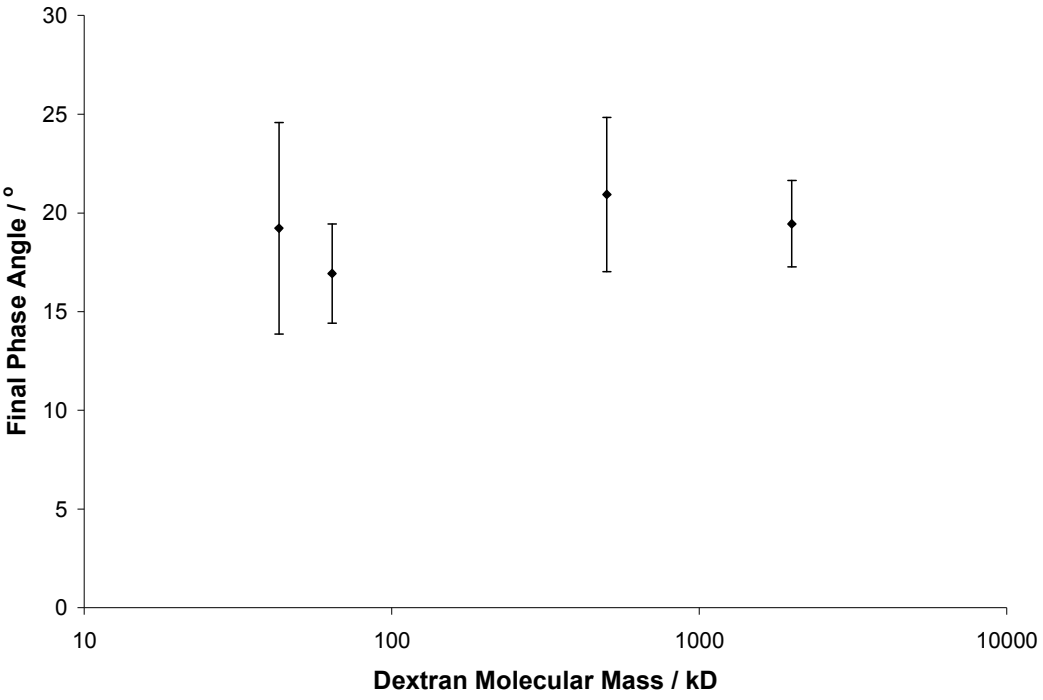

Figure 5-11 Final phase angle of hydrogel (43, 64, 500 and 2000kD – average of three replicates, error bars show +/- 1 standard deviation)

The final phase angle of the gels is relatively constant. The phase angle, a measure of the fluidity of the gel, is going to be based on the amount of water present within the gel and the strengths of the interactions. The amount of water is the same for each mixture and as such it is expected that the final phase angle is constant.

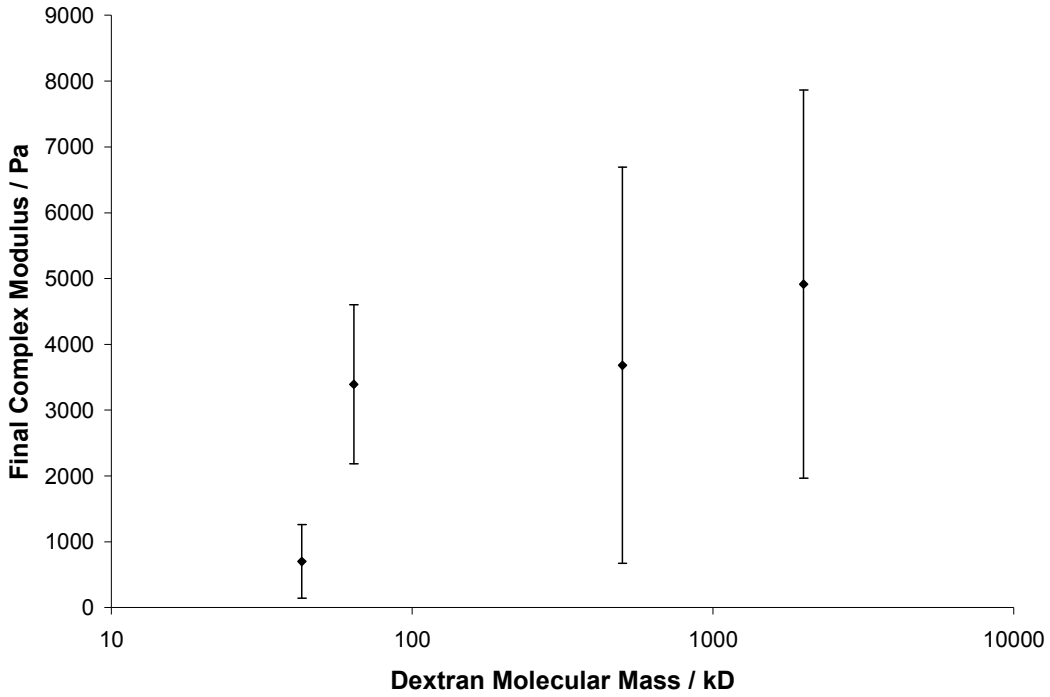

Figure 5-12 Final complex modulus of hydrogel (43, 64, 500 and 2000kD – average of three replicates, error bars show +/- 1 standard deviation)

The final complex modulus is very variable. This is primarily due to very few of the experiments having reached steady state. This is partly due to evaporation of the remaining water once gelation has finished. It is also due to the continued breakage and creation of the affinity cross-links.

Section 5.3.5. Conclusions

The rheology experiments have shown that there is a strong correlation between the molecular mass of the dextran and the complex modulus of the gel at the gel point. This corresponds to the increase in association constant seen in Section 3 as well as the increase in viscosity of pure dextran mixtures seen in Section 5.2. The ratio of the peak stress to peak strain of the system will be dependent upon both the inherent viscosity of the materials and the new bonds being formed by the gelation process.

The remaining features of the gelation process are either roughly constant, in the case of the time to reach the gel point, or show no correlation to the dextran molecular mass. The hydrogels produced within the system will not be responding exactly as expected due to the

deformation caused by the oscillatory tests. It is likely that the final complex modulus would have a similar relationship as the gel point complex modulus, but the hydrogels are damaged as they become more solid.

Section 5.4. Nomenclature

G	Spring Modulus (Pa)
v	Velocity (ms^{-1})
ω	Angular velocity ($rads^{-1}$)
r	Radius (m)
z	Thickness of fluid between plates (m)
α	Angle of upper plate to the horizontal (^{o})
γ	Shear strain
$\dot{\gamma}$	Shear strain rate (s^{-1})
η	Viscosity (Pas)
σ	Shear stress (Pa)
$\dot{\sigma}$	Shear stress rate (Pas^{-1})

Section 6. Diffusion Rate Experiments

Diffusion rate experiments were carried out using a Shimadzu UV1601 and an in house produced flow chamber. The primary aim of the hydrogels produced in this work was for there to be a change in the swelling of the hydrogel in the presence of glucose, thus increasing the diffusion rate of a protein through the material.

Section 6.1. Hydrogel Theory

The hydrogels are a mixture of conA and CM-dextran. The covalent bonds between the carboxylic acid groups and amine groups on the conA molecule provide a base structure which is supplemented by the reversible interactions of the terminal glucose groups of the dextran and the saccharide binding sites on the conA. A hydrogel, as implied by its name, is a highly hydrated system. This results in the hydrogel acting like a concentrated solution rather than a solid material within a liquid. Therefore there are strong osmotic forces acting on the hydrogel, trying to dilute the system. When some of the reversible interactions are stopped by the presence of glucose in solution, there are fewer resistances to the osmotic forces, resulting in a swelling of the hydrogel. The swelling of the hydrogel causes the inherent mesh size of the system to increase, allowing diffusion of larger molecules and of greater diffusion of smaller molecules.

Section 6.2. Hydrogel Production

The original technique for casting hydrogels of CM-dextran and conA devised by Zhang [101] was found to be difficult to use reliably. It was therefore necessary to perfect the production method prior to the experimental work of this section.

The original approach involved casting a mass of gel between two clingfilm coated glass plates, the plates being large enough to contain three usable hydrogels. Nylon gauze, to increase the strength of the hydrogel, was placed into the hydrogel mixture before the upper plate was placed on top. Spacers were used to ensure the desired thickness of hydrogel. In order to be able to cast the hydrogels, the final mixture was allowed a period of 30 minutes to partially set, thus increasing the viscosity and allowing the mixture to be poured onto the glass sheet without it overflowing the sides of the glass plate.

Removing one of the glass plates, to enable removal of the cast hydrogel, proved very difficult. In order to successfully separate them it was necessary to submerge the plates, allowing the hydrogels to hydrate and therefore not adhere as strongly to the clingfilm. However this was sometimes still not sufficient. It also resulted in several hydrogels being fully hydrated before required, resulting in wastage of protein.

For the mixtures involving the lower molecular mass dextrans the period of time the mixture was allowed to partially set increased to several hours. This was deemed unworkable, due to the possibility of the mixture setting in the beaker before it was poured. The combination of these two problems resulted in the decision to make individual moulds.

The resulting moulds were still problematic due to the clingfilm adhering to the hydrogels. Parafilm was therefore tried instead. The more robust nature of the parafilm made preparation of the moulds simpler, both physically and visually. The removal of the glass plates from the parafilm was much simpler than for clingfilm and a small droplet of ethanol between the parafilm and the hydrogel edge resulted in rapid separation - the hydrogel then being rinsed in distilled water to remove residual ethanol.

Casting the hydrogel mixtures in the moulds, particularly of hydrogels involving lower molecular mass dextran, involved pouring the freshly combined final mixture into the mould. These hydrogels were found to not swell as much as the hydrogels cast after the 30 minute pause. It was assumed that there were some covalent bonds being formed between the mixture and the nylon support mesh. The hydrogels were therefore cast without the mesh support. Instead, an additional mesh support was placed in the diffusion cell, upon which was placed a hydrated hydrogel.

Section 6.3. Experimental Conditions and Data Analysis

Section 6.3.1. In-House Diffusion Chamber

A diffusion cell was contructed to test the hydrogels. It consisted of two matching halves: one to act as the donor chamber, the other to be the receptor chamber (see Figure 6-1). Each chamber had baffles so as to aid mixing. The open surface area between the two chambers, where the hydrogel would be positioned was $4.6 \times 10^{-4} m^2$. On opposite sides of each chamber were inlet and outlet holes for connecting the necessary tubing. In the four corners are holes that pass through the whole depth to allow the system to be bolted together.

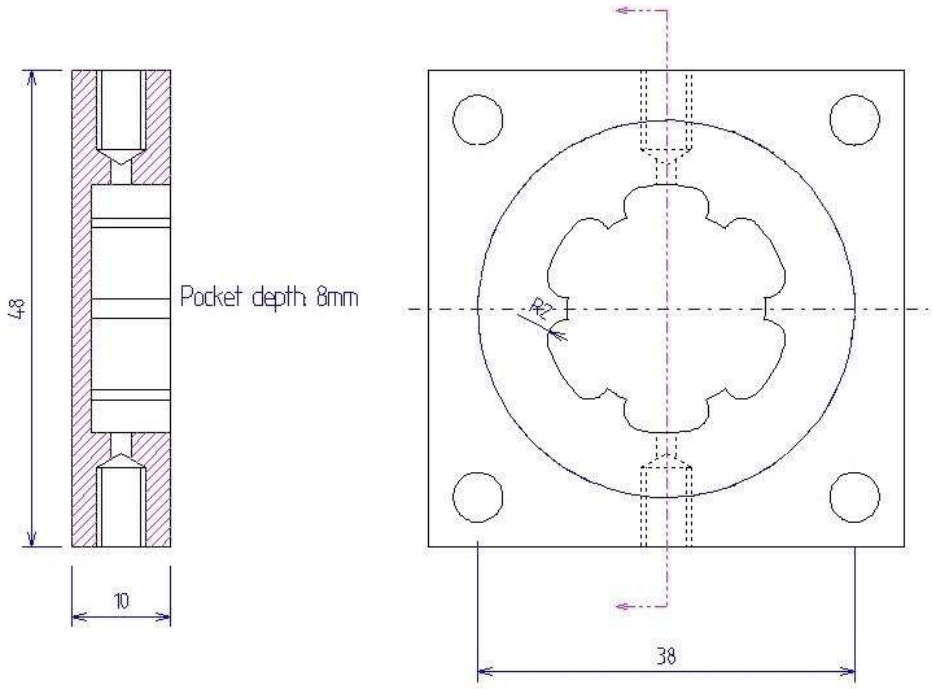

Figure 6-1 Schematic of diffusion cell.

Side view shows baffled chamber with two connection holes. Plan view shows central hollow chamber, with baffles. The surrounding ring is the indented step for placement of the membrane. The four corner holes are for bolts to hold the two halves together.

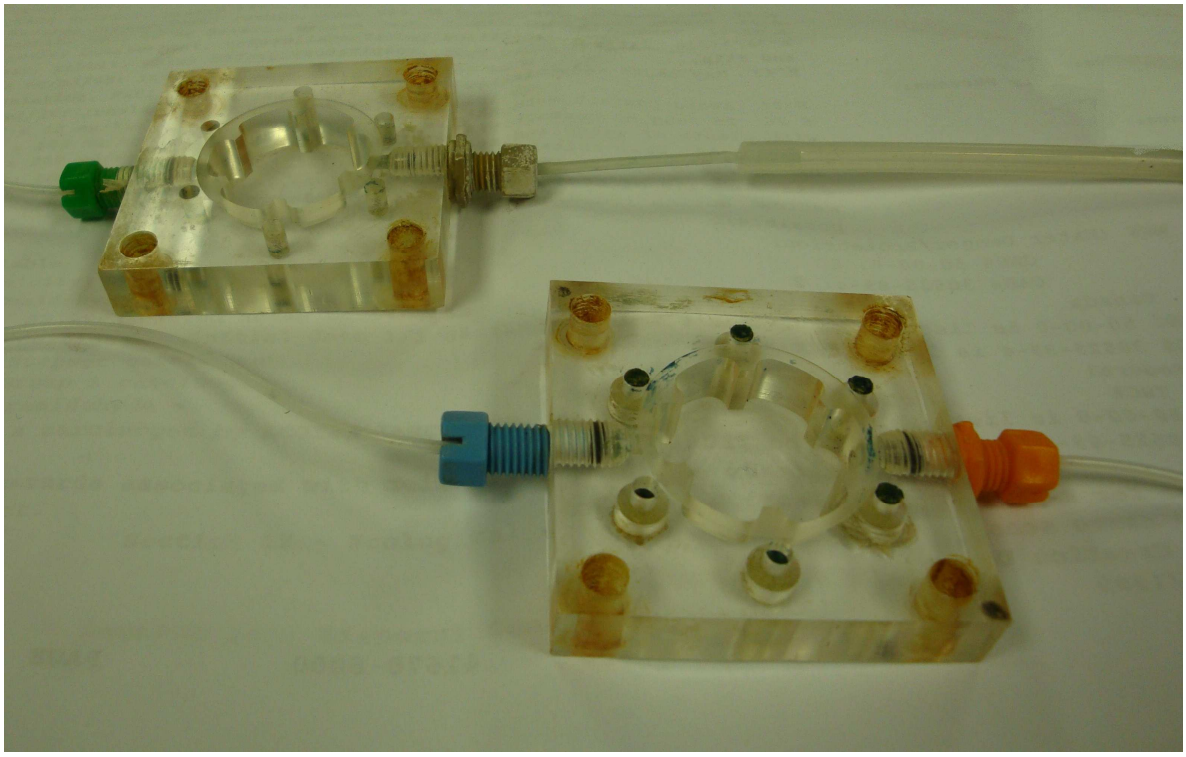

Figure 6-2 Photograph of diffusion cell.

The two halves of the diffusion cell. The additional holes (seen as dark blue marks) around the central chamber were for a separate purpose and for these tests have been filled with silicon sealant.

Section 6.3.2. Experimental Conditions

The key characteristic of hydrogel performance is the rate of diffusion of protein. In order to find this the hydrogel membrane was placed in a flow cell which had a known volume on each side. Through the donor chamber a solution was pumped containing the target molecule (e.g. insulin) and, where applicable, the molecule which causes the hydrogel to swell or contract (D-glucose). The liquid in the receptor chamber was passed through a UV Spectrophotometer, which monitored the protein transmitted from changes in absorption of the receiving solution at the appropriate wavelength.

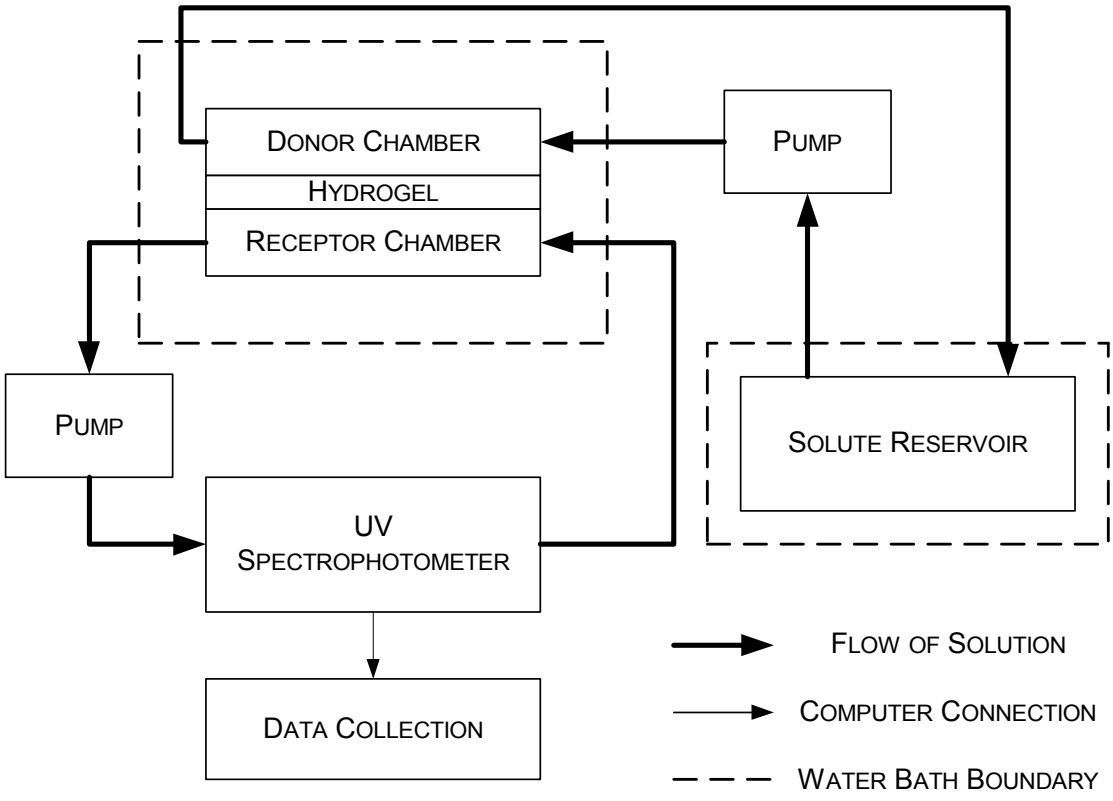

Figure 6-3 Schematic of flow cell set-up.

The receptor chamber / UV half is a closed loop. The donor chamber / solute reservoir side has a sufficient excess of solution to ensure constant concentration on the donor side.

The solute reservoir and the flow cell were kept in a waterbath at 37^{o}C reflecting physiological conditions. The standard buffer (see Section 2.2) was also used for this reason. The receptor chamber was agitated with a magnetic flea at 180 rpm to prevent a stagnant layer of protein from forming beneath the hydrogel. Both pumps operated at recycle flow of 10ml min^{-1}.

Cytochrome C (cytC) was used as the solute during flow experiments in place of insulin due to cost and ease of detection. It is a heme protein of 12kD, making it approximately twice the mass of an insulin monomer. Work by Kataoka *et al.* and Bohidar on cytC and insulin has shown that at 37^{o}C and pH 7.4 the hydrodynamic radii are 1.7 and 7.5nm respectively [116, 117]. The insulin is larger than expected due to aggregation. The liquid

phase diffusivities of cytC and insulin are 11.4 and 5.5 $x10^{-11}m^2s^{-1}$ [116-118]. These were considered sufficiently similar to justify the use of cytC.

As can be seen in Figure 6-4, cytC has a very vivid red colour allowing for simple detection in the UV spectrophotometer. The use of 410nm as the target wavelength, rather than a wavelength associated with general protein absorption is that there will be no interference from any possible leakage of conA from the hydrogel.

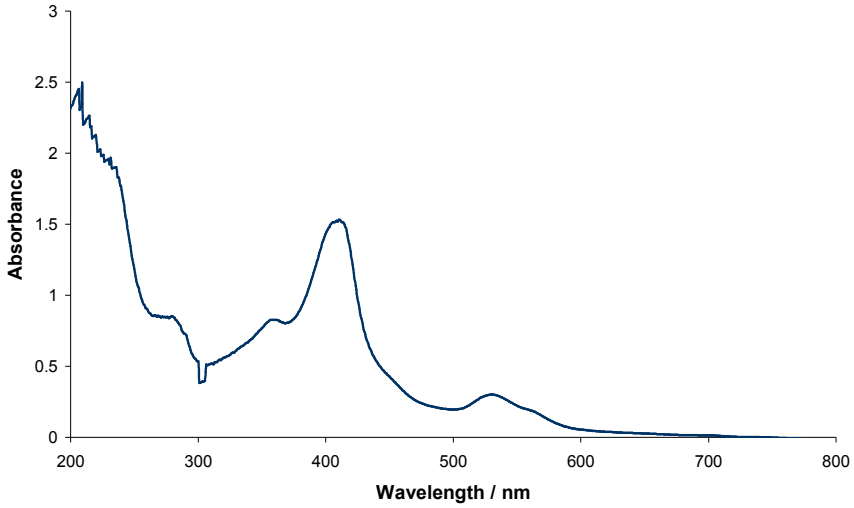

Figure 6-4 Absorption spectrum of cytochrome C showing the strong absorbance at 410nm.

The absorption of 410nm wavelength radiation is linear with respect to concentration, enabling simple conversion of absorption data into terms of concentration of cytC.

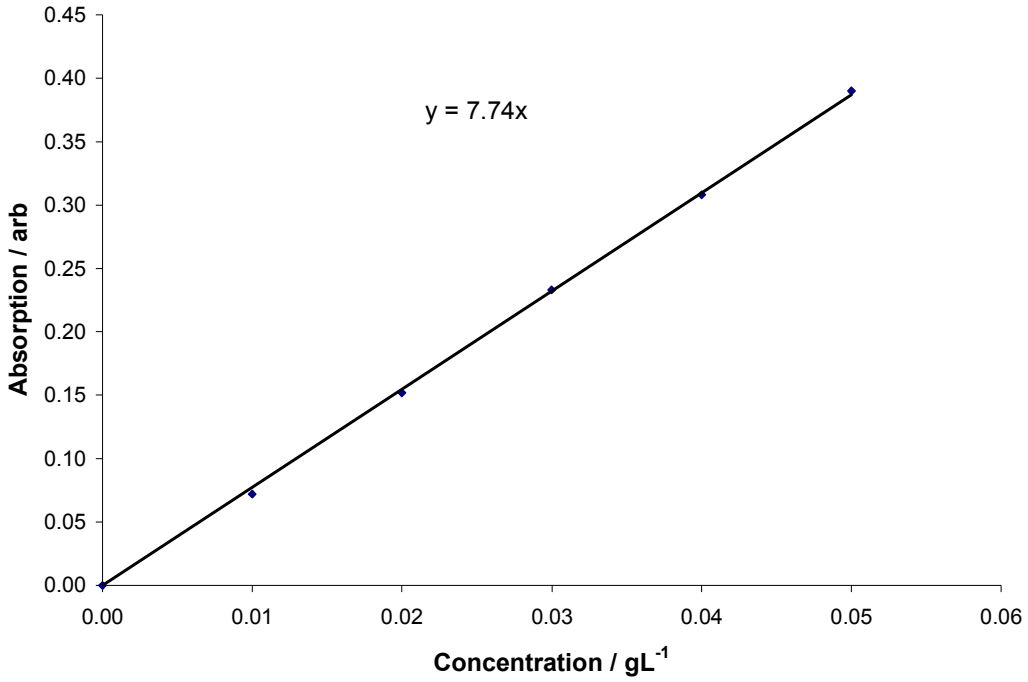

Figure 6-5 Calibration graph of various concentrations of cytochrome C, enabling conversion of spectrometric data from absorbance units to concentration units.

Hydrogels were produced using the method detailed in Section 2.6. Hydrogels containing 50% 6, 11 or 64KD dextran were found to not form solid hydrogels. This corresponds to the dextrans which were found to have less than one carboxylic acid per molecule (see Section 2.3). In the case of the two smallest dextrans there would also be a limited amount of affinity cross-linking per molecule which again resulted in a weak hydrogel.

Once cast, gels were allowed to come to room temperature before being removed from the mould and placed into the flow cell. Once in the flow cell, buffer was circulated through the system to allow full hydration for 30 minutes. In this situation the receptor side piping is operated as an open loop so that it can be flushed of any remaining cytC. Once hydrated the following procedure was followed:

- Magnetic stirrer was set to agitate the receptor chamber.
- Flow cell was placed in water bath with cytC reservoir.
- Receptor side piping was made a closed loop (ensuring minimal air bubbles enter the system).

- Open ends of donor side piping were placed in reservoir of $0.05gL^{-1}$ cytC.
- Pump and UV data logger were turned on simultaneously.
- CytC circulated through donor side for 10 minutes.
- Pump stopped and piping moved to $0.05gL^{-1}$ cytC reservoir containing desired concentration of glucose.
- Pump turned on and glucose / cytC mixture allowed to circulate for 10 minutes.
- Pump stopped, receptor side closed loop opened and both sides flushed with buffer for 10 minutes.

Each hydrogel was used until destruction or for one day. The concentration of glucose in the second reservoir was raised incrementally over the course of the experiments, with at least two replicates being performed at each concentration.

Section 6.3.3. Data Analysis

The flow cell experiments produced data such as that shown in Figure 6-6.

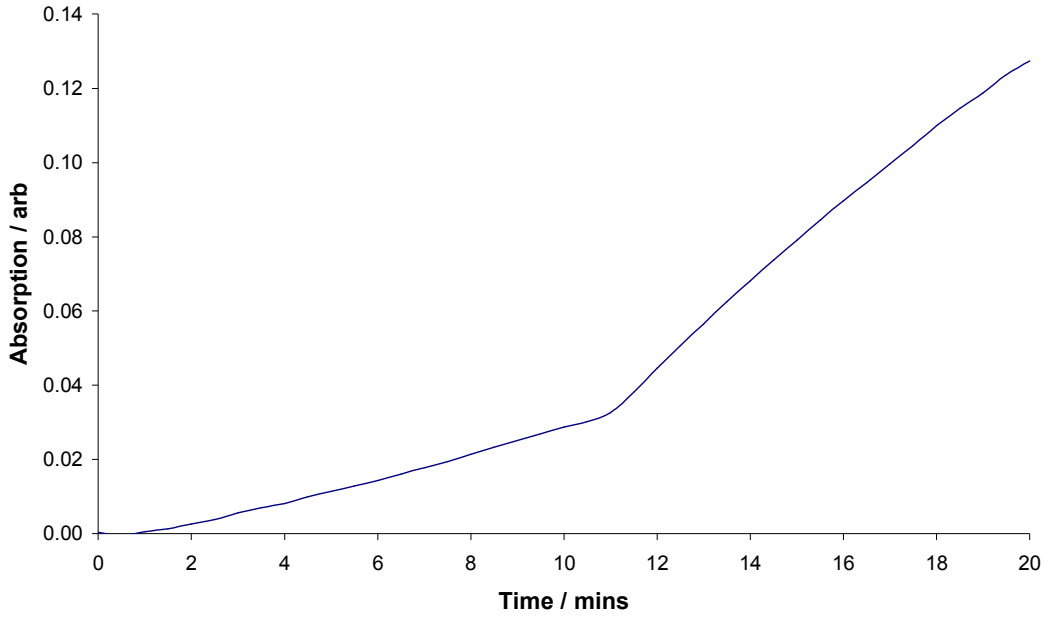

Figure 6-6 Time course of cytC passage through a 500kD dextran hydrogel. Addition of 0.075M Glucose at 10 minutes

The data was first converted into concentration of cytC from the absorption data using the calibration curve, Figure 6-5. The gradient of the data is the concentration flux through the

hydrogel, in $gL^{-1}min^{-1}$. The initial gradient, between 0 and 10 minutes is the rate at which cytC passes through the hydrogel without additional swelling effects caused by the presence of glucose. There is a lag phase, after the introduction of glucose at 10 minutes, before the rate of concentration flux increases. This is due to the finite period of time required for the concentration of glucose to reach steady state in the donor chamber and for the cytC that has diffused through the hydrogel to reach the UV beam. The perceived tail-off of the concentration flux, at approximately 19 minutes is due to the rate of diffusion through the hydrogel ceasing to be the limiting factor.

Therefore the concentration flux before and after introduction of glucose was taken as the gradient between 7 and 10 minutes and between 12 and 15 minutes respectively. For each experiment, the ratio of the pre- and post-glucose concentration flux was the quoted figure. This compensates for the fact that each hydrogel has a different concentration flux in the absence of glucose.

Section 6.3.4. Swelling Model

Diffusion through a hydrogel can be modelled by assessing the cross-linked structure and calculating the mesh size created by the degree of swelling. Within the conA – CM-dextran hydrogels there are covalent cross-links between the carboxymethyl groups and the amine groups of the conA and there are affinity cross-links between the terminal glucose groups and the conA binding sites. Together these hold the two components together forming the hydrogel.

The mixture of conA and CM-dextran, when fully hydrated, acts as a concentrated solution and osmotic forces try to force the hydrogel to swell. The combination of the covalent and affinity cross-links cause the gel to act as a spring which opposes this force. When the competitor, glucose, is introduced the number of affinity cross-links decreases resulting in a weaker opposition to the osmotic forces leading to swelling.

Flory-Rehner [119, 120] proposed a theory to explain the relationship between crosslink density and swelling in rubber compounds. Peppas and Merrill [121] have modified this original equation to produce a relationship which allows the calculation of the swelling ratio of hydrogel based materials:

$$\frac{1}{\overline{M}_c} = \frac{2}{\overline{M}_n} - \frac{\frac{\bar{\upsilon}}{V_1}\left[\ln\left(1-\upsilon_{2,s}\right)+\upsilon_{2,s}+\chi_1\upsilon_{2,s}^2\right]}{\upsilon_{2,r}\left[\left(\frac{\upsilon_{2,s}}{\upsilon_{2,r}}\right)^{\frac{1}{3}}-0.5\left(\frac{\upsilon_{2,s}}{\upsilon_{2,r}}\right)\right]}$$

Equation 6-1

Where: $\overline{M_c}$ – Number average molecular mass of the polymer chain between cross-links

$\overline{M_n}$ – Number average molecular mass of the polymer chain

$\bar{v}$ – Partial specific volume of the polymer

V_1 – Molar volume of water

χ_1 – Flory polymer-solvent interaction parameter

$v_{2,s}$ – Polymer fraction of the gel at equilibrium swelling

$v_{2,r}$ – Polymer fraction of the gel after gel formation

The total number of cross-links was determined by finding the respective number of affinity and covalent bonds. The number of covalent bonds was assumed to equal the number of carboxymethyl groups measured for the dextran material used (see Section 2.3) as it was assumed that each binds to a conA molecule. Affinity cross-links were calculated by solving the binding equation. It was assumed that there was only one dextran binding per tetramer. Although this is not strictly rigorous, the modelling was greatly simplified. Once swelling had been calculated the gel mesh size could be estimated and used to determine the gel phase diffusion coefficient of the solute molecule. (see Appendix 12).

The following equation can be used to calculate the mesh size:

$$\xi = v_{2,s}^{-1/3}\left(\frac{2C_n\overline{M_c}}{M_r}\right)^{1/2} l$$

Equation 6-2

Where: C_n – Flory characteristic ratio

M_r – Molecular mass of repeat unit

l – Unit length along the polymer backbone

The swelling ratio can be found by dividing the polymer fraction of the gel after formation by the polymer fraction after swelling. The volume increase due to the swelling will be seen as a reduction in the polymer fraction, therefore the swelling ratio will be greater than 1:

$$Q = \frac{v_{2,r}}{v_{2,s}} \qquad \textbf{Equation 6-3}$$

The mesh size can then be used to calculate the rate of diffusion, based on the deviation from the liquid phase diffusivity [122, 123]:

$$D_{gel} \cong D_l\left(1 - \frac{r}{\xi}\right)e^{\frac{-1}{Q-1}} \qquad \textbf{Equation 6-4}$$

Where: D_l – Liquid phase diffusivity of the solute

r – Hydrodynamic radius of the solute

This diffusivity value can be used to calculate the concentration flux through a hydrogel. The amount of protein that diffuses through the membrance can be found using Fick's first law:

$$J = D\frac{dC}{dy} = \frac{D(C_D - C_R)}{\delta_G} \qquad \textbf{Equation 6-5}$$

Where J is the flux through the hydrogel per unit area per unit time, δ_G is the swollen membrane thickness and C_D and C_R are the donor and receiving chamber concentrations respectively.

A mass balance can then be taken on the receiving side of the flow cell to obtain the concentration flux:

Mass at time, t = Mass at time, 0 + Flux through the hydrogel

$$VC_{R,t} = VC_{R,0} + JAt$$
$$VdC_R = JAdt$$
$$J_C = \frac{dC_R}{dt} = \frac{D_{gel}(C_D - C_R)A}{\delta_G V} \qquad \textbf{Equation 6-6}$$

Where A is the surface area of the membrane and V is the receiving chamber volume [124]:

It can be assumed that the concentration of cytC in the receiving chamber is significantly less than the bulk concentration of the donor chamber:

$$J_C = \frac{D_{gel} A}{\delta_G V} C_D \qquad \textbf{Equation 6-7}$$

The swelling calculated in Equation 6-3 has a twofold effect on the proceeding calculations. The thickness of the hydrogel increases (it is assumed that the cross-sectional area is constrained by the flow cell and does not change), thus the path length for diffusion increases. It also, however, dilutes the conA and glucose terminal groups within the hydrogel, thus reducing the number of affinity cross-links. The modelling must therefore be done iteratively to find the values for the swelling and thus the concentration flux (A Power Basic model for this can be found in Appendix 13).

Several of the parameters are known from the literature or can be calculated directly from the masses used. For the calculation of the swelling:

Table 6-1 Swelling model parameters for 500kD hydrogel

Parameter	Value	Reference
Flory interaction parameter	0.473 (dextran/water)	[125]
	0.48 (dextran/salt water)	[126]
Partial volume of dextran	0.62 cm^3g^{-1} - 0.644cm^3g^{-1}	[125, 127, 128]
Polymer fraction of the gel	0.099gg^{-1}	Section 2.6
Number average molecular mass between covalent cross-links	4050$gmol^{-1}$	Section 2.3
Number average molecular mass of polymer chain	500kD	
Molar volume of water	18cm^3mol^{-1}	
Association constant, conA/dextran	2220M	Section 3
Association constant, conA/glucose	170M	Section 3
Concentration of conA [M_{tot}]	1.49 x10^{-4} M	Section 2.6
Concentration of terminal glucose groups [X_{tot}]	3.4 x10^{-2} M	Section 2.6

The calculation of the concentration flux from the swelling ratio of the hydrogel is performed using the parameters in Table 6-2.

Table 6-2 Mesh size, diffusivity and flux calculation parameters for 500kD hydrogel

Parameter	Value	Reference
Flory characteristic ratio	1.8 - 10	[124, 129]
Molecular mass of repeat unit	$162 gmol^{-1}$	
Unit length along polymer backbone	0.46nm	[129]
Liquid phase diffusivity of cytC	$11.4 \times 10^{-11} m^2 s^{-1}$	[118]
Hydrodynamic radius of cytC	1.7nm	[117]
Conc. of solute in donor chamber	$0.05 gL^{-1}$	
Thickness of cast hydrogel	0.48mm	
Volume of receiving chamber	$4.6 \times 10^{-6} m^3$	
Surface area of hydrogel	$4.6 \times 10^{-4} m^2$	

Initial estimates of the association constants for conA-dextran and conA-glucose were taken from the ITC work (see Section 3). However, those values are for reactions in free solution, whereas within the hydrogel there will be spatial constraints which might be expected to modify these values.

Section 6.4. Results and Discussion

Section 6.4.1. Experimental Data

Hydrogels were produced using mixtures of 50% 500kD CM-dextran with 50% of either 17, 43, 500 or 2000kD CM-Dextran (see Section 2.6) and used in the flow cell. The data in Figure 6-7 to Figure 6-10 represents the average of two or three replicates.

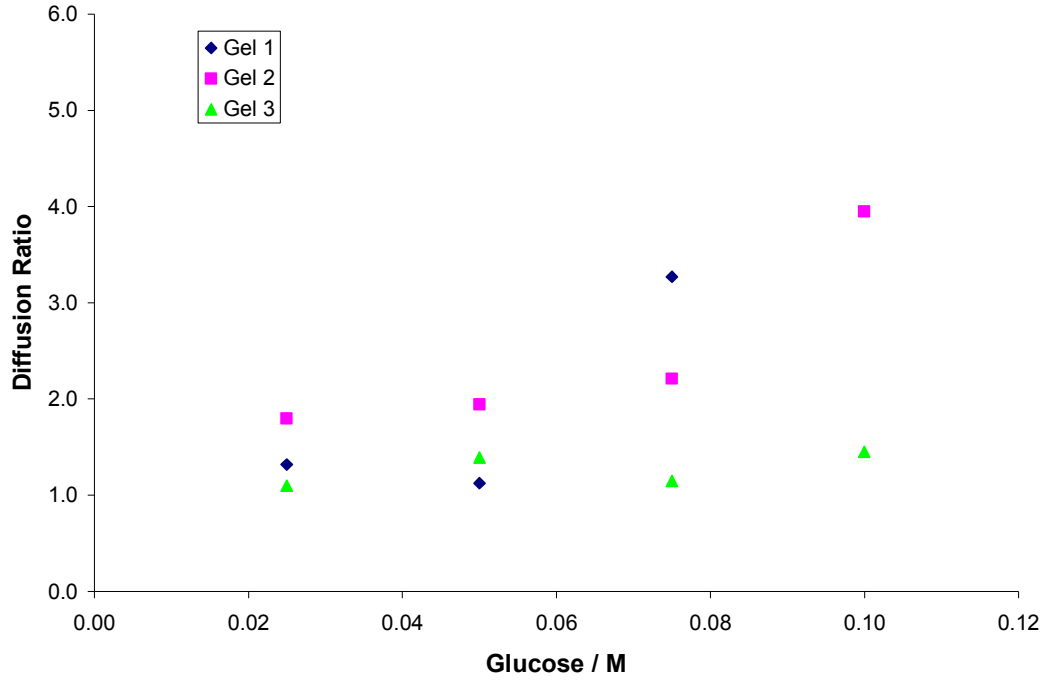

Figure 6-7 Diffusion ratio with respect to glucose concentration for 17-500kD hydrogels

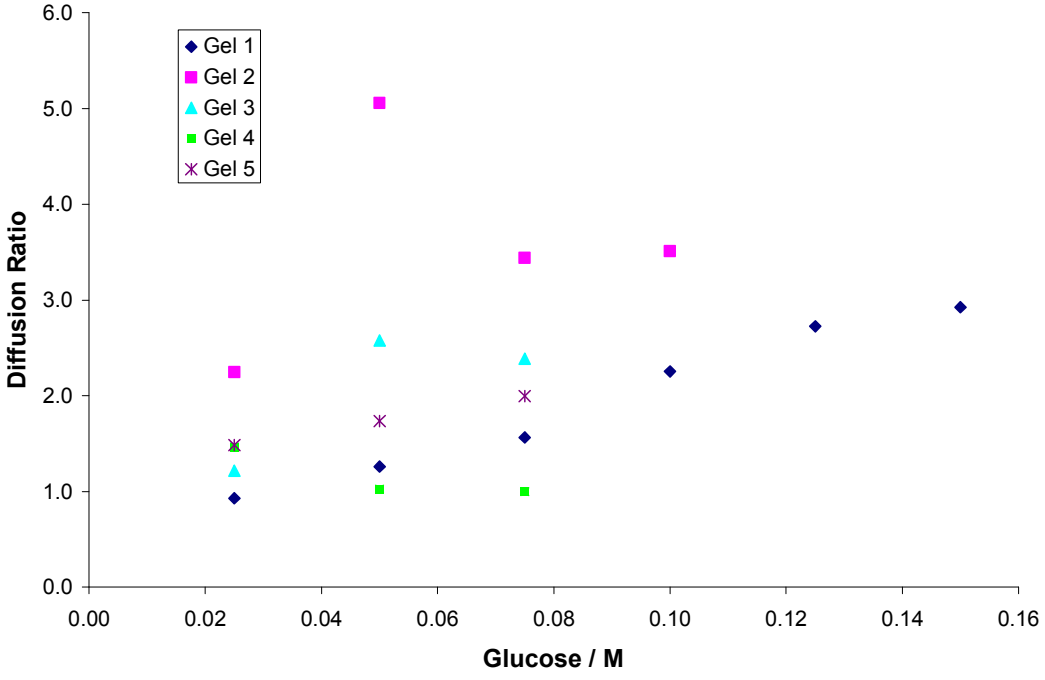

Figure 6-8 Diffusion ratio with respect to glucose concentration for 43-500kD hydrogels

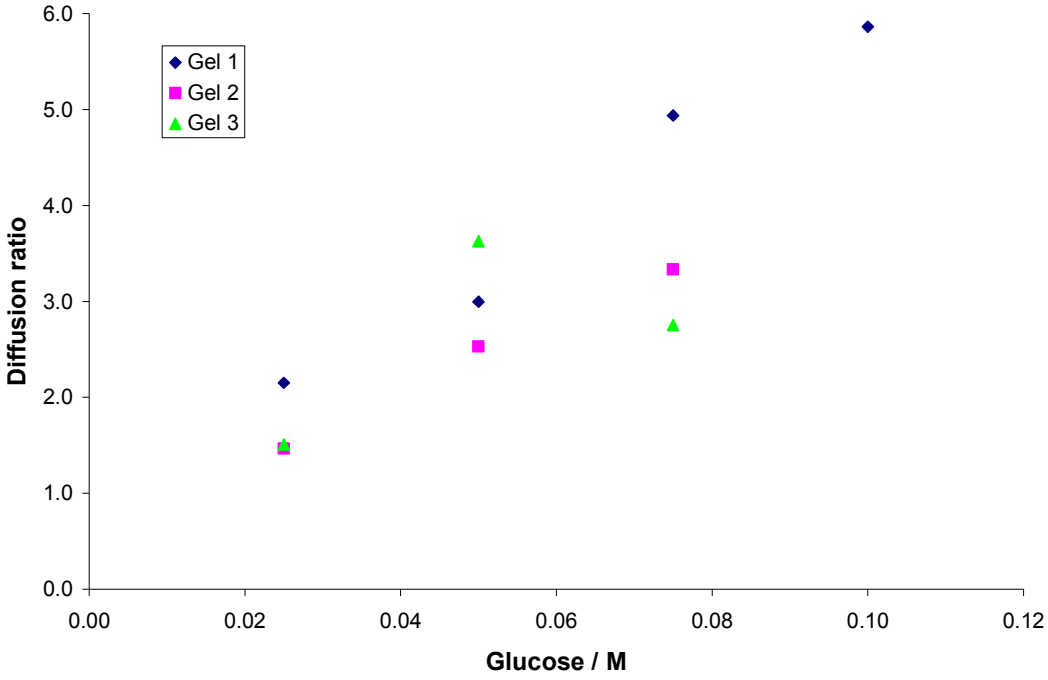

Figure 6-9 Diffusion ratio with respect to glucose concentration for 500kD hydrogels

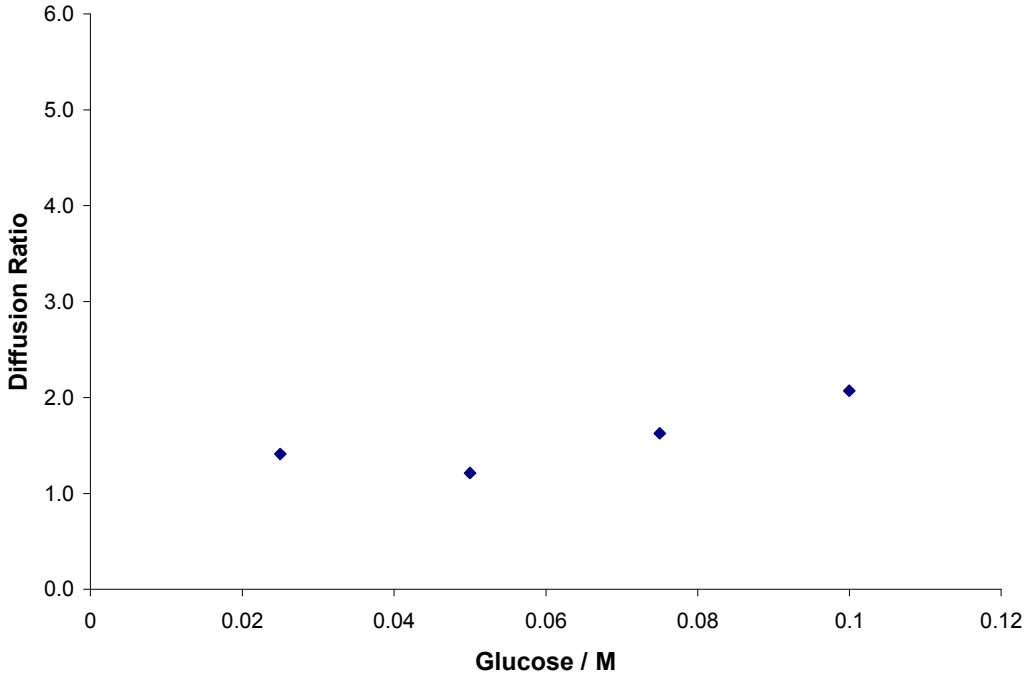

Figure 6-10 Diffusion ratio with respect to glucose concentration for 500-2000kD hydrogels

The majority of the hydrogels show a general trend of the diffusion ratio increasing with increasing glucose concentration. The 500kD hydrogel shows the greatest response to glucose concentration whereas the 500-2000kD hydrogel does not respond as much. The amount of data available was limited by the difficulty in removing the hydrogels from the mould. The 500-2000kD hydrogel was particularly difficult to extract without causing irreparable damage. There were a few instances of hydrogels suffering tears in the surface, normally by large air bubbles forcing through the surface. However it was possible to push the sides of the tears back together and the hydrogel could continue to be used with only a slight increase in diffusion rate. This was the cause of the jumps in the data where a low glucose concentration has a higher diffusion ratio than later tests with higher concentrations, e.g. 43-500kD gel 2.

Section 6.4.2. Swelling Model

The swelling model was used to replicate the behaviour of a 500kD hydrogel using the data in Table 6-1 and Table 6-2.

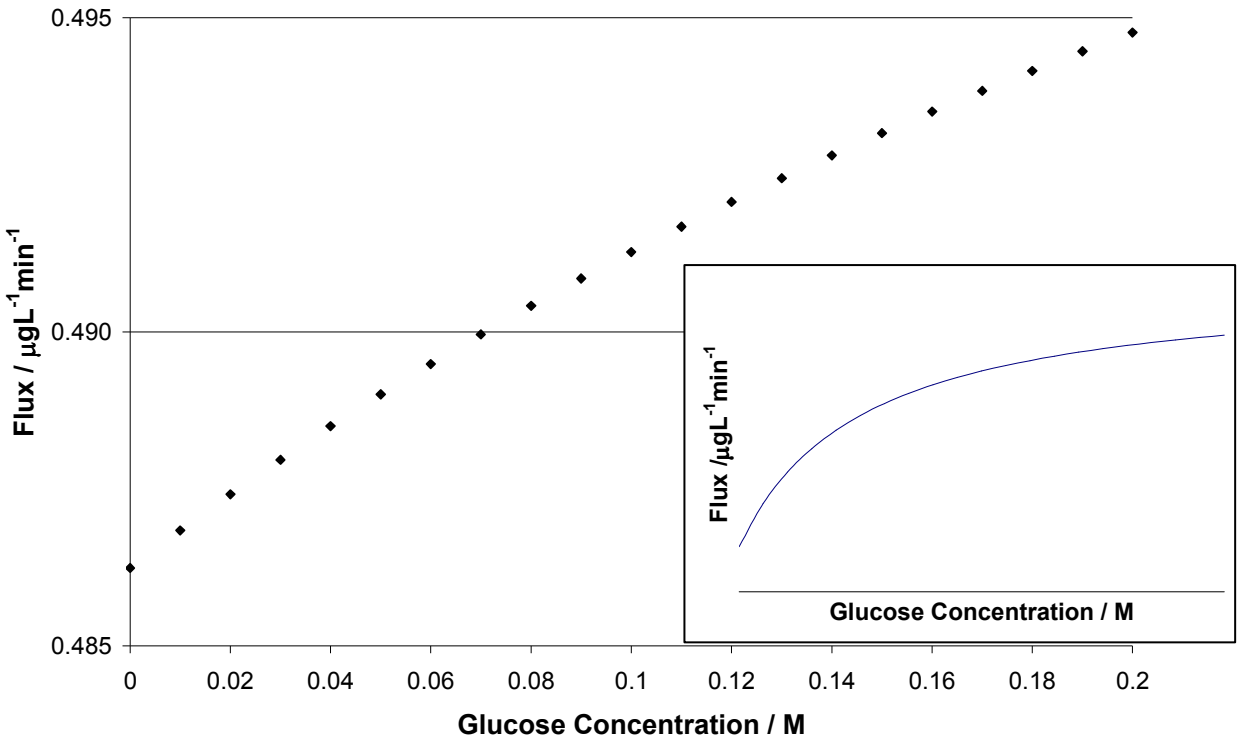

Figure 6-11 Concentration flux variation with glucose for 500kD hydrogel – Base model using data from Table 6-1 and Table 6-2. (Inset displays trend for all glucose concentrations)

The swelling model, when using the values from literature and direct calculations from this work is shown in Figure 6-11. Although this appears to show good variation with glucose concentration, the concentration flux variation is over a small scale and is very low. The inset graph shows the overall trend, that as the concentration of glucose increases it ceases to be the limiting factor. The hydrogels used in this work, at these glucose concentrations, are represented by the linear portion of this curve. The data shown in Figure 6-6 has a pre-glucose concentration flux of $0.45 mgL^{-1}min^{-1}$ and a concentration flux of $1.5 mgL^{-1}min^{-1}$ after the introduction of 0.075M glucose. In contrast, the model gives these values as $4.86x10^{-4}$ and $4.90x10^{-4}$ $mgL^{-1}min^{-1}$ for no glucose and 0.075M glucose resepectively. The data is therefore three orders of magnitude too high, compared to the swelling model: if the diffusion rate is assumed to be equal to the liquid phase diffusivity the rate is still only $7.13x10^{-2} mgL^{-1}min^{-1}$.

Of the data used in the swelling model, some of the parameter values are not necessarily accurate. Those that are from literature (such as the Flory Interaction parameter) and those that are definite calculations from experiments (such as the cytC concentration being $0.05 gL^{-1}$) will be assumed correct. However the concentrations of binding groups, the association constants, the Flory characteristic ratio, the backbone unit length and the membrane thickness were not definite values. Therefore a series of tests were performed whereby the stated parameter was increased and decreased by 20% to see which had noticeable effects upon the concentration flux through the hydrogel.

Section 6.4.2.1. Terminal Glucose Group Variation

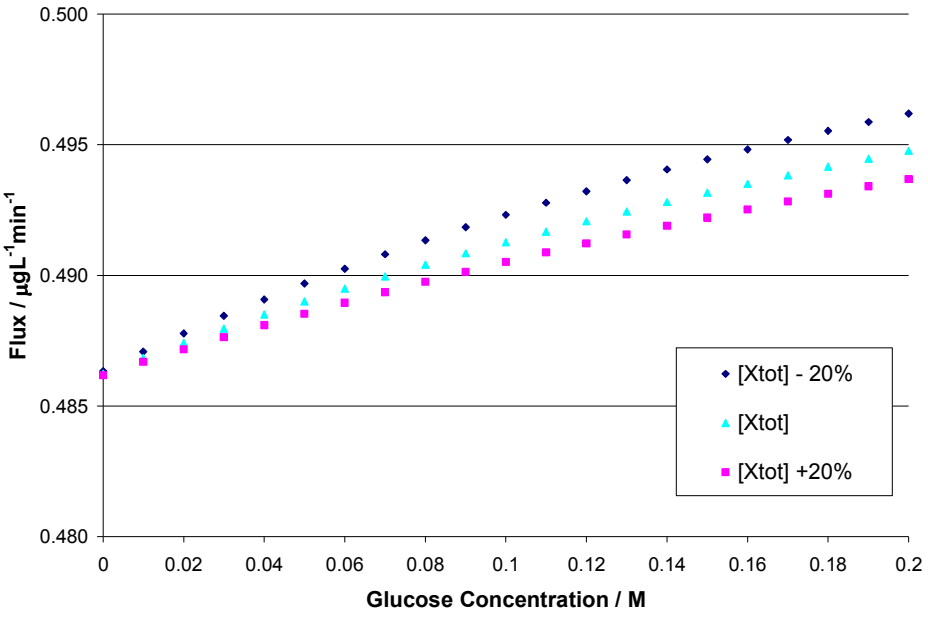

Figure 6-12 Concentration flux variation with glucose for 500kD hydrogel – Terminal glucose group variation

The model has been recalculated in Figure 6-12 with the concentration of terminal glucose groups altered. An inverse relationship is seen between concentration flux and terminal group concentration. This is expected. The number of groups available to form affinity cross-links with conA is likely to be lower than the maximum available due to the spatial restrictions caused by the covalent cross-links. However the change in concentration flux is minimal compared to the three orders of magnitude difference when compared to the experimental results.

Section 6.4.2.2. ConA Variation

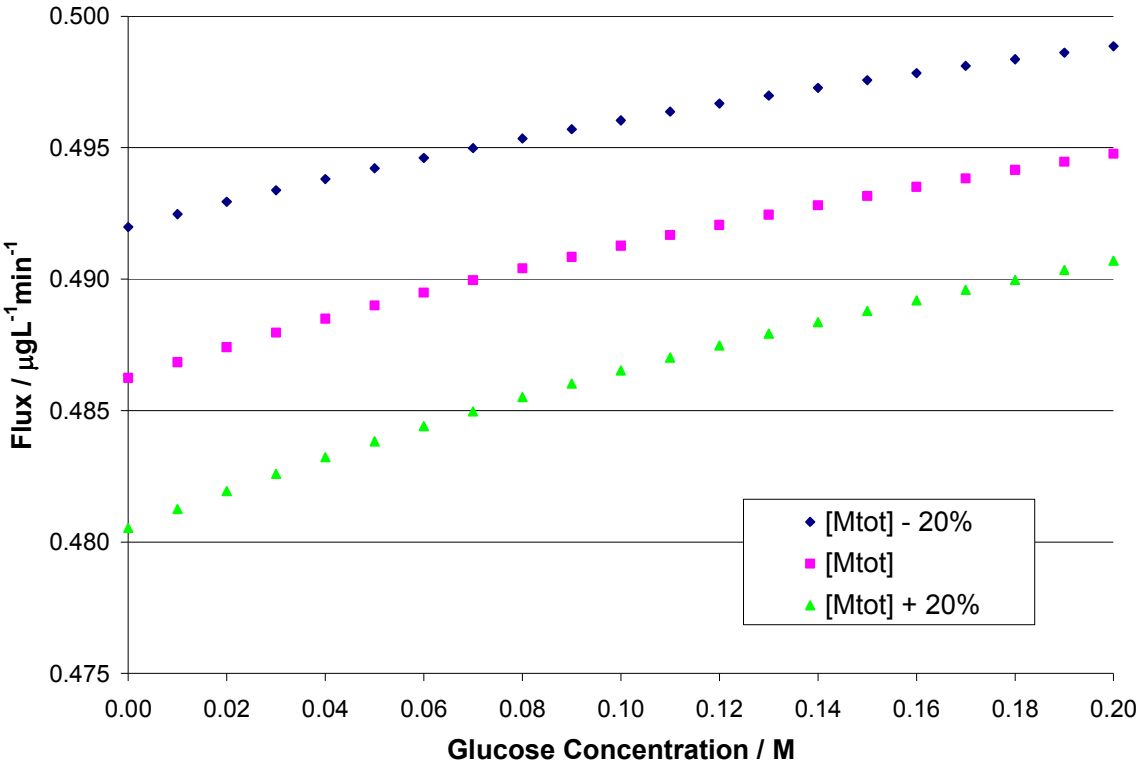

Figure 6-13 Concentration flux variation with glucose for 500kD hydrogel – ConA concentration variation

The concentration of conA in the hydrogel has a similar, though greater, effect on the concentration flux as the concentration of terminal glucose groups. A reduction in concentration allows greater concentration flux of glucose, but the variation is not sufficient to cause an order of magnitude change.

Section 6.4.2.3. Covalent Cross-Link Variation

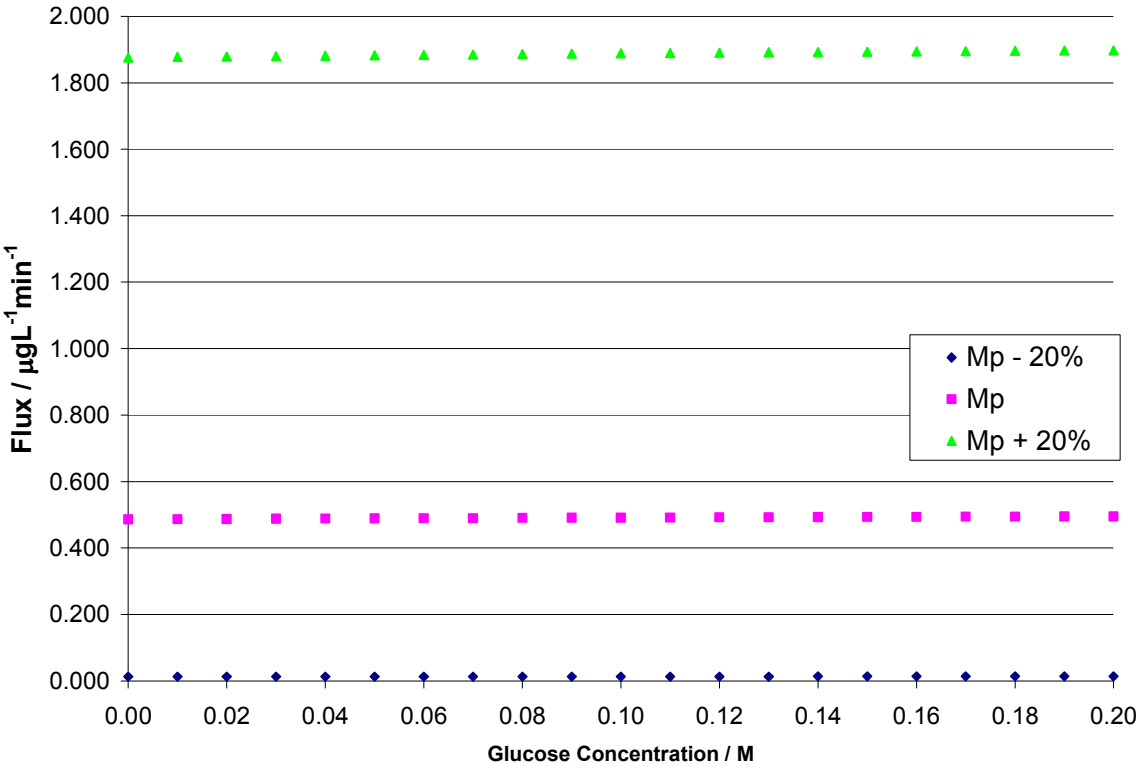

Figure 6-14 Concentration flux variation with glucose for 500kD hydrogel – Number average molecular mass between covalent cross-links variation

The average molecular mass between the covalent cross-links has a strong effect on the concentration flux through the hydrogel. It is plausible that, though the number of possible covalent cross-links per dextran is known, this is a maximum value and the number actually formed is lower than this (corresponding to a higher M_p value). This is capable of increasing the concentration flux by an order of magnitude, making the model slightly more realistic compared to the experimental data.

Section 6.4.2.4. Association Constant Variation

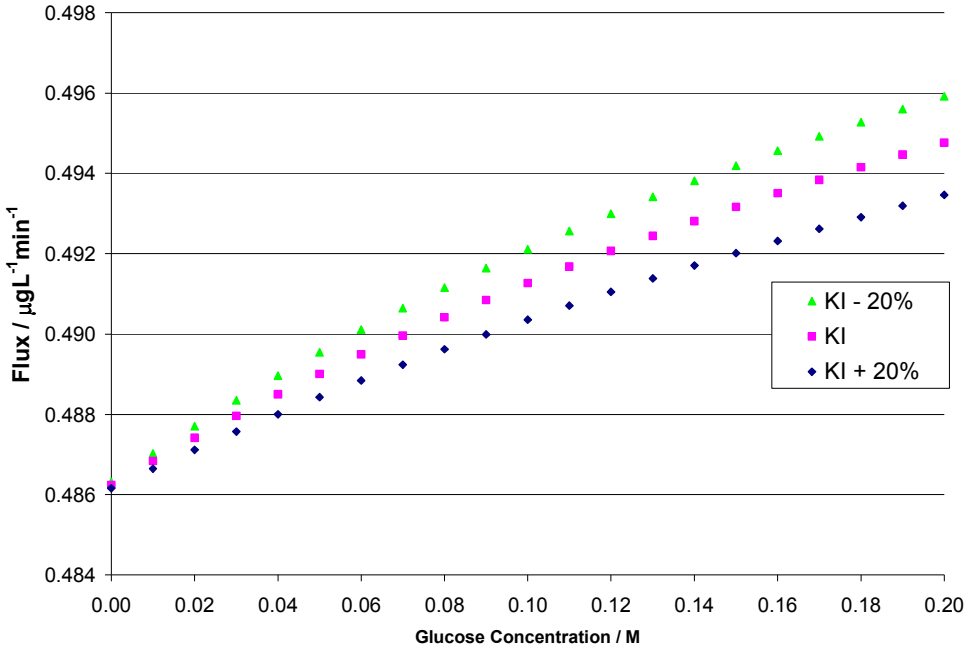

Figure 6-15 Concentration flux variation with glucose for 500kD hydrogel – ConA/dextran association constant variation

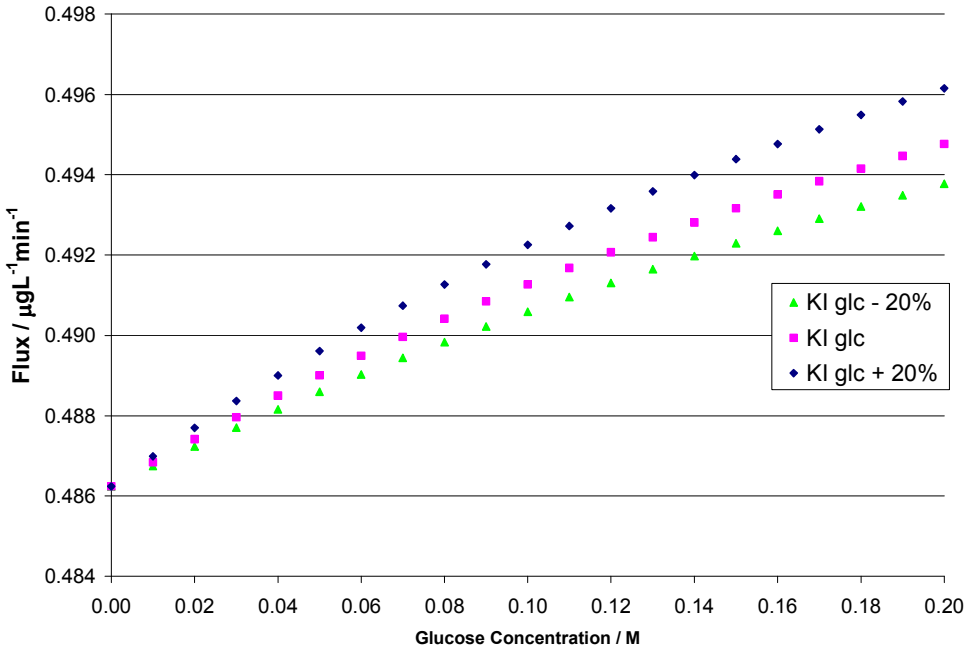

Figure 6-16 Concentration flux variation with glucose for 500kD hydrogel – ConA/glucose association constant variation

Decreasing the association constant between conA/dextran makes the hydrogel weaker, resulting in greater concentration flux. The difference is, however, only slight. The change in concentration flux caused by a variation in the conA/glucose association constant, Figure 6-16, is equally slight. The response is reversed as glucose is a competitor and therefore stronger affinity bonds with the conA will reduce the number of bonds available to the dextran.

Section 6.4.2.5. Flory Characteristic Ratio Variation

The value of the Flory characteristic ratio is not known from the literature. It can be seen from Figure 6-17 that over the range of feasible values it does not have a significant effect upon the concentration flux.

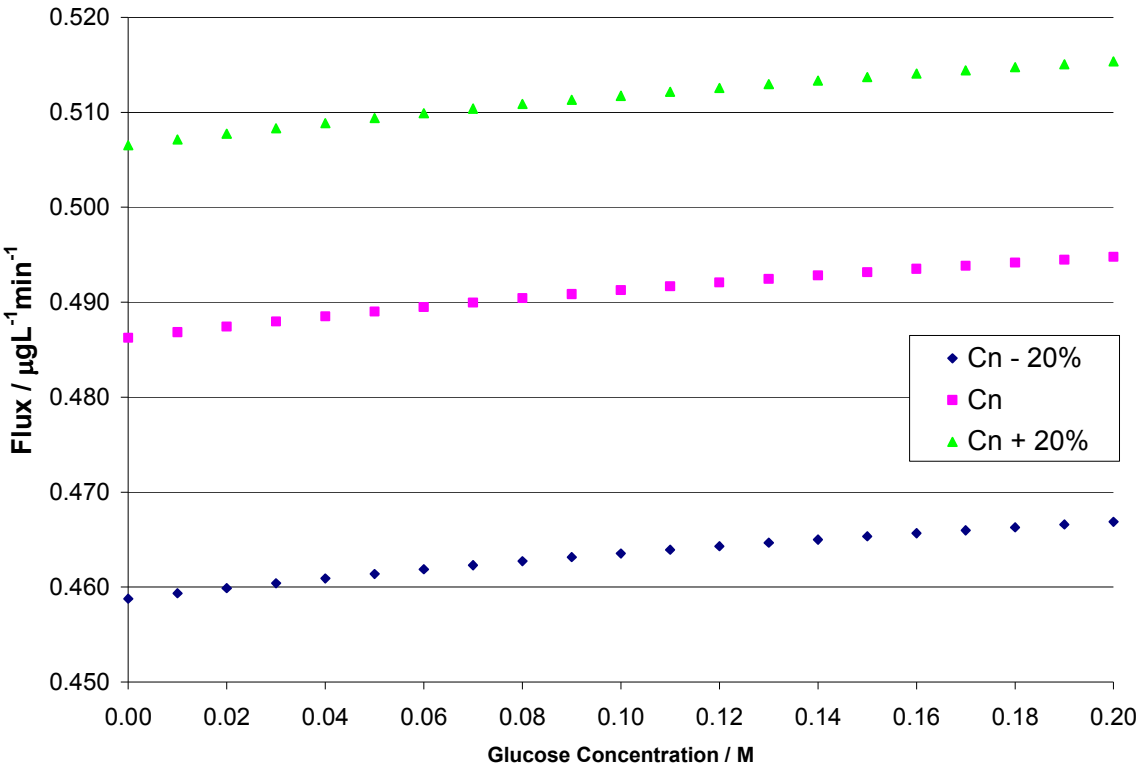

Figure 6-17 Concentration flux variation with glucose for 500kD hydrogel – Flory characteristic ratio variation

Section 6.4.2.6. Backbone Unit Length Variation

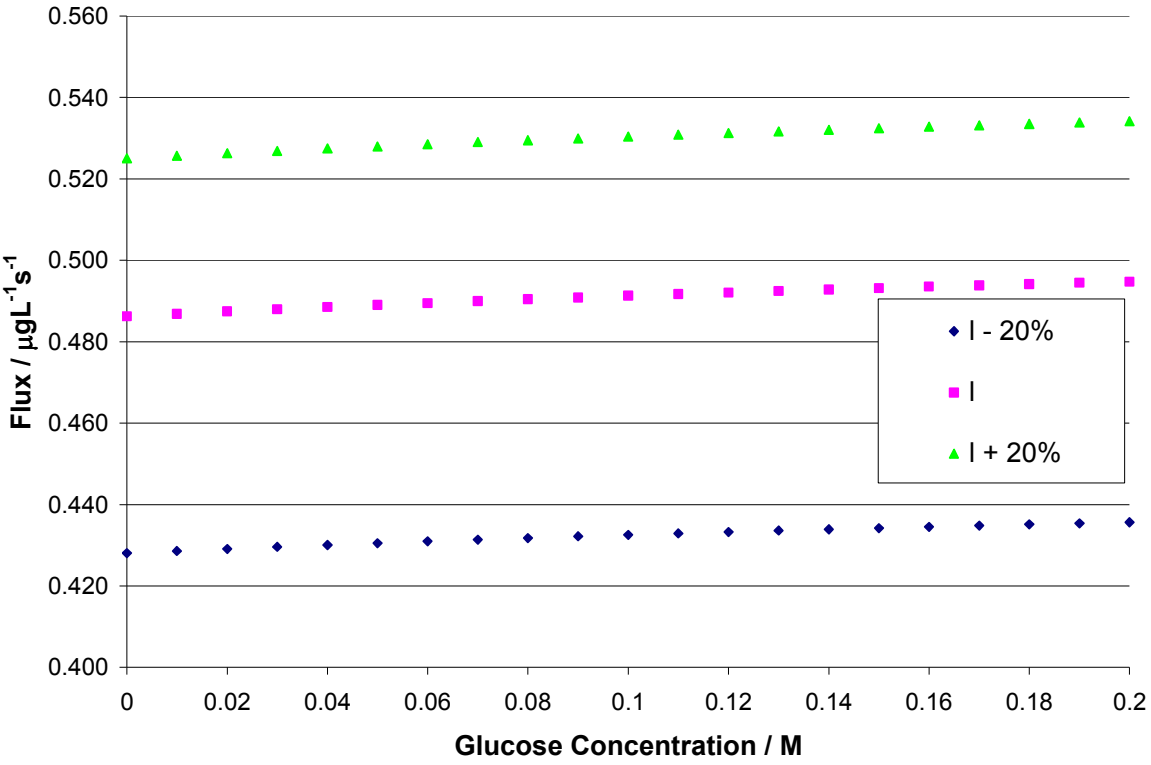

Figure 6-18 Concentration flux variation with glucose for 500kD hydrogel – Unit length of backbone variation

The unit length of the backbone, together with the average molecular mass between cross-links, controls the physical distance between bonds in the hydrogel. This relates directly to the mesh size of the hydrogel and therefore its diffusivity. This is shown by the noteworthy effect it has on the concentration flux.

Section 6.4.2.7. Membrane Thickness Variation

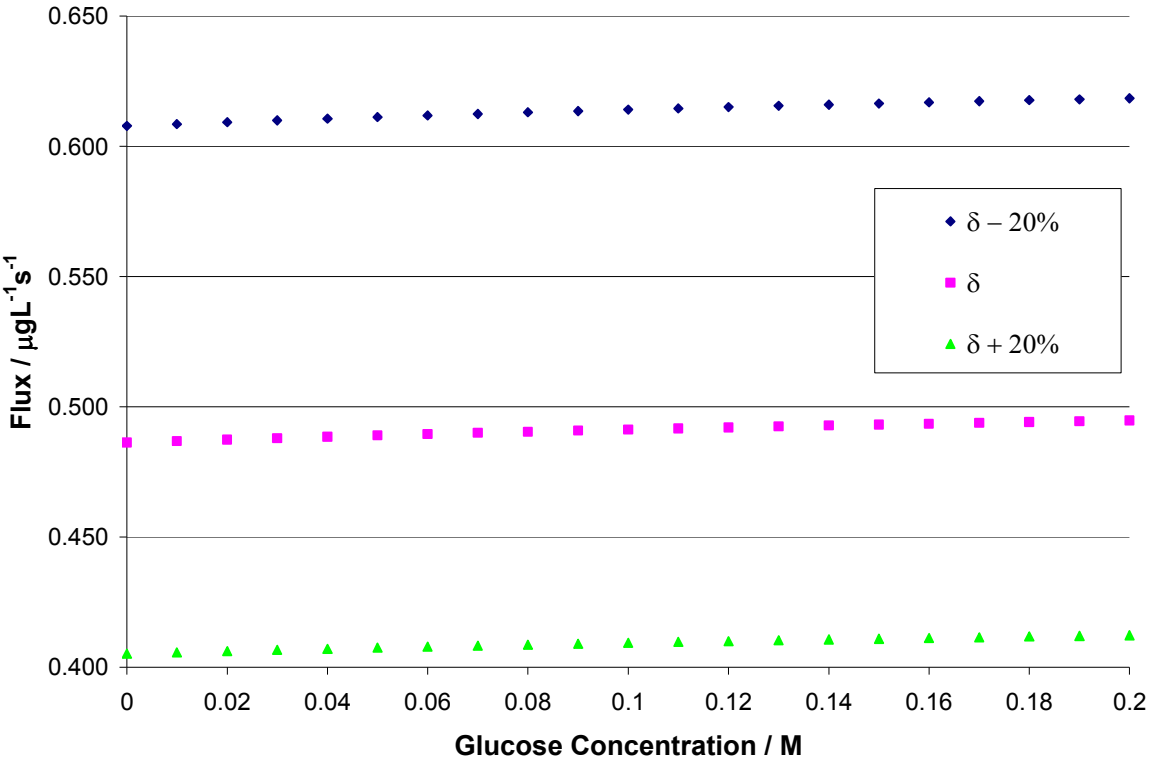

Figure 6-19 Concentration flux variation with glucose for 500kD hydrogel – Membrane thickness variation

The membrane thickness has a noticeable effect upon the concentration flux. The membrane thickness is the shortest path length available to cytC as it diffuses through the hydrogel, therefore it is expected that it would have a strong influence on the concentration flux.

Section 6.4.2.8. Membrane Surface Area Variation

The surface area of the membrane was initially calculated based on the open area between the two sides of the diffusion cell. However it was observed during experiments that the swelling resulted in the hydrogel 'ballooning' up into the donor chamber. This was approximately to a height of 5mm above the starting position, with the rim of the hydrogel not moving due to it being clamped in place. If it is assumed that the swelling is the upper portion of a perfect sphere it can be calculated that the surface area will have increased by 17%.

Section 6.5. Conclusions

A more robust method has been produced for the casting of dextran / conA hydrogels, resulting in simpler production and reduced protein wastage.

The experimental data has shown that glucose responsive hydrogels can be produced from a combination of different dextrans and conA. However, it has also shown that the hydrogels have a variable degree of response from batch to batch as well as from recipe to recipe.

The swelling model has shown that the hydrogels do not respond as the literature data would suggest. A sensitivity analysis covering the uncertainty of the model parameters has shown that the strength and concentration of the affinity bonds has a weaker effect upon the swelling than the thickness of the hydrogel and the number of covalent linkages. Using the data from the base model, each molecule of 500kD dextran will have fewer than one affinity bond and over 100 covalent cross-links attached. It is therefore unsurprising that altering the strength and number of affinity bonds does not greatly influence the total number of bonds. The number of covalent bonds actually created between dextran molecules is likely to be lower than this maximum.

The thickness of the hydrogel, and thus the minimum path length, is likely to be the main cause of error between the swelling model concentration flux and the experimental concentration flux. The swelling model assumes that the entire hydrogel is a homogenous

phase of uniform thickness and of the calculated mesh size. SEM images of conA/dextran hydrogels [1] show that the hydrogel is a honeycomb of conA/dextran with voids of approximately 1μm:

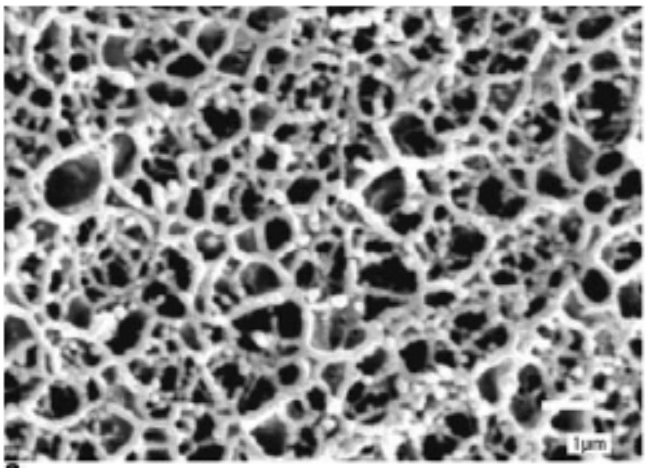

Figure 6-20 SEM image of conA/dextran hydrogel.Taken from [1].

Hydrogel is fully swollen in standard buffer (Section 2.2).10000x Magnification.

Therefore the cytC has to diffuse through very thin phases of hydrogel between voids that do not hinder liquid phase diffusion. This results in a very small active thickness. This is supported by the observation that torn hydrogels could reseal sufficiently to continue producing concentration fluxes of a similar magnitude. Any covalent bonds will be permanently broken by the tear, but the affinity cross-links will be able to reform. This would only be able to produce very thin sections of hydrogel in the presence of glucose. As such the active thickness of the hydrogel must be equally thin for this phenomenon to be correct. It is also likely that the cast hydrogel is not of uniform thickness, but will have parts that are thinner (including voids) than wanted. It was also observed that whilst the edges of the gel were constrained so that it could not swell sideways, the gels did wrinkle and balloon once swollen. This would have the potential to increase the surface area of the gel by a significant amount.

Section 6.6. Nomenclature

A	Surface area of hydrogel (m^2)
C_d	Concentration of cytC, donor side (mgL^{-1})
C_n	Flory characteristic ratio
C_r	Concentration of cytC, receiving side (mgL^{-1})
D_{gel}	Gel phase diffusivity (m^2s^{-1})
D_l	Liquid phase diffusivity of the solute (m^2s^{-1})
J	Flux ($mgm^{-2}min^{-1}$)
J_C	Concentration flux ($mgL^{-1}min^{-1}$)
l	Unit length along the polymer backbone (m)
$\overline{M_c}$	Number average molecular mass of the polymer chain between cross-links ($gmol^{-1}$)
$\overline{M_n}$	Number average molecular mass of the polymer chain ($gmol^{-1}$)
M_r	Molecular mass of repeat unit ($gmol^{-1}$)
Q	Swelling ratio
r	Hydrodynamic radius of the solute (m)
$\bar{v}$	Partial specific volume of the polymer
V	Volume of receiving side (m^3)
V_1	Molar volume of water (m^3g^{-1})
$v_{2,r}$	Polymer fraction of the gel after gel formation (gg^{-1})
$v_{2,s}$	Polymer fraction of the gel at equilibrium swelling (gg^{-1})
δ_G	Thickness of hydrogel (m)
χ_1	Flory polymer-solvent interaction parameter
ξ	Mesh size (m)

Section 7. Swelling Rate of Hydrogels

Swelling rate experiments were carried out using a Shimadzu UV1601. The achievable flux of a conA/dextran hydrogel will not be usable in a glucose responsive implant if the rate of change of flux with the introduction of glucose is too slow.

Section 7.1. Swelling Rate Theory

The swelling rate of the hydrogels could not be taken directly from the diffusion cell experiments due to the lag between cytC diffusing through the hydrogel and being pumped to the flow cuvette in the UV-VIS spectrophotometer. Noomrio *et al.* developed a simple experimental system to find the rate of swelling [130]. A batch of hydrogel material is mixed and cast on the inside (non optical) face of a spectrophotometer cuvette. Once this has set the opposite face is similarly cast with hydrogel, leaving a gap in between for the spectrophotometer beam to pass through the liquid phase and two optical faces of the cuvette. A solution of a very high molecular mass dye, in this case 2000kD blue dextran, is poured into the gap and the cuvette placed in the spectrophotometer. As the hydrogel swells the dye becomes more concentrated as it is too big to diffuse into the hydrogel. The corresponding change in absorption can be converted to a change in concentration and thus a change in swelling.

Section 7.1.1. Calculations

A simple mass balance is required to calculate the swelling ratio. The volume of a blank cuvette, V_{tot}, is known and the volume of added dye solution, V_l, for each experiment was recorded. Therefore:

$$V_G = V_{tot} - V_l \qquad \textbf{Equation 7-1}$$

The concentration of the dye initially added is known, therefore the total mass of dye, M_D, present in the cuvette is easily found. The concentration of dye during the experiment is found from a calibration curve and the absorption data from the spectrophotometer.

Therefore the swelling ratio:

$$SR = \frac{\left(V_{tot} - V_l^t\right) - \left(V_{tot} - V_l^0\right)}{\left(V_{tot} - V_l^0\right)}$$

$$SR = \frac{\left(V_{tot} - \frac{M_D}{[D_t]}\right) - \left(V_{tot} - \frac{M_D}{[D_0]}\right)}{\left(V_{tot} - \frac{M_D}{[D_0]}\right)} \qquad \textbf{Equation 7-2}$$

Section 7.2. Experimental Conditions

The cuvettes were cast with hydrogel using the standard recipe (Section 2.6). Each side was allowed to set overnight before the opposing side was cast. The blue dextran was dissolved in buffer (Section 2.2) at a concentration of 0.18mgml^{-1} at room temperature. It was not possible to heat the spectrophotometer chamber to 37^{o}C, so the experiments occurred at room temperature (~20^{o}C). The volume of liquid required was found by pippetting buffer into the space between the hydrogel. This was used to zero the spectrophotometer before being poured out and replaced with an equal volume of blue dextran solution. The cuvette was placed in the spectrophotometer and the experiment allowed to proceed for five hours.

Section 7.3. Results and Discussion

The swelling rate experiment was performed for each hydrogel mixture (6, 11, 17, 43, 64, 500 and 2000kD) with glucose concentrations of 0, 25 and 50mM.

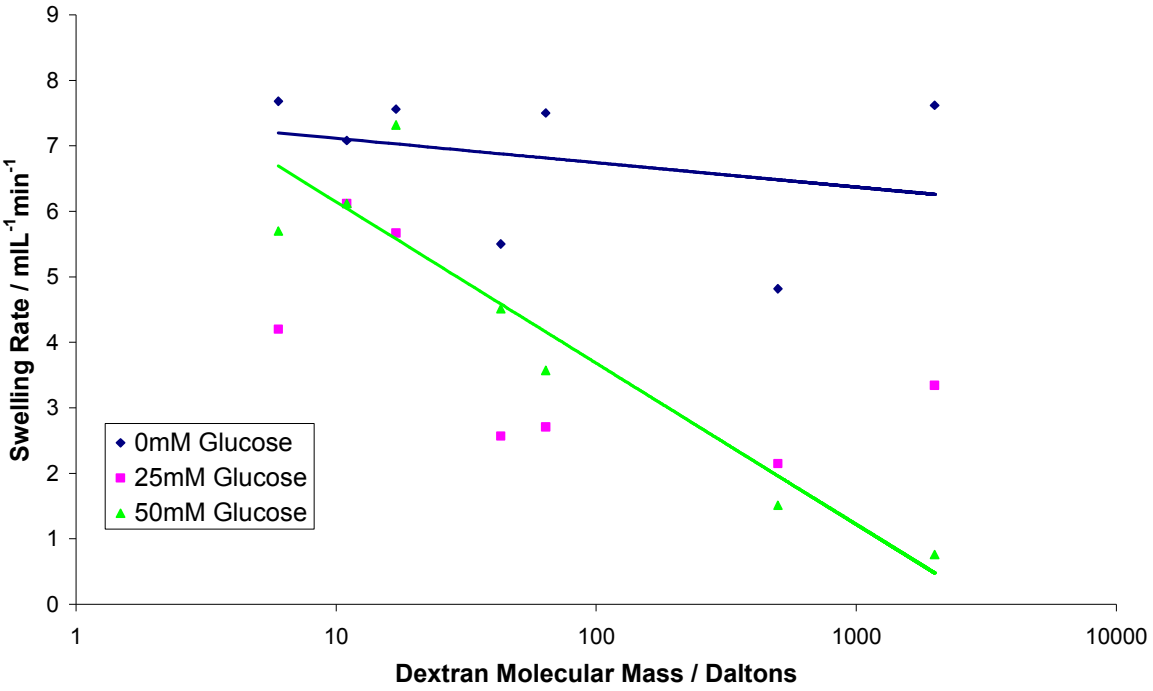

Figure 7-1 Swelling rate with respect to dextran molecular mass.

The swelling rate in the absence of glucose is consistently greater than the swelling rates in the presence of glucose (The data for 25mM is too scattered to justify a trendline). This is surprising as the glucose should facilitate the swelling process. The reason for this is that the hydrogels were not hydrated before the experiments were performed. Therefore osmotic forces created by the presence of the glucose will be acting to prevent water from entering the hydrogel.

Osmotic pressure is calculated using the van't Hoff equation [131]:

$$\Pi = \frac{CRT}{M} \qquad \textbf{Equation 7-3}$$

Where C is the concentration of the solute in gm^{-3}, R is the universal gas constant, T is the absolute temperature and M is the molecular mass of the solute.

It can be seen from this equation that the smaller molecular mass components have a greater effect upon the osmotic pressure than larger molecules. Using the data in Section 6.3.4, the osmotic pressures of the system have been calculated, Table 7-1. It is clear that the osmotic pressure of the glucose dominates the system, therefore restricting the hydration of the hydrogel.

Table 7-1 Osmotic Pressures of cuvette swelling experiments, 500kD hydrogel

Ingredient	Osmotic Pressure / Pa
Dextran in hydrogel	~500
ConA in hydrogel	~400
Blue Dextran ($0.18 mgml^{-1}$)	~1
Glucose (25mM)	$\sim 6x10^4$

Swelling rates for the 25mM glucose hydrogels shows no clear pattern, however the 50mM glucose shows a clear trend of decreasing swelling rate with increasing molecular mass. This is likely to be due to the corresponding increase in association constant that was found in Section 3.

Section 7.4. Conclusions

The swelling rate experiments shown are actually showing the rate of hydration of the hydrogel. The data shows that hydrogels do not hydrate effectively in the presence of glucose. This is due to the high osmotic pressure generated within the solution phase of the cuvette experiments. Future tests would be more effective if the hydrogel layers were pre-hydrated in buffer for a fixed period of time. The buffer solution would then be carefully pipetted out before the introduction of glucose in blue dextran solution. It is also possible that the layers of hydrogel were too thick. This would cause additional mass transfer problems for the hydration of the hydrogels. Once fully hydrated, the glucose is a sufficiently small molecule to mean it would diffuse rapidly through the water in the hydrogel.

Section 7.5. Nomenclature

C	Concentration of solute / gm^{-3}
D	Concentration of dye / gml^{-1}
M	Molecular mass of solute / $gmol^{-1}$
M_D	Mass of dye / g
R	Universal gas constant = 8.314 $JK^{-1}mol^{-1}$
SR	Swelling Ratio
T	Absolute temperature / K
V_g	Volume of gel / ml
V_l	Volume of liquid / ml
V_{tot}	Total volume / ml
Π	Osmotic pressure / Pa

Part 2 - Conclusions

The rheological tests have shown that increasing both the molecular mass and the concentration of the dextran increases the viscosity of the solution. The oscillatory rheological tests have shown that the hydrogels follow the same pattern as the dextran solutions, that is that the greater the length of the dextran chain, the greater the complex viscosity.

The conA / dextran hydrogels produced have been shown to swell in the presence of glucose, increasing the diffusion rate of protein. There isn't an apparent link between diffusion rate through the gels and the complex viscosity of the hydrogels. This is due to the non-reproducible nature of the hydrogels. The heterogeneity of the dextran material resulted in it not being possible to produce a hydrogel using a given recipe and be able to predict what the diffusion rate would be for a given glucose concentration.

The swelling rate experiments showed that hydration of the hydrogels is decreased by the osmotic pressure of the glucose in the solution.

Part 3 – Overall Conclusions and Future Work

Section 8. Overall Conclusions

Dextran and conA have been used to produce hydrogels which swell in the presence of glucose. The strength of the association between conA and dextran has been shown to have a slight increasing trend as the molecular mass is increased. For these hydrogels to be viable for human implantation, the swelling of the hydrogel must be triggered in the physiological range of glucose concentrations, approximately 5mM. The diffusion cell experiments performed at 10mM glucose showed minimal swelling, whereas those at 25mM and 50mM showed greater swelling. Therefore it can be said that these hydrogels will not successfully swell in physiological conditions. This is confirmed by considering the dissociation constants of the dextran / conA complexes (the dissociation constant is equal to the reciprocal of the association constants quoted in Section 3). The dissociation constant of 17kD dextran is the highest at approximately 3mM, the lowest is that of 2000kD dextran at approximately 0.4mM. For glucose to competitively bind to the conA the dextran must have a dissociation constant roughly equal or higher than the glucose concentration. Therefore this confirms that glucose at physiological concentrations cannot outcompete the larger molecular mass dextrans. This is, however, dependent upon the components within the hydrogel binding with the same strength as they do when in free solution.

The smaller dextran samples did not produce fully set hydrogels. This made them unusable for these experiments. The beading effect had a twofold effect. Firstly, the number of branch end groups accessible to a conA molecule is decreased due to some of the dextran molecules being encapsulated within other dextran material. The smaller dextran molecules also had fewer carboxylic acid groups for the same reason. The quantities of the EDC and NHS within the gelation mixture give an approximate 1:1 ratio of binder to carboxylic acid group for the 500kD dextran. Those dextrans with fewer carboxylic groups will therefore not combine with all of the binding groups available in the initial 10 minute mixing stage.

When the conA is added to this mixture, some of the unused binding groups will react with carboxylic acid groups present on the protein, potentially resulting in clumps of protein. If this is the case, the spatial constraint of having protein tetramers bound together will result in fewer possible affinity cross-links, thereby weakening the hydrogel.

The physical robustness of the hydrogels, when measured as the complex viscosity, also showed an increase with increasing molecular mass of the dextran. This effect, as well as being caused by the degree of carboxymethylation, was caused by the greater viscosity of the high molecular mass dextrans.

The heterogeneous nature of the dextran material, caused by the uncontrolled batch production, resulted in unpredictable responses of the hydrogels. Kim *et al.* [82] showed that not controlling the batch conditions of dextran production would result in variable molecular mass and branching ratio. Both of these factors effect the binding strength of the affinity interaction and thus control of these factors would result in greater homogeneity.

The diffusion rate through the hydrogel was found to be several orders of magnitude higher, within the fluctuations, than the predicted value from Flory-Rehner model calculations. It is likely that this was caused by the hydrogel having large voids which greatly reduced the active thickness of the hydrogel. There is also a suggestion that the hydrogel structure stretched with time. The ITC tests showed that the majority of conA tetramers only have one dextran group capable of attaching due to the spatial constraints with occasional secondary attachments. This is particularly true once covalent attachment of the conA to the dextran has occurred. Therefore, once free glucose had disrupted this affinity linkage and the hydrogel swelled, it was unlikely that the conA would rebind to the same terminal group. This resulted in the hydrogel stretching within the flow cell, increasing the surface area for diffusion. However, due to the voids previously discussed, the active thickness of the hydrogel did not greatly change, as evidenced by the zero free glucose diffusion rate being relatively stable for a given hydrogel.

This thesis has shown that the multivalency of the conA is not advantageous in the manner expected. For a protein to be effective in this type of system it must have the following characteristics. Firstly it must bind to glucose with a dissociation constant of approximately

5mM, so that the physiological glucose concentration will have an effect upon swelling. Secondly, the protein must be of sufficient size to enable an affinity cross-link to form when there is already a covalent attachment to the protein. Therefore, though it is unlikely that more than one dextran terminal group will form an affinity cross-link to a single conA tetramer, the presence of four saccharide binding sites increases the probability that one will not be spatially effected by the covalently bound dextran present.

This work has shown that, though working hydrogels can be produced from these ingredients, the repeatability is not high. It has also been shown that high multivalency of the binding protein used is not essential. A monomeric protein could be used with covalent cross-linking and would have the same number of affinity cross-links as a seemingly more multivalent protein, due to the spatial restrictions. A spatial study of the protein and ligand is as important as a study of the thermodynamics of the system.

Section 9. Future Work Plans

This research has revealed several opportunities for further work.

The carboxymethylation process has been found to not attach the same number of carboxylic acid groups to each mass range of dextran and for the smaller dextran molecules almost none were attached. For the dextrans where significant amounts were attached, the time allowed for carboxymethylation could be altered to give the same for each sample. For those dextrans that had very little carboxymethylation (primarily the smaller dextrans) it is possible that this is caused by very small beads of dextran forming - the precursors to those found by Stenekes *et al.* and Mellors *et al.* [86, 94]. Stenekes found that heating the beads to 100^{o}C for 60 minutes resulted in the breakdown of the structures, returning the dextran to solution. It should therefore be possible to achieve carboxymethylation of these dextrans by performing one of two options. Either pre-heating the dextran solution to 100^{o}C for 60 minutes, then cooling the solution to 60^{o}C and proceeding with the standard carboxymethylation protocol. Alternatively the whole carboxymethylation process could be performed at 100^{o}C. Once dextrans of similar degrees of carboxymethylation have been produced the diffusion cell experiments could be repeated to see if the smaller dextrans, with more appropriate dissociation constant values, are viable.

The beading effect of the smaller molecular mass dextrans is, itself, promising. Colleagues have shown the beads to be very stable, once formed, and have also shown it is possible to both incorporate proteins within the structure and to create the beads within a glass fibre membrane [94, 132]. The formation of responsive hydrogels within a glass fibre membrane removes the problem of mechanical weakness. The creation of storable dextran beads could be of use for drug delivery.

The ITC work showed a trend of increasing association constant with increasing molecular mass. The CM-dextrans were assumed to cross-link to the conA in the same manner. Additional experiments should be performed on the CM-dextrans to test this assumption. The smaller molecular mass dextrans should also be retested after being heated to melt the beads. The ITC data shown assumed all branch ends were available for binding, this would not have been the case if small beads had formed.

The mechanical strength of the hydrogels was a problem when placing them into the diffusion cell and would prove problematic in any future uses of this technique. Tests could be carried out whereby the gelation is performed with some fibres of carboxymethyl cellulose added to the dextran mixture. These will not enter solution, but the carboxylic acid groups should still be available for some cross-linking. These fibres may then provide structural support without restricting the swelling of the hydrogel.

For the larger molecular mass dextrans, the heterogeneity caused problems in reproducibility. Work in the literature has shown that it is possible to produce dextrans with a reliable size and branching ratio if the growth conditions are controlled. This could be an avenue for generating reproducible dextrans and therefore reproducible hydrogels.

This thesis has shown that the conA tetramer is effective at producing glucose responsive membranes, but has also shown that a multivalent protein is perhaps not essential. Therefore a study of available glucose binding proteins should be performed to identify any other proteins that may be effective. Multivalency of the protein provides a higher probability of an active site being available after covalent cross-linking, but mono- or divalent proteins should not be dismissed. Smaller monomeric proteins could be just as effective.

Section 10. References

1. Zhang, R., Tang, M., Bowyer, A., Eisenthal, R., Hubble, J., *Synthesis and Characterization of a D-glucose Sensitive Hydrogel Based on CM-dextran and Concanavalin A.* Reactive and Functional Polymers, 2006. **66**: p. 757-767.
2. Voet, D., Voet, J.G., *Biochemistry*. 2nd ed. 1995, New York City: Wiley.
3. Tuch, B., Dunlop, M., Proietto, J., *Diabetes Research - A Guide for Postgraduates*. 1st ed. 2000, Amsterdam: Harwood Academic Publishers.
4. McNally, R.J.Q., Feltbower, R.G., Parker, L., Bodansky, H.J., Campbell, F., McKinney, P.A., *Space-Time Clustering Analyses of Type I Diabetes Among 0 - 29-year-olds in Yorkshire, UK.* Diabetologia, 2006. **49**: p. 900-904.
5. Montague, W., *Diabetes and the Endocrine Pancreas*. Croom Helm Biology in Medicine Series. 1983, Guildford: Croom Helm.
6. Emilien, G., Maloteaux, J.M., Ponchon, M., *Pharmacological Management of Diabetes: Recent Progress and Future Perspective in Daily Drug Treatment.* Pharmacology and Therapeutics, 1999. **81**: p. 37-51.
7. Shier, D., Butler, J., Lewis, R., *Hole's Essentials of Human Anatomy and Physiology*. 8th ed. 2003, London: McGaw-Hill Higher Education.
8. Patel, A., *Diabetes in Focus*. 1st ed. 1999, London: Pharmaceutical Press.
9. Voet, D., Voet, J.G., *Sugars and Polysaccharides*, in *Biochemistry*. 1995, Wiley: New York City. p. 251-263.
10. Kim, C.K., Im, E.B., Lim, S.J., Oh, Y.K., Han, S.K., *Development of Glucose-Triggered pH-Sensitive Liposomes for a Potential Insulin Delivery.* International Journal of Pharmaceutics, 1994. **101**(3): p. 191-197.
11. Jeandidier, N., Boivin, S., *Current Status and Future Prospects of Parenteral Insulin Regimens, Strategies and Delivery Systems for Diabetes Treatment.* Advanced Drug Delivery Reviews, 1999. **35**: p. 179-198.
12. Hinchcliffe, M., Illum, L., *Intranasal Insulin Delivery and Therapy.* Advanced Drug Delivery Reviews, 1999. **35**: p. 199-234.
13. Garg, S., Rosenstock, J., Silverman, B.L., Sun, B., Konkoy, C.S., de la Pena, A., Muchmore, D.B., *Efficacy and Safety of Preprandial Human Insulin Inhalation Powder Versus Injectable Insulin in Patients with Type I Diabetes.* Diabetologia, 2006. **49**: p. 891-899.
14. Muchmore, D.B., Silverman, B., De La Pena, A. and Tobian, J., *The AIR Inhaled Insulin System: System Components and Pharmokinetic / Glucodynamic Data.* Diabetes Technology and Therapeutics, 2007. **9**: p. S-41-S-47.
15. Hao, E., Tyrberg, B., Itkin-Ansari, P., Lakey, J.R.T., Geron, I., Monosov, E.Z., Barcova, M., Mercola, M., Levine, F., *Beta-Cell Differentiation From Nonendocrine Epithelial Cells Of The Adult Pancreas.* Nature Medicine, 2006. **12**(3): p. 310-316.
16. Langer, R., *Drug Delivery And Targeting.* Nature, 1998. **392**(6679 Suppl. S): p. 5-10.
17. Peppas, N.A., *Physiologically Responsive Hydrogels.* Journal of Bioactive and Compatible Polymers, 1991. **6**(3): p. 241-246.
18. Galaev, I.Y., Mattiasson, B., *'Smart' Polymers and what they could do in Biotechnology amd Medicine.* Trends in BIotechnology, 1999. **17**: p. 335-340.
19. Miyata, T., Uragami, T., Nakamae, K., *Biomolecule-Sensitive Hydrogels.* Advanced Drug Delivery Reviews, 2002. **54**: p. 79-98.

20. Qiu, Y., Park, K., *Environment-Sensitive Hydrogels for Drug Delivery.* Advanced Drug Delivery Reviews, 2001. **53**: p. 321-339.
21. Ratner, B.D., Hoffman, A.S., *Synthetic Hydrogels for Biomedical Applications.* ACS Symposium Series, 1976(31): p. 1-36.
22. Bae, Y.H., Okano, T., Kim, S.W., *Insulin Permeation Through Thermo-Sensitive Hydrogels.* Journal of Controlled Release, 1989. **9**(3): p. 271-279.
23. Serizawa, T., Kazuhisa, N., Yamamoto, K., Akashi, M., *Thermoresponsive Ultrathin Hydrogels Prepared by Sequential Chemical Reactions.* Macromolecules, 2002. **35**: p. 2184-2189.
24. Ni, C., Zhu, X.-X.,, *Synthesis And Swelling Behaviour Of Thermosensitive Hydrogels Based On N-Substituted Acrylamides And Sodium Acrylate.* European Polymer Journal, 2004. **40**: p. 1075-1080.
25. Akala, E.O., Kopeckova, P., Kopecek, J., *Novel pH-Sensitive Hydrogel with Adjustable Swelling Kinetics.* Biomaterials, 1998. **19**: p. 1037-1047.
26. Heller, J., *Chemically Self-Regulated Drug Delivery Systems.* Journal of Controlled Release, 1988. **8**(2): p. 111-125.
27. Hassan, C.M., Doyle , F.J., Peppas, N.A., *Dynamic Behaviour of Glucose-Responsive Poly(methacrylic acid - g-ethylene glycol) Hydrogels.* Macromolecules, 1997. **30**(20): p. 6166-6173.
28. Klumb, L.A., Horbett, T.A., *Design Of Insulin Delivery Devices Based On Glucose Sensitive Membranes.* Journal of Controlled Release, 1992. **18**: p. 59-80.
29. Guiseppi-Elie, A., Brahim, S.I., Narinesingh, D., *A Chemically Synthesized Artificial Pancreas: Release Of Insulin From Glucose-Responsive Hydrogels.* Advanced Materials, 2002. **14**(10): p. 743-746.
30. Kost, J., Horbett, T.A., Ratner, B.D., Singh, M., *Glucose Sensitive Membranes Containing Glucose Oxidase: Activity, Swelling And Permeability Studies.* Journal of Biomedical Materials Research, 1985. **19**(9): p. 1117-1133.
31. Miyata, T., Asami, N., Uragami, T., *Preparation of an Antigen-Sensitive Hydrogel Using Antigen-Antibody Bindings.* Macromolecules, 1999. **32**: p. 2082-2084.
32. Miyata, T., Asami, N., Uragami, T., *A Reversibly Antigen-Responsive Hydrogel.* Nature, 1999. **399**: p. 766-769.
33. Shiino, D., Murata, Y., Kubo, A., Kim, Y.L., Kataoka, K., Koyama, Y., Kikuchi, A., Yokoyama, M., Sakurai, Y., Okano, T., *Amine Containing Phenylboronic Acid Gel For Glucose-Responsive Insulin Release Under Physiological pH.* Journal of Controlled Release, 1995. **37**: p. 269-276.
34. Shiino, D., Murata, Y., Kataoka, K., Koyama, Y., Yokoyama, M., Okano, T., Sakurai, Y., *Preparation And Characterisation Of A Glucose-Responsive Insulin-Releasing Polymer Device.* Biomaterials, 1994. **15**(2): p. 121-128.
35. Kitano, S., Koyama, Y., Kataoka, K., Okano, T., Sakurai, Y., *A Novel Drug Delivery System Utilizing A Glucose Responsive Polymer Complex Between Poly(vinyl alcohol) And Poly(N-vinyl-2-pyrrolidone) With A Phenyl Boronic Acid Moiety.* Journal of Controlled Release, 1992. **19**: p. 162-170.
36. Hisamitsu, I., Kataoka, K., Okano, T., Sakurai, Y., *Glucose-Responsive Gel from Phenylborate Polymer and Polyvinyl Alcohol: Prompt Response at Physiological pH through the Interaction of Borate with Amino Group in the Gel.* Pharmaceutical Research, 1997. **14**(3): p. 289-293.
37. Kataoka, K., Miyazaki, H., Bunya, M., Okano, T., Sakurai, Y., *Totally Synthetic Polymer Gels Responding To External Glucose Concentration: Their Preparation*

And Application To On-Off Regulation Of Insulin Release. Journal of the American Chemical Society, 1998. **120**: p. 12694-12695.
38. Wang, J.L., Cunningham, B.A., Waxdal, M.J., Edelman, G.M., *The Covalent and Three-Dimensional Structure of Concanavalin A: I. Amino Acid Sequence of Cyanogen Bromide Fragments F_1 and F_2.* The Journal of Biological Chemistry, 1975. **250**(4): p. 1490-1502.
39. Obaidat, A.A., Park, K., *Characterization of Glucose Dependent Gel-Sol Phase Transition of Polymeric Glucose-Concanavalin A Hydrogel System.* Pharmaceutical Research, 1996. **13**: p. 989-995.
40. Obaidat, A.A., Park, K., *Characterization of Protein Release Through Glucose-Sensitive Hydrogel Membranes.* Biomaterials, 1997. **18**: p. 801-806.
41. Tanna, S., Taylor, M.J., Adams, G., *Insulin Delivery Governed by Covalently Modified Lectin-Glycogen Gels Sensitive to Glucose.* Journal of Pharmacy and Pharmacology, 1999. **51**: p. 1093-1098.
42. Tanna, S., Sahota, T., Clark, J., Taylor, M.J., *Covalent Coupling of Concanavalin A to a Carbopol 934P and 941P Carrier in Glucose-Sensitive Gels for Delivery of Insulin.* Journal of Pharmacy and Pharmacology, 2002. **54**: p. 1461-1469.
43. Tanna, S., Taylor, M.J., *A Self-Regulating System Using High-Molecular Weight Solutes In Glucose-Sensitive Gel Membranes.* Journal of Pharmacy and Pharmacology, 1994. **46**: p. 1051a.
44. Taylor, M.J., Tanna, S., Cockshott, S., Vaitha, R., *A Self-Regulated Delivery System Using Unmodified Solutes In Glucose-Sensitive Gel Membranes.* Journal of Pharmacy and Pharmacology, 1994. **46**: p. 1051a.
45. Tanna, S., Taylor, M.J., Sahota, T., Sawicka, K., *Glucose-Responsive UV Polymerised Dextran-Concanavalin A Acrylic Derivatised Mixtures For Closed Loop Insulin Delivery.* Biomaterials, 2006. **27**: p. 1586-1597.
46. Brownlee, M., Cerami, A., *A Glucose-Controlled Insulin-Delivery System: Semisynthetic Insulin Bound to Lectin.* Science, 1979. **206**: p. 1190-1191.
47. Makino, K., Mack, E.J., Okano, T., Kim, S.W., *A Microcapsule Self-Regulating Delivery System for Insulin.* Journal of Controlled Release, 1990. **12**(3): p. 235-239.
48. Kim, S.W., Pai, C.M., Makino, K., Seminoff, L.A., Holmberg, D.L., Gleeson, J.M., Wilson, D.E., Mack, E.J., *Self-Regulated Glycosylated Insulin Delivery.* Journal of Controlled Release, 1990. **11**: p. 193-201.
49. Seminoff, L.A., Olsen, G.B., Kim, S.W., *A Self-Regulating Insulin Delivery System I: Characterization of a Synthetic Glycosylated Insulin Derivative.* International Journal of Pharmaceutics, 1989. **54**(3): p. 241-249.
50. Seminoff, L.A., Gleeson, J.M., Zheng, J., Olsen, G.B., Holmberg, D., Mohammad, S.F., Wilson, D., Kim, S.W., *A Self-Regulating Insulin Delivery System II: In Vivo Characteristics of a Synthetic Glycosylated Insulin.* International Journal of Pharmaceutics, 1989. **54**(3): p. 251-257.
51. Kim, S.W., Jacobs, H.A., *Self-Regulated Insulin Delivery - Artificial Pancreas.* Drug Development and Industrial Pharmacy, 1994. **20**: p. 575-580.
52. Tang, M., Zhang, R., Bowyer, A., Eisenthal, R., Hubble, J., *A Reversible Hydrogel Membrane for Controlling the Delivery of Macromolecules.* Biotechnology and Bioengineering, 2002. **82**(1): p. 47-53.
53. Ballerstadt, R., Ehwald, R., *Suitability Of Aqueous Dispersions Of Dextran And Concanavalin A For Glucose Sensing In Different Variants Of The Affinity Sensor.* Biosensors and Bioelectronics, 1994. **9**(8): p. 557-567.

54. Imanishi, Y., Ito, Y., *Glucose-Sensitive Insulin-Releasing Molecular Systems.* Pure and Applied Chemistry, 1995. **67**(12): p. 2015-2021.
55. Ito, Y., Casolaro, M., Kono, K., Yukil, I., *An Insulin-Releasing System That Is Responsive To Glucose.* Journal of Controlled Release, 1989. **10**(2): p. 195-203.
56. Ito, Y., Chung, D.J., Imanishi, Y., *Design And Synthesis Of A Protein Device That Releases Insulin In Response To Glucose Concentration.* Bioconjugate Chemistry, 1994. **5**(1): p. 84-87.
57. Cartier, S., Horbett, T.A., Ratner, B.D., *Glucose-Sensitive Membrane-Coated Porous Filters for Control of Hydraulic Permeability and Insulin Delivery from a Pressurized Reservoir.* Journal of Membrane Science, 1995. **106**: p. 17-24.
58. Chung, D.J., Ito, Y., Imanishi, Y., *An Insulin-Releasing Membrane System On The Basis Of Oxidation Of Glucose.* Journal of Controlled Release, 1992. **18**(1): p. 45-53.
59. Iobst, S.T., Wormald, M.R., Weis, W.I., Dwek, R.A., Drickamer, K., *Binding Of Sugar Ligands To Ca^{2+}-Dependent Animal Lectins: I. Analysis Of Mannose Binding By Site-Directed Mutagenesis And NMR.* Journal of Biological Chemistry, 1994. **269**(22): p. 15505-15511.
60. Turner, M.W., *The Role Of Mannose-Binding Lectin In Health And Disease.* Molecular Immunology, 2003. **40**: p. 423-429.
61. Weis, W.I., Drickamer, K., Hendrickson, W.A., *Structure Of A C-type Mannose-Binding Protein Complexed With An Oligosaccharide.* Nature, 1992. **360**: p. 127-134.
62. Liener, I.E., Sharon, N., Goldstein, I.J., *The Lectins. Properties, Functions And Applications In Biology And Medicine*. 1st ed. Molecular Biology - An International Series Of Monographs And Textbooks. 1986, London: Academic Press Inc. Ltd.
63. Singh, R.s., Tiwary, A.K., Kennedy, J.F., *Lectins: Sources, Activities and Applications.* Critical Reviews in Biotechnology, 1999. **19**(2): p. 145-178.
64. Sharon, N., Lis, H, *Lectins As Cell Recognition Molecules.* Science, 1989. **246**: p. 227-234.
65. Cunningham, B.A., Wang, J.L., Waxdal, M.J., Edelman, G.M., *The Covalent and Three-Dimensional Structure of Concanavalin A: II. Amino Acid Sequence of Cyanogen Bromide Fragment F_3.* The Journal of Biological Chemistry, 1975. **250**(4): p. 1503-1512.
66. Becker, J.W., Reeke, G.N., Wang, J.L., Cunningham, B.A., Edelman, G.M., *The Covalent and Three-Dimensional Structure of Concanavalin A: III. Structure of the Monomer and its Interactions with Metals and Saccharides.* The Journal of Biological Chemistry, 1975. **250**(4): p. 1513-1524.
67. Reeke, G.N., Becker, J.W., Edelman, G.M., *The Covalent and Three-Dimensional Structure of Concanavalin A: IV. Atomic Coordinates, Hydrogen Bonding and Quarternary Structure.* The Journal of Biological Chemistry, 1975. **250**(4): p. 1525-1547.
68. Dam, T.K., Roy, R., Das, S.K., Oscarson, S., Brewer, C.F., *Binding Of Multivalent Carbohydrates To Concanavalin A And Dioclea grandiflora Lectin.* The Journal of Biological Chemistry, 2000. **275**(19): p. 14223-14230.
69. Kim, J.J., Park, K., *Glucose-Binding Property Of Pegylated Concanavalin A.* Pharmaceutical Research, 2001. **18**(6): p. 794-799.
70. Garcia-Hernandez, E., Hernandez-Arana, A., *Structural Bases of Lectin-Carbohydrate Affinities: Comparison with Protein-Folding Energetics.* Protein Science, 1999. **8**: p. 1075-1086.

71. Mandal, D.K., Kishore, N., Brewer, C.F., *Thermodynamics of Lectin-Carbohydrate Interactions. Titration Microcalorimetry Measurements of the Binding of N-Linked Carbohydrates and Ovalbumin to Concanavalin A*. Biochemistry, 1994. **33**: p. 1149-1156.
72. Loris, R., Hameryck, T., Bouckaert, J., Wyns, L., *Lectin Legume Structure.* Biochimica et Biophysica Acta, 1998. **1383**: p. 9-36.
73. Ballerstadt, R., Evans, C., McNichols, R., Gowda, A., *Concanavalin A for In Vivo Glucose Senseing: A Biotoxicity Review.* Biosensors and Bioelectronics, 2006. **22**: p. 275-284.
74. Sharon, N., *Lectin Carbohydrate Complexes Of Plants And Animals - An Atomic View.* Trends in Biochemical Sciences, 1993. **18**(6): p. 221-226.
75. Jeanes, A., Haynes, W.C., Wilham, C.A., Rankin, J.C., Melvin, E.H., Austin, M.J., Cluskey, J.E., Fisher, B.E., Tsuchiya, H.M., Rist, C.E., *Characterization And Classification Of Dextrans From Ninety-Six Strains Of Bacteria.* Journal of the American Chemical Society, 1954. **76**: p. 5041-5052.
76. Jeanes, A., Wilham, C.A., *Periodate Oxidation Of Dextran.* Journal of American Chemical Society, 1950. **72**: p. 2655-2657.
77. Jeanes, A., Seymour, F.R., *The α-D-Glucopyranosidic Linkages Of Dextrans: Comparison Of Percentages From Structural Analysis By Periodate Oxidation And By Methylation - Unusual Dextrans, Part VII.* Carbohydrate Research, 1979. **74**: p. 31-40.
78. Dimler, R.J., Wolff, I.A., Sloan, J.W., Rist, C.E., *Interpretation Of Periodate Oxidation Data On Degraded Dextran.* Journal of American Chemical Society, 1955. **77**: p. 6568-6573.
79. Bovey, F.A., *Enzymatic Polymerization. I. Molecular Weight And Branching During The Formation Of Dextran.* Journal Of Polymer Science, 1959. **35**: p. 167-182.
80. Larm, O., Lindberg, B., Svensson, S., *Studies On The Length Of The Side Chains Of The Dextran Elaborated By Leuconostoc Mesenteroides NRRL B-512.* Carbohydrate Research, 1971. **20**: p. 39-48.
81. Lindberg, B., Svensson, S., *Structural Studies On Dextran From Leuconostoc Mesenteroides NRRL B-512.* Acta Chemica Scandinavica, 1968. **22**: p. 1907-1912.
82. Kim, D., Robyt, J.F., Lee, S.-Y., Lee, J.-H., Kim, Y.-M., *Dextran Molecular Size And Degree Of Branching As A Function Of Sucrose Concentration, pH And Temperature Of Reaction Of Leuconostoc Mesenteroides B-512FMCM Dextransucrase.* Carbohydrate Research, 2003. **338**: p. 1183-1189.
83. Dam, T.K., Brewer, C.F., *Multivalent Protein-Carbohydrate Interactions: Isothermal Titration Microcalorimetry Studies.* Methods in Enzymology, 2004. **379**: p. 107-128.
84. Dam, T.K., Roy, R., Page, D., Brewer, C.F., *Negative Cooperativity associated with Binding of Multivalent Carbohydrates to Lectins, Thermodynamic Analysis of the "Multivalency Effect".* Biochemistry, 2002. **41**: p. 1351-1358.
85. Dam, T.K., Roy, R., Page, D., Brewer, C.F., *Thermodynamic Binding Parameters of Individual Epitopes of Multivalent Carbohydrates to Concanavalin A as Determined by "Reverse" Isothermal Titration Microcalorimetry.* Biochemistry, 2002. **41**: p. 1359-1363.
86. Stenekes, R.J.H., Talsma, H., Hennink, W.E., *Formation Of Dextran Hydrogels By Crystallization.* Biomaterials, 2001. **22**: p. 1891-1898.

87. Zhang, R., Tang, M., Bowyer, A., Eisenthal, R., Hubble, J., *A Novel pH- and Ionic Strength-Sensitive Carboxy Methyl Dextran Hydrogel.* Biomaterials, 2005. **26**: p. 4677-4683.
88. Williams, D., Fleming, I., *Spectroscopic Methods in Organic Chemistry*. 6th ed. 2008, Maidenhead: McGraw-Hill Higher Education.
89. Pasika, W.M., Cragg, L.H., *The Detection and Estimation of Branching in Dextran by Proton Magnetic Resonance Spectroscopy.* Canadian Journal of Chemistry, 1962. **41**: p. 293-299.
90. Seymour, F.R., Knapp, R.D., Bishop, S.H., *Correlation of the Structure of Dextrans to their 1H-NMR Spectra.* Carbohydrate Research, 1979. **74**: p. 77-92.
91. Sokolov, V.B., Krasnov, K.A., Matyushichev, I., Yu., Passet, B.V., *1H NMR Study of Distribution of Functional Groups in Carboxymethyl Dextran.* Russian Journal of Applied Chemistry, 1999. **72**(4): p. 701-703.
92. Cheetham, N.W.H., Fiala-Beer, E., *Dextran Structural Details from High-Field Proton NMR Spectroscopy.* Carbohydrate Polymers, 1991. **14**: p. 149-158.
93. Maina, N.H., Tenkanen, M., Maaheimo, H., Juvonen, R. and Virrki, L., *NMR Spectroscopic Analysis of Exopolysaccharides Produced by Leuconostoc citreum and Weissella confusa.* Carbohydrate Research, 2008. **343**: p. 1446-1455.
94. Mellors, R., Benzeval, I., Eisenthal, R., Hubble, J., *Preparation of Self-Assambled Microspheres and their Potential for Drug Delivery.* Submitted for Publication.
95. MicroCal, L., *VP-ITC MicroCalorimeter User's Manual*, Northampton, MA: MicroCal.
96. Cornish-Bowden, A., *Fundamentals of Enzyme Kinetics*. 1st ed. 1979, Southampton: Butterworths. P.154.
97. Baldwin, J.M., *A Model Of Co-Operative Oxygen Binding To Haemoglobin.* British Medical Bulletin, 1976. **32**(3): p. 213-218.
98. Michel, D., *Co-operative Equilibrium Curves Generated By Ordered Ligand Binding To Multi-Site Molecules.* Biophysical Chemistry, 2007. **129**: p. 284-288.
99. Wiseman, T., Williston, S., Brandts, J.F., Lin, L.-N., *Rapid Measurement of Binding Constants and Heats of Binding Using a New Titration Calorimeter.* Analytical Biochemistry, 1989. **179**: p. 131-137.
100. Santori, F., *Lectin Affinity Chromatography of Monosaccharides*, in *Department of Chemical Engineering*. 2002, University of Bath: Bath. p. 159.
101. Zhang, R., *Dextran Hydrogel Preparation and Applications in Biomedical Engineering*, in *Department of Chemical Engineering*. 2004, University of Bath: Bath. p. 250.
102. Mangold, S.L., Cloninger, M.J., *Binding of Monomeric and Dimeric Concanavalin A to Mannose-Functionalized Dendrimers.* Organic & Biomolecular Chemistry, 2006. **4**: p. 2458-2465.
103. Ioan, C.E., Aberle, T., Burchard, W., *Structure Properties of Dextran. 2. Dilute Solution.* Macromolecules, 2000. **33**: p. 5730-5739.
104. Saltzman, W.M., *Drug Delivery: Engineering Principles for Drug Therapy*. 1st ed. 2001, New York: Oxfor University Press.
105. Elgavish, S., Shaanan, B., *Lectin-Carbohydrate Interactions: Different Folds, Common Recognition Principles.* Trends in Biochemical Sciences, 1997. **22**(12): p. 462-467.
106. Mann, D.A.K., M., Maly, D.J., Kiessling, L.L., *Probing Low Affinity and Multivalent Interactions with Surface Plasmon Resonance: Ligands for*

Concanavalin A. Journal of American Chemical Society, 1998. **120**(41): p. 10575-10582.
107. Hubble, J., *Affinity Cell Separations: Problems and Prospects.* Trends in Biotechnology, 1997. **15**(7): p. 249-255.
108. Hubble, J., *A Model of Multivalent Ligand-Receptor Equilibria Which Explains the Effect of Multivalent Binding Inhibitors.* Molecular Immunology, 1999. **36**: p. 13-18.
109. Sidebotham, R.L., *Dextrans.* Advances in Carbohydrate Chemistry and Biochemistry, 1974. **30**: p. 371-444.
110. Eirich, F.R., *Rheology - Theories and Applications*. 1st ed. Vol. 4. 1967, New York: Academic Press, Inc.
111. Ferry, J.D., *Viscoelastic Polymers of Properties*. 3rd ed. 1980, USA: John Wiley and Sons, Inc.
112. Goodwin, J.W., Hughes, R.W., *Rheology for Chemists*. 1st ed. 2000, Cambridge: The Royal Society of Chemistry.
113. Walters, K., *Rheometry*. 1st ed. 1975, Whitstable: Whitstable Litho.
114. Bohlin, *A Basic Introduction to Rheology*. MAN0334 Issue 2 ed. 1994.
115. Weng, L., Chen, X., Chen, W., *Rheological Characterization of in situ Crosslinkable Hydrogels Formulated from Oxidized Dextran and N-Carboxyethyl Chitosan.* Biomacromolecules, 2007. **8**: p. 1109-1115.
116. Bohidar, H.B., *Light Scattering and Viscosity of Heat Aggregation of Insulin.* Biopolymers, 1998. **45**: p. 1-8.
117. Kataoka, M., Hagihara, Y., Mihara, K., Goto, Y., *Molten Globule of Cytochrome C Studied by Small Angle X-Ray Scattering.* Journal of Molecular Biology, 1993. **229**: p. 591-596.
118. Young, M.E., Carroad, P.A., Bell, R.L., *Estimation of Diffusion Coefficients of Proteins.* Biotechnology and Bioengineering, 1980. **22**: p. 947-955.
119. Flory, P.J., Rehner Jr, J., *Statistical Mechanics of Cross-Linked Polymer Networks.* Journal of Chemical Physics, 1943. **11**: p. 512-520.
120. Flory, P.J., *Principles of Polymer Chemistry*. 1st ed. 1959, Ithaca: Cornell University Press.
121. Peppas, N.A., Barr-Howell, B.D., Gombotz, W.R., Hoffman, A.S., Horbett, T.A., Lustig, S.R., Mikos, A.G., Ratner, B.D., *Hydrogels in Medicine and Pharmacy*, ed. N.A. Peppas. Vol. 1 - Fundamentals. 1986, Boca Raton: CRC Press Inc.
122. Lustig, S.R., Peppas, N.A., *Solute Diffusion in Swollen Membranes. Part IX. Scaling Laws for Solute Diffusion in Gels.* Journal of Applied Polymer Science, 1988. **36**: p. 735-747.
123. Peppas, N.A., Reinhaart, F., *Solute Diffusion in Swollen Membranes. Part 1. A New Theory.* Journal of Membrane Science, 1983. **15**: p. 275-287.
124. Hubble, J., Zhang, R., *Bio-responsive Hydrogel Membranes*, in *Handbook of Membrane Separations. Chemical, Pharmaceutical, Food and Biotechnology Applications*, A.N. Pabby, Rizvi, S.S.H., Sastre, A.M., Editor. 2009, CRC Press: Boca Raton.
125. Ferreira, L., Gil, M.H., Dordick, J.S., *Enzymatic Synthesis of Dextran-Containing Hydrogels.* Biomaterials, 2002. **23**: p. 3957-3967.
126. Tuinier, R., Brulet, A., *On The Long-Range Attraction Between Proteins Due To Nonadsorbing Polysaccharide.* Biomacromolecules, 2003. **4**: p. 28-31.

127. van Dijk-Wolthuis, W.N.E., Hoogeboom, J.A.M., van Steenbergen, M.J., Tsang, S.K.Y., Hennink, W.E., *Degradation and Release Behaviour of Dextran-Based Hydrogels.* Macromolecules, 1997. **30**: p. 4639-4645.
128. Cheng, T.-W., Wu, J.-G., *Modified Boundary Layer Resistance Model for Membrane Ultrafiltration.* Tamkang Journal of Science and Engineering, 2001. **4**: p. 111-117.
129. Paradossi, G., Cavalieri, F., Chiessi,E., *Proton Fluctuations and Water Diffusion in Dextran Chemical Hydrogels Studied by Incoherent Elastic and Quasielastic Neutron Scattering.* Carbohydrate Research, 2005. **340**: p. 921-927.
130. Noomrio, M.H., Zhang, R., Eisenthal, R., Hubble, J., *Characterisation of Hydrogel Gel Swelling by Molecular Exclusion.* Biotechnology Letters, 2005. **27**: p. 1587-1590.
131. Morris, J.G., *A Biologist's Physical Chemistry*. 2nd ed. 1974, Colchester: William Clowes & Sons, Limited.
132. Yu, S., Benzeval, I.D., Bowyer, A., Hubble, J., *Preparation of Pore-Filled Responsive Membranes using Dextran Precipitation* Journal of Membrane Science, Submitted for Publication.
133. Goodwin, J.W., Hughes, R.W., *Rheology for Chemists; An Introduction*. 1st ed. 2000, Cambridge: Royal Society of Chemistry.
134. Tongue, B.H., *Principles of Vibration*. 2nd ed. 2002, New York: Oxford University Press.
135. Bird, R.B., Armstrong, R.C., Hassager, O., *Dynamics of Polymeric Liquids - Fluid Mechanics*. 1st ed. Vol. 1. 1977, USA: John Wiley and Sons.
136. Flory, P.J., *Statistical Mechanics of Swelling of Network Structures.* Journal of Chemical Physics, 1950. **18**: p. 108-111.
137. Peppas, N.A., Merrill, E.W., *Crosslinked Poly(vinyl Alcohol) Hydrogels as Swollen Elastic Networks.* Journal of Applied Polymer Science, 1977. **21**: p. 1763-1779.
138. Canal, T., Peppas, N.A., *Correlation Between Mesh Size and Equilibrium Degree of Swelling of Polymeric Networks.* Journal of Biomedical Materials Research, 1989. **23**: p. 1183-1193.

Appendix 1. NMR Traces

This appendix contains the NMR traces of glucose, maltose and the seven dextran samples.

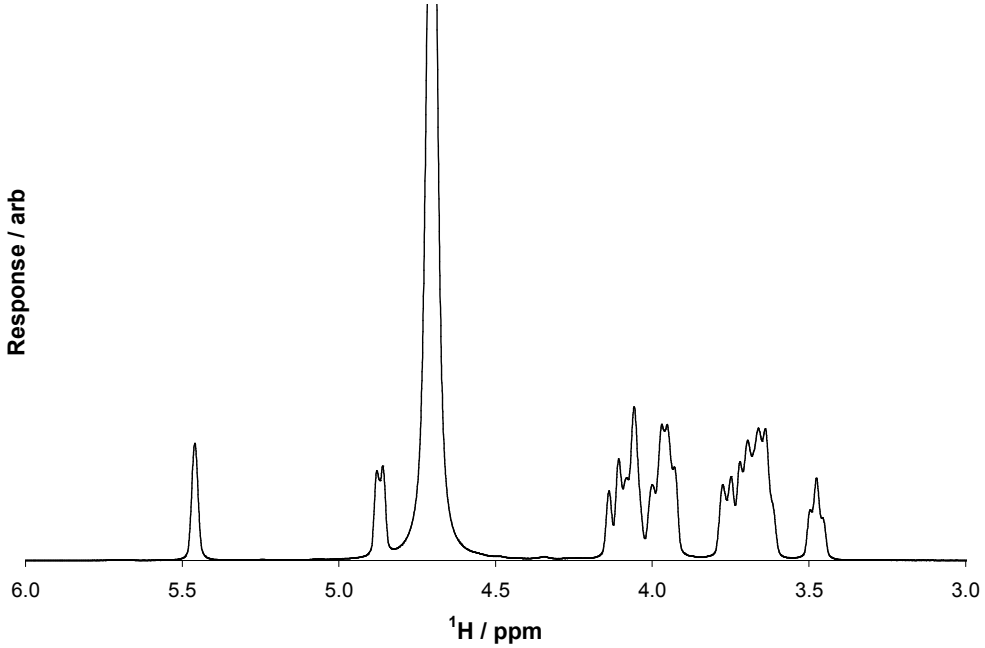

^{1}H NMR trace of glucose

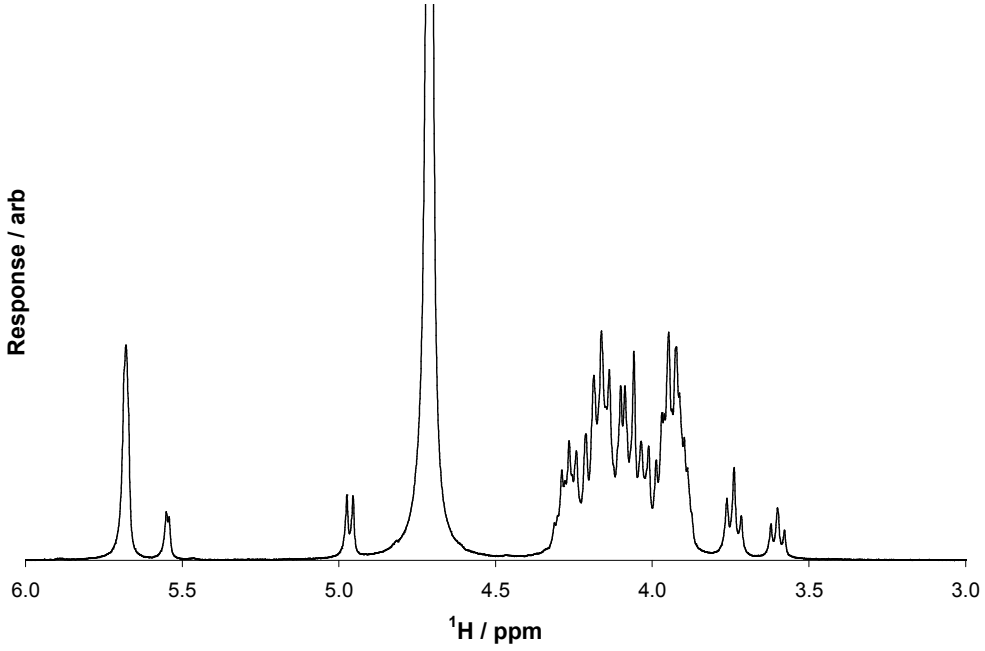

^{1}H NMR trace of maltotriose

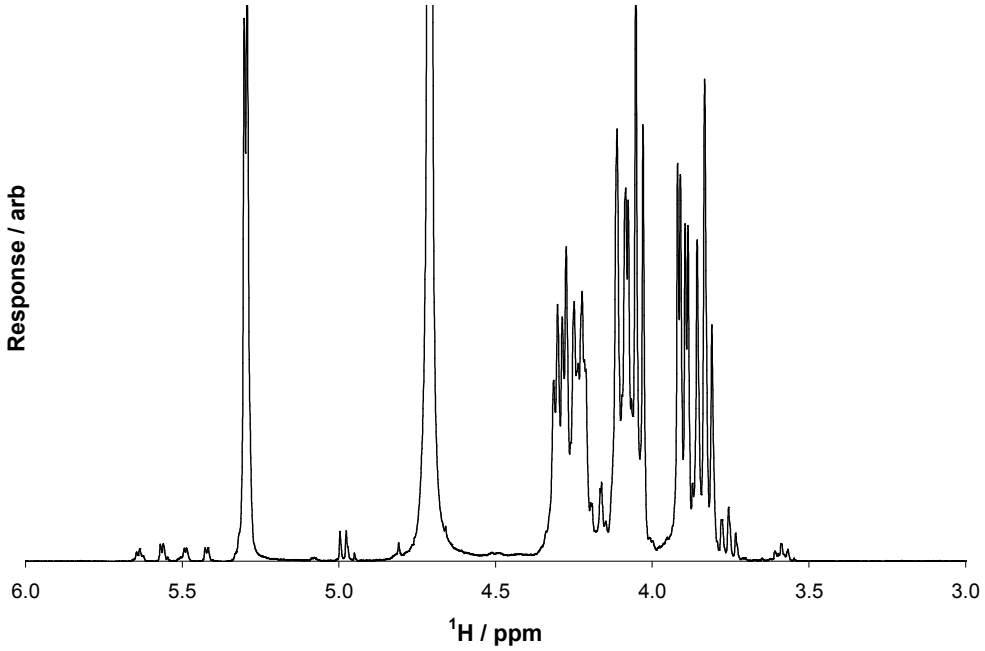

^{1}H NMR trace of 6kD dextran

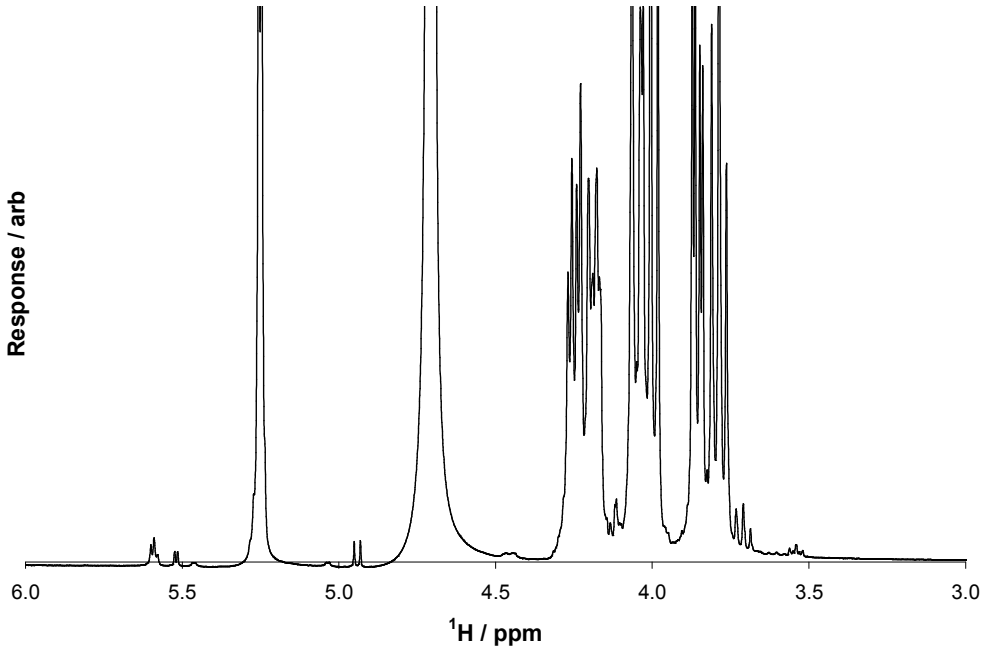

^{1}H NMR trace of 11kD dextran

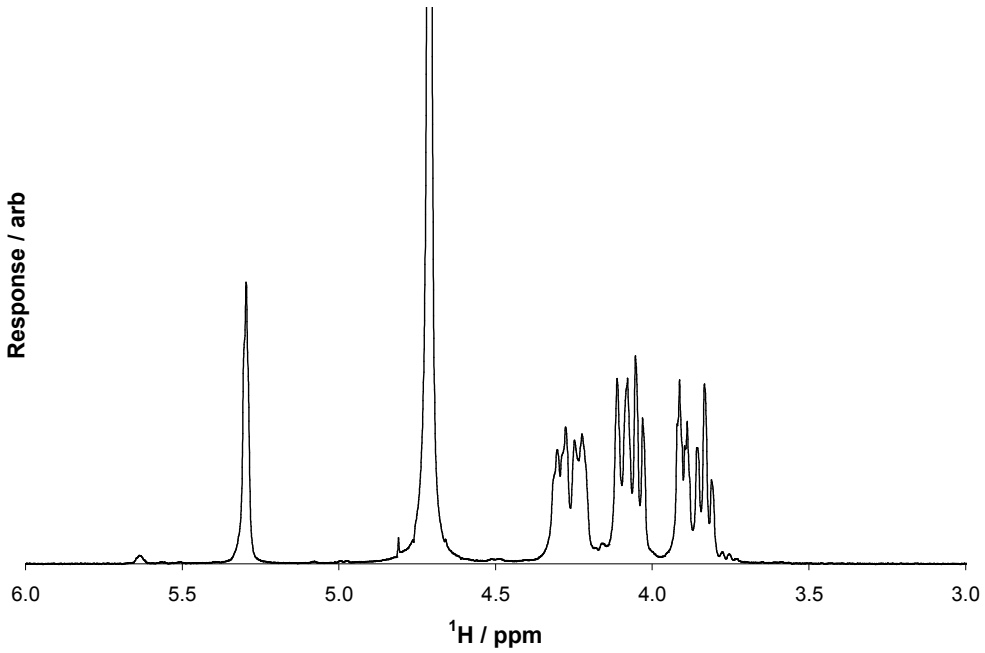

^{1}H NMR trace of 17kD dextran

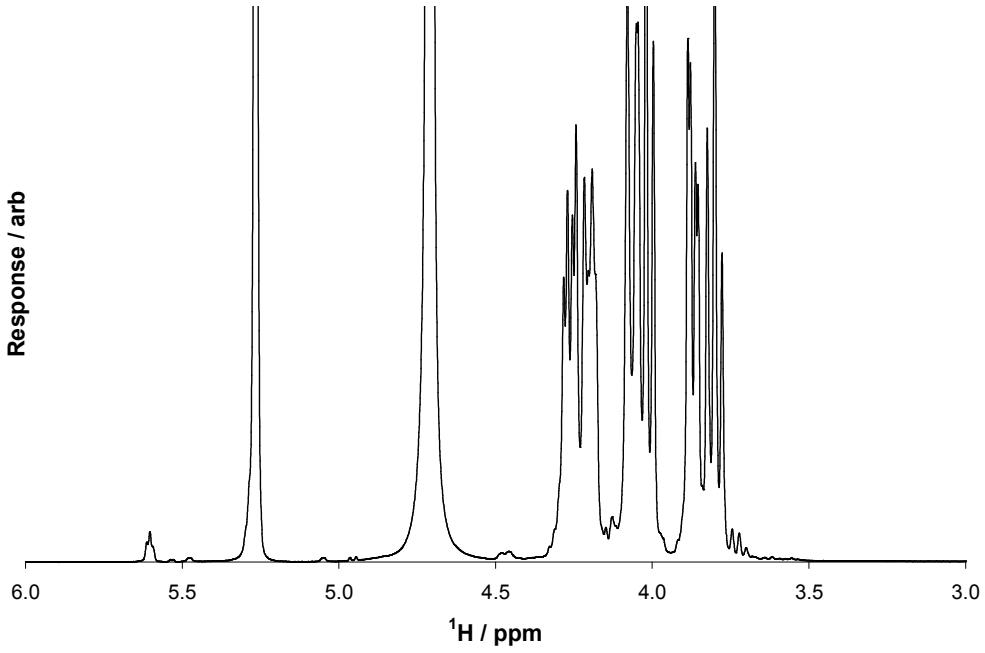

^{1}H NMR trace of 43kD dextran

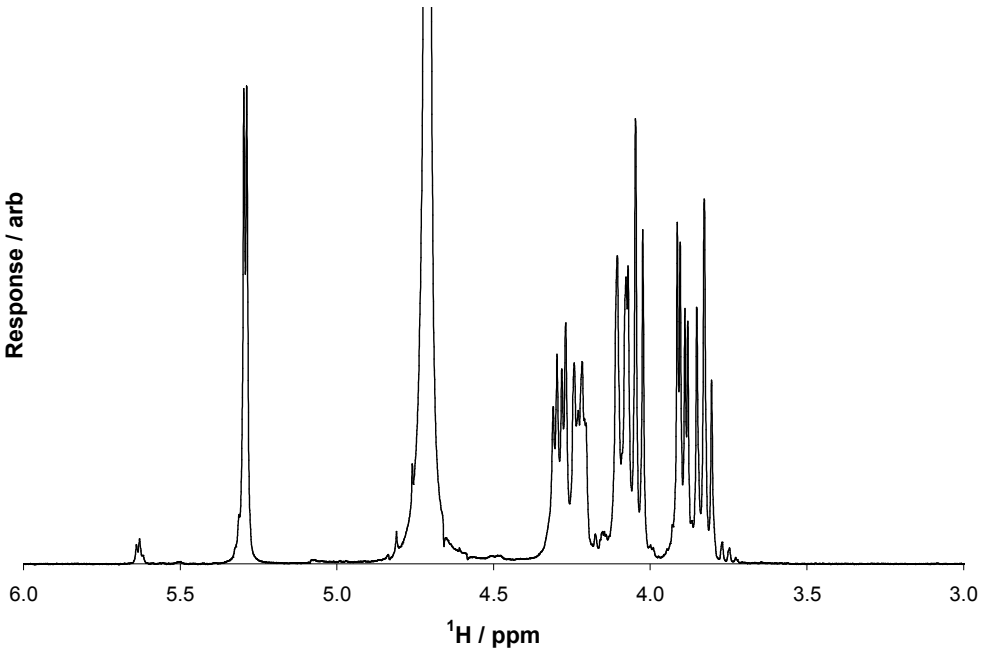

^{1}H NMR trace of 64kD dextran

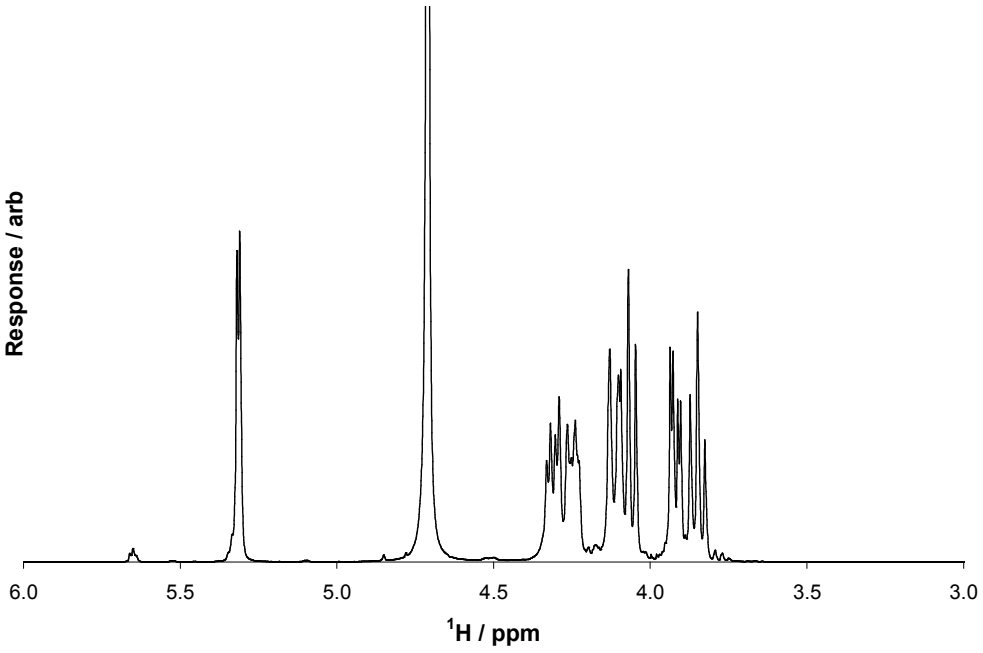

^{1}H NMR trace of 500kD dextran

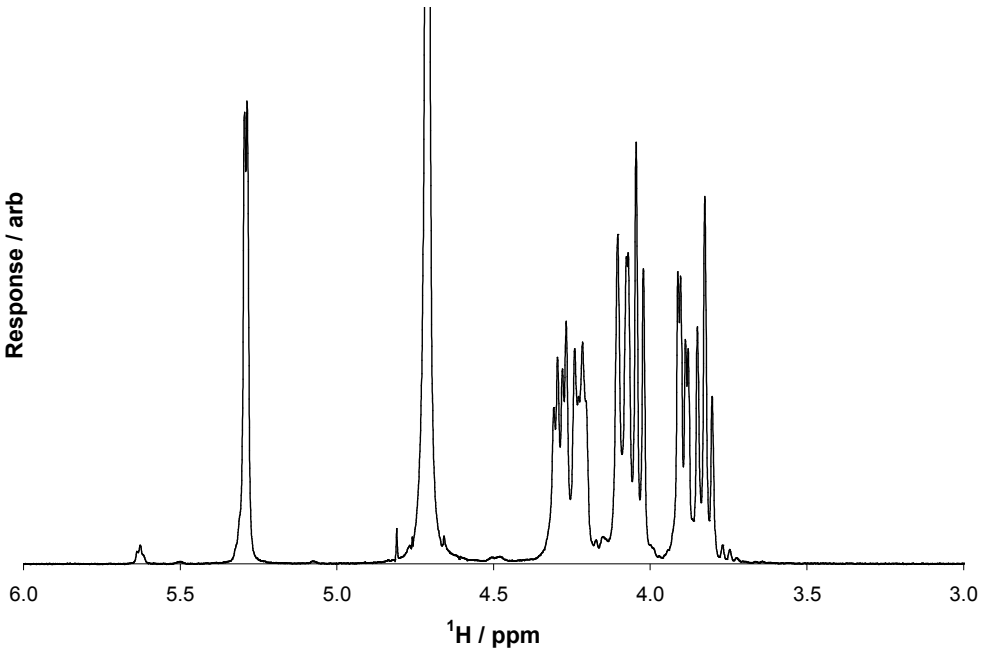

^{1}H NMR trace of 2000kD dextran

Appendix 2. Isothermal Titration Calorimetry Binding Theory

This appendix contains the derivation of the equations necessary to model data from the ITC.

Appendix 2.1. One Site Model

The rate equation for a single site interaction of the lectin, [*M*], and the ligand, [*X*], (conA and dextran respectively) can be described as:

$$\frac{d[MX]}{dt} = k_a[M][X] - k_d[MX] \qquad \textbf{Equation A2-1}$$

At equilibrium, the association and dissociation rates of the conA/dextran complex are equal to each other and can be rearranged in terms of the association constant:

$$k_a[M][X] = k_d[MX] \qquad \textbf{Equation A2-2}$$

$$K = \frac{k_a}{k_d} = \frac{[MX]}{[M][X]} \qquad \textbf{Equation A2-3}$$

Equation A2-1 is equivalent to the mass balance for the conA/dextran complex during an injection. The mass balance for the total conA and total dextran during an injection can similarly be written:

$$V_C \frac{d[X_{TOT}]}{dt} = V_{inj}[X_{inj}] - V_{inj}[X_{TOT}] \qquad \textbf{Equation A2-4}$$

$$V_C \frac{d[M_{TOT}]}{dt} = -V_{inj}[M_{TOT}] \qquad \textbf{Equation A2-5}$$

Equation A2-4 and Equation A2-5 can be simplified to give the total conA and dextran after the completion of the injection. This is done by assuming that the material lost during the injection is equivalent to the average, before (subscript 0) and after (subscript 1) the injection, of the concentrations:

$$V_C[X_{TOT}]_1 = V_C[X_{TOT}]_0 - V_{inj}\frac{[X_{TOT}]_1 + [X_{TOT}]_0}{2} + V_{inj}[X_{inj}] \qquad \textbf{Equation A2-6}$$

This can be rearranged to:

$$[X_{TOT}]_1 = \frac{2V_{inj}[X_{inj}] + [X_{TOT}]_0(2V_C - V_{inj})}{2V_C + V_{inj}} \qquad \textbf{Equation A2-7}$$

And

$$V_C[M_{TOT}]_1 = V_C[M_{TOT}]_0 - V_{inj}\frac{[M_{TOT}]_1 + [M_{TOT}]_0}{2} \qquad \textbf{Equation A2-8}$$

This can be rearranged to:

$$[M_{TOT}]_1 = [M_{TOT}]_0\frac{2V_C - V_{inj}}{2V_C + V_{inj}} \qquad \textbf{Equation A2-9}$$

Equation A2-3 can be rewritten in terms of the individual mass balances of conA and dextran:

$$[X_{TOT}] = [X] + [MX] \qquad \textbf{Equation A2-10}$$

$$[M_{TOT}] = [M] + [MX] \qquad \textbf{Equation A2-11}$$

$$K = \frac{[MX]}{([M_{TOT}] - [MX])([X_{TOT}] - [MX])} \qquad \textbf{Equation A2-12}$$

This can be rearranged for [*MX*], giving a quadratic equation, and solved for the physically meaningful root:

$$[MX] = \frac{-b - \sqrt{b^2 - 4[M_{TOT}][X_{TOT}]}}{2} \qquad \textbf{Equation A2-13}$$

Where:

$$b = -\left([M_{TOT}] + [X_{TOT}] + \frac{1}{K}\right)$$

Equation A2-13 can therefore be solved using Equation A2-7 and Equation A2-9. The energy released for a calculated quantity of [*MX*] can then be found:

$$Q = [MX]V_C\Delta H \qquad \textbf{Equation A2-14}$$

The energy released by an individual injection can be calculated as the difference between the energy for the amount of [*MX*] before the injection and the amount of [*MX*] after the injection. As with previous calculations, a term must be included for what occurs outside of the sample cell:

$$dQ_i = Q_i + \frac{V_{inj}}{V_C}\left(\frac{Q_i + Q_{i-1}}{2}\right) - Q_{i-1} \qquad \textbf{Equation A2-15}$$

The preceding set of equations can be entered into a spreadsheet or mathematical package and fitted against an experimental data set by estimating values for the parameters *K* and *ΔH*.

Appendix 2.2. Two Site Model

When considering conA as more than a monomer, the mass balances must be rewritten. For a dimer:

$$[X_{TOT}] = [X] + [MX] + 2[MXX]$$

$$[M_{TOT}] = [M] + [MX] + [MXX] \qquad \textbf{Equation A2-16}$$

The following four equations enable calculation of the free conA and dextran and the two complexes:

$$[X] = \frac{[X_{TOT}]}{1 + KI_1[M] + 2KI_1KI_2[M][X]}$$

$$[M] = \frac{[M_{TOT}]}{1 + KI_1[M] + KI_1KI_2[X]^2} \qquad \textbf{Equation A2-17}$$

$$[MX] = KI_1[M][X]$$

$$[MXX] = KI_1KI_2[M][X]^2$$

The amount of energy released is calculated:

$$Q = V_C[MX]\Delta H_1 + V_C[MXX](\Delta H_1 + \Delta H_2) \qquad \textbf{Equation A2-18}$$

Equation A2-17 and Equation A2-16 must be solved numerically, estimating the two association constants and two enthalpy changes. The system is completed by using Equation A2-15 in the same manner as the single site model.

Nomenclature:

ΔG	Gibbs free energy change ($Jmol^{-1}$)
ΔH	Enthalpic change ($Jmol^{-1}$)
K	Apparent association constant (M^{-1})
KI	Intrinsic association constant (M^{-1})
k_a	Association rate ($M^{-1}s^{-1}$)
k_d	Dissociation rate (s^{-1})
$[M]$	Concentration of free lectin (conA) (M)
$[MX]$	Concentration of conA/dextran complex (M)
$[MXX]$	Concentration of conA/dextran/dextran complex (M)
$[M_{TOT}]$	Total conA sites, bound and unbound (M)
Q_i	Total energy released (J)
dQ_i	Energy change over one injection (J)
R	Universal gas constant = 8.31 $Jmol^{-1}K^{-1}$
ΔS	Entropic change ($Jmol^{-1}K^{-1}$)
t	Time (s)
T	Temperature (K)
V_C	Volume of sample cell (L)
V_{inj}	Volume of injection i (L)
$[X]$	Free dextran binding ligands at injection, i (M)
$[X_{TOT}]$	Total dextran ligands, bound and unbound (M)

Appendix 3. Isothermal Titration Calorimetry Models

This appendix contains the programs for the ITC experiments which were entered into Scientist® in order to model the data.

Appendix 3.1. One Site Model

```
// ITC 1 site model
// Iterative solution
// n = number of injections
// bf = branch factor - number of branches per molecule
// occ = ligand molecular concentration in syringe
// cc = ligand branch end concentration in syringe
// mtoi = initial concentration of macromolecule in the cell
// mto = concentration of macromolecule in the cell after first injection
// fvi = volume of first injection
// vi = volume of second and subsequent injections
// vc = cell volume
// mt = total macromolecule, [m]tot
// me = free macromolecule, [m]
// xt = total ligand, [x]tot
// xe = free ligand, [x]
// mx11 = total complex, [mx]
// Q = total energy release
// dq = energy release for given injection

IndVars: n
DepVars: dq

Params: vi,fvi,vc,mtoi,K1,dh1,bf,occ

// Effect of first injection, fvi, receptor concentration in the cell prior to recorded injections

mto=mtoi*((2*vc-fvi)/(2*vc+fvi))
cc=occ*bf

//Energy released from all injections up to the previous injection
// Add volume of initial injection to volume added up to previous injection

dv1=fvi+(n-1)*vi
mt1=mtoi*((2*vc-dv1)/(2*vc+dv1))
xt1=(2*dv1*cc)/(2*vc+dv1)

me1=mt1/(1+K1*xe1)
xe1=xt1/(1+K1*me1)
mx11=K1*me1*xe1

Q1=(mx11*dh1)*vc

//Energy released from all injections including the current injection
// Add volume of initial injection to volume added up to current injection

dv2=fvi+n*vi
mt2=mtoi*((2*vc-dv2)/(2*vc+dv2))
xt2=(2*dv2*cc)/(2*vc+dv2)
```

```
me2=mt2/(1+K1*xe2)
xe2=xt2/(1+K1*me2)
mx21=K1*me2*xe2

Q2=(mx21*dh1)*vo


//Heat evolved from current injection

dq=(Q2+(vi/vo)*((Q2+Q1)/2)-Q1)*1000000

// Molar ratio of titrant to macromolecule
y=xt2/mt2

***
0<xe1<xt1
0<me1<mt1
0<xe2<xt2
0<me2<mt2
```

Appendix 3.2. Two Site Model with Constant K and ΔH values

```
// ITC 2 site model with constant K and dH values
// Iterative solution
// n = number of injections
// bf = branch factor - number of branches per molecule
// occ = ligand molecular concentration in syringe
// cc = ligand branch end concentration in syringe
// mtoi = initial concentration of macromolecule in the cell
// mto = concentration of macromolecule in the cell after first injection
// fvi = volume of first injection
// vi = volume of second and subsequent injections
// vc = cell volume
// mt = total macromolecule, [m]tot
// me = free macromolecule, [m]
// xt = total ligand, [x]tot
// xe = free ligand, [x]
// mx11 = total one site complex, [mx]
// mx12 = total two site complex, [mxx]
// Q = total energy release
// dq = energy release for given injection

// K values are intrinsic association constants

IndVars: n
DepVars: dq

Params: vi,fvi,vc,mtoi,K1,dh1,bf,occ

// Effect of first injection, fvi, receptor concentration in the cell prior to recorded injections

mto=mtoi*((2*vc-fvi)/(2*vc+fvi))
cc=occ*bf

//Energy released from all injections up to the previous injection
// Add volume of initial injection to volume added up to previous injection
```

```
dv1=fvi+(n-1)*vi
mt1=mtoi*((2*vc-dv1)/(2*vc+dv1))
xt1=(2*dv1*cc)/(2*vc+dv1)

me1=mt1/(1+2*K1*xe1+K1^2*xe1^2)
xe1=xt1/(1+2*K1*me1+2*K1^2*me1*xe1)
mx11=2*K1*me1*xe1
mx12=K1^2*me1*xe1^2

Q1=(mx11*dh1+mx12*(dh1*2))*vc

//Energy released from all injections including the current injection
// Add volume of initial injection to volume added up to current injection

dv2=fvi+n*vi
mt2=mtoi*((2*vc-dv2)/(2*vc+dv2))
xt2=(2*dv2*cc)/(2*vc+dv2)

me2=mt2/(1+2*K1*xe2+K1^2*xe2^2)
xe2=xt2/(1+2*K1*me2+2*K1^2*me2*xe2)
mx21=2*K1*me2*xe2
mx22=K1^2*me2*xe2^2

Q2=(mx21*dh1+mx22*(dh1*2))*vc

//Heat evolved from current injection

dq=(Q2+(vi/vc)*((Q2+Q1)/2)-Q1)*1000000

// Molar ratio of titrant to macromolecule
y=xt2/mt2

***
0<xe1<xt1
0<me1<mt1
0<xe2<xt2
0<me2<mt2
```

Appendix 3.3. Two Site Model with Variable K and ΔH Values

```
// ITC 2 site model with variable K and dH values
// Iterative solution
// n = number of injections
// bf = branch factor - number of branches per molecule
// occ = ligand molecular concentration in syringe
// cc = ligand branch end concentration in syringe
// mtoi = initial concentration of macromolecule in the cell
// mto = concentration of macromolecule in the cell after first injection
// fvi = volume of first injection
// vi = volume of second and subsequent injections
// vc = cell volume
// mt = total macromolecule, [m]tot
// me = free macromolecule, [m]
// xt = total ligand, [x]tot
// xe = free ligand, [x]
```

```
// mx11 = total one site complex, [mx]
// mx12 = total two site complex, [mxx]
// Q = total energy release
// dq = energy release for given injection

// K values are intrinsic association constants

IndVars: n
DepVars: dq

Params: vi,fvi,vc,mtoi,K1,K2,dh1,dh2,bf,occ

// Effect of first injection, fvi, receptor concentration in the cell prior to recorded injections

mto=mtoi*((2*vc-fvi)/(2*vc+fvi))
cc=occ*bf

//Energy released from all injections up to the previous injection
// Add volume of initial injection to volume added up to previous injection

dv1=fvi+(n-1)*vi
mt1=mtoi*((2*vc-dv1)/(2*vc+dv1))
xt1=(2*dv1*cc)/(2*vc+dv1)

me1=mt1/(1+2*K1*xe1+K1*K2*xe1^2)
xe1=xt1/(1+2*K1*me1+2*K1*K2*me1*xe1)
mx11=2*K1*me1*xe1
mx12=K1*K2*me1*xe1^2

Q1=(mx11*dh1+mx12*(dh1+dh2))*vc

//Energy released from all injections including the current injection
// Add volume of initial injection to volume added up to current injection

dv2=fvi+n*vi
mt2=mtoi*((2*vc-dv2)/(2*vc+dv2))
xt2=(2*dv2*cc)/(2*vc+dv2)

me2=mt2/(1+2*K1*xe2+K1*K2*xe2^2)
xe2=xt2/(1+2*K1*me2+2*K1*K2*me2*xe2)
mx21=2*K1*me2*xe2
mx22=K1*K2*me2*xe2^2

Q2=(mx21*dh1+mx22*(dh1+dh2))*vc

//Heat evolved from current injection

dq=(Q2+(vi/vc)*((Q2+Q1)/2)-Q1)*1000000

// Molar ratio of titrant to macromolecule
y=xt2/mt2

***
0<xe1<xt1
0<me1<mt1
0<xe2<xt2
0<me2<mt2
```

Appendix 3.4. Three Site Model with Constant K and ΔH Values

```
// ITC 3 site model with constant K and dH values
// Iterative solution
// n = number of injections
// bf = branch factor - number of branches per molecule
// occ = ligand molecular concentration in syringe
// cc = ligand branch end concentration in syringe
// mtoi = initial concentration of macromolecule in the cell
// mto = concentration of macromolecule in the cell after first injection
// fvi = volume of first injection
// vi = volume of second and subsequent injections
// vc = cell volume
// mt = total macromolecule, [m]tot
// me = free macromolecule, [m]
// xt = total ligand, [x]tot
// xe = free ligand, [x]
// mx11 = total one site complex, [mx]
// mx12 = total two site complex, [mxx]
// mx13 = total three site complex, [mxxx]
// Q = total energy release
// dq = energy release for given injection

// K values are intrinsic association constants

IndVars: n
DepVars: dq

Params: vi,fvi,vc,mtoi,K1,dh1,bf,occ

// Effect of first injection, fvi, receptor concentration in the cell prior to recorded injections

mto=mtoi*((2*vc-fvi)/(2*vc+fvi))
cc=occ*bf

// Energy released from all injections up to the previous injection
// Add volume of initial injection to volume added up to previous injection

dv1=fvi+(n-1)*vi
mt1=mtoi*((2*vc-dv1)/(2*vc+dv1))
xt1=(2*dv1*cc)/(2*vc+dv1)

me1=mt1/(1+3*K1*xe1+3*K1^2*xe1^2+K1^3*xe1^3)
xe1=xt1/(1+3*K1*me1+3*K1^2*me1*xe1+K1^3*me1*xe1^2)
mx11=3*K1*me1*xe1
mx12=3*K1^2*me1*xe1^2
mx13=K1^3*me1*xe1^3

Q1=(mx11*dh1+mx12*(dh1*2)+mx13*(dh1*3))*vc

// Energy released from all injections including the current injection
// Add volume of initial injection to volume added up to current injection

dv2=fvi+n*vi
mt2=mtoi*((2*vc-dv2)/(2*vc+dv2))
xt2=(2*dv2*cc)/(2*vc+dv2)

me2=mt2/(1+3*K1*xe2+3*K1^2*xe2^2+K1^3*xe2^3)
```

```
xe2=xt2/(1+3*K1*me2+3*K1^2*me2*xe2+K1^3*me2*xe2^2)
mx21=3*K1*me2*xe2
mx22=3*K1^2*me2*xe2^2
mx23=K1^3*me2*xe2^3

Q2=(mx21*dh1+mx22*(dh1*2)+mx23*(dh1*3))*vc

// Heat evolved from current injection

dq=(Q2+(vi/vc)*((Q2+Q1)/2)-Q1)*1000000

// Molar ratio of titrant to macromolecule
y=xt2/mt2

***
0<xe1<xt1
0<me1<mt1
0<xe2<xt2
0<me2<mt2
```

Appendix 3.5. Three Site Model with Variable K and ΔH Values

```
// ITC 3 site model with variable K and dH values
// Iterative solution
// n = number of injections
// bf = branch factor - number of branches per molecule
// occ = ligand molecular concentration in syringe
// cc = ligand branch end concentration in syringe
// mtoi = initial concentration of macromolecule in the cell
// mto = concentration of macromolecule in the cell after first injection
// fvi = volume of first injection
// vi = volume of second and subsequent injections
// vc = cell volume
// mt = total macromolecule, [m]tot
// me = free macromolecule, [m]
// xt = total ligand, [x]tot
// xe = free ligand, [x]
// mx11 = total one site complex, [mx]
// mx12 = total two site complex, [mxx]
// mx13 = total three site complex, [mxxx]
// Q = total energy release
// dq = energy release for given injection

// K values are intrinsic association constants

IndVars: n
DepVars: dq

Params: vi,fvi,vc,mtoi,K1,K2,K3,dh1,dh2,dh3,bf,occ

// Effect of first injection, fvi, receptor concentration in the cell prior to recorded injections

mto=mtoi*((2*vc-fvi)/(2*vc+fvi))
cc=occ*bf

// Energy released from all injections up to the previous injection
```

```
// Add volume of initial injection to volume added up to previous injection

dv1=fvi+(n-1)*vi
mt1=mtoi*((2*vc-dv1)/(2*vc+dv1))
xt1=(2*dv1*cc)/(2*vc+dv1)

me1=mt1/(1+3*K1*xe1+3*K1*K2*xe1^2+K1*K2*K3*xe1^3)
xe1=xt1/(1+3*K1*me1+3*K1*K2*me1*xe1+K1*K2*K3*me1*xe1^2)
mx11=3*K1*me1*xe1
mx12=3*K1*K2*me1*xe1^2
mx13=K1*K2*K3*me1*xe1^3

Q1=(mx11*dh1+mx12*(dh1+dh2)+mx13*(dh1+dh2+dh3))*vc

// Energy released from all injections including the current injection
// Add volume of initial injection to volume added up to current injection

dv2=fvi+n*vi
mt2=mtoi*((2*vc-dv2)/(2*vc+dv2))
xt2=(2*dv2*cc)/(2*vc+dv2)

me2=mt2/(1+3*K1*xe2+3*K1*K2*xe2^2+K1*K2*K3*xe2^3)
xe2=xt2/(1+3*K1*me2+3*K1*K2*me2*xe2+K1*K2*K3*me2*xe2^2)
mx21=3*K1*me2*xe2
mx22=3*K1*K2*me2*xe2^2
mx23=K1*K2*K3*me2*xe2^3

Q2=(mx21*dh1+mx22*(dh1+dh2)+mx23*(dh1+dh2+dh3))*vc

// Heat evolved from current injection

dq=(Q2+(vi/vc)*((Q2+Q1)/2)-Q1)*1000000

// Molar ratio of titrant to macromolecule
y=xt2/mt2

***
0<xe1<xt1
0<me1<mt1
0<xe2<xt2
0<me2<mt2
```

Appendix 3.6. Four Site Model with Constant K and ΔH Values

```
// ITC 4 site model with variable K and dH values
// Iterative solution
// n = number of injections
// bf = branch factor - number of branches per molecule
// occ = ligand molecular concentration in syringe
// cc = ligand branch end concentration in syringe
// mtoi = initial concentration of macromolecule in the cell
// mto = concentration of macromolecule in the cell after first injection
// fvi = volume of first injection
// vi = volume of second and subsequent injections
// vc = cell volume
// mt = total macromolecule, [m]tot
```

```
// me = free macromolecule, [m]
// xt = total ligand, [x]tot
// xe = free ligand, [x]
// mx11 = total one site complex, [mx]
// mx12 = total two site complex, [mxx]
// mx13 = total three site complex, [mxxx]
// mx14 = total four site complex, [mxxxx]
// Q = total energy release
// dq = energy release for given injection

// K values are intrinsic association constants

IndVars: n
DepVars: dq

Params: vi,fvi,vc,mtoi,K1,dh1,bf,occ

// Effect of first injection, fvi, receptor concentration in the cell prior to recorded injections

mto=mtoi*((2*vc-fvi)/(2*vc+fvi))
cc=occ*bf

// Energy released from all injections up to the previous injection
// Add volume of initial injection to volume added up to previous injection

dv1=fvi+(n-1)*vi
mt1=mtoi*((2*vc-dv1)/(2*vc+dv1))
xt1=(2*dv1*cc)/(2*vc+dv1)

me1=mt1/(1+4*K1*xe1+6*K1^2*xe1^2+4*K1^3*xe1^3+K1^4*xe1^4)
xe1=xt1/(1+4*K1*me1+12*K1^2*me1*xe1+12*K1^3*me1*xe1^2+4*K1^4*xe1^4)
mx11=4*K1*me1*xe1
mx12=6*K1^2*me1*xe1^2
mx13=4*K1^3*me1*xe1^3
mx14=K1^4*me1*xe1^4

Q1=(mx11*dh1+mx12*(dh1*2)+mx13*(dh1*3)+mx14*(dh1*4))*vc

// Energy released from all injections including the current injection
// Add volume of initial injection to volume added up to current injection

dv2=fvi+n*vi
mt2=mtoi*((2*vc-dv2)/(2*vc+dv2))
xt2=(2*dv2*cc)/(2*vc+dv2)

me2=mt2/(1+4*K1*xe2+6*K1^2*xe2^2+4*K1^3*xe2^3+K1^4*xe2^4)
xe2=xt2/(1+4*K1*me2+12*K1^2*me2*xe2+12*K1^3*me2*xe2^2+4*K1^4*xe1^4)
mx21=4*K1*me2*xe2
mx22=6*K1^2*me2*xe2^2
mx23=4*K1^3*me2*xe2^3
mx24=K1^4*me2*xe2^4

Q2=(mx21*dh1+mx22*(dh1*2)+mx23*(dh1*3)+mx24*(dh1*4))*vc

// Heat evolved from current injection

dq=(Q2+(vi/vc)*((Q2+Q1)/2)-Q1)*1000000

// Molar ratio of titrant to macromolecule
```

```
y=xt2/mt2

***
0<xe1<xt1
0<me1<mt1
0<xe2<xt2
0<me2<mt2
```

Appendix 3.7. Four Site Model with Variable K and ΔH Values

```
// ITC 4 site model with variable K and dH values
// Iterative solution
// n = number of injections
// bf = branch factor - number of branches per molecule
// occ = ligand molecular concentration in syringe
// cc = ligand branch end concentration in syringe
// mtoi = initial concentration of macromolecule in the cell
// mto = concentration of macromolecule in the cell after first injection
// fvi = volume of first injection
// vi = volume of second and subsequent injections
// vc = cell volume
// mt = total macromolecule, [m]tot
// me = free macromolecule, [m]
// xt = total ligand, [x]tot
// xe = free ligand, [x]
// mx11 = total one site complex, [mx]
// mx12 = total two site complex, [mxx]
// mx13 = total three site complex, [mxxx]
// mx14 = total four site complex, [mxxxx]
// Q = total energy release
// dq = energy release for given injection

// K values are intrinsic association constants

IndVars: n
DepVars: dq

Params: vi,fvi,vc,mtoi,K1,K2,K3,K4,dh1,dh2,dh3,dh4,bf,occ

// Effect of first injection, fvi, receptor concentration in the cell prior to recorded injections

mto=mtoi*((2*vc-fvi)/(2*vc+fvi))
cc=occ*bf

// Energy released from all injections up to the previous injection
// Add volume of initial injection to volume added up to previous injection

dv1=fvi+(n-1)*vi
mt1=mtoi*((2*vc-dv1)/(2*vc+dv1))
xt1=(2*dv1*cc)/(2*vc+dv1)

me1=mt1/(1+4*K1*xe1+6*K1*K2*xe1^2+4*K1*K2*K3*xe1^3+K1*K2*K3*K4*xe1^4)
xe1=xt1/(1+4*K1*me1+12*K1*K2*me1*xe1+12*K1*K2*K3*me1*xe1^2+4*K1*K2*K3*K4*xe1^4)
mx11=4*K1*me1*xe1
mx12=6*K1*K2*me1*xe1^2
mx13=4*K1*K2*K3*me1*xe1^3
```

```
mx14=K1*K2*K3*K4*me1*xe1^4

Q1=(mx11*dh1+mx12*(dh1+dh2)+mx13*(dh1+dh2+dh3)+mx14*(dh1+dh2+dh3+dh4))*vc

// Energy released from all injections including the current injection
// Add volume of initial injection to volume added up to current injection

dv2=fvi+n*vi
mt2=mtoi*((2*vc-dv2)/(2*vc+dv2))
xt2=(2*dv2*cc)/(2*vc+dv2)

me2=mt2/(1+4*K1*xe2+6*K1*K2*xe2^2+4*K1*K2*K3*xe2^3+K1*K2*K3*K4*xe2^4)
xe2=xt2/(1+4*K1*me2+12*K1*K2*me2*xe2+12*K1*K2*K3*me2*xe2^2+4*K1*K2*K3*K4*xe1^4)
mx21=4*K1*me2*xe2
mx22=6*K1*K2*me2*xe2^2
mx23=4*K1*K2*K3*me2*xe2^3
mx24=K1*K2*K3*K4*me2*xe2^4

Q2=(mx21*dh1+mx22*(dh1+dh2)+mx23*(dh1+dh2+dh3)+mx24*(dh1+dh2+dh3+dh4))*vc

// Heat evolved from current injection

dq=(Q2+(vi/vc)*((Q2+Q1)/2)-Q1)*1000000

// Molar ratio of titrant to macromolecule
y=xt2/mt2

***
0<xe1<xt1
0<me1<mt1
0<xe2<xt2
0<me2<mt2
```

Appendix 3.8. One Site Model with Two Populations of Dextran

```
// ITC 1 site model with two populations of dextran
// Iterative solution
// n = number of injections
// bf = branch factor - number of branches per molecule
// occ = molecular concentration
// cc = concentration of branch ends in syringe
// mtoi = initial concentration of macromolecule in the cell
// mto = concentration of macromolecule in the cell after first injection
// fvi = volume of first injection
// vi = injection volume
// vc = cell volume
// mt = total macromolecule [m]t
// me = free macromolecule [m]
// xat = total dextran, length a [xa]t
// xae = free dextran, length a [xa]
// xbt = total dextran, length b [xb]t
// xbe = free dextran, length b [xb]
// xratio = xat/(xat+xbt)
// mxa = [mxa]
// mxb = [mxb]
// Q = total energy release
// dq = energy release for given injection
```

```
IndVars: n
DepVars:dq

// K values are intrinsic

Params: vi,fvi,vo,mtoi,Ka,Kb,dha,dhb,bf,occ,xratio

// Effect of first injection, fvi, on receptor concentration in the cell prior to recorded injections

mto=mtoi*((2*vc-fvi)/(2*vc+fvi))
cc=occ*bf

//Energy released from all injections up to the previous injection

dv1=fvi+(n-1)*vi
mt1=mtoi*((2*vc-dv1)/(2*vc+dv1))
xt1=(2*dv1*cc)/(2*vc+dv1)

me1=mt1/(1+Ka*xae1+Kb*xbe1)
xae1=(xt1*xratio)/(1+Ka*me1)
xbe1=(xt1*(1-xratio))/(1+Kb*me1)
mxa1=Ka*me1*xae1
mxb1=Kb*me1*xbe1

Q1=(mxa1*dha+mxb1*dhb)*vc

//Energy released from all injections including the current injection
// Add volume of initial injection to volume added up to current injection

dv2=fvi+n*vi
mt2=mtoi*((2*vc-dv2)/(2*vc+dv2))
xt2=(2*dv2*cc)/(2*vc+dv2)

me2=mt2/(1+Ka*xae2+Kb*xbe2)
xae2=(xt2*xratio)/(1+Ka*me2)
xbe2=(xt2*(1-xratio))/(1+Kb*me2)
mxa2=Ka*me2*xae2
mxb2=Kb*me2*xbe2

Q2=(mxa2*dha+mxb2*dhb)*vc

//Heat evolved from current injection

dq=(Q2+(vi/vc)*((Q2+Q1)/2)-Q1)*1000000

// Molar ratio of titrant to macromolecule
y=xt2/mt2

***
0<xae1<xt1
0<xbe1<xt1
0<me1<mt1
0<xae2<xt2
0<xbe2<xt2
0<me2<mt2
***
```

Appendix 4. Isothermal Titration Calorimetry Raw Data

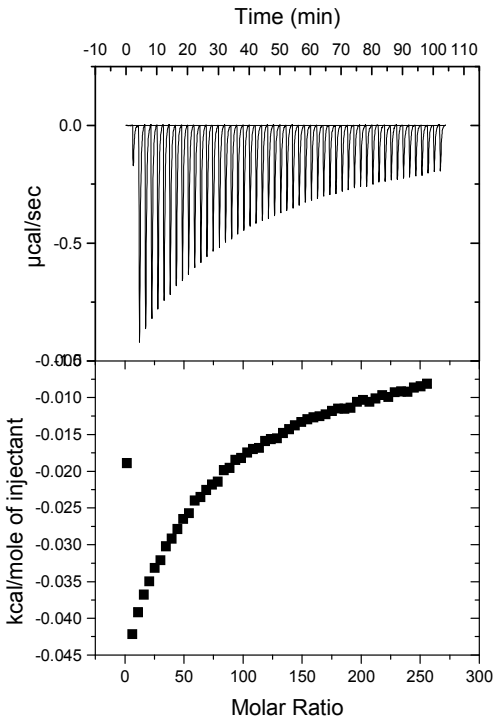

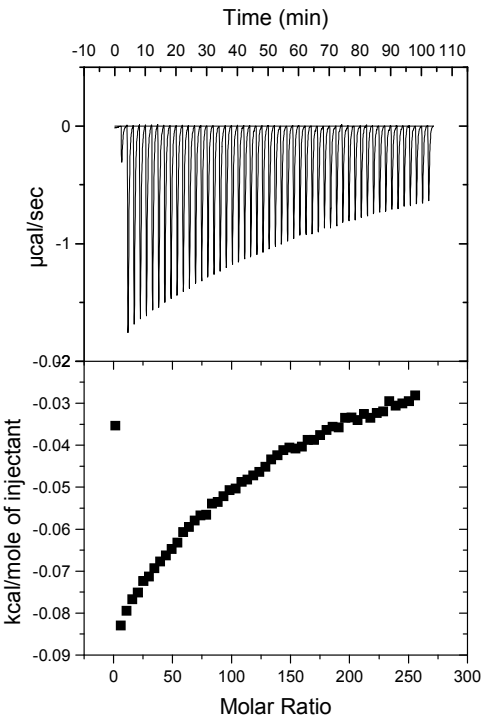

ITC Raw Data, Glucose

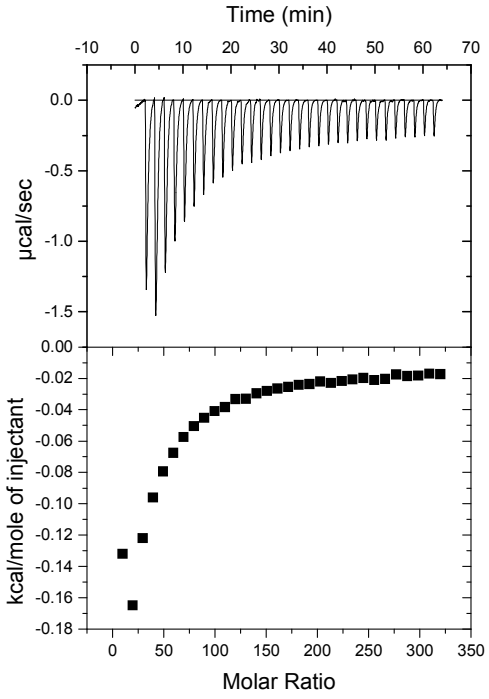

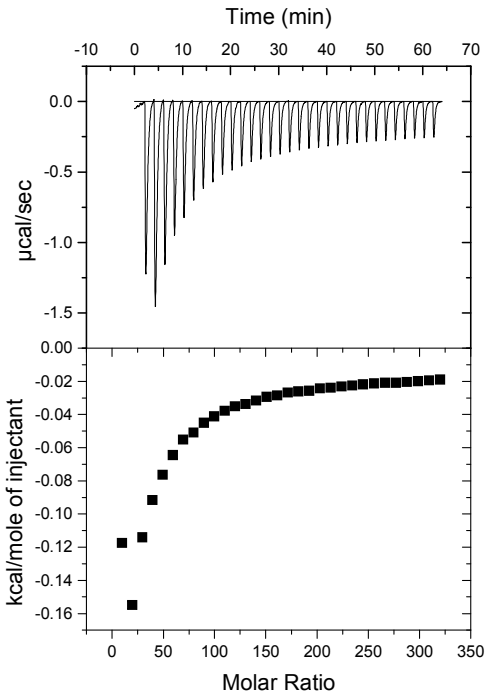

ITC Raw Data, Maltose

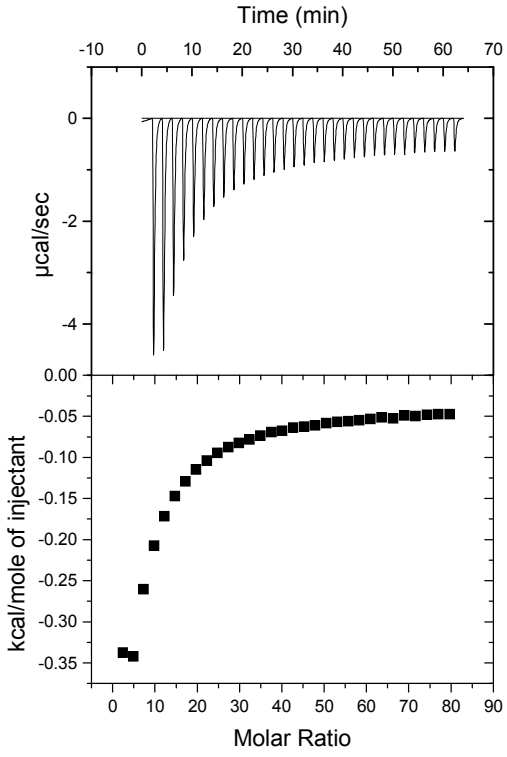

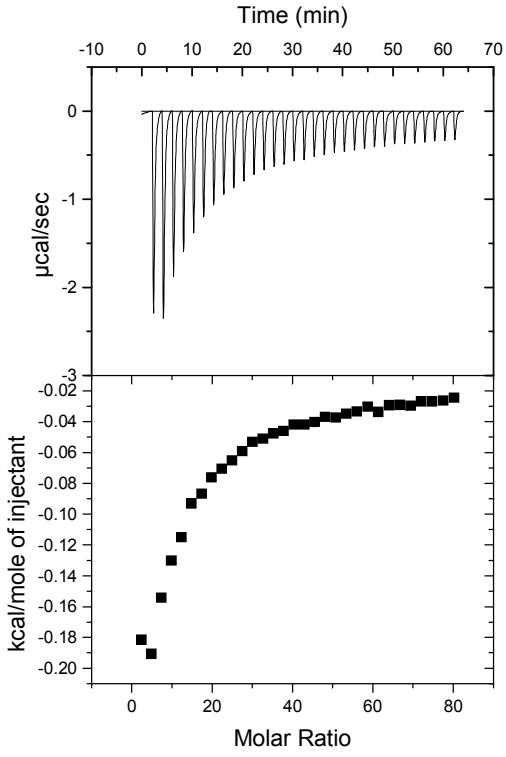

ITC Raw Data, Maltotriose

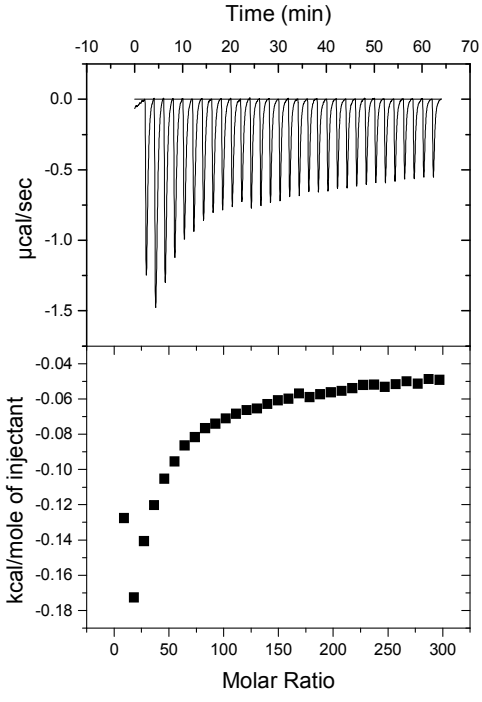

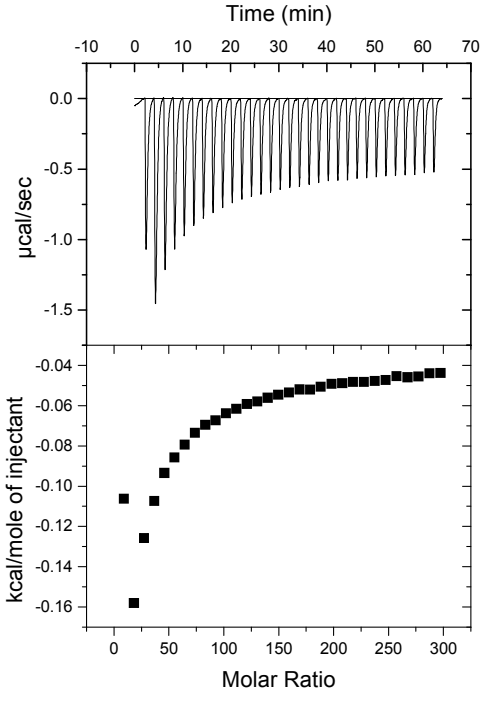

ITC Raw Data, 6kD dextran

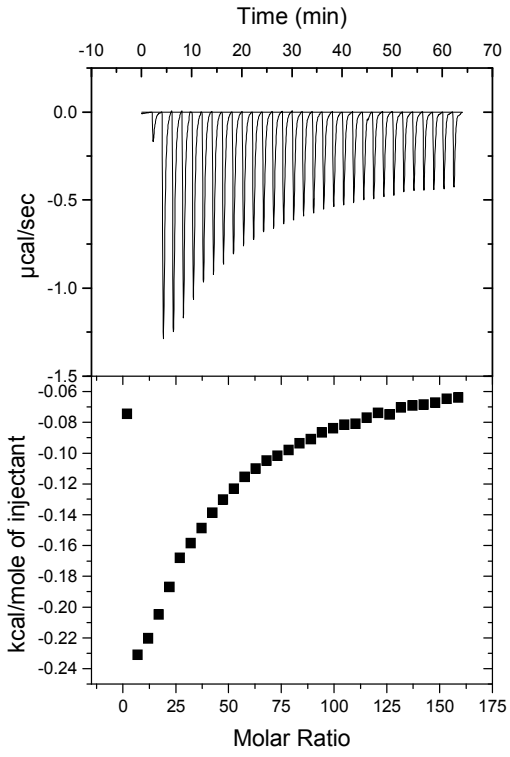

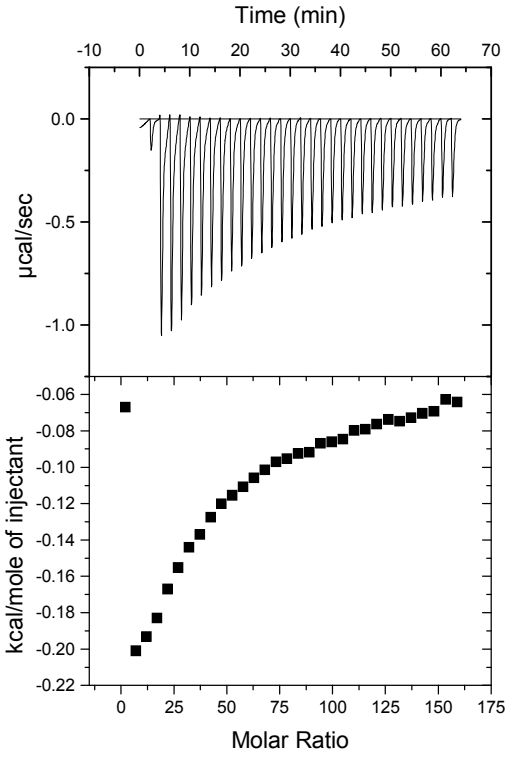

ITC Raw Data, 11kD dextran

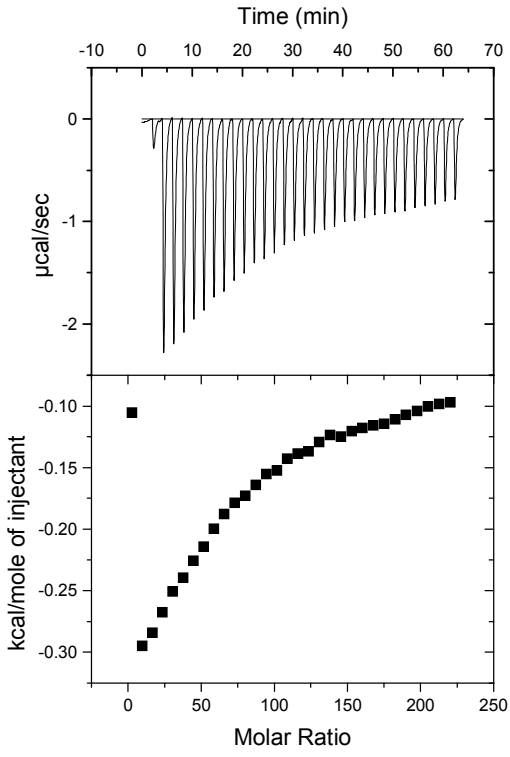

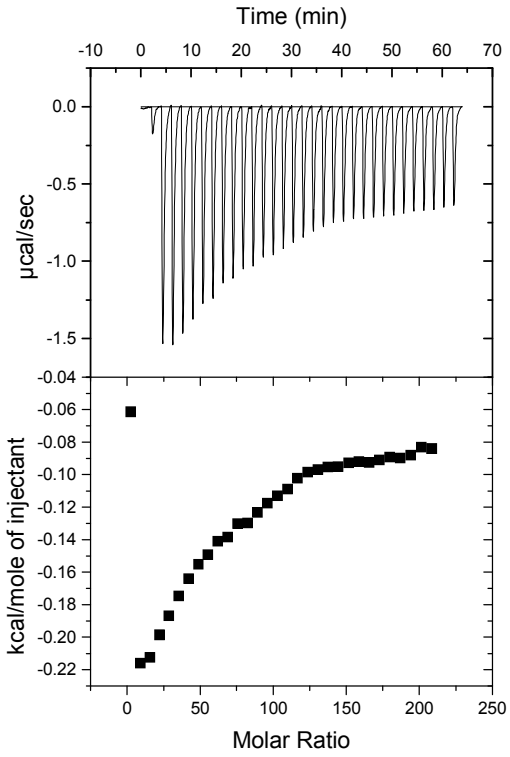

ITC Raw Data, 17kD dextran

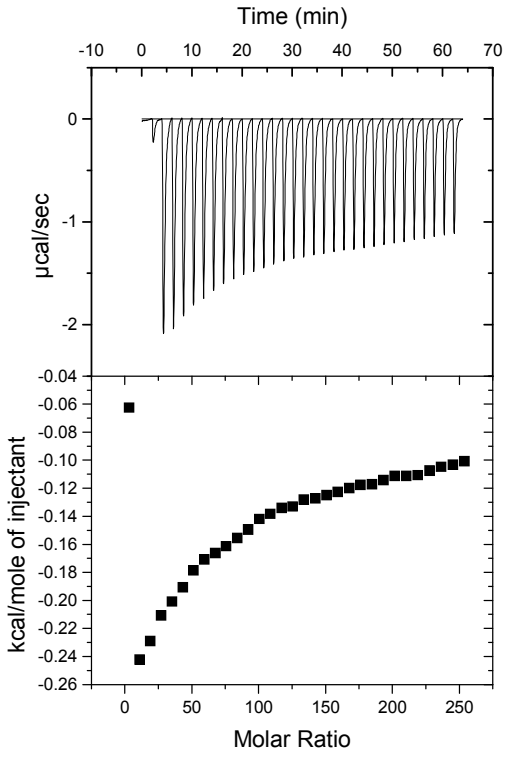

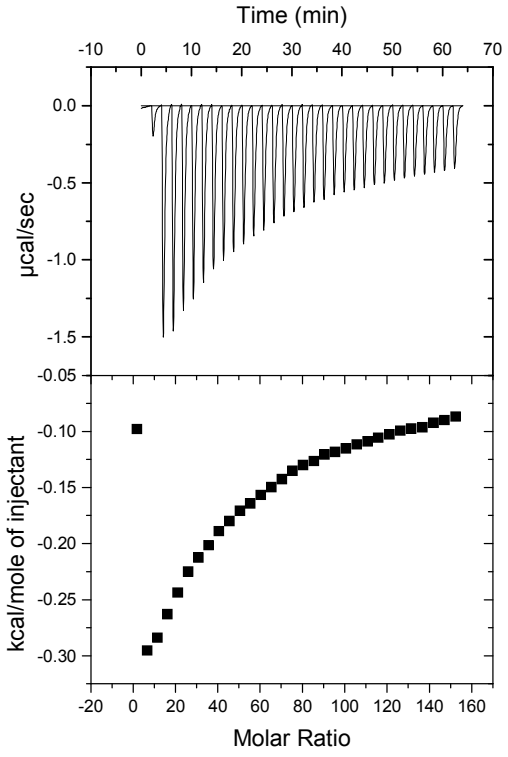

ITC Raw Data, 43kD dextran

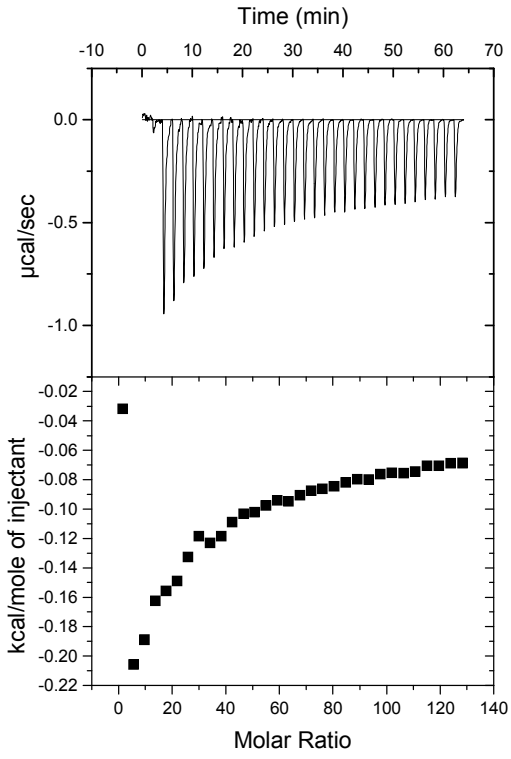

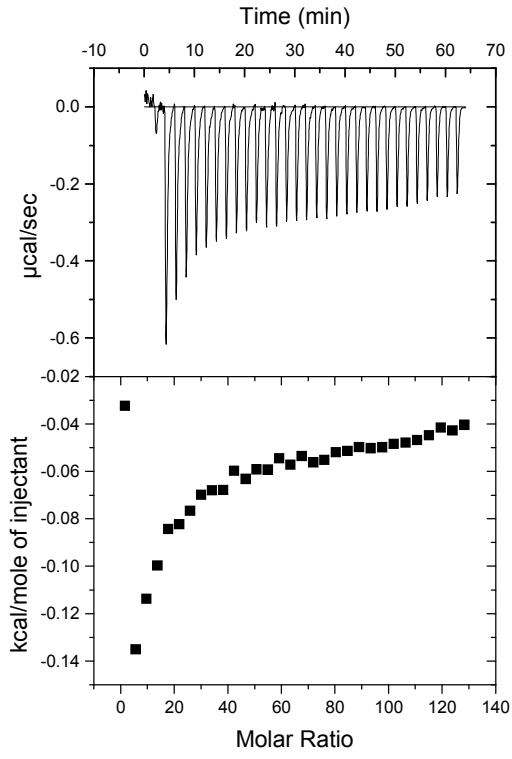

ITC Raw Data, 64kD dextran

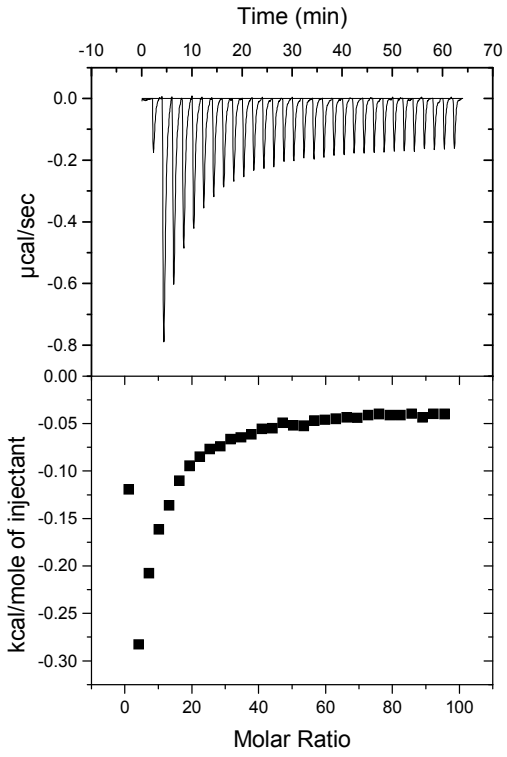

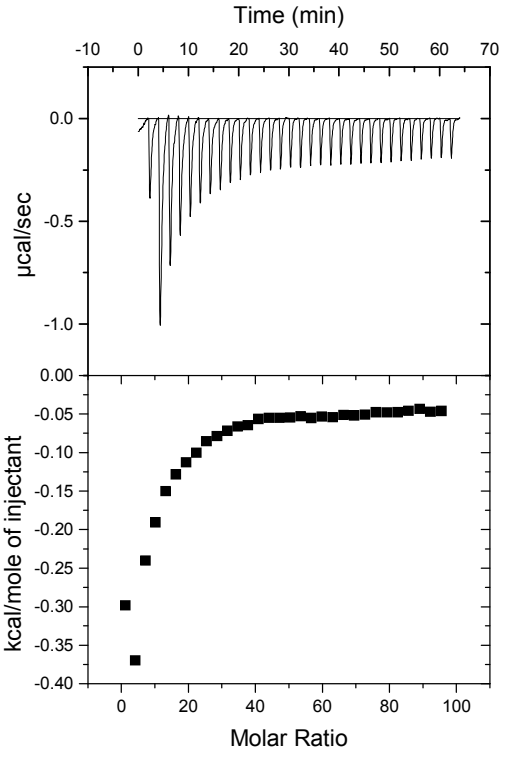

ITC Raw Data, 500kD dextran

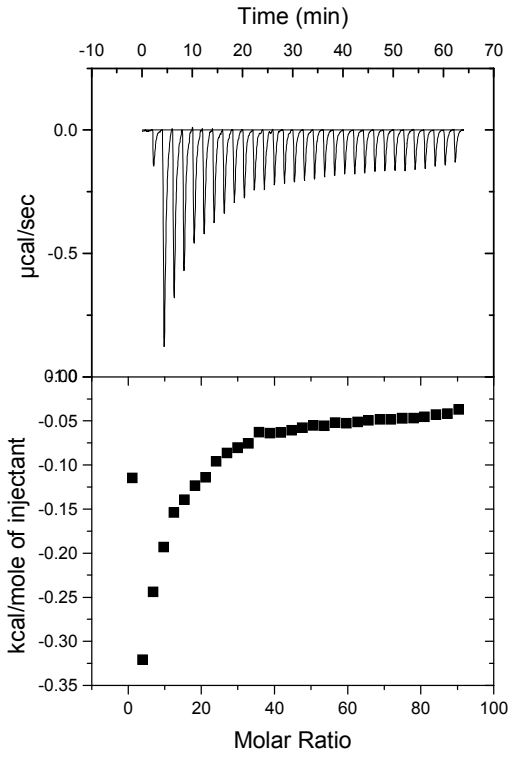

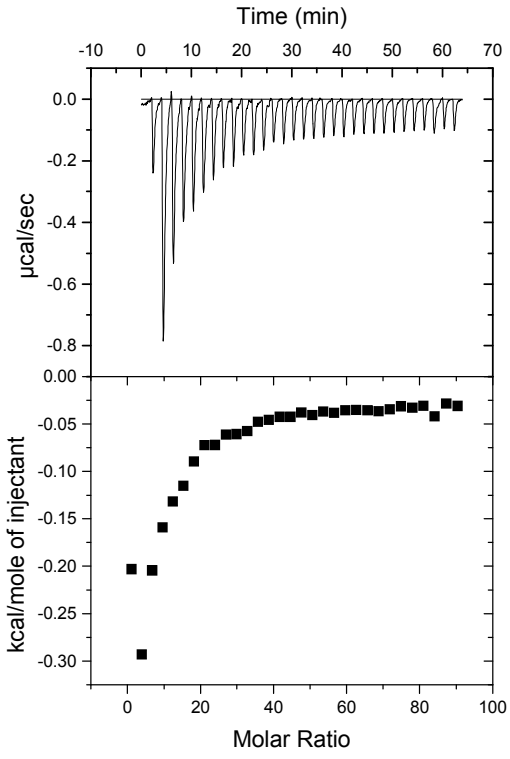

ITC Raw Data, 2000kD dextran

Appendix 5. Surface Plasmon Resonance Binding Theory

This appendix contains the derivation of the equations necessary to model data from the SPR.

Appendix 5.1. Langmuir Model

The analysis of the SPR data is based around the type of interaction it is believed is occurring. The most simple of which is a Langmuir binding:

$$[M]+[X]=[MX] \qquad \textbf{Equation A5-19}$$

$$\frac{d[MX]}{dt}=k_a[M][X]-k_d[MX] \qquad \textbf{Equation A5-20}$$

$$[X]=[X_{TOT}]-[MX] \qquad \textbf{Equation A5-21}$$

Equation A5-21 is substituted into Equation A5-20 as it is not possible to calculate the concentration of unbound dextran ligands. The total concentration, of bound and unbound dextran, is estimated as part of the data analysis (an explanation of why dextran, rather than conA, is bound to the sensor chip surface can be found in Section 4.2.2). Equation A5-20, once *[X]* has been replaced, can be rewritten in terms of the SPR signal:

$$\frac{dR}{dt}=k_a[M](R_{\max}-R)-k_dR \qquad \textbf{Equation A5-22}$$

During the association phase the whole of Equation A5-22 is active. During dissociation the concentration of lectin, *C*, is negligible and so Equation A5-22 becomes:

$$\frac{dR}{dt}=-k_dR \qquad \textbf{Equation A5-23}$$

Once the data is loaded into the software that is supplied by BIAcore, a least squares fit can be performed using Equation A5-22 (least squares fit is similar to Section 3.2.2, but without the denominator).

Appendix 5.2. Bivalent Model

The bivalent model assumes that the binding of a second dextran ligand to a conA tetramer has different association and dissociation rates than the primary bind:

$$[MX]+[X]=[MXX] \qquad \textbf{Equation A5-24}$$

$$\frac{d[MXX]}{dt}=k_{a2}[MX][X]-k_{d2}[MXX] \qquad \textbf{Equation A5-25}$$

Both of these equations are then fitted with an extended form of Equation A5-19, taking into account the additional removal and production of *[MX]* in the second binding (Equation A5-27). The unbound dextran term is now substituted using :

$$[X]=[X_{TOT}]-[MX]-[MXX] \qquad \textbf{Equation A5-26}$$

$$\frac{d[MX]}{dt}=k_{a1}[M][X]-k_{d1}[MX]-\left(k_{a2[}[MX][X]-k_{d2}[MXX]\right) \qquad \textbf{Equation A5-27}$$

The difference between the first and second bind to a conA molecule could have a positive or a negative effect. There may be conformational changes caused by the first binding which facilitate the other binding sites, or there could be problems caused by the dextran molecules once the conA is no longer free-floating in solution.

Appendix 5.3. Heterogeneous Ligand Population Model

This binding model assumes that there are two populations of *[X]*, which in total account for all of the binding:

$$[M]+[X_1]=[MX_1] \qquad \textbf{Equation A5-28}$$

$$\frac{d[MX_1]}{dt}=k_{a1}[M][X_1]-k_{d1}[MX_1] \qquad \textbf{Equation A5-29}$$

$$[M]+[X_2]=[MX_2] \qquad \textbf{Equation A5-30}$$

$$\frac{d[MX_2]}{dt}=k_{a2}[M][X_2]-k_{d2}[MX_2] \qquad \textbf{Equation A5-31}$$

In this case the total of bound and unbound dextran ligands is divided into two populations, both of which must be estimated in the analysis. This is done most simply by setting a fixed ratio, *Y*, and then estimating the total, Equation A5-29 and Equation A5-31 can therefore be rewritten in terms of the SPR signal:

$$\frac{dR_1}{dt}=k_{a1}C\left(YR_{\max}-R_1\right)-k_{d1}R_1 \qquad \textbf{Equation A5-32}$$

$$\frac{dR_2}{dt}=k_{a2}C\left((1-Y)R_{\max}-R_2\right)-k_{d2}R_2 \qquad \textbf{Equation A5-33}$$

Appendix 5.4. Additional Effects

Langmuir binding, with mass transfer effect, MT:

$$\frac{d[M_s]}{dt}=k_t\left([M]-[M_s]\right)-\left(k_a[M_s][X]-k_d[MX]\right) \qquad \textbf{Equation A5-34}$$

[M_s] is then used in the proceeding equations rather than *[M]*. Similar equations can be written for the bivalent binding and heterogeneous binding analyses.

Bulk refractive index (RI) effect, incorporated as a simple multiple of the conA concentration:

$$R_t=R+[M]R_i \qquad \textbf{Equation A5-35}$$

Nomenclature:

K_a	Association constant (M^{-1})
k_a	Association rate ($M^{-1}s^{-1}$)
k_d	Dissociation rate (s^{-1})
$[M]_i$	Concentration of free lectin (conA) (M)
$[MX]_i$	Concentration of conA/dextran complex (M)
$[MXX]_i$	Concentration of conA/dextran/dextran complex (M)
R	Response (RU)
R_t	Total response (RU)
R_{max}	Max. dextran binding capacity (RU)
R_i	Refractive index effect (RU M^{-1})
t	Time (s)
$[X]_i$	Free dextran binding ligands at injection, i (M)
$[X]_{TOT}$	Total dextran ligands, bound and unbound (M)
χ^2	Size of error

Appendix 6. Surface Plasmon Resonance Models

This appendix contains the programs for the SPR experiments which were entered into Scientist® in order to model the data.

Appendix 6.1. Langmuir Model

```
// SPR Langmuir model
// Iterative solution
// T = Time
// c1 – c5 = concentration of injections 1 – 5
// rt1 – rt5 = response, at time t of injections 1 -5
// rm = maximum response of activated surface
// r11 – r51 = response of injection 1 to 5 from complex [MX]
// ka1 = association rate
// kd1 = dissociation rate
// ri = refractive index factor

IndVars: T,c1,c2,c3,c4,c5
DepVars: rt1,rt2,rt3,rt4,rt5
Params: rm,ka1,kd1,ri

r11'=ka1*c1*(rm-r11)-kd1*r11
rt1=r11+c1*ri

r21'=ka1*c2*(rm-r21)-kd1*r21
rt2=r21+c2*ri

r31'=ka1*c3*(rm-r31)-kd1*r31
rt3=r31+c3*ri

r41'=ka1*c4*(rm-r41)-kd1*r41
rt4=r41+c4*ri

r51'=ka1*c5*(rm-r51)-kd1*r51
rt5=r51+c5*ri

// Initial conditions
t=0

r11=0
r21=0
r31=0
r41=0
r51=0

***
```

Appendix 6.2. Langmuir Model with Mass Transfer

```
// SPR Langmuir model with mass transfer
// Iterative solution
// T = Time
// c1 – c5 = concentration of injections 1 – 5
// cs1 – cs5 = concentration at activated surface
// rt1 – rt5 = response, at time t of injections 1 -5
// rm = maximum response of activated surface
// r11 – r51 = response of injection 1 to 5 from complex [MX]
// ka1 = association rate
// kd1 = dissociation rate
// ri = refractive index factor
// kt = mass transfer coefficient

IndVars: T,c1,c2,c3,c4,c5
DepVars: rt1,rt2,rt3,rt4,rt5
Params: rm,ka1,kd1,ri,kt

cs1'=kt*(c1-cs1)-(ka1*cs1*(rm-r11)-kd1*r11)
r11'=ka1*cs1*(rm-r11)-kd1*r11
rt1=r11+c1*ri

cs2'=kt*(c2-cs2)-(ka1*cs2*(rm-r21)-kd1*r21)
r21'=ka1*cs2*(rm-r21)-kd1*r21
rt2=r21+c2*ri

cs3'=kt*(c3-cs3)-(ka1*cs3*(rm-r31)-kd1*r31)
r31'=ka1*cs3*(rm-r31)-kd1*r31
rt3=r31+c3*ri

cs4'=kt*(c4-cs4)-(ka1*cs4*(rm-r41)-kd1*r41)
r41'=ka1*cs4*(rm-r41)-kd1*r41
rt4=r41+c4*ri

cs5'=kt*(c5-cs5)-(ka1*cs5*(rm-r51)-kd1*r51)
r51'=ka1*cs5*(rm-r51)-kd1*r51
rt5=r51+c5*ri

// Initial conditions
t=0

cs1=0   cs2=0   cs3=0   cs4=0   cs5=0
r11=0   r21=0   r31=0   r41=0   r51=0

***
```

Appendix 6.3. Bivalent Model

```
// SPR Bivalent model
// Iterative solution
// T = Time
// c1 – c5 = concentration of injections 1 – 5
// rt1 – rt5 = response, at time t of injections 1 -5
// rm = maximum response of activated surface
// r11 – r51 = response of injection 1 to 5 from complex [MX]
// r12 – r52 = response of injection 1 to 5 from complex [MXX]
```

```
// ka1, ka2 = association rate of [MX] and [MXX]
// kd1, kd2 = dissociation rate of [MX] and [MXX]
// ri = refractive index factor

IndVars: T,c1,c2,c3,c4,c5
DepVars: rt1,rt2,rt3,rt4,rt5
Params: rm,ka1,ka2,kd1,kd2,ri

r11'=2*ka1*c1*(rm-r11-2*r12)-kd1*r11-(ka2*r11*(rm-r11-2*r12)-2*kd2*r12)
r12'=ka2*r11*(rm-r11-2*r12)-2*kd2*r12
rt1=r11+r12+c1*ri

r21'=2*ka1*c2*(rm-r21-2*r22)-kd1*r21-(ka2*r21*(rm-r21-2*r22)-2*kd2*r22)
r22'=ka2*r21*(rm-r21-2*r22)-2*kd2*r22
rt2=r21+r22+c2*ri

r31'=2*ka1*c3*(rm-r31-2*r32)-kd1*r31-(ka2*r31*(rm-r31-2*r32)-2*kd2*r32)
r32'=ka2*r31*(rm-r31-2*r32)-2*kd2*r32
rt3=r31+r32+c3*ri

r41'=2*ka1*c4*(rm-r41-2*r42)-kd1*r41-(ka2*r41*(rm-r41-2*r42)-2*kd2*r42)
r42'=ka2*r41*(rm-r41-2*r42)-2*kd2*r42
rt4=r41+r42+c4*ri

r51'=2*ka1*c5*(rm-r51-2*r52)-kd1*r51-(ka2*r51*(rm-r51-2*r52)-2*kd2*r52)
r52'=ka2*r51*(rm-r51-2*r52)-2*kd2*r52
rt5=r51+r52+c5*ri

// Initial conditions
t=0

r11=0   r12=0   r21=0   r22=0   r31=0   r32=0   r41=0   r42=0   r51=0   r52=0

***
```

Appendix 6.4. Heterogeneous Model

```
// SPR Heterogeneous model
// Iterative solution
// T = Time
// c1 – c5 = concentration of injections 1 – 5
// rt1 – rt5 = response, at time t of injections 1 -5
// rm = maximum response of activated surface
// r11 – r51 = response of injection 1 to 5 from complex [MX1]
// r13 – r53 = response of injection 1 to 5 from complex [MX2]
// ka1, ka3 = association rate of [MX1] and [MX2]
// kd1, kd3 = dissociation rate of [MX1] and [MX2]
// ri = refractive index factor
// y = ratio of [MX1] to [MX2]

IndVars: T,c1,c2,c3,c4,c5
DepVars: rt1,rt2,rt3,rt4,rt5
Params: rm,ka1,ka3,kd1,kd3,y,ri

r11'=ka1*c1*(y*rm-r11)-kd1*r11
r13'=ka3*c1*((1-y)*rm-r13)-kd3*r13
rt1=r11+r13+c1*ri
r21'=ka1*c2*(y*rm-r21)-kd1*r21
```

```
r23'=ka3*c2*((1-y)*rm-r23)-kd3*r23
rt2=r21+r23+c2*ri

r31'=ka1*c3*(y*rm-r31)-kd1*r31
r33'=ka3*c3*((1-y)*rm-r33)-kd3*r33
rt3=r31+r33+c3*ri

r41'=ka1*c4*(y*rm-r41)-kd1*r41
r43'=ka3*c4*((1-y)*rm-r43)-kd3*r43
rt4=r41+r43+c4*ri

r51'=ka1*c5*(y*rm-r51)-kd1*r51
r53'=ka3*c5*((1-y)*rm-r53)-kd3*r53
rt5=r51+r53+c5*ri

// Initial conditions
t=0

r11=0   r13=0   r21=0   r23=0   r31=0   r33=0   r41=0   r43=0   r51=00  r53=0

***
```

Appendix 6.5. Heterogeneous Bivalent Model

```
// SPR Heterogeneous bivalent model
// Iterative solution
// T = Time
// c1 – c5 = concentration of injections 1 – 5
// rt1 – rt5 = response, at time t of injections 1 -5
// rm = maximum response of activated surface
// r11 – r51 = response of injection 1 to 5 from complex [MX1]
// r12 – r52 = response of injection 1 to 5 from complex [MXX1]
// r13 – r53 = response of injection 1 to 5 from complex [MX2]
// r14 – r54 = response of injection 1 to 5 from complex [MXX2]
// ka1 – ka4 = association rate of [MX1], [MXX1], [MX2] and [MXX2]
// kd1 – kd4 = dissociation rate of [MX1], [MXX1], [MX2] and [MXX2]
// ri = refractive index factor
// y = ratio of [MX1] to [MX2]

IndVars: t,c1,c2,c3,c4,c5
DepVars: rt1,rt2,rt3,rt4,rt5
Params: rm,ka1,ka2,kd1,kd2,ka3,kd3,ka4,kd4,y,ri

r11'=2*ka1*c1*(rm*y-r11-2*r12)-kd1*r11-(ka2*r11*(rm*y-r11-2*r12)-2*kd2*r12)
r12'=ka2*r11*(rm*y-r11-2*r12)-2*kd2*r12
r13'=2*ka3*c1*(rm*(1-y)-r13-2*r14)-kd3*r13-(ka4*r13*(rm*(1-y)-r13-2*r14)-2*kd4*r14)
r14'=ka4*r13*(rm*(1-y)-r13-2*r14)-2*kd4*r14
rt1=r11+r12+r13+r14+c1*ri

r21'=2*ka1*c2*(rm*y-r21-2*r22)-kd1*r21-(ka2*r21*(rm*y-r21-2*r22)-2*kd2*r22)
r22'=ka2*r21*(rm*y-r21-2*r22)-2*kd2*r22
r23'=2*ka3*c2*(rm*(1-y)-r23-2*r24)-kd3*r23-(ka4*r23*(rm*(1-y)-r23-2*r24)-2*kd4*r24)
r24'=ka4*r23*(rm*(1-y)-r23-2*r24)-2*kd4*r24
rt2=r21+r22+r23+r24+c2*ri

r31'=2*ka1*c3*(rm*y-r31-2*r32)-kd1*r31-(ka2*r31*(rm*y-r31-2*r32)-2*kd2*r32)
r32'=ka2*r31*(rm*y-r31-2*r32)-2*kd2*r32
r33'=2*ka3*c3*(rm*(1-y)-r33-2*r34)-kd3*r33-(ka4*r33*(rm*(1-y)-r33-2*r34)-2*kd4*r34)
```

```
r34'=ka4*r33*(rm*(1-y)-r33-2*r34)-2*kd4*r34
rt3=r31+r32+r33+r34+c3*ri

r41'=2*ka1*c4*(rm*y-r41-2*r42)-kd1*r41-(ka2*r41*(rm*y-r41-2*r42)-2*kd2*r42)
r42'=ka2*r41*(rm*y-r41-2*r42)-2*kd2*r42
r43'=2*ka3*c4*(rm*(1-y)-r43-2*r44)-kd3*r43-(ka4*r43*(rm*(1-y)-r43-2*r44)-2*kd4*r44)
r44'=ka4*r43*(rm*(1-y)-r43-2*r44)-2*kd4*r44
rt4=r41+r42+r43+r44+c4*ri

r51'=2*ka1*c5*(rm*y-r51-2*r52)-kd1*r51-(ka2*r51*(rm*y-r51-2*r52)-2*kd2*r52)
r52'=ka2*r51*(rm*y-r51-2*r52)-2*kd2*r52
r53'=2*ka3*c5*(rm*(1-y)-r53-2*r54)-kd3*r53-(ka4*r53*(rm*(1-y)-r53-2*r54)-2*kd4*r54)
r54'=ka4*r53*(rm*(1-y)-r53-2*r54)-2*kd4*r54
rt5=r51+r52+r53+r54+c5*ri

// Initial conditions
t=0

r11=0   r12=0   r13=0   r14=0   r21=0   r22=0   r23=0   r24=0   r31=0   r32=0   r33=0
r34=0   r41=0   r42=0   r43=0   r44=0   r51=0   r52=0   r53=0   r54=0

***
```

Appendix 7. Surface Plasmon Resonance Data

Appendix 7.1. Deconvoluted SPR data

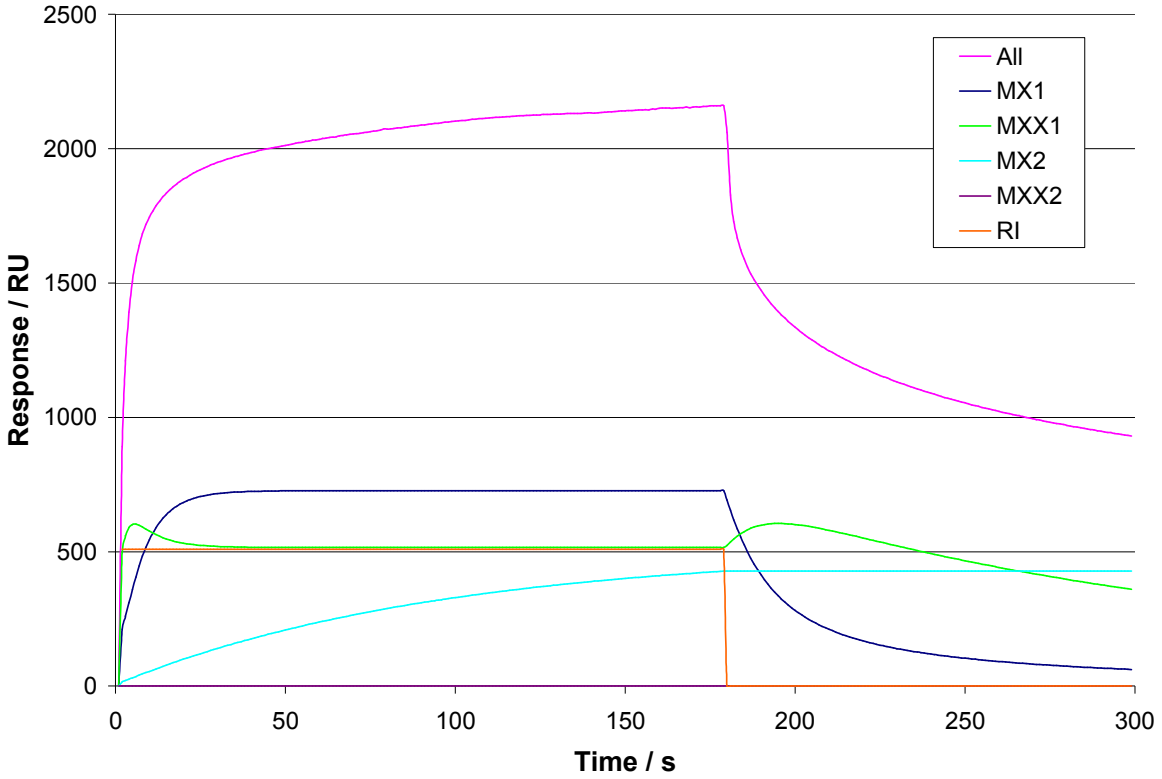

Graph of response components that comprise the total seen response of an injection of 10.2μM conA over a blank sensor surface.

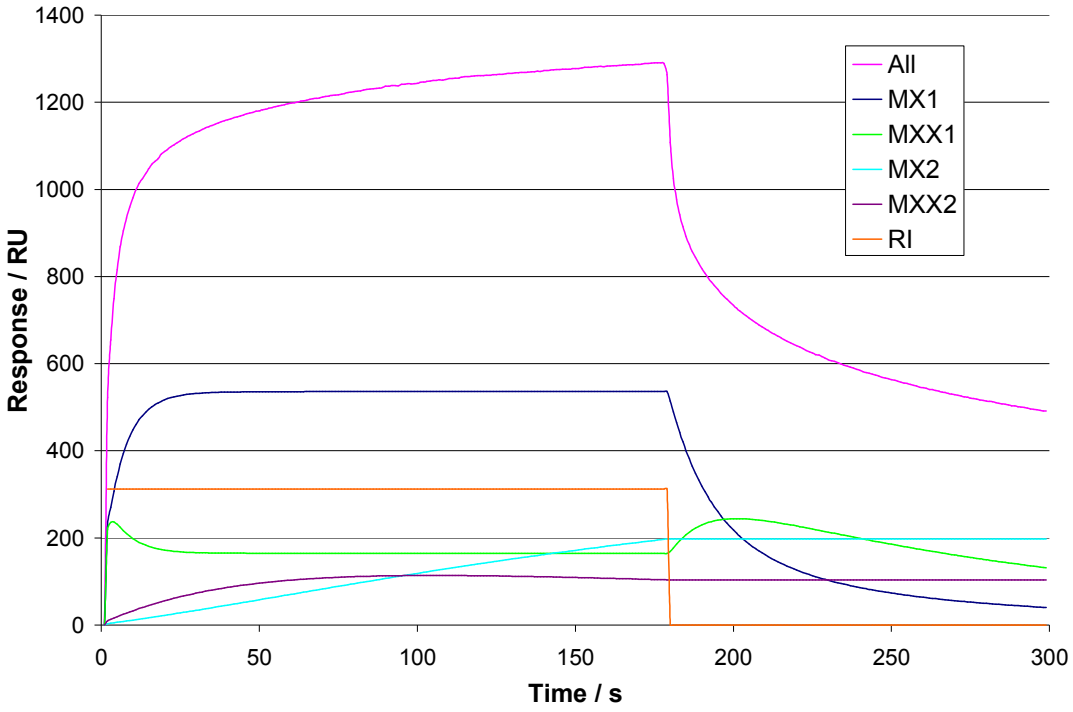

Graph of response components that comprise the total seen response of an injection of 10.2µM conA over 43kD dextran.

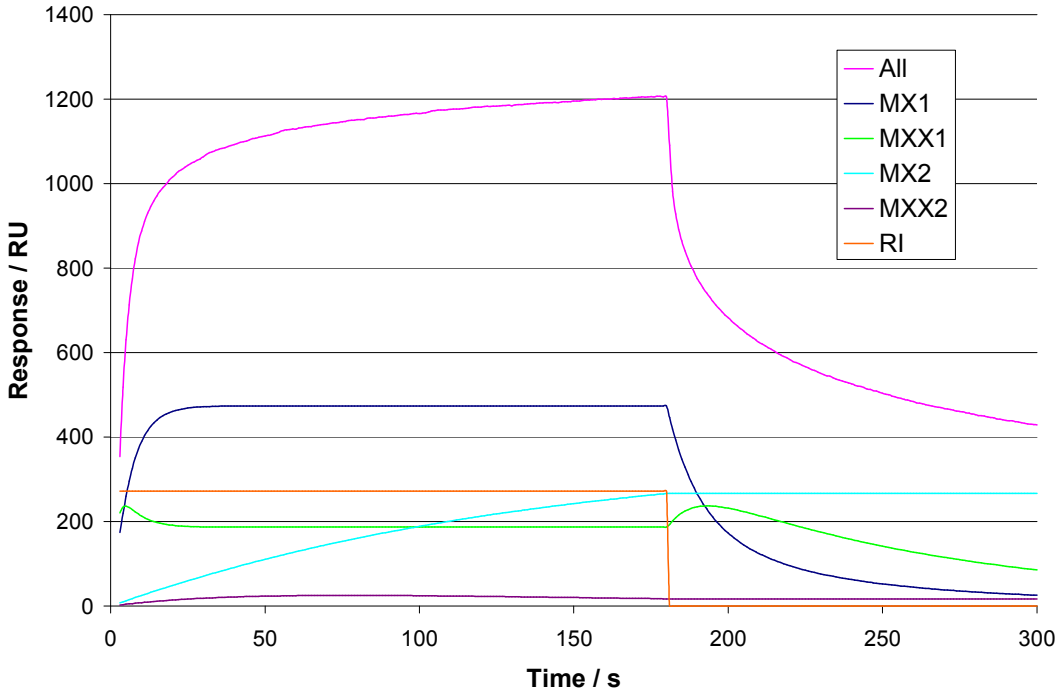

Graph of response components that comprise the total seen response of an injection of 10.2µM conA over 500kD dextran.

Appendix 7.2. SPR Raw Data

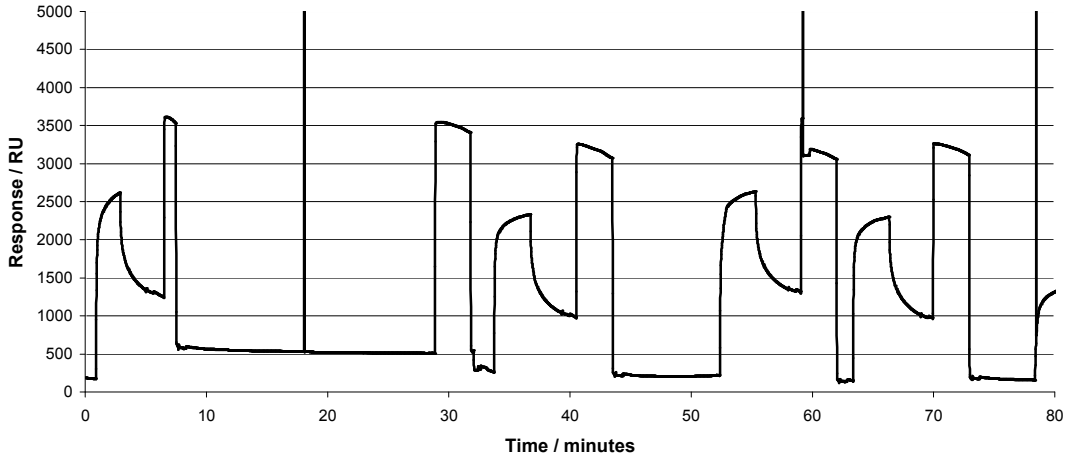

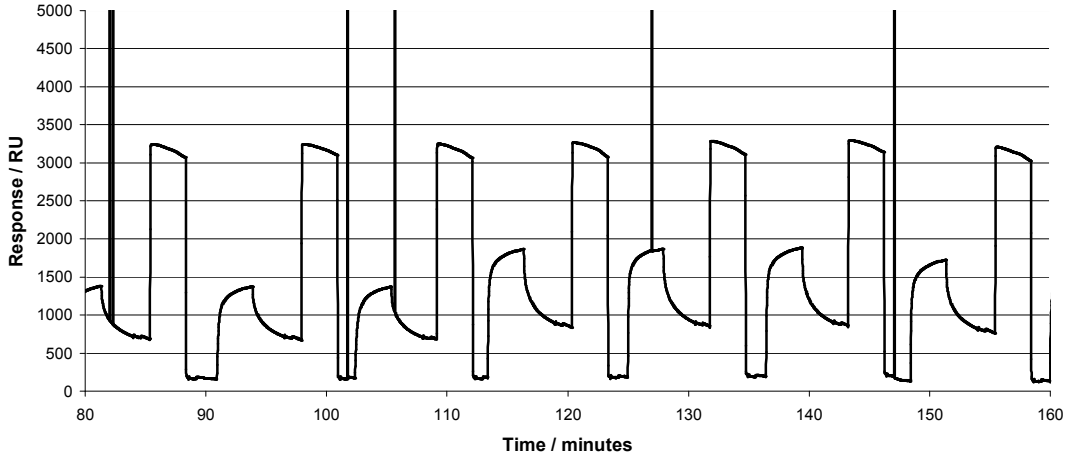

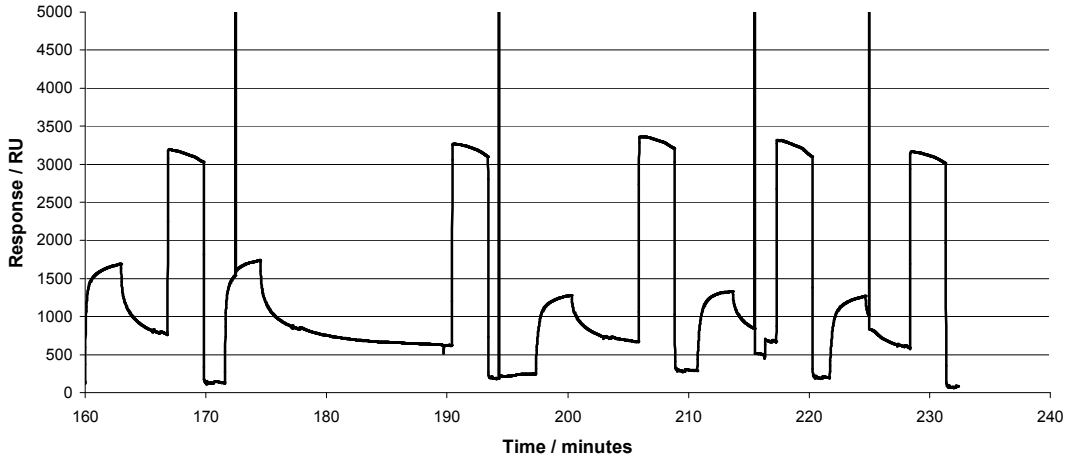

SPR Blank bind raw data

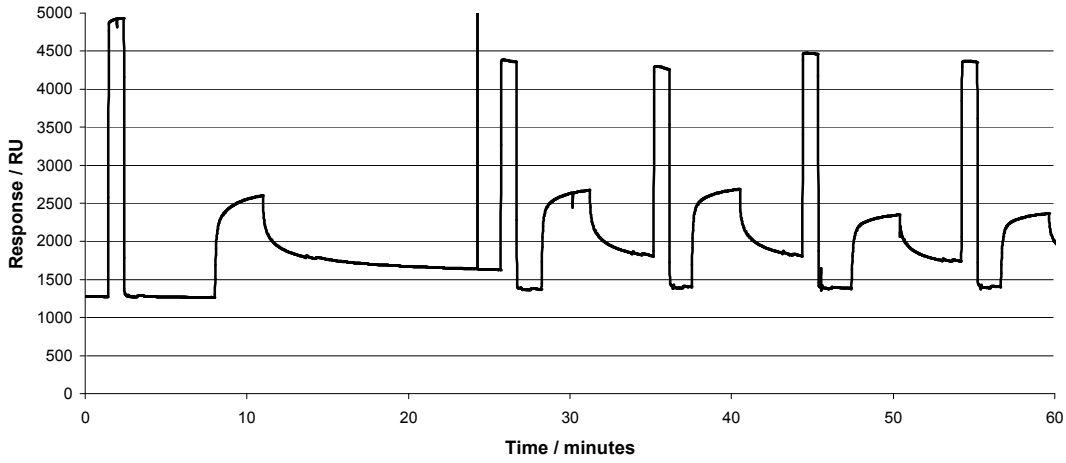

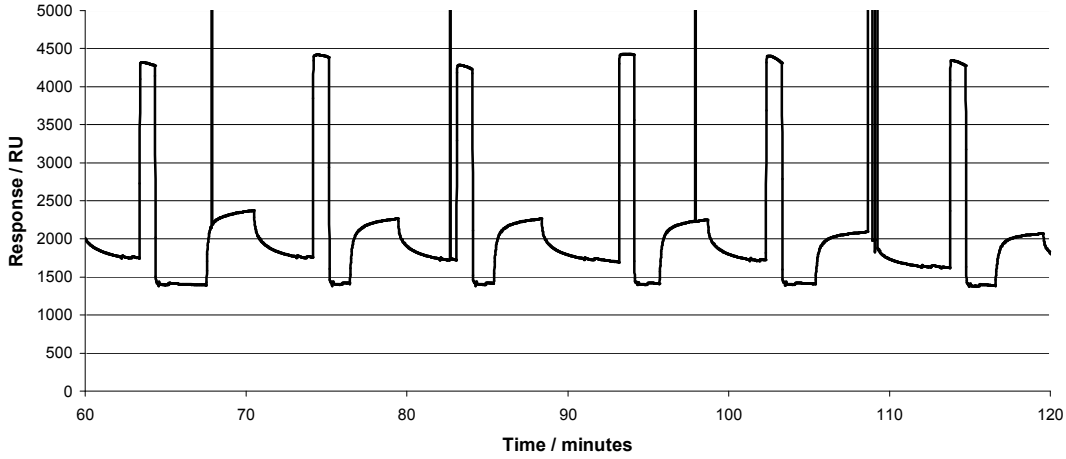

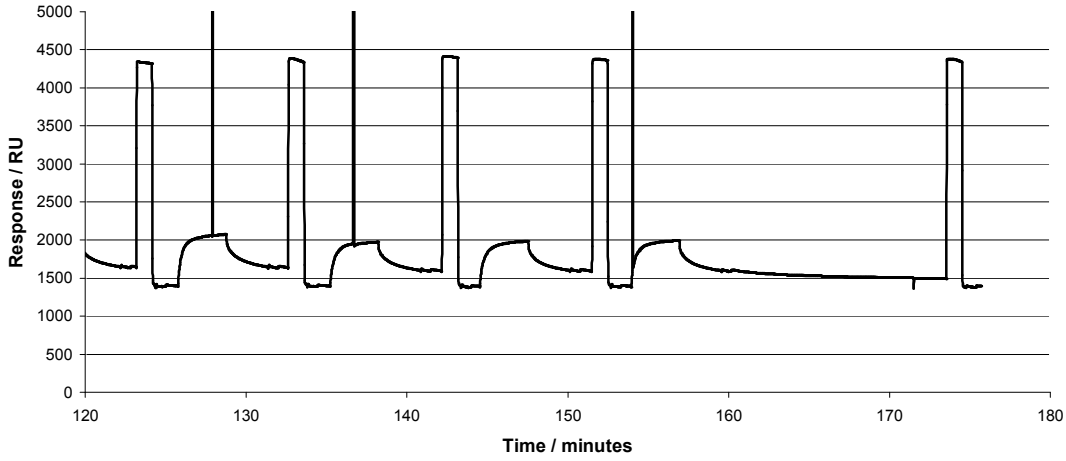

SPR Raw data,43kD bind

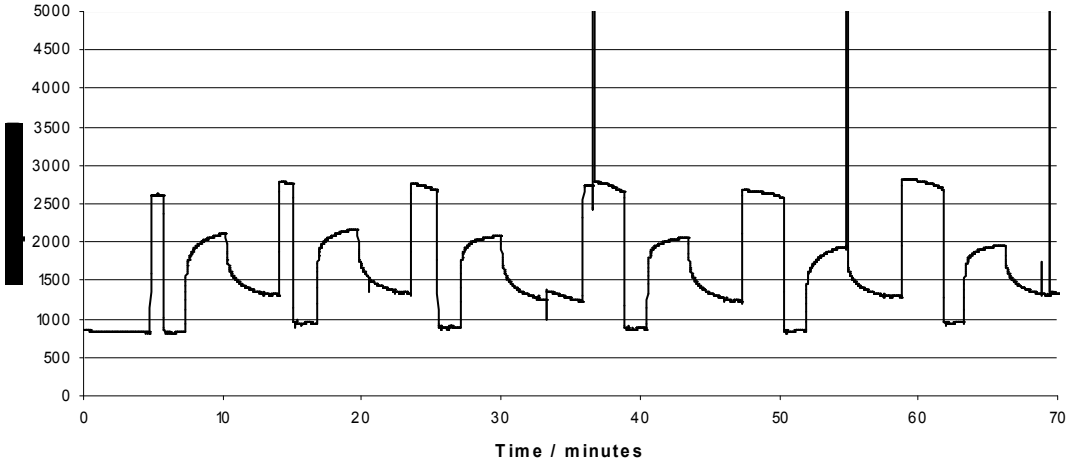

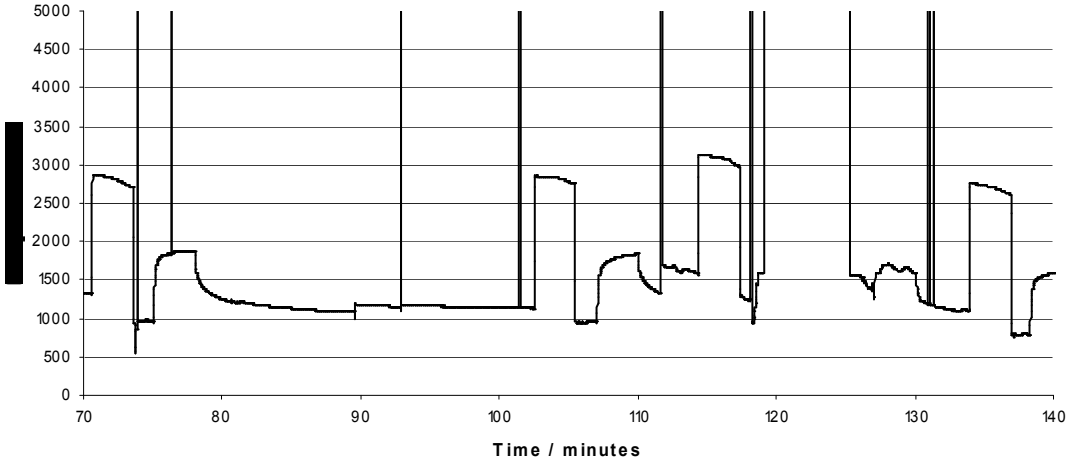

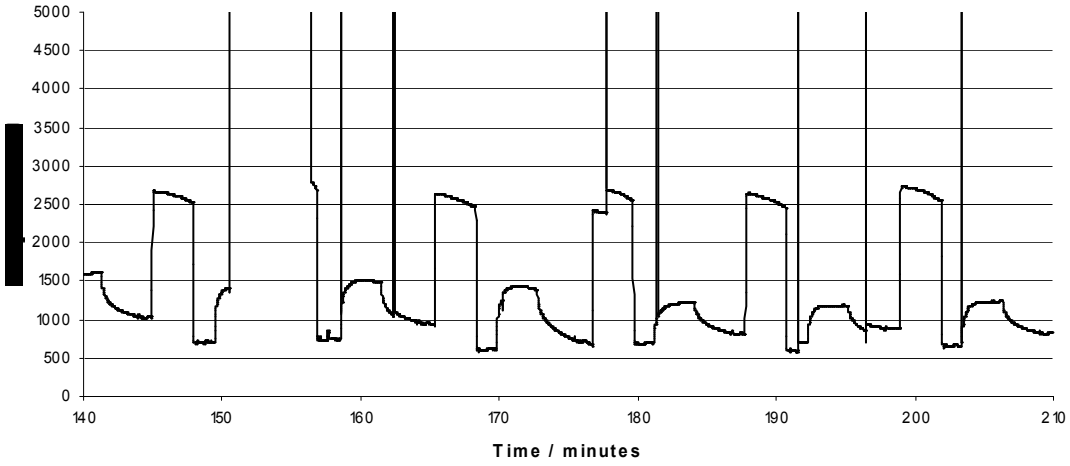

SPR Raw data, 500kD bind

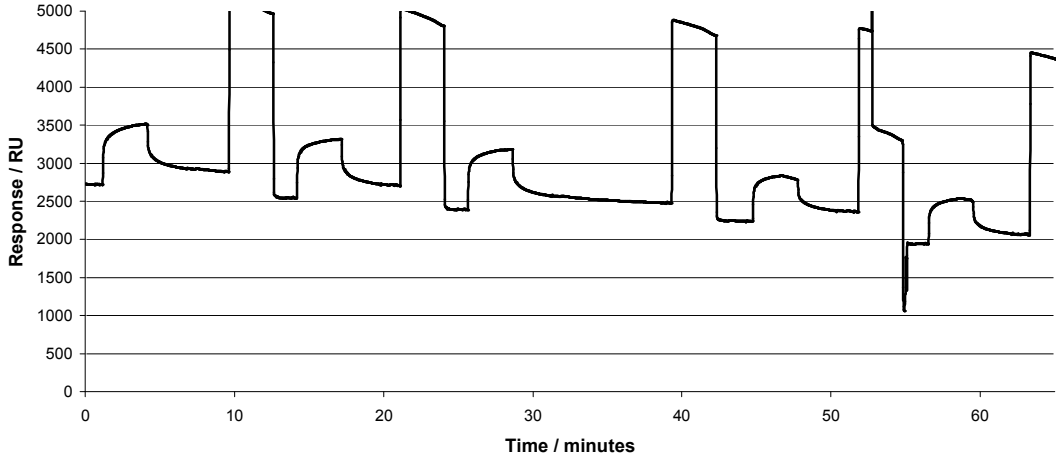

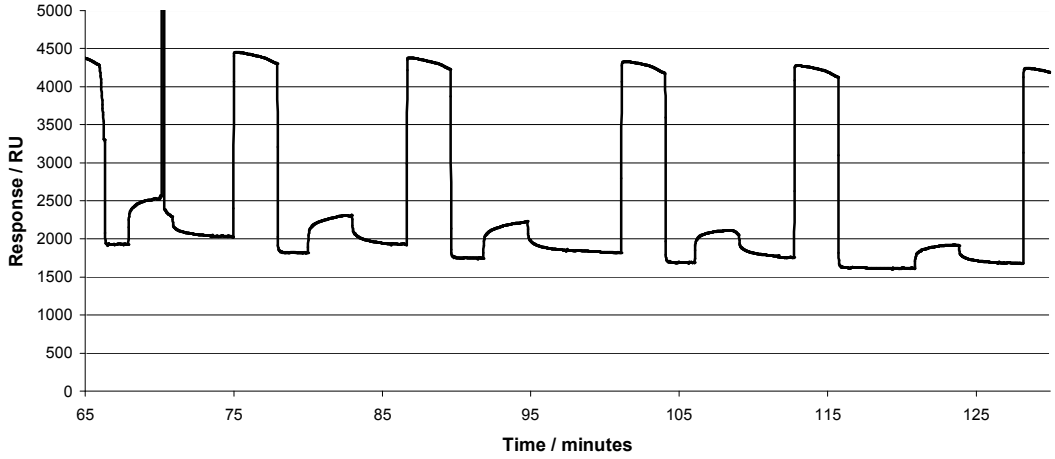

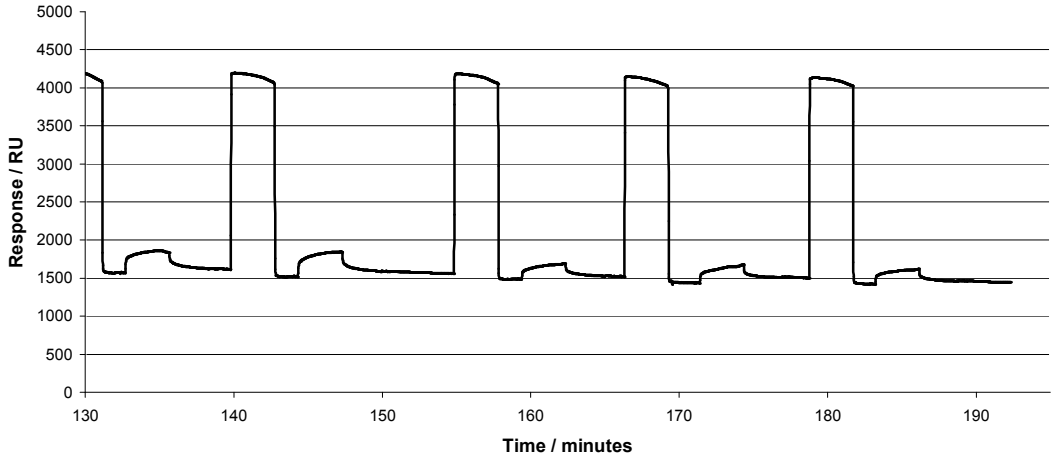

SPR Raw data, 2000kD bind

Appendix 8. Rheology - Maxwell Model for Viscoelasticity

This appendix contains the derivation of the Maxwell model for a viscoelastic material [133].

Given the equations for a Newtonian solution and by Hooke's law for a spring:

$$\sigma = \eta\dot{\gamma} \qquad \textbf{Equation A8-36}$$

$$\sigma = G\gamma \qquad \textbf{Equation A8-37}$$

It can be seen from these two equations that the shear stress for a solution is proportional to the rate at which it is being sheared. For a spring the stress is proportional to the magnitude of the strain.

Maxwell [111] developed a model which contained a Hookean spring and a Newtonian dashpot in series.

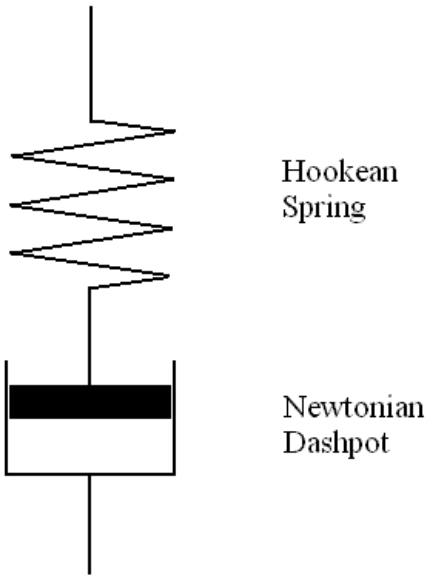

For a finite shear strain applied constantly over time, the spring will respond, giving a maximum stress. The dashpot will gradually release that stress through movement of the piston in the fluid. The release of the stress can be viewed as a first-order rate process:

$$\frac{d\sigma}{dt} = -k\sigma \qquad \textbf{Equation A8-38}$$

Integrating Equation A8-38 gives:

$$\ln\sigma(t) - \ln\sigma(0) = -kt \qquad \textbf{Equation A8-39}$$

Rearranging and replacing the rate constant with a time constant, τ_m:

$$\sigma(t) = \sigma_0 e^{-\frac{t}{\tau_m}} \qquad \textbf{Equation A8-40}$$

The decay time constant controls the rate at which a stress is released and can be viewed as the ratio of the viscosity and the shear modulus:

$$\tau_{\mathrm{m}} = \frac{\eta}{G} \qquad \textbf{Equation A8-41}$$

Therefore it can be seen that a solution with a relatively strong viscous component would take a long time to release the stress. Conversely, a solution with a relatively high elastic component would more rapidly.

The relaxation function, G(t), can be calculated by dividing Equation A8-40 by the applied strain, γ:

$$G(t) = \frac{\sigma(t)}{\gamma} = \frac{\sigma_0}{\gamma} e^{-\frac{t}{\tau_m}}$$

$$G(t) = Ge^{-\frac{t}{\tau_m}} \qquad \textbf{Equation A8-42}$$

To mathematically describe the Maxwell model the rate of strain of the two parts must be added together (taking the first derivative of Equation A8-37):

$$\dot{\gamma} = \frac{\dot{\sigma}}{G} + \frac{\sigma}{\eta} \qquad \textbf{Equation A8-43}$$

The Maxwell model, Equation A8-43, along with the decay time constant can be used to analyse the viscometric tests which were carried out.

Nomenclature:

G	Spring Modulus (Pa)
t	Time (s)
γ	Shear strain
$\dot{\gamma}$	Shear strain rate (s^{-1})
η	Viscosity (Pas)
σ	Shear stress (Pa)
$\dot{\sigma}$	Shear stress rate (Pas^{-1})
τ_m	Time constant = η/G (s)

Appendix 9. Mathematics of an Oscillator

Given a mass on a spring [134]:

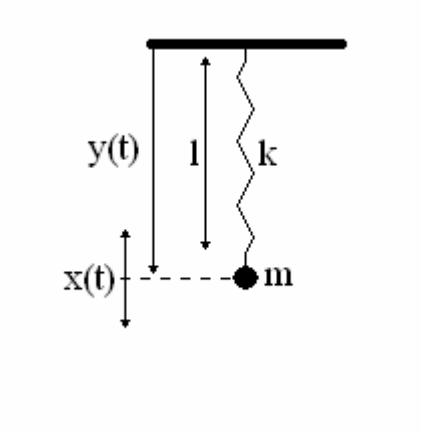

Assuming Newton's second law of motion and that the forces acting on the mass are gravity and the spring:

$$F = m\ddot{y}(t) = -k\left(y(t) - l\right) + mg \qquad \textbf{Equation A9-44}$$

At equilibrium, there is no acceleration (where $y_0 = y(t)$ at equilibrium):

$$k\left(y_0 - l\right) = mg$$

$$y(t) = y_0 + x(t)$$

$$m\ddot{x}(t) = -k\left(y_0 + x(t) - l\right) + mg$$
$$m\ddot{x}(t) = -k\left(y_0 + x(t) - l\right) + k\left(y_0 - l\right) = -kx(t)$$
$$\ddot{x}(t) = -\frac{k}{m}x(t)$$

This final equation is a non-forcing LDE and as such will have a solution of the form:

$$x(t) = ae^{\lambda t}$$

Taking the natural frequency, ω_n, to be the square root of the ratio of the spring constant and the mass and realising that the second derivative must be negative:

$$\omega_n = \sqrt{\frac{k}{m}}$$
$$\therefore \lambda = i\omega_n$$

Therefore:

$$x(t) = ae^{i\omega t_n}$$

This can be viewed as Euler's formula:

$$x(t) = ae^{i\omega t} = a(\cos(\omega t) + i\sin(\omega t)) \qquad \textbf{Equation A9-45}$$

It can be shown that a is the amplitude of the oscillator.

Nomenclature:

a = amplitude of the wave

F = force (N)

g = gravitational force = $9.81 ms^{-2}$

i = imaginary number = $-1^{0.5}$

k = the spring constant of the spring (Nm^{-1})

l = length of unstretched spring (m)

m = the mass (kg)

t = time (s)

$x(t)$ = displacement from equilibrium position (m)

$y(t)$ = displacement from baseline (m)

λ = LDE factor (s^{-1})

ω_n = natural frequency (s^{-1})

Appendix 10. Oscillatory Rheology

This appendix contains the derivation of the oscillatory rheological tests, based on a Maxwell model [110-112, 114, 135].

Given an oscillatory applied strain:

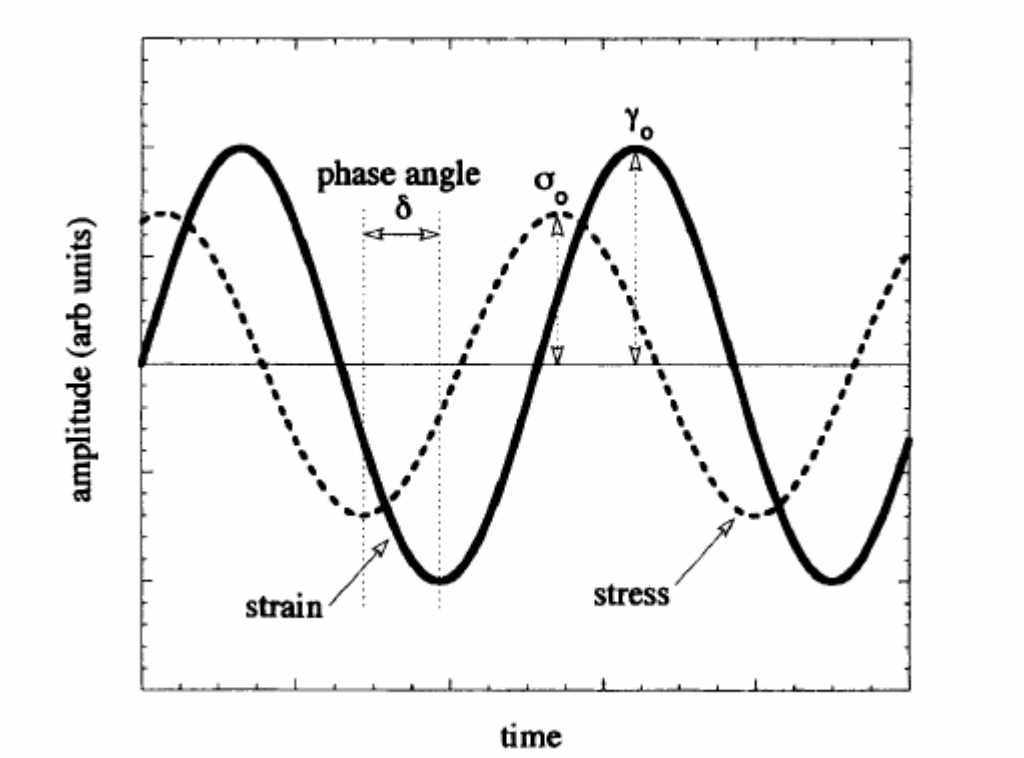

It can be shown that an oscillator has the formula (see Appendix 9):

$$x(t) = Ae^{i\omega t} = A(\cos(\omega t) + i\sin(\omega t)) \qquad \textbf{Equation A10-46}$$

Where A is the amplitude of the oscillation and ω is the frequency. For this system this gives a shear strain and shear stress:

$$\gamma^* = \gamma_0 e^{i\omega t} \qquad \textbf{Equation A10-47}$$

$$\sigma^* = \sigma_0 e^{i(\omega t+\delta)} \qquad \textbf{Equation A10-48}$$

To use the Maxwell model (Equation A8-43), the rate of shear strain and shear stress must be known:

$$\dot{\gamma}^* = i\omega\gamma_0 e^{i\omega t} = i\omega\gamma^* \qquad \textbf{Equation A10-49}$$

$$\dot{\sigma}^* = i\omega\sigma_0 e^{i(\omega t \backslash + \delta)} = i\omega\sigma^* \qquad \textbf{Equation A10-50}$$

Therefore:

$$i\omega\gamma^* = \frac{iw\sigma^*}{G} + \frac{\sigma^*}{\eta} \qquad \textbf{Equation A10-51}$$

Rearranging and using the decay time constant, Equation A8-41:

$$\frac{G\gamma^*}{\sigma^*} = 1 + \frac{1}{i\omega\tau_m} \qquad \textbf{Equation A10-52}$$

Further rearrangement and use of the complex modulus gives:

$$G^* = \frac{\sigma^*}{\gamma^*}$$

$$G^* = G\left(\frac{i\omega\tau_m}{1 + i\omega\tau_m}\right) \qquad \textbf{Equation A10-53}$$

Multiplying through by the complex conjugate of the denominator ($1\text{-}i\omega\tau_m$) gives:

$$G^* = G\left(\frac{(w\tau_m)^2}{1 + (w\tau_m)^2}\right) + iG\left(\frac{w\tau_m}{1 + (w\tau_m)^2}\right) \qquad \textbf{Equation A10-54}$$

The real part of this complex number is known as the storage modulus, G', and the imaginary part is the loss modulus, G''. These two terms can also be calculated directly from the data achieved during oscillation experiments, the phase difference and the complex modulus:

$$G^* = \frac{\sigma^*}{\gamma^*}$$

$$G^* = \frac{\sigma_0 e^{i(\omega t + \delta)}}{\gamma_0 e^{i\omega t}} = \frac{\sigma_0\left(e^{i\omega t} e^{i\delta}\right)}{\gamma_0 e^{i\omega t}}$$

$$G^* = \frac{\sigma_0 e^{i\delta}}{\gamma_0} = \left|G^*\right|\left(\cos\delta + i\sin\delta\right) \qquad \textbf{Equation A10-55}$$

The likelihood of a viscoelastic solution being described by a single combination of a spring and a dashpot is highly unlikely. The total stress on a system can be viewed as a summation of the shear strains applied multiplied by the resulting relaxation moduli:

$$\sigma(t) = \sum_{t_i=-\infty}^{t_i=t} \gamma_i G(t - t_i)$$ **Equation A10-56**

This can be expressed as an integral, thus enabling calculation of the total stress for a given strain history:

$$\sigma(t) = \int_{-\infty}^{t} G(t - t_i)\dot{\gamma}(t_i)dt_i$$ **Equation A10-57**

This is the Boltzmann Superposition Principle.

For an oscillating shear strain of frequency ω and being applied as a sine wave, the shear strain rate is:

$$\dot{\gamma} = \omega\gamma_0 \cos(\omega t)$$ **Equation A10-58**

Applying this to Equation A10-57 gives:

$$\sigma(t) = \omega\gamma_0 \int_{-\infty}^{t} G(t - t_i)\cos(\omega t_i)dt_i$$ **Equation A10-59**

Changing the integral limits by assuming $s = t - t_i$ and using trigonometry

$$\sigma(t) = \gamma_0 \sin(\omega t)\left(\omega\int_0^{\infty} G(s)\sin(\omega s)ds\right) + \gamma_0 \cos(\omega t)\left(\omega\int_0^{\infty} G(s)\cos(\omega s)ds\right)$$ **Equation A10-60**

The shear strain was applied as a sine wave. Therefore the term preceded by $\gamma_0 sin(\omega t)$ is in phase with this shear strain and the term preceded by $\gamma_0 cos(\omega t)$ is out of phase. As discussed previously, the elastic modulus is the in phase term and the loss modulus is the out of phase term.

Therefore, it can be written that:

$$\sigma(t) = \gamma_0 \sin(\omega t) G'(\omega) + \gamma_0 \cos(\omega t) G''(\omega) \qquad \textbf{Equation A10-61}$$

The phase difference, δ, can be used to describe the shear stress based on the applied shear strain:

$$\sigma(t) = \sigma_0 \sin(\omega t + \delta) \qquad \textbf{Equation A10-62}$$

Using the same trigonometry as for Equation A10-60:

$$\sigma(t) = \sigma_0 \cos\delta \sin(\omega t) + \sigma_0 \sin\delta \cos(\omega t) \qquad \textbf{Equation A10-63}$$

Equating Equation A10-61 and Equation A10-63 gives:

$$G'(\omega) = \frac{\sigma_0}{\gamma_0} \cos(\delta) = G^* \cos(\delta) \qquad \textbf{Equation A10-64}$$

$$G''(\omega) = \frac{\sigma_0}{\gamma_0} \sin(\delta) = G^* \sin(\delta) \qquad \textbf{Equation A10-65}$$

Nomenclature:

G	Spring Modulus (Pa)
G^*	Complex modulus (Pa)
G'	Storage modulus (Pa)
G''	Loss modulus (Pa)
t	Time (s)
γ^*	Complex shear strain
γ_0	Peak shear strain
$\dot{\gamma}$	Shear strain rate (s^{-1})
δ	Phase angle (^{o})
η	Viscosity (Pas)
σ^*	Complex shear stress (Pa)
σ_0	Peak shear stress (Pa)
τ_m	Time constant = η/G (s)
ω	Frequency of oscillation (Hz)

Appendix 11. Complex Number Theory

Complex numbers are written in the form:

$$z = x + iy$$

where $i = (-1)^{0.5}$, x is the real part of the number ($x = \mathcal{R}e\, z$) and y the Imaginary part ($y = \mathcal{I}m\, z$).

Complex numbers can be represented on an Argand diagram, where the two real numbers, x and y, can be used as Cartesian coordinates.

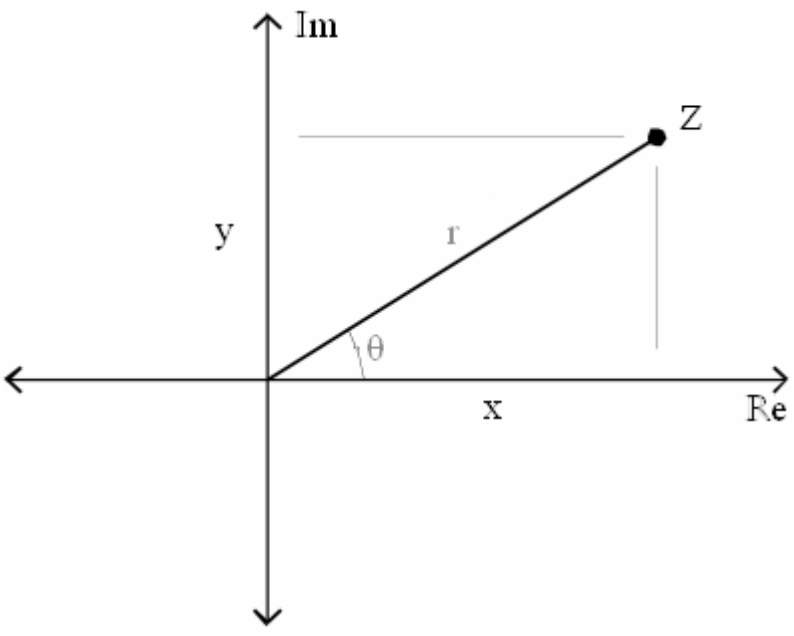

Where:

$$|z| = r = \sqrt{x^2 + y^2}$$

$$\theta = \arg z$$

$$\cos\theta = \frac{x}{r}$$

$$\sin\theta = \frac{y}{r}$$

The modulus of a complex number, $|z|$, can be found using Pythagoras' theorem and the angle, θ, by simple trigonometry. It is possible, therefore, to represent a complex number as:

$$z = r\cos\theta + ir\sin\theta$$

If these coordinates are plotted on an Argand diagram for $-\pi < \theta < \pi$ a circle would be drawn. This can be used to describe an oscillator, such as that used in Section 5 of this work [110, 135]. The result is easier to manage, mathematically, when Euler's formula is used:

$$z = re^{i\theta} = r\cos\theta + ir\sin\theta$$

Nomenclature:

i	Imaginary number = $-1^{0.5}$
r	Modulus of complex number
z	Complex number
θ	Argument of complex number

Appendix 12. Swelling Model for a Hydrogel

This appendix contains the derivation of the hydrogel swelling model [124].

Peppas and Merrill adapted the work of Flory and Rehner to develop an equation for the swelling of a polymer network [119, 120, 136, 137]:

$$\frac{1}{\overline{M_c}} = \frac{2}{\overline{M_n}} - \frac{\frac{\bar{v}}{V_1}\left[\ln\left(1-v_{2,s}\right)+v_{2,s}+\chi_1\left(v_{2,s}\right)^2\right]}{v_{2,r}\left[\left(\frac{v_{2,s}}{v_{2,r}}\right)^{\frac{1}{3}}-0.5\left(\frac{v_{2,s}}{v_{2,r}}\right)\right]} \qquad \textbf{Equation A12-66}$$

Where: $\overline{M_c}$ – Number average molecular mass of the polymer chain between cross-links

$\overline{M_n}$ – Number average molecular mass of the polymer chain

$\bar{v}$ – Partial specific volume of the polymer = 0.62 [127]

V_1 – Molar volume of water

χ_1 – Flory polymer-solvent interaction parameter = 0.473 [127]

$v_{2,s}$ – Polymer fraction of the gel at equilibrium swelling

$v_{2,r}$ – Polymer fraction of the gel after gel formation

The swelling ratio can be found:

$$Q = \frac{v_{2,r}}{v_{2,s}} \qquad \textbf{Equation A12-67}$$

The number of covalent cross-links can be equated to the number of carboxymethyl groups attached to a given dextran molecule (see Section 2.3). The number of affinity cross-links is dependent upon the association constant of the interaction (where *[MC]* is the concentration of cona – glucose interactions):

$$K = \frac{[MX]}{[M][X]} = \frac{[MX]}{([M_{TOT}]-[MX]-[MC])([X_{TOT}]-[MX])} \qquad \textbf{Equation A12-68}$$

$$K_c = \frac{[MC]}{[M][C]} = \frac{[MC]}{([M_{TOT}]-[MX]-[MC])[C]} \qquad \textbf{Equation A12-69}$$

In order to calculate *[MX]* Equation A12-69 must be rearranged in terms of the cona-glucose complex and substituted into Equation A12-68. This results in a quadratic equation:

$$0 = K[MX]^2 - \left(K[X_{TOT}] + K[M_{TOT}] + K_C[C] + 1\right)[MX] + K[M_{TOT}][X_{TOT}] \quad \textbf{Equation A12-70}$$

Calculation of *[MX]* allows the number average molecular mass between affinity crosslinks to be calculated:

$$\overline{M}_c^{aff} = \frac{[P]\overline{M}_n}{[MX]} \quad \textbf{Equation A12-71}$$

Where *[P]* is the concentration of the polymer in the gel.

The concentrations of the components is governed by the degree of swelling, therefore calculation of the swelling from Equation A12-66 must be done iteratively with Equation A12-70. The swollen polymer fraction can be used to calculate the mesh size of the gel [138]:

$$\xi = v_{2,s}^{-1/3}\left(\frac{2C_n\overline{M}_c}{M_r}\right)^{1/2} l \quad \textbf{Equation A12-72}$$

Where: C_n - Flory characteristic ratio

M_r - Molecular mass of repeat unit

l - Unit length along the polymer backbone

The mesh size can be used to calculate the rate of diffusion, based on the deviation from the liquid phase diffusivity [122, 123]:

$$D_{gel} \cong D_l\left(1 - \frac{r}{\xi}\right)e^{\frac{-1}{Q-1}} \quad \textbf{Equation A12-73}$$

Where: D_l – Liquid phase diffusivity of the solute

r – hydrodynamic radius of the solute

This diffusivity value can be used to calculate the concentration flux through the a hydrogel of known swollen membrane thickness, δ_G, and receiving chamber volume, V [124]:

$$J = \frac{AD_{gel}}{V\delta_G}\left(C_D - C_R\right) \qquad \textbf{Equation A12-74}$$

Where C_D and C_R are the donor and receiving chamber concentrations respectively.

Modelling of the rate of diffusion of a solute through a hydrogel can be achieved using Equation A12-66 to Equation A12-74.

Nomenclature:

A	Surface area of hydrogel (m^2)
C_d	Concentration of cytC, donor side (mgL^{-1})
C_n	Flory characteristic ratio
C_r	Concentration of cytC, receiving side (mgL^{-1})
D_{gel}	Gel phase diffusivity (m^2s^{-1})
D_l	Liquid phase diffusivity of the solute (m^2s^{-1})
J	Flux ($mgL^{-1}min^{-1}$)
l	Unit length along the polymer backbone (m)
$\overline{M_c}$	Number average molecular mass of the polymer chain between cross-links ($gmol^{-1}$)
$\overline{M_n}$	Number average molecular mass of the polymer chain ($gmol^{-1}$)
M_r	Molecular mass of repeat unit ($gmol^{-1}$)
Q	Swelling ratio
r	Hydrodynamic radius of the solute (m)
$\bar{v}$	Partial specific volume of the polymer
V	Volume of receiving side (m^3)
V_1	Molar volume of water (m^3g^{-1})
$v_{2,r}$	Polymer fraction of the gel after gel formation (gg^{-1})
$v_{2,s}$	Polymer fraction of the gel at equilibrium swelling (gg^{-1})
χ_1	Flory polymer-solvent interaction parameter
ξ	Mesh size (m)

Appendix 13. Power Basic Model of Hydrogel Swelling

This appendix contains the Power Basic model for hydrogel swelling.

```
' Affinity membrane model

' J. Hubble, June 2005   -   I. Benzeval, September 2008

   DEFDBL a-z
   FUNCTION PBMAIN()
   CLS
   DIM a(20)

'Data section

'Ligand receptor properties
   a(1)=1.49e-4    '[Mtot] Concentration of ConA in gel (M)
   a(2)=0.034      '[Xtot] Concentration of terminal glucose groups in gel (M)
   a(3)=4.5e-4     'Kd     Dissociation constant, ConA-Dextran (M)
   a(4)=5.9e-3     'Kc     Dissociation constant, ConA-Glucose (M)
   a(5)=4050       'mp     Average MM between covalent cross-links (g/mol)

'Polymer properties
   a(6)=500000     'mn     Dextran mol mass (g/mol)
   a(7)=162        'mr     Molecular mass of repeat unit (glucose) (g/mol)
   a(8)=0.62       'vb     Partial specific volume of dextran (cm^3/g)
   a(9)=18         'v1     Molar volume of water (cm^3/g)
   a(10)=0.099     'vr     Dextran fraction of gel after formation (g/g)
   a(11)=0.473     'xi     Flory solvent polymer interaction constant (-)
   a(12)=5         'cn     Flory characteristic ratio (-)
   a(13)=4.6e-10   'l      Unit length along the polymer back bone (m)
   a(14)=a(10)*1000/a(6)  'pc Dextran concentration (M)

'Solute properties
   a(15)=11.4e-11  'diff   Liquid phase diffusivity of CytC (m^2/s)
   a(16)=3.8e-9    'r      Radius of CytC (m)

'Transport properties
   a(17)=4.8e-4    'mt     Membrane thickness (m)
```

```
      a(18)=4.6e-4    'area   Membrane area (m^2)
      a(19)=4.6e-6    'vol    Volume of receiving chamber (m^3)
      a(20)=50        'sol    Solute concentration (mg/L)

     'Data output routine
     f$="test2.txt"
     OPEN f$ FOR OUTPUT AS #2

      cfin=0.2       'Maximum glucose concentration
      cs=.01
        FOR c=0 TO cfin  STEP cs
           CALL crosslink(c,a(),j,na,np,diffg,namax)
           PRINT c,j,na,np,diffg,namax
           PRINT #2,c,j,na,np,diffg,namax
        NEXT i1
     CLOSE #2

     print"Error sum =";es

1111       END FUNCTION

SUB crosslink(c,a(),j,na,np,diffg,namax)

      namax=a(1)/a(14)     'Maximum number of affinity cross-links in absence of glucose
      rlo=(a(3)+a(1)+a(2)-SQR(a(3)^2+2*a(3)*a(1)+2*a(3)*a(2)+a(1)^2-2*a(1)*a(2)+a(2)^2))/2    '[MX]
no competitor.
      yo=rlo/a(1)          'Fraction of [Mtot] to [MX]
      np=(a(6)/a(5))       'Number of covalent cross-links per polymer chain
      nao=namax*yo         'Number of affinity cross-links in absence of competitor
      mco=a(6)/(nao+np)    'Molecular mass between ALL cross-links

         CALL bisect(a(),mco,cx)  'Find root

      vso=cx
      vsp=0                'set initial vs value to zero for convergence test
      lt=a(2)              'reset concentrations for next competitor value
      rt=a(1)

1000    aa=a(3)*a(4)+a(3)*c+rt*a(4)+a(4)*lt
```

```
bb=a(3)^2*a(4)^2+2*a(3)^2*a(4)*c+2*a(3)*a(4)^2*rt+2*a(3)*a(4)^2*lt+a(3)^2*c^2
cc=2*a(3)*c*rt*a(4)+2*a(3)*c*a(4)*lt+rt^2*a(4)^2-2*a(4)^2*rt*lt+a(4)^2*lt^2
dd=SQR(bb+cc)
rl=(aa-dd)/(2*a(4))  '[MX] with competitor
y=rl/rt              'Ratio of new [MX] to previous [MX]

na=namax*y           'Number of affinity cross-links in presence of glucose
bonds=na+np          'Total number of cross-links, covalent + affinity
mc=a(6)/bonds        'Molecular mass between all cross-links

   IF bonds < 2 THEN
         PRINT "Dissolution - bonds per chain =",bonds   'Insufficient bonds to form a gel
      GOTO 111
   END IF

      CALL bisect(a(),mc,cx) 'Find root
vs=cx
sr=vso/vs        'Swelling ratio - computed with reference to the swollen gel with no glucose

'Recompute concentrations after swelling

lt=a(2)/sr
rt=a(1)/sr

'Check for convergence of swelling calculations

   IF ABS((vs-vsp)/vsp)>=1e-4 THEN
      vsp=vs
      GOTO 1000
   END IF

'mesh - Hydrogel mesh size

mesh=vs^(-.33)*(a(12)*mc/a(7))^0.5*a(13)
'q - Volume degree of swelling - computed with reference to the formation volume
q=a(10)/vs
'diffg - Gel diffusivity
diffg=a(15)*(1-a(16)/mesh)*EXP(-1/(q-1))
```

```
      IF diffg <= 0 THEN
         diffg=0
      END IF

   'j - Flux

   j=60*((a(18)*diffg)/(a(17)*sr*a(19)))*a(20)


111   END SUB

'Bisection root finding routine
   SUB bisect(a(),mco,cx)

   x1 = a(10)      'Set maximum possible value of vso=vr
   x2 = 1e-8       'Set minimum possible value of vs0 = a fraction above 0

      CALL func(a(),x2,mco,fmid)
      CALL func(a(),x1,mco,f)

      IF f * fmid >= 0 THEN
         PRINT "Root not bracketed",fmid,f
      GOTO 200
      END IF

      IF f < 0 THEN   'Orients search
         cx = x1
         dx = x2 - x1
      ELSE
      cx = x2
      dx = x1 - x2
      END IF

   'Bisection loop

   acc = .000001 * (x1 + x2) / 2
      FOR ii = 1 TO 500
         dx = .5 * dx
         xmid = cx + dx
```

```
            CALL func(a(),xmid,mco,xr)
        IF xr <= 0 THEN
           cx = xmid
        END IF
        IF ABS(dx) < acc THEN GOTO 200
        NEXT ii
      PRINT "too many bisections"

200    END SUB

'_____________________________________________________

   SUB func (a(),vso,mco,x)

      x=2/a(6)-(a(8)/a(9))*(LOG(1-vso)+vso+a(11)*vso^2)/(a(10)*((vso/a(10))^(1/3)-0.5*(vso/a(10))))-
1/mco

   END SUB

'_____________________________________
```